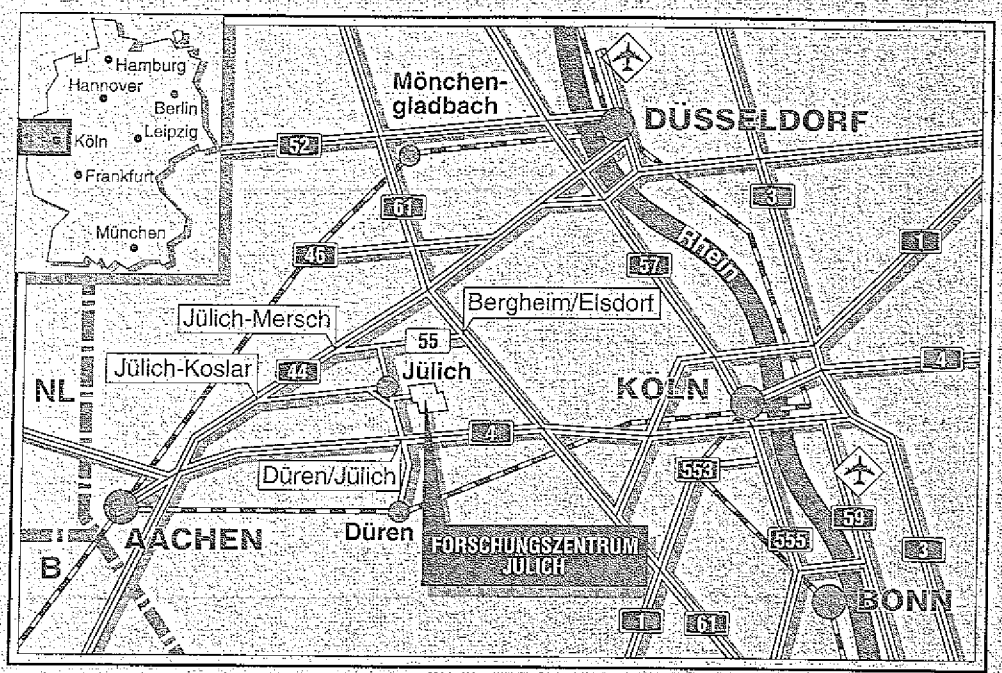

Berichte des Forschungszentrums Jülich ; 3031
ISSN 0944-2952
Institut für Festkörperforschung Jül-3031

Zu beziehen durch : Forschungszentrum Jülich GmbH · Zentralbibliothek
D-52425 Jülich · Bundesrepublik Deutschland
Telefon : 02461/61-6102 · Telefax : 02461/61-6103 · Telex : 833556-70 kfa d

Origins of scale invariance in growth processes

Joachim Krug

This work was submitted in November 1994 as a Habilitation Thesis to the Heinrich-Heine-Universität Düsseldorf.

O sweet spontaneous
earth how often have
the
doting

fingers of
prurient philosophers pinched
and
poked

thee
, has the naughty thumb
of science prodded
thy

beauty . how
often have religions taken
thee upon their scraggy knees
squeezing and

buffeting thee that thou mightest conceive
gods
(but
true

to the incomparable
couch of death thy
rhythmic
lover

thou answerest

them only with

spring)

e.e. cummings

Contents

1. Introduction

The study of growth processes has always constituted, explicitly or implicitly, an integral part of solid state physics and materials science. Indeed, most properties of real materials depend crucially on the presence of imperfections - bulk vacancies, dislocations, surface roughness - that are remnants of the nonequilibrium conditions under which the material has formed. Over the centuries the art and science of crystal growth has progressed to ever more closely approximate the ideal of a perfect, crystalline solid, as evidenced impressively by modern techniques such as molecular beam epitaxy (MBE), which allow for the engineering of solid state devices at the level of individual atomic planes. Nevertheless, the success of this and other techniques depends crucially on the ability to control the disordering effects of the nonequilibrium growth conditions, and to assess, at least empirically, the relationship between the growth conditions and the resulting structure.

Apart from its eminent technological significance, the growth of solids is of considerable fundamental interest, since it may provide us with important clues to the way in which complex structures form in Nature, through the agglomeration of simple, microscopic processes operating in a highly disordered, noisy environment. This aspect was dramatically brought to the attention of the theoretical physics community in 1981, with the invention of the diffusion-limited aggregation model (DLA) by Witten and Sander [1], which has since been found to describe a wide variety of naturally occurring patterns [2, 3]. To add to the excitement, it was found that the structures generated by DLA and related models typically show spatial *scale invariance*, thus requiring for their quantitative characterization the notions of fractal geometry pioneered by Mandelbrot [4]. Mandelbrot has presented a vast amount of empirical evidence in support of his thesis that fractal structures occur quite commonly in Nature, as the outcome of many complex physical, geological, biological and even social processes. As has been remarked by Kadanoff [5] and others, Mandelbrots observation raises a fundamental scientific problem insofar as not many *mechanisms* are known that could account for the genericity of scale invariant behavior.

The problem was posed in more pointed form in 1987 by Bak, Tang and Wiesenfeld [6],who suggested the concept of *self-organized criticality* (SOC) as a framework within which to formulate general principles that are responsible for scale invariance in Nature. The term is motivated by viewing the ubiquity of scale invariant behavior against the background of equilibrium statistical mechanics, where scale invariance is associated, since the advent of the renormalization group, with critical point phenomena. Given that in Nature no experimentators are available to tune systems to their critical points, the argument goes, natural systems can show scale invari-

ance only if they tune themselves, as it were, through some kind of self-organization mechanism. While this line of reasoning is appealing and has stimulated a tremendous amount of work on extended nonequilibrium systems, it should be kept in mind that the association of scale invariance with critical point behavior has its roots in a somewhat arbitrary historical development, in which equilibrium critical phenomena happened to provide the first example of nontrivial scale invariance that could be understood on a fundamental level. There is no guarantee that the analogy with critical phenomena will serve as a reliable guide when venturing into the vast unknown territory of scale invariance far from equilibrium.

With hindsight, it appears rather unlikely that principles of the generality originally envisioned by Bak and coworkers [6] will be found at the origin of all, or even a significant fraction of instances where scale invariance is encountered in natural processes. Consequently, workers in the field now tend to reserve the term SOC to describe a more specific class of mechanisms which produce scale invariance through a separation of time scales between driving and relaxation (as, for example, in earthquakes; see [7]). Nevertheless, growth processes such as DLA (and other, less spectacular examples which will form the main part of these notes) come quite close to fulfilling the requirements for a robust, ubiquitous mechanism for scale invariant behavior: Nonequilibrium growth processes are involved in the formation of virtually any natural structure; they can be classified according to some broad characteristics such as the presence of a Laplacian field (as in DLA), the presence of a well-defined growth interface with approximately local dynamics (in kinetic roughening phenomena, see below), symmetries, conservation laws etc.; and for many such classes it is possible to formulate simple models and theories that can be used to extract quantitative, sometimes universal information about the scale invariant structures that form.

This article describes some recent progress in our understanding of how scale-invariant structures emerge through far-from-equilibrium growth processes. Since exhaustive reviews on various aspects of the subject are available [2, 3, 8, 9, 10], the emphasis here will be on a few key concepts, which are developed as comprehensively as possible. Simplicity is favored over generality; priority is given to elementary arguments based on scaling ideas and dimensional analysis, which provide the maximum yield in terms of intuitive insights. For details and technicalities the reader is referred to the extensive bibliography.

1.1 Outline

It is evident already from a very superficial look at a growth process like DLA that the *competition* between different parts of the growing structure plays a central role in developing long-ranged spatial correlations and scale invariance. Of course, it is an altogether different matter to turn this qualitative insight into a quantitative theory. **Chapter 2** is devoted to a restricted class of *needle models for competitive growth* which allow a detailed analysis of the relation between competition and scale invariance. Competition mediated by a Laplacian field (as in DLA) as well as through geometric shadowing will be considered, and special attention will be paid to the role of fluctuations and the extent of universality of the resulting scaling properties. Sections 2.1 and 2.2 mainly summarize results that have been presented in detail elsewhere, while the discussion of the shadowing instability (Section 2.3) and Laplacian needle growth (Section 2.4) considerably extends the brief published accounts [11, 12].

The main part of the article - chapters 3, 4 and 5 - deals with growth processes that can be reduced to the motion of a well-defined interface with approximately local dynamics. This explicitly excludes diffusion-limited growth, but includes many technologically relevant vapor deposition techniques. In this case scale-invariant behavior appears in the form of *kinetically induced surface roughness* [8, 9, 10]. The underlying mechanism is the interaction of microscopic fluctuations with the slow dynamics of the long-wavelength interface degrees of freedom.

The basic concepts are introduced in **Chapter 3**, in a (hopefully!) pedagogical manner. The starting point are macroscopic interface equations of motion, derived from thermodynamic and kinetic considerations in the spirit of the classic work of Mullins [13]. Special attention is paid to terms in the equations which originate from the nonequilibrium character of the process. Two types of terms are generally encountered - *kinematic* terms (such as the celebrated Kardar-Parisi-Zhang (KPZ) nonlinearity [14]) that appear simply because the interface is moving, and *dynamic* terms that reflect changes in the interface relaxation processes due to the nonequilibrium conditions. Terms of the latter type play an important role in the description of crystal growth from atomic beams [15].

Given a macroscopic interface equation of motion, a continuum theory of kinetic roughening is obtained by adding appropriate noise terms that describe the (equilibrium or nonequilibrium) fluctuations in the problem. In Chapter 3, this program will be carried out at the level of *linear* fluctuation theory. While mathematically undemanding, the linear theory already contains most key features of kinetic roughening phenomena; moreover, as will be explained in Section 3.4, physically relevant situations exist in which the linear theory is exact.

In Chapters 4 and 5, the discussion is specialized to two broad classes of kinetic roughening phenomena, which can be distinguished according to whether or not the surface relaxation processes conserve the volume of the growing structure. The generic description for *nonconserved* dynamics is provided by the Kardar-Parisi-Zhang equation introduced in 1986 [14]. In view of the excellent accounts that have appeared during the last few years [8, 9, 10], only the most important properties of the equation - tilt invariance, the fluctuation-dissipation theorem, and the mapping to directed polymers in random media - will be presented in **Chapter 4**. The remainder of the chapter describes some recent developments which have not been summarized previously, notably the topics of amplitude universality, finite size effects, chaotic interfaces and inhomogeneous growth.

Conserved growth equations apply to MBE-type vapor deposition processes, where desorption of material from the surface, as well as the formation of bulk defects can be neglected. They represent a distinct class of kinetic roughening phenomena, which has been the focus of much activity over the last four years. **Chapter 5** attempts to provide a unified picture of the current understanding of these processes. The central goal will be to identify the microscopic mechanisms underlying the relevant dynamic nonequilibrium terms in the large scale dynamics; most of the material presented here has not been published previously. Since one of the main motivations for these studies has been to more closely approximate the conditions under which epitaxial growth is actually conducted in the laboratory, Chapter 5 also contains, in Sections 5.2.4 and 5.4.2, a preliminary assessment of pertinent experiments.

The chapters are written such as to be reasonably self-contained. Each chapter contains a few introductory paragraphs that place it into the general context. In particular, Chapter 2 is largely independent of the rest of the article. While Chapter 3 is a prerequisite for the discussions in Chapters 4 and 5, readers who have some familiarity with kinetic roughening phenomena should be able to turn directly to the last two chapters.

2. Competitive growth

In this chapter a sequence of models is introduced, in which one-dimensional structures ('needles') grow from linear or planar substrates and interact through some kind of screening or shadowing mechanism. We shall investigate in detail how the competition gives rise to a scale-invariant, power law distribution of needle heights,

$$N(h) \sim h^{-\gamma} \tag{2.1}$$

and, correspondingly, a density profile

$$n(h) = \int_h^\infty dh\, N(h) \sim h^{-(\gamma-1)}, \tag{2.2}$$

both relations being understood to hold for the frozen, stationary structure which evolves after a long time; in some cases the power laws are modified by logarithmic corrections. The models are discussed in the order of increasing complexity of the competition mechanism, which ranges from unidirectional geometric shadowing to Laplacian (that is, electrostatic) screening.

While the models are mainly motivated by their simplicity and should not be expected to precisely describe any specific system, physical situations are conceivable in which the competing structures are, to a good approximation, linear, and insights gained from the study of needle models could prove useful. Examples are patterns of linear cracks driven into a solid by thermal shock [16], and arrays of dendritic side branches [17, 18].

2.1 Ballistic deposition at oblique incidence

Ballistic deposition is a simple model for the deposition of amorphous thin films at low temperatures [19]. In this model, particles are released at random positions above the surface and move towards the deposit along straight line ('ballistic') trajectories which form a fixed angle, θ, with the substrate normal. Corresponding to the assumption of low temperature and, hence, negligible atomic mobility, the particles stick permanently at the point of first contact with the deposit. It has long been recognized [20] that the structures grown by this simple rule attain a characteristic *columnar* morphology when the deposition angle θ is increased towards the limit of grazing incidence, $\theta \to 90°$ (Figure 1). The deposit breaks up into columns which grow more or less independently of each other and interact only through geometric shadowing. The columns are needle-shaped in the case of growth from a one-dimensional (linear) substrate, and have a sheet-like structure when grown from a plane [21, 22]. Much experimental interest has focused on the growth angle of the columns, which is distinct from the angle of deposition [20]. In fact this angle is

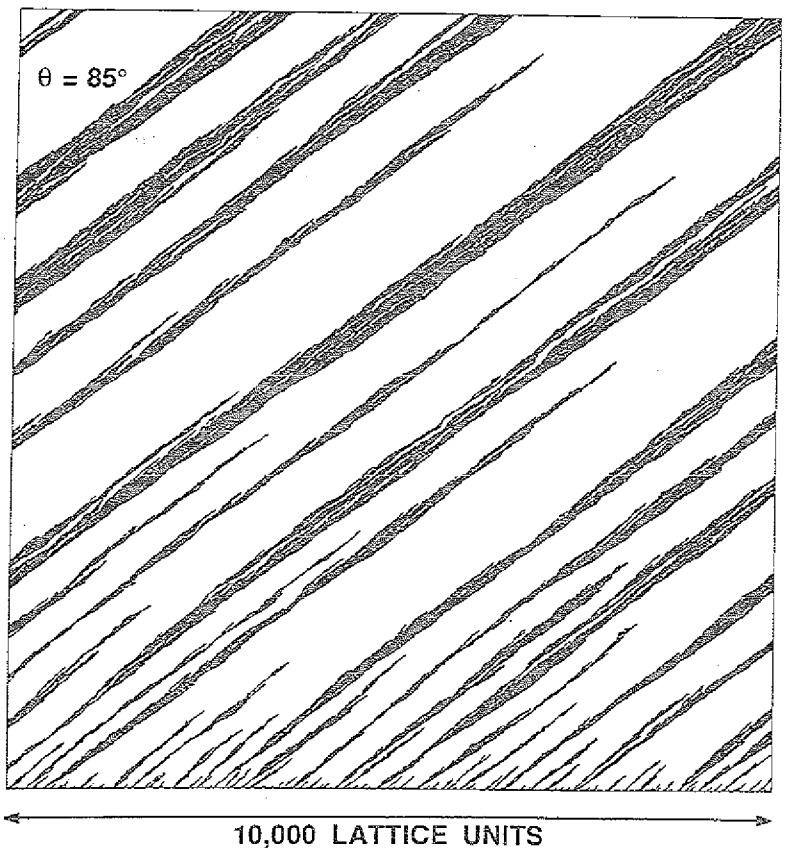

Figure 1: Lattice simulation of ballistic deposition onto a one-dimensional substrate. Particles enter from the right, following trajectories which form an angle of 85° with respect to the surface normal. In this particular model the columns (black) grow at an angle of about 52° relative to the normal. The picture shows part of a larger system. Courtesy of Paul Meakin.

related to the angular dependence of the deposit density, and can be computed in a mean-field approximation [23].

A closer look at Figure 1 suggests the idealization depicted in Figure 2: The columns are replaced by needles which grow independently by the accretion of flux at their tips. In this view, the competition is seen to be *noise driven*: While the average growth rate is the same for all needles, the shot noise in the particle flux makes it possible for some needles to temporarily grow ahead of their neighbors. Once a needle has been completely shaded, it is forever excluded from further growth: The competition mechanism is *exclusive* in the sense that needles are either completely unaffected by the presence of others (the *active* state), or else completely shaded.

These qualitative considerations can be turned into precise predictions by exploiting the mapping [24] to coalescing random walks indicated in Figure 2. The

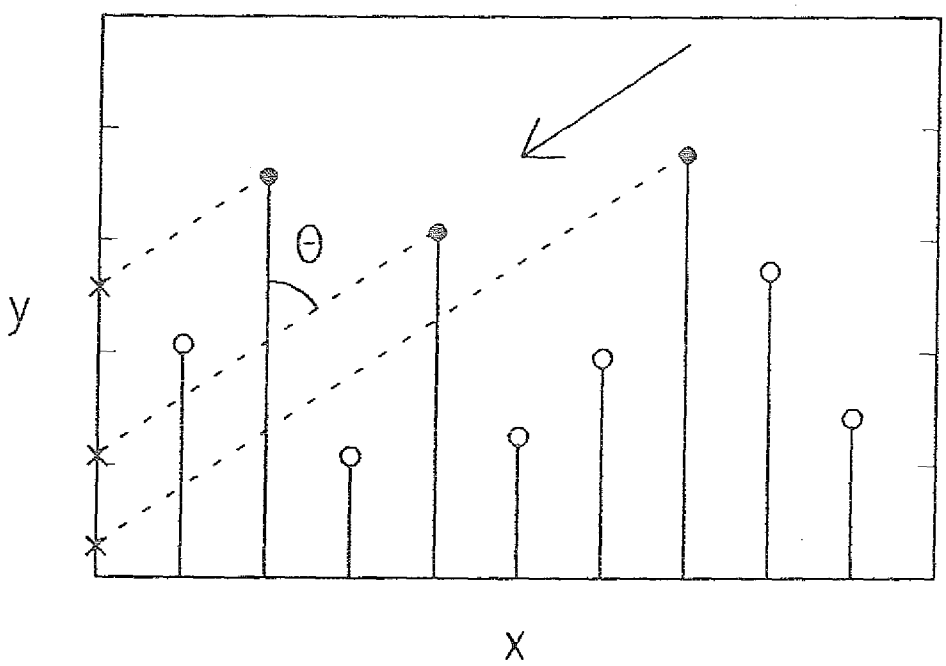

Figure 2: Schematic of the needle model for oblique incidence ballistic deposition. Active (shaded) needles are identified by full (open) tips. The arrow shows the direction of the beam incident at an angle θ. The dotted lines indicate the mapping of the tip positions onto coalescing particles.

positions of the *active* needle tips are projected onto a line perpendicular to the substrate, and are interpreted as the positions of point particles. Due to the growth of the needles, the particles have an (unessential) constant upward drift, superimposed by independent random walks. The shading of one needle by another corresponds to the coalescence of the walkers. The crucial advantage of this mapping, then, is that the *nonlocal* geometric shadowing interaction between needles is turned into a *local* contact interaction among random walkers.

An elementary property of coalescing random walks is that their average distance increases with time t as $\sqrt{t}$. This is simply a consequence of the fact that, apart from the contact interactions, the walkers are independent: After a time t, a *free* walker has explored a region of size $\sqrt{t}$; in the presence of other walkers, it can survive up to time t only if it has depleted a region of that size around it. Similarly, in the needle model, the height fluctuations of an active needle grow with time t or, equivalently, with height h as $\delta h \sim \sqrt{h}$. Through the geometric shadowing mechanism this vertical length scale is translated into a horizontal *shadowing length* $\xi(h) \sim \delta h$ over which a surviving needle of height h is expected to have shaded other

needles. The density at height h can then be estimated as $n(h) \sim 1/\xi(h) \sim h^{-1/2}$, so $\gamma = 3/2$ in (2.1).

More precisely, the mapping to coalescing random walks yields an expression for the asymptotic fraction of surviving needles [24, 25],

$$\rho(t) \approx \cot\theta/\sqrt{\pi t}. \tag{2.3}$$

Since shaded needles stop growing entirely, only those which are active at time t contribute to the density profile for $h \gtrsim h_a(t)$, where $h_a(t)$ denotes the average height of active needles. We therefore have the identity

$$\rho(t) = n(h_a(t)) \tag{2.4}$$

and, since $h_a(t) = t$ in the present case (unit deposition rate),

$$N(h) = -\frac{dn}{dh} \approx \frac{\cot\theta}{2\sqrt{\pi}} \frac{1}{h^{3/2}}. \tag{2.5}$$

Equation (2.4) expresses a particularly simple relation between the dynamics of competition - as described by the survivor density ρ - and the scaling of the frozen structure; the relation is a consequence of the exclusive nature of shadowing in the present model, and can only approximately be generalized to other situations. At some finite time t the height distribution is a superposition of the distribution of shaded needles, which follows (2.5) up to $h \approx h_a(t)$, and a Gaussian of width $\sim \sqrt{t}$ and total weight $\rho(t)$, centered around $h_a(t)$, which contains the active part of the population; of course in a finite system eventually a state is reached in which only a single needle is growing [24].

Within the idealized needle model, the value $\gamma = 3/2$ is evidently *universal*, i.e. it is independent of deposition angle, growth rate and such [25]. The needle model also seems to give an accurate description of several versions of the full ballistic deposition problem, provided θ is chosen sufficiently large to ensure the formation of well-separated columns [23, 24]. In the full problem it is more natural to consider the distribution of column masses, s, rather than heights h. The two are related as follows [24]. The shape of individual columns is characterized by exponents $\nu_{||}$, $\nu_\perp$ which describe how their height h and width w scales with mass, $h \sim s^{\nu_{||}}$ and $w \sim s^{\nu_\perp}$. The mass distribution is therefore given by

$$N(s) = \frac{dh}{ds} N(h) \sim s^{-\tau} \tag{2.6}$$

with $\tau = 1 + \nu_{||}(\gamma - 1)$. For processes like ballistic deposition, where both the individual columns and the deposit as a whole are compact, we also have the general relation [26] $\nu_{||} = 2 - \tau$. Together these relations imply

$$\tau = 2 - 1/\gamma, \tag{2.7}$$

so $\tau = 4/3$ in the present case.

In conclusion, unidirectional geometric shadowing in conjunction with deposition flux shot noise is an example of competitive growth which gives rise to scale-invariant structures, eq. (2.1), with robust, universal scaling exponents. To a certain extent these ideas also apply to deposition onto a plane, where the coalescing objects are lines rather than point particles [21, 22].

2.2 Noisy vs. deterministic competition

2.2.1 Nagatani's forest formation model

Nagatani [27] proposed a modification of the needle model described above, in which the growth rate v_i of an active needle depends on its height h_i as $v_i \sim h_i^\alpha$. One particular realization of this idea is a model [25] in which all active needles are chosen for growth with equal probability, but the height of the chosen needle is incremented by an amount proportional to h_i^α. The scaling approach of the preceding section is directly applicable here: The height fluctuation of a surviving needle increases with height as $\delta h \sim h^{(1+\alpha)/2}$; estimating $n(h) \sim 1/\xi(h) \sim 1/\delta h$, one obtains the height distribution exponent

$$\gamma = \frac{3+\alpha}{2}, \tag{2.8}$$

in good agreement with simulations [25].

A conceptually interesting feature of the Nagatani model is the possibility, for $\alpha > 0$, of purely *deterministic* competition. Let us consider the following deterministic growth model [25]: On each site i of the integer lattice we define a real positive height variable $h_i(t)$. Each height grows independently, according to

$$\frac{dh_i}{dt} = h_i^\alpha, \tag{2.9}$$

as long as the needle is not shaded, i.e. as long as the condition

$$h_i > h_j - (j-i)\cot\theta \tag{2.10}$$

is fulfilled for all $j > i$ (Figure 2); shaded needles stop growing entirely. The initial values $h_i(0)$ are drawn at random from some distribution $P(h)$.

For $\alpha > 0$ the initial height fluctuations are amplified by the growth process, and needles of large initial heights are able to shade those who are less fortunate. Due to the simplicity of eqs. (2.9) and (2.10) it is possible to write down an explicit expression [25] for the fraction of surviving needles in terms of $P(h)$, for general α. Here we sketch the special case $\alpha = 1$, in which the active needles grow exponentially, $h_i(t) = h_i(0)e^t$. From (2.10) the surviving fraction can be written as

$$\rho(t) = \int_0^\infty dh\, P(h) \prod_{i=1}^{\infty} \int_0^{h+i/\ell} dh'\, P(h'), \tag{2.11}$$

where $\ell = e^t \tan\theta$.

Consider first a uniform distribution, $P(h) = 1$ for $0 < h < 1$. In this case the product in (2.11) only extends to $i_{\max} = \ell(1-h)$. We replace the product by the exponential of a sum and approximate the sum by an integral. A change of variables then yields

$$\rho \approx \int_0^1 dh\, e^{-\ell(1-h)-\ell(h+1/\ell)\ln(h+1/\ell)+1} \approx \sqrt{\frac{\pi}{2\ell}}; \tag{2.12}$$

in the last step a saddle point integration was performed. Not surprisingly, the form of the integrand in (2.12) shows that the survival probability is dominated, for large ℓ, by the needles with the largest initial heights, around $h = 1 - 1/\ell$. Since the average height of active needles grows as $h_a(t) = (1/2)e^t = (\ell/2)\cot\theta$, we can use (2.4) to conclude that

$$N(h) \approx (\sqrt{\pi \cot\theta}/4)\, h^{-3/2}, \tag{2.13}$$

and thus $\gamma = 3/2$ in (2.1).

It is instructive to repeat this calculation for an unbounded initial distribution, such as $P(h) = e^{-h}$. Proceeding as before we obtain, in analogy with (2.12), the expression

$$\rho \approx \int_0^\infty dh\, e^{-h-\ell e^{-h}}. \tag{2.14}$$

Here the integral is dominated by contributions around $h \sim \ln\ell$, and the saddle point integration results in $\rho \approx \sqrt{\pi/2}(e\ell)^{-1}$. With $h_a(t) = e^t = \ell\cot\theta$ we obtain, from (2.4),

$$N(h) \approx \sqrt{\frac{\pi}{2}}\frac{\cot\theta}{e} h^{-2}, \tag{2.15}$$

so in contrast to (2.13), here the height distribution exponent is $\gamma = 2$.

The important lesson to be learned is that, in deterministic competition processes, the properties of the emerging scale invariant structure depend not only on the dynamical rule (encoded e.g. in the exponent α in (2.9)), but also on the statistics of the random initial conditions; in that sense, there is less robustness (or universality) than in noisy processes. The reason can be traced to the fact that, in contrast to the noisy model discussed in Section 2.1, the survivors in the deterministic case are not *typical*; instead, they are recruited from the needles of largest initial height [25]. Consequently, the statistics of the active needle population at some given time t, which determines the further evolution of the structure, is related to the *extremal statistics* [28] of the initial height distribution $P(h)$, that is, the probability distribution of the *largest* initial height among $\ell(t)$ independent samples. The sensitivity of deterministic growth processes to the statistical properties of initial conditions has been noted before in various contexts [8, 29, 30], and will be a recurrent theme throughout this chapter.

2.2.2 Self-thinning in plant populations

Competition for sunlight is believed to play an important role in the dynamics of plant populations. Through a process referred to as *self-thinning*, larger plants cause increased mortality among smaller ones by depriving them of light. Empirically, this process is observed to proceed according to a universal scaling law relating the mean weight of survivors, m, to their number density per unit area ρ as [31]

$$m \sim \rho^{-3/2}. \tag{2.16}$$

If we plausibly assume that plant weight is related to plant height as $m \sim h^3$, we see that this implies the lateral distance between plants, $\xi = \rho^{-1/2}$, increasing proportional to h. In the traditional explanation of (2.16), ξ is identified with the crown diameter which, on dimensional grounds, is also assumed to scale as $m^{1/3}$, and therefore $\xi \sim h$. The weakness of this argument lies in the complicated allometry of real plants, i.e. in the fact that different linear size measures such as stem diameter, crown diameter, or height, empirically scale with different powers of plant weight [32].

It is therefore of some interest to attempt a *dynamical* explanation based on simple screening models of the kind discussed in the previous section. Following Nagatani [27], we consider a one-dimensional geometry, as in Figure 2, with sunlight streaming in from the right at a fixed angle θ. We further assume that shadowing is exclusive, i.e. fully shaded plants die instantaneously while those which still receive some light grow as if there were no shading at all.

As a first step in the modeling procedure, the growth dynamics of individual (non-interacting) plants has to be ascertained. There is empirical evidence [33] that the increase in plant height can be characterized by a (possibly time-dependent) relative growth rate r, such that

$$\frac{dh_i}{dt} = r(t) h_i. \tag{2.17}$$

The essential point is that the growth rate is proportional to the height; the time dependence of $r(t)$ can be eliminated through a redefinition of time, which reduces (2.17) to the deterministic Nagatani model, eq. (2.9), with $\alpha = 1$.

Next it has to be decided whether the competition process is noise-driven, i.e. due to random fluctuations of the growth rate r, or whether it is primarily deterministic and merely expresses the exponential amplification of randomness in the initial conditions (that is, the sizes of seedlings). In the first case the stochastic version of Nagatani's model described briefly in the previous section (model II of Meakin and Krug [25]) would provide an appropriate starting point. With $\alpha = 1$, eq. (2.8) gives $\gamma = 2$, which implies that the lateral distance between survivors scales as $\xi = 1/n \sim h$,

in agreement with the empirical law (2.16). If, on the other hand, the competition were mainly deterministic, the initial distribution of seedling heights would have to be known. Heuristically, one expects the distribution to be unbounded but rapidly decaying, such as a Gaussian or exponential distribution. For such distributions the calculation sketched in the previous section shows that, again, $\xi \sim h$, possibly with logarithmic corrections [25]. Thus, in this particular case, noisy and deterministic competition leads to similar results.

The relative success of these simple, one-dimensional models should not be over-interpreted; e.g. the relation $\xi \sim h$ is equivalent to the empirical rule (2.16) only if the conventional, and questionable [32], allometric relation $m \sim h^3$ is used. However they do show that the shadowing length ξ need not be related, as is traditionally done, to the allometry of individual plants (indeed, in the model no lateral length scale is associated with individual needles), but rather can emerge from the competitive *interaction* between individuals.

2.3 The shadow instability

In the ballistic deposition model described in Section 2.1, the deposition flux is assumed to be collimated and unidirectional. While this is a reasonable approximation in some situations, other growth processes such as sputter deposition are characterized by particle trajectories approaching the surface from a wide range of directions. It was first pointed out by Karunasiri, Bruinsma and Rudnick [34] (KBR) that this leads to a deterministic *shadow instability* in that valleys receive less flux than hills and are therefore left behind. Subsequent studies [35, 36, 37, 38, 39] have explored various aspects of the instability.

2.3.1 The grass model

A needle model for the shadow instability is illustrated in Figure 3. We focus on the simplest nontrivial case, neglecting both roughening through shot noise and smoothening by surface relaxation processes. The growth rate of the ith needle is given by [11]

$$\frac{dh_i}{dt} = V(\theta_i), \tag{2.18}$$

where the *exposure angle* θ_i, $0 \leq \theta_i \leq \pi$, describes the range of directions in which straight lines can be drawn from the tip of needle i without intersecting any of the other needles (Figure 3), and V is a monotonically increasing function with $V(0) = 0$. As in Section 2.2, the initial values $h_i(0)$ are drawn independently from a distribution $P(h)$.

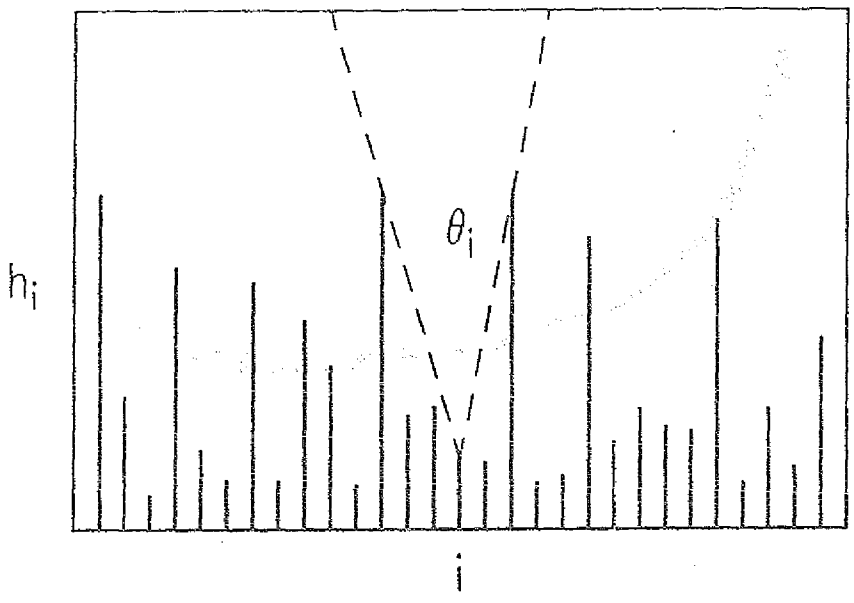

Figure 3: The grass model for the shadow instability.

Some insight into the competition process is gained from the distribution $P_t(\theta)$ of exposure angles at time t (Figure 4). As the growth progresses, the distribution becomes increasingly bimodal. The peak close to $\theta = 0$ contains needles which are essentially excluded from further growth, while the (diminishing) peak close to $\theta = \pi$ contains those which have not yet been subject to shadowing; only a small fraction of needles resides between the peaks. The structure of the distribution allows us to extend the distinction between active and shaded needles, developed in the unidirectional case, to the present, more involved situation in which no needle ever entirely ceases to grow. We *define* a surviving (*active*) needle through the condition $\theta_i(t) > \theta_{\rm th}$, for some arbitrary threshold angle $\theta_{\rm th}$, say, $\theta_{\rm th} = \pi/2$. The surviving fraction $\rho(t)$ can then be written as

$$\rho(t) = \int_{\theta_{\rm th}}^{\pi} d\theta \, P_t(\theta). \tag{2.19}$$

While the simple identity (2.4) between the surviving fraction and the density profile does not hold here, a similar, approximate relation can be derived as follows. Note first that averaging the equations of motion (2.18) over initial conditions yields

$$\int_0^{\pi} d\theta \, P_t(\theta) V(\theta) = \frac{d}{dt}\langle h \rangle = \frac{d}{dt}\int_0^{\infty} dh \, h N_t(h), \tag{2.20}$$

where a time index has been added to the height distribution $N(h)$ to express that we are considering the transient behavior. Using the definition (2.2) of the density profile and performing a partial integration, the right hand side of (2.20) can be

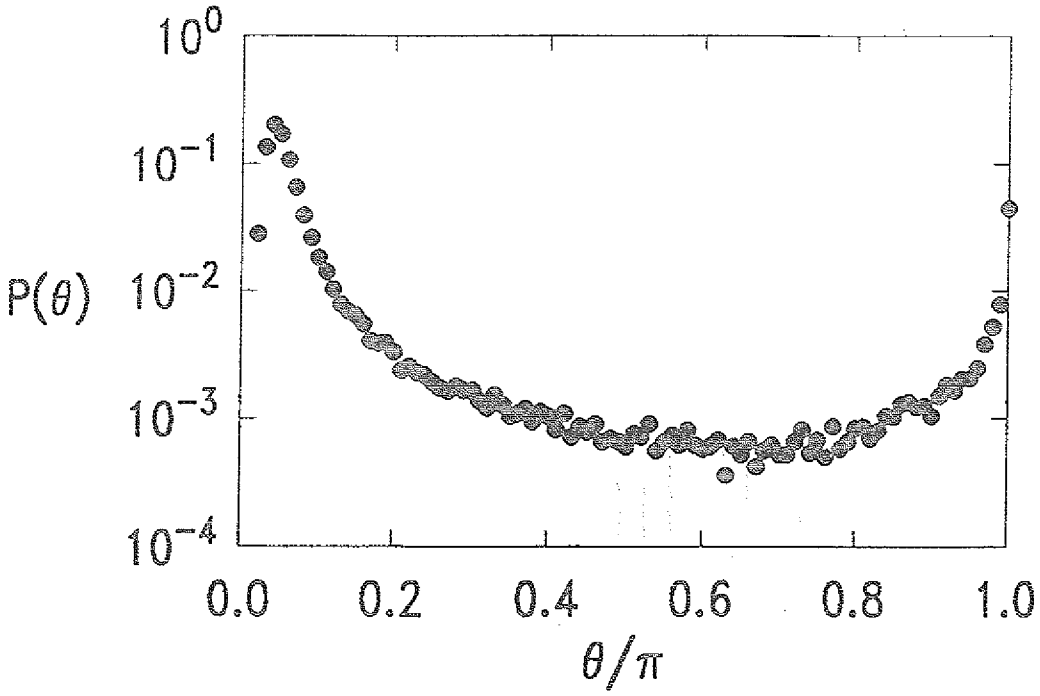

Figure 4: Distribution of exposure angles at time $t = 20$, from simulations using $V(\theta) = \theta$. The data constitute an average over 100 runs for a system of 500 needles. [11]

written as

$$\frac{d}{dt}\langle h\rangle = \frac{d}{dt}\int_0^{V(\pi)t} dh\, n_t(h) = V(\pi)n_t(V(\pi)t) + \int_0^{V(\pi)t} dh\, \frac{\partial n_t}{\partial t}, \tag{2.21}$$

introducing explicitly the maximal height $V(\pi)t$. On the other hand, from its definition (2.19) the surviving fraction can be bounded by

$$\rho(t) \leq \int_{\theta_{\rm th}}^{\pi} d\theta\, P_t(\theta)[V(\theta)/V(\theta_{\rm th})] \leq V(\theta_{\rm th})^{-1}\int_0^{\pi} d\theta\, P_t(\theta)V(\theta) \tag{2.22}$$

(recall that $V(\theta)$ is monotonic!). Inserting (2.20) and (2.21) we see that $\rho(t)$ is bounded by $[V(\pi)/V(\theta_{\rm th})]n(V(\pi)t)$ *provided* the term arising from the explicit time dependence of n_t in (2.21) can be neglected; as we shall see below, this is not always true. We will nevertheless assume a relation of the form

$$\rho(t) \sim n(h_a(t)), \tag{2.23}$$

with $h_a(t) \approx V(\pi)t$ the typical height of active needles, to relate the dynamics of competition to the frozen structure.

The analysis [11] focuses on the transfer of the needle population from the 'active' to the 'shaded' peak in Figure 4. We consider a late stage in the process, when the typical distance between active needles is $\xi \gg 1$. For the sake of simplicity we use a *periodic* array of active needles (Figure 5), with spacing ξ and alternating heights $h_1 = h_{\rm max} = V(\pi)t$ and $h_2 = h_1 - \Delta$, with $\Delta \ll \xi$; any effect from the shaded needles will be disregarded. In the course of time the shorter of the active needles

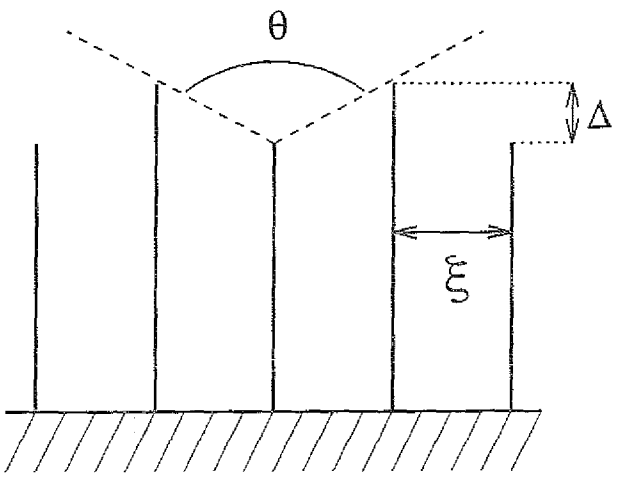

Figure 5: Periodic needle array used in the analysis of the shadowing model.

increasingly lag behind the longer ones and eventually join the shaded majority. For a quantitative description one introduces an exponent ν to characterize the behavior of $V(\theta)$ close to $\theta=\pi$, $V(\pi)-V(\theta)\sim(\pi-\theta)^\nu$ for $\theta\to\pi$. Elementary geometry then yields

$$\frac{d\Delta}{dt}=V(\pi)-V(\theta)\sim(\pi-\theta)^\nu\sim\left(\frac{\Delta}{\xi}\right)^\nu. \tag{2.24}$$

The solution of this equation is

$$\Delta(t)=[\Delta(0)^{1-\nu}+(1-\nu)t/\xi^\nu]^{1/(1-\nu)} \tag{2.25}$$

for $\nu\neq 1$ and $\Delta(t)=\Delta(0)e^{t/\xi}$ for $\nu=1$. As a measure for the time scale of shadowing we introduce t^* through $\Delta(t^*)=\xi$; in our simplified situation, the exposure angle of the shorter needles has decrased to $\theta(t^*)=\theta_{\rm th}=\pi/2$ at time t^*. From (2.25) we obtain

$$t^*=\frac{\xi}{1-\nu}\left[1-\left(\frac{\Delta(0)}{\xi}\right)^{1-\nu}\right] \tag{2.26}$$

for $\nu\neq 1$, and

$$t^*=\xi\ln[\xi/\Delta(0)] \tag{2.27}$$

for $\nu=1$. In the relevant limit $\Delta(0)/\xi\ll 1$, eq.(2.26) behaves as $t^*\sim\xi$ for $\nu<1$, and $t^*\sim\xi^\nu/\Delta(0)^{\nu-1}$ for $\nu>1$.

The origin of scale invariance in this class of competitive growth processes lies in the fact that the shadowing time t^* increases with ξ: Further shadowing is slowed down as active needles become scarce. This is analogous to the coarsening of a one-dimensional phase separating system, where the interaction between domain walls, providing the thermodynamic driving force for coarsening, decreases (exponentially) with increasing domain size; Langer's treatment of spinodal decomposition [40] is

in fact similar to the present approach in that it is based upon an estimate of the lifetime, t^*, of metastable periodic order parameter profiles, which decay via the disappearance of every second domain.

The analogy with coarsening gives an important clue on how to proceed: Since, in the simplified periodic configuration analyzed here, the active needle spacing doubles when the shorter needles are shaded, we may interpret $1/t^*$ as *the growth rate of the needle spacing* ξ, and write

$$\frac{d\xi}{dt} \sim \frac{\xi}{t^*(\xi)}. \tag{2.28}$$

In evaluating this relation we are faced with the problem that t^* depends, for $\nu \geq 1$, on the initial height difference $\Delta(0)$ as well as on the needle spacing. In the deterministic process considered here, $\Delta(0)$ generally acquires a ξ-dependence due to the fact that the active needles which survive up to a time t are those with the largest initial height in a region of size $\xi(t)$, see Section 2.2. The estimate of $\Delta(0)$ for a given distribution of initial values is an exercise in extremal statistics [11, 25, 28]. The result is a relation of the type

$$t^*(\xi) \sim \xi^z \tag{2.29}$$

where the *dynamic exponent* $z > 1$ depends, for $\nu > 1$, both on ν and on the initial distribution; e.g., for uniform, bounded initial distributions $z = 2\nu - 1$, while for unbounded, rapidly decaying distributions $z = \nu$ [11]. This is another instance of the lack of robust universality in deterministic growth processes alluded to previously. For $\nu = 1$ we always have $t^* \sim \xi \ln \xi$ and the initial distribution merely affects the prefactor.

Integrating (2.28) we obtain the *coarsening law*

$$\xi(t) \sim t^p, \tag{2.30}$$

where p takes the universal value $p = 1$ for $\nu < 1$ and $p = 1/z$ for $\nu > 1$. In the borderline case $\nu = 1$ (2.30) is replaced by

$$\xi(t) \sim t/\ln t. \tag{2.31}$$

The density of survivors is $\rho(t) \sim 1/\xi(t)$ and, using (2.23), we have

$$\gamma = 1 + p. \tag{2.32}$$

In particular, we obtain the universal result $\gamma = 2$ for $\nu \leq 1$, with a logarithmic correction,

$$N(h) \sim \frac{\ln h}{h^2} \tag{2.33}$$

for $\nu = 1$. These predictions are in excellent agreement with simulations carried out for a range of values of ν, $1/2 \leq \nu \leq 5$, and a variety of initial distributions [11].

2.3.2 Shaded needles

Two examples of numerically determined height distributions are shown in Figure 6. The graphs nicely illustrate the decomposition into a time-independent ('frozen') power law part and a peak at $h \approx h_a(t)$ which contains the active needles. However, Figure 6b indicates that this is not the whole story: A second peak is seen to develop and to move towards increasing height at a sublinear rate. This peak is associated with the dynamics of the *shaded* needles.

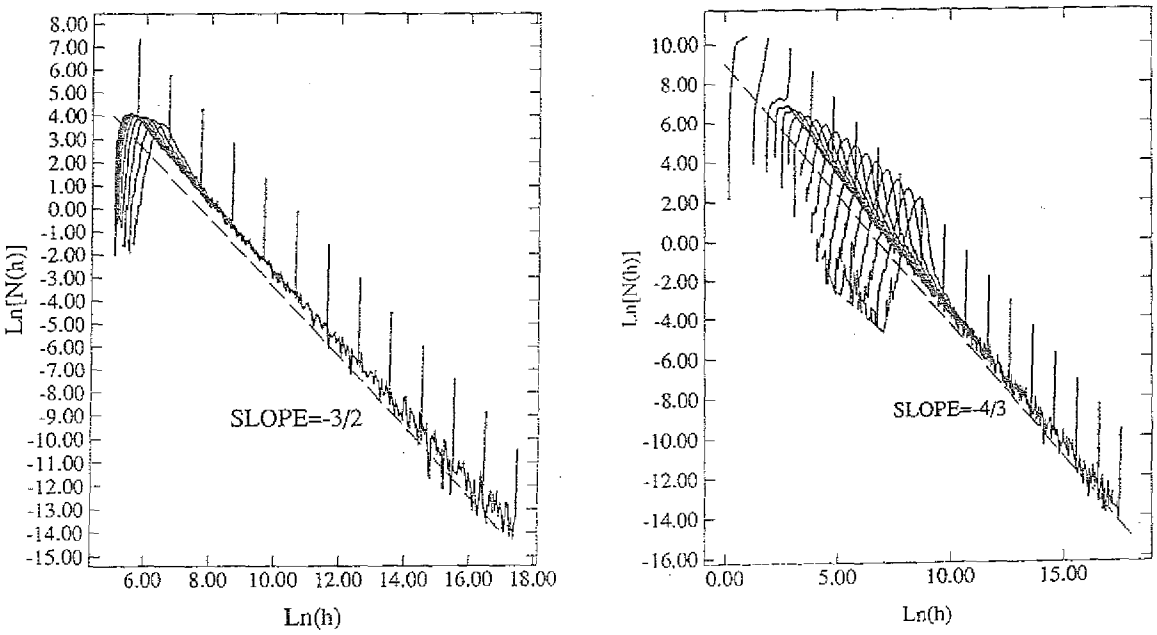

Figure 6: Height distributions of the needle model for shadowing, with growth rate function (a) $V(\theta) = \pi^{3/2} - (\pi - \theta)^{3/2}$ and (b) $V(\theta) = (1 - \cos\theta)^{3/8}$. In both cases the initial heights were drawn from a uniform distribution. The dashed lines indicate the theoretical predictions for the height distribution exponent γ.

Suppose that the growth rate behaves as $V(\theta) \sim \theta^\eta$ for $\theta \to 0$. We need to estimate the typical exposure angle, θ_s, characteristic of the shaded needles. An upper bound on θ_s is obtained by taking into account only the shadowing due to the highest, active needles; their spacing being ξ, we have $\theta_s \leq \xi / h_a(t) \sim \xi / t$, and hence the typical height $h_s(t)$ of the shaded needles evolves as

$$dh_s/dt = V(\theta_s) \leq (\xi/t)^\eta \sim t^{-\eta(1-p)}. \tag{2.34}$$

The height of the shaded needles remains bounded for all times if $\eta > 1/(1-p)$; in

general, however, we may only conclude that $h_s \sim t^\mu$ with

$$\mu \leq 1 - \eta(1-p) \leq 1. \tag{2.35}$$

Numerically, it appears [11] that this bound overestimates the value of μ, in particular in the case $p=1$ where the bound becomes trivial; this implies that considerable shadowing must go on also *within* the population of shaded needles. Nevertheless, in most cases μ is found to be positive, e.g. $\mu \approx 0.3$ when $V(\theta)=\theta$. Consequently, the $t \to \infty$ limit of the height distribution $N(h)$ is trivial for any fixed h, since for sufficiently long times *all* needles have grown beyond height h. Instead, the scaling behavior (2.1) is encountered in the scaling range $h_s(t) < h < h_a(t)$, as is clearly seen in Figure 6b. In other words, the typical form of the density profile is

$$n_t(h) \begin{cases} =1 & : \quad 0 \leq h \leq h_s(t) \sim t^\mu \\ \sim h^{-p} & : \quad h_s(t) \leq h \leq h_a(t) \sim t \\ =0 & : \quad h > h_a(t) \end{cases} \tag{2.36}$$

Note that there is a sharp drop in $n(h)$ at $h \sim h_s$, corresponding to the peak seen in $N(h)$ (Figure 6b).

To delineate the limits of consistency of our approach, we now use the approximate form (2.36) of the density profile to evaluate the right hand side of (2.21). We find two contributions to the averaged growth rate, one of the order $dh_s(t)/dt \sim t^{\mu-1}$ from the shaded needles and one of the order t^{-p} from the active ones. The fundamental assumption of our approach has been that the dynamics is *dominated* by the active needles. This requires $\mu < 1-p$; using the bound (2.35), a *sufficient* condition is

$$\eta > p/(1-p). \tag{2.37}$$

One can also derive this condition by evaluating the left hand side of (2.20) with the following simple Ansatz for the exposure angle distribution $P_t(\theta)$,

$$P_t(\theta) = (1-\rho(t))\delta(\theta - \theta_s(t)) + \rho(t)\delta(\theta - \pi). \tag{2.38}$$

Again, this gives rise to two competing contributions to the average growth rate, and with the bound $\theta_s \leq \xi/t$ the peak at $\theta = \pi$ is found to dominate if (2.37) is fulfilled. Surely, the condition (2.37) is too restrictive to be useful; e.g. it is only marginally satisfied in the case depicted in Figure 6a ($p=1/2$ and $\eta=1$), although in this case the shaded needles are seen to play no significant role.

2.3.3 The effect of noise

Consider adding random forces $f_i(t)$ on the right hand side of (2.18). The shadowing dynamical equation (2.24) then becomes

$$\frac{d\Delta}{dt} = \left(\frac{\Delta}{\xi}\right)^{\nu} + f(t) \tag{2.39}$$

where we take f to be Gaussian with zero mean and covariance

$$\langle f(t)f(t')\rangle = D\delta(t-t'). \tag{2.40}$$

The solution of this equation is straightforward in the linear case $\nu = 1$ (compare to Section 3.2.2). In a situation where initially all active needles have the same height, $\Delta(0) = 0$, the height difference grows according to

$$\langle \Delta(t)^2 \rangle = \frac{D\xi}{2}(e^{2t/\xi} - 1), \tag{2.41}$$

and the shadowing time, obtained by equating (2.41) to ξ^2, is

$$t^*(\xi) = (\xi/2)\ln(1 + 2\xi/D). \tag{2.42}$$

For large ξ this is of the form (2.27), with an effective initial height difference $\Delta(0)_{\text{eff}} \sim D$.

The comparison indicates how (2.39) may be approximately solved for arbitrary values of ν. Eq.(2.41) describes two distinct regimes. For $t \ll \xi/2$, the process is noise dominated and $\langle \Delta(t)^2 \rangle \approx Dt$, while for $t \gg \xi/2$ the deterministic term in (2.39) takes over. It is plausible that the succession of a noise-dominated early time regime and a late time regime dominated by deterministic shadowing should be a general feature of (2.39). We can therefore match the early time behavior, $\Delta(t) = \sqrt{Dt}$, to the deterministic solution (2.25), requiring continuity of Δ and $d\Delta/dt$ at the crossover time t_c; such an approach was first suggested by Rossi [41] in the context of Laplacian needle growth, see Section 2.4. The two conditions serve to fix t_c, as well as the initial condition $\Delta(0) = \Delta(0)_{\text{eff}}$ in (2.25), thereby selecting a particular trajectory from the one-parameter family of deterministic solutions. The result is

$$t_c = (1/2)(D/2)^{\frac{1-\nu}{1+\nu}} \xi^{\frac{2\nu}{1+\nu}} \tag{2.43}$$

and

$$\Delta(0)_{\text{eff}} = [(1+\nu)/2]^{1/(1-\nu)} (D/2)^{1/(1+\nu)} \xi^{\nu/(1+\nu)}. \tag{2.44}$$

The first important observation is that $\Delta(0)_{\text{eff}}/\xi \to 0$ for $\xi \to \infty$, for any value of ν. This implies that the prediction $p = 1$ in the universal regime $\nu < 1$ is unaffected

by the noise, since $t^*(\xi) = \xi/(1-\nu)$ for large ξ as before (eq.(2.26)). On the other hand, for $\nu > 1$, insertion of (2.44) into (2.26) yields the shadowing time

$$t^* = \frac{\nu+1}{\nu-1} t_c \sim \xi^{\frac{2\nu}{1+\nu}} \tag{2.45}$$

for large ξ. The coarsening exponent is

$$p = \frac{1+\nu}{2\nu} < 1. \tag{2.46}$$

Somewhat remarkably, the shadowing time in (2.45) is of the same order (though always greater than) the crossover time t_c from the noise-dominated regime, which might raise doubts concerning the consistency of the approach. Nevertheless, Rossi [41] found good agreement with (2.46) from an exact enumeration analysis of a discrete version of (2.39).

2.3.4 Beyond the needle model

We conclude this section by commenting on numerical work on the shadowing instability that includes fluctuations (due to the shot noise in the deposition flux) and surface tension effects. These studies have considered either discretized continuum equations, or lattice models in which particles are deposited ballistically from a range of directions. The most general continuum equation is of the form

$$\frac{\partial}{\partial t} h(x,t) = \sigma \nabla^2 h - \kappa \nabla^4 h + \frac{\lambda}{2} (\nabla h)^2 + \theta[h(x,t)] + f(x,t), \tag{2.47}$$

where $h(x,t)$ is the continuous version of the height variables $h_i(t)$, and the exposure angle θ is defined as before, in Figure 3, as a functional of the instantaneous surface configuration; it is assumed that the vertical local growth rate is proportional to the exposure angle, with a factor of proportionality (the deposition flux) that has been set to unity. The coefficients $\sigma, \kappa > 0$ are related to the surface tension; the σ-term describes surface relaxation due to evaporation-condensation processes, while the κ-term captures smoothening through surface diffusion, see Chapter 3. The $(\nabla h)^2$-nonlinearity was first proposed in the celebrated work of Kardar, Parisi and Zhang [14] (KPZ), and will be thoroughly discussed in Chapter 4. Finally, $f(x,t)$ is a Gaussian random force with short range correlations in space and time, and variance D (see eqs.(2.40) and (3.16)). The needle model discussed in the bulk of this section corresponds to the simplest case where $\sigma = \kappa = \lambda = D = 0$, and the linear appeareance of θ in (2.47) implies that one is dealing with the 'borderline' situation $\nu = 1$.

A serious deficiency of (2.47) lies in the fact that all coupling terms appearing in the equation are the result of a small gradient expansion (see Chapter 3), which is

clearly inappropriate in view of the large modulations caused by the shadow instability. A more satisfactory continuum description, in which the local normal growth rate is proportional to the normal projection of the incident flux, integrated over the exposure angle, was proposed by Bales and Zangwill [36]. The surface morphology generated by this model is quite different from that obtained with needle models and continuum equations of the type (2.47), which assume a single-valued height function at all times; in fact, the surface develops a structure of domed columns, separated by deep narrow grooves that occasionally close, due to the formation of overhangs, and leave chains of vacancies in the bulk. However, because of the high computational cost associated with the Bales-Zangwill model, it has not been possible so far to quantitatively study its scaling and coarsening properties.

In their original paper [34] on the shadow instability, KBR studied (2.47) with $\sigma = \lambda = D = 0$, i.e. the deterministic problem with surface diffusion relaxation. For small values of κ, $\kappa \leq 10^{-4}$, they found a power law density profile with an exponent $p = \gamma - 1$ *increasing* from $p \approx 1$ for $\kappa = 0$ to $p \approx 1.5$ for $\kappa = 10^{-4}$; for larger values of κ an abrupt transition, from compact growth with a flat interface to a spiky morphology, is observed at a critical height $h^* \sim \kappa^{1/3}$, but the spikes do not appear to have a power law height distribution. The result $p > 1$ is very surprising in view of our interpretation of p as a *coarsening* exponent, as in (2.30); indeed, $p > 1$ would correspond to superlinear coarsening, and it is hard to see how such a behavior could arise from a local coupling as in (2.47) (it is *not* due to the shadowing interaction because then it should appear also in the needle model). It is possible that KBR in fact observed the steep transition region between the constant plateau and the power law decay in the density profile (2.36), which may give rise to large, spurious values of p; another possibility is that the coupling by the κ-term enhances the growth of the shaded background of needles to such an extent that, at least for larger values of κ, the power law regime disappears altogether. Clearly this case requires further investigation.

Yao, Roland and Guo [37] considered (2.47) with $\kappa = 0$, $\sigma > 0$ and $\lambda \neq 0$. They found linear coarsening, $p = 1$, both in the presence and absence of noise. Apart from the logarithmic correction in (2.31), which may have been too weak to detect, this result agrees with our analysis of the needle model. On the other hand, a subsequent study of the case $\lambda = 0$, $\sigma > 0$, reported by Yao and Guo [38], resulted in a smaller coarsening exponent $p \approx 0.7$. The main contribution of Yao and Guo [38] was an extension of (2.47), with $\lambda = 0$ and $\sigma > 0$, to two-dimensional surfaces, where the coarsening was found to progress surprisingly slowly, with $p \approx 0.33$.

Lattice models for the shadow instability were introduced by Roland and Guo [37, 42] and by Tang and Liang [39]. The model of Roland and Guo is subject to the

solid-on-solid (SOS) constraint, i.e. overhangs and bulk vacancies are not allowed to form; surface sites are selected for deposition by launching particles towards the surface along randomly directed ballistic trajectories, but the success of the deposition attempt is decided by energetic considerations, thereby bringing surface tension and temperature into play. In contrast, the model of Tang and Liang is very close in spirit to standard ballistic deposition (Section 2.1), i.e. particles stick permanently at the site of first impact, and the deposit is highly defective. In both models the maximal exposure angle $\theta_{\max}$ is treated as a control parameter, and both models show evidence of a phase transition from a 'flat' phase at small $\theta_{\max}$, in which the surface roughens as predicted by KPZ-theory (see Chapter 4), to a grooved, columnar phase dominated by shadowing at large $\theta_{\max}$. However the scaling in the grooved phase is quite different in the two models. While Tang and Liang [39] find a column mass distribution exponent $\tau \approx 1.47$, consistent, via the relation (2.7), with the needle model prediction $\gamma = 2$, Roland and Guo [37, 42] report a coarsening exponent $p \approx 0.56$. These results suggest that the Tang/Liang model might be appropriately described by the continuum equation (2.47) with $\sigma > 0$ and $\lambda \neq 0$, while the Roland/Guo model corresponds, roughly, to the case $\lambda = 0$. It is obvious, however, that we are still far from a coherent picture of the various approaches to modeling the shadow instability, let alone an understanding of universality classes of possible asymptotic behaviors.

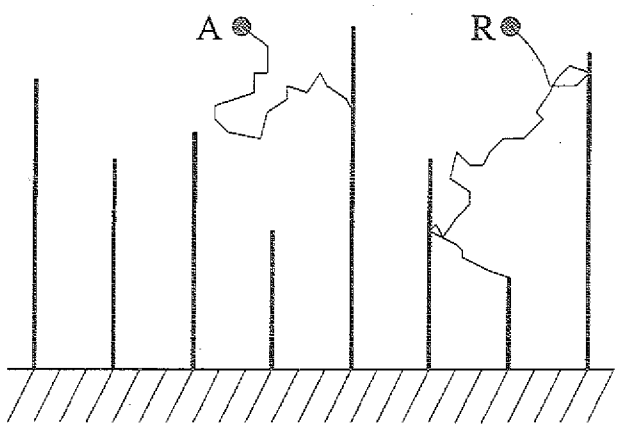

Figure 7: Illustration of the two versions of Laplacian needle growth. In model A, the random walker is absorbed at the sides of needles, while in model R it is reflected.

2.4 Laplacian needles

Diffusion-limited needle growth was considered independently by Meakin [43] and Rossi [41, 44] as a simplification of the notoriously difficult DLA problem. In this

model, needles grow perpendicular to a d-dimensional substrate plane by the accretion of individual random walkers. The walkers are released, one by one, from randomly chosen lateral positions at the height of the highest needle (Figure 7). Growth occurs only if the walker hits the tip of a needle. In the original version [41, 43, 44] of the model, walkers that hit the side of a needle are reflected. Here we shall also discuss a version [12] referred to as *model A*, in which walkers are *absorbed* at the sides of needles, this boundary condition being, as will be argued below, somewhat more faithful to DLA; the original version with *reflecting* boundary conditions then constitutes *model R*. A typical configuration generated by model A is shown in Figure 8. Since the positional probability distribution of the random walker satisfies the Laplace equation, with appropriate (absorbing or reflecting) boundary conditions at the sides of the needles, this model is a simple example of *Laplacian growth* [2, 3].

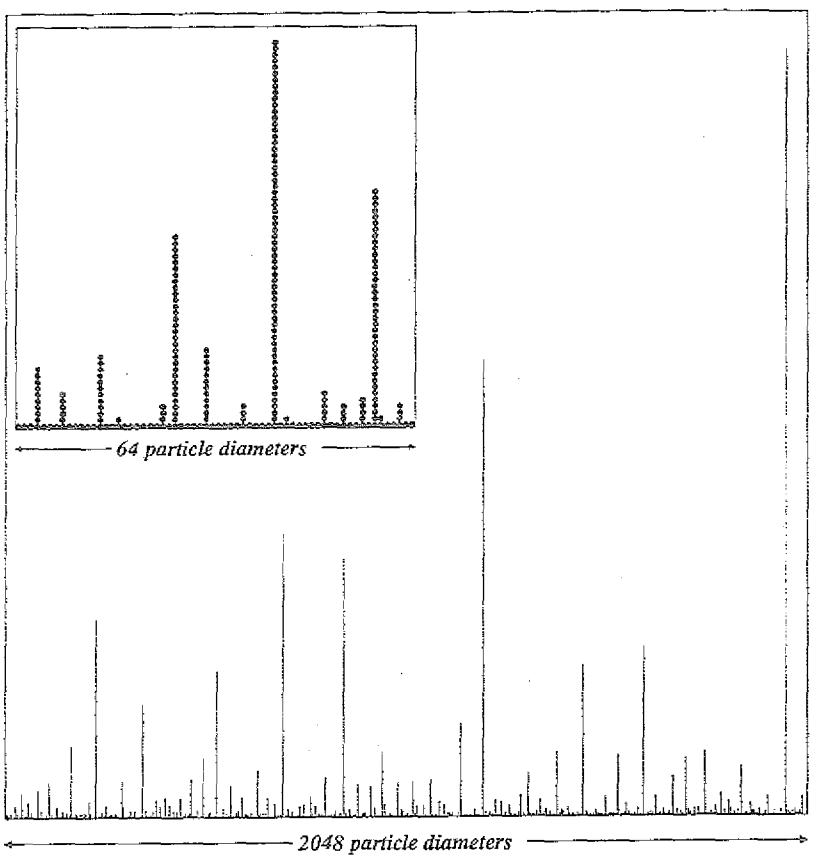

Figure 8: Needle forest generated in a two-dimensional off-lattice simulation of Laplacian growth, with absorbing boundary conditions at the sides of the needles. The forest consists of 20000 particles. The inset shows a magnification of the lower left corner. Courtesy of Thomas Rage.

Rossi [41] proposed to analyze the problem within a two-absorber approximation, which is closely analogous to the approach applied to the shadow instability in Section 2.3. He considered the initial stage of screening for a configuration of two needles in the plane (i.e. growth occurs from a line, $d=1$) with lateral spacing ξ and heights h_1 and $h_2 = h_1 - \Delta$, with $\Delta/\xi \ll 1$, and supplemented with periodic boundary conditions (see Figure 5). The quantity of interest is the probability $\mathcal{P}(\xi,\Delta)$ that the next walker to be launched onto this configuration is absorbed by the tallest needle, h_1. Rossi observes that, in the continuum limit where ξ and Δ are large compared to the lattice spacing (or particle size), the scale invariance of the Laplace equation implies that $\mathcal{P}$ should depend only on the ratio Δ/ξ and, since $\mathcal{P}(\xi,0) = 1/2$, one expects an expansion of the form

$$\mathcal{P}(\xi,\Delta) \approx \frac{1}{2}\left[1 + C\left(\frac{\Delta}{\xi}\right)^{\nu}\right] \tag{2.48}$$

for $\Delta/\xi \ll 1$. The rate at which the height difference Δ increases due to screening is proportional to $2\mathcal{P}-1$, and hence Δ satisfies an equation of the form (2.24), or rather, since the process is manifestly noisy, its stochastic counterpart (2.39). The analysis of Section 2.3 can then be taken over, and a prediction for the height distribution exponent γ (equivalently, the coarsening exponent p) follows in terms of the (unknown) exponent ν in (2.48). For example, under the plausible assumption that a walker launched at a random lateral position and height h_1 will invariably be absorbed at the needle tip that is closer to its starting point one has

$$\mathcal{P} = 1/2 + \Delta^2/2\xi^2, \tag{2.49}$$

so $\nu = 2$ and (2.46) would predict that $p = 3/4$, which is close to (but smaller than) the early numerical estimate [41, 43] $p \approx 0.83$. It is interesting to note that the value $p = 0.78 \pm 0.02$ was obtained numerically in a model of 'shortest-path' aggregation, for which (2.49) is exact [45].

Krug, Kassner, Meakin and Family [12] extended Rossi's analysis in two directions. First, they pointed out that, for model A in $d=1$, the probability $\mathcal{P}(\xi,\Delta)$ can be computed using the conformal mapping technique. The calculation, which will be sketched shortly, shows that in fact $\nu = 1$, and therefore the density profile is found (from (2.2) and (2.33)) to decay as

$$n(h) \sim \frac{\ln h}{h}, \tag{2.50}$$

see Figure 9; while the conformal mapping calculation applies only to model A, scaling arguments and numerical simulations [12] indicate that (2.50) holds for model R as well. Second, the breakdown of the two-absorber picture in high dimensions -

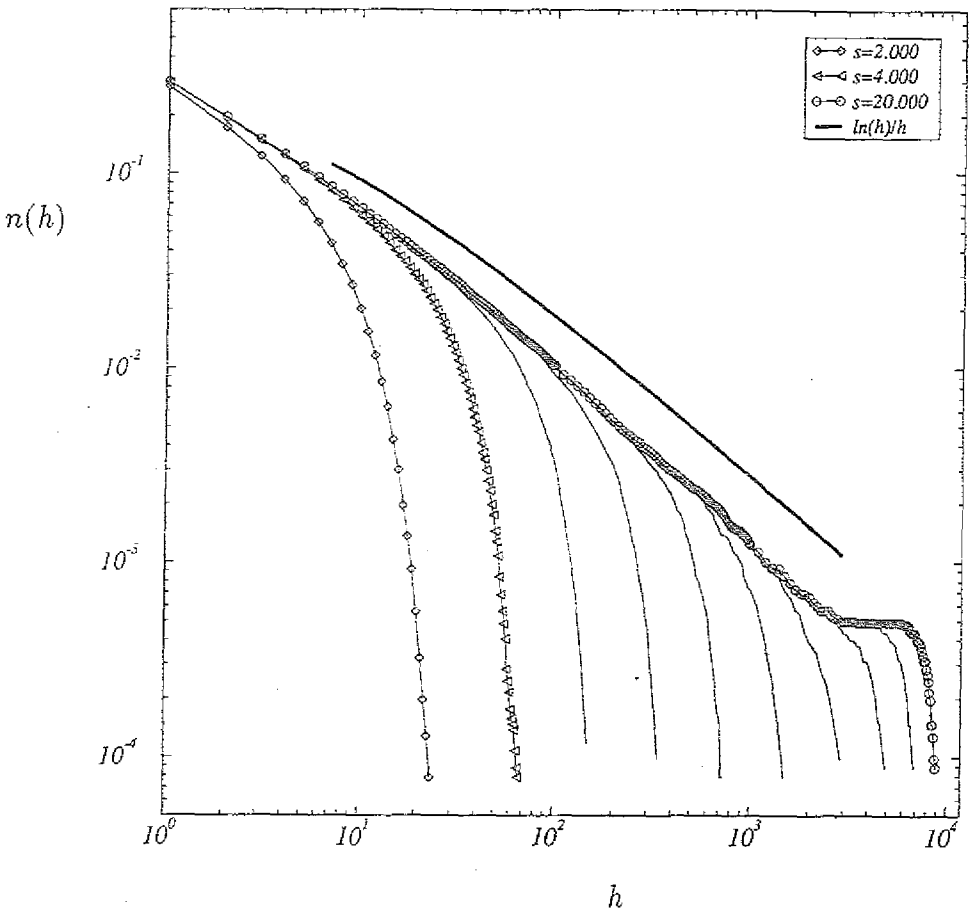

Figure 9: Density profiles obtained by averaging 50 independent off-lattice simulations of model A, in $d=1$. The figure shows a series of curves obtained at different stages of growth. At the latest stage, when 20000 particles (per run) have been deposited, the plateau in the density indicates that only a single needle remains. The bold line is the prediction (2.50). Courtesy of Thomas Rage.

more precisely, above an upper critical dimension d_c - was predicted. This breakdown is expected to occur because, in high dimensionalities, the needle deposit becomes increasingly transparent to the random walkers and the screening capacity of an individual needle becomes small. For $d \geq d_c$ screening is a *collective* effect involving many needles. This regime can be described by a continuum theory of mean field type [46, 47], which will be discussed in Section 2.4.3. Presently we focus on $d=1$, which is below d_c both for model R and A.

2.4.1 Caveats and preliminaries

Before taking a closer look at the conformal mapping approach, we should issue one word of caution. Even in the regime $d < d_c$, in which screening is dominated by

individual needles, it is far from clear that the two-absorber approximation captures the essence of the full problem. The tacit assumption of the approximation is that the screening interaction between the dominant, tallest needles can be isolated from the influence of the background of shorter needles that have been screened previously. In the shadowing model of Section 2.3 this assumption was, to some extent, justified by the observation that the needle population naturally decomposes into a group of 'shaded' and a group of 'active' individuals, as evidenced by the two peaks in the exposure angle distribution (Figure 4). In the Laplacian case there is no evidence that the distribution of growth probabilities has a similar, bimodal structure.

An impression of the dynamic significance of the background of 'screened' needles is gained by comparing the time evolution of the height distribution $N_t(h)$, as shown for model R e.g. in Figure 2 of Ref.[43], with the corresponding behavior in the shadowing model, Figure 6a. While in the latter case a clear distinction between the frozen bulk of the deposit, and a small subpopulation of active needles is seen to evolve, in the Laplacian model growth appears to occur simultaneously at all levels (all values of h), indicating that a considerable flux of random walkers penetrates the deposit far below the height of the tallest, 'active' needles. Model A seems to be better behaved in this respect - the time evolution of the density profile shown in Figure 9 indicates that the bulk of the deposit is essentially frozen once several particles per site have been deposited.

For a preliminary assessment of screening effects in the two versions of the Laplacian needle model, we consider the penetration of a random walker into a periodic needle array in $d=1$ lateral dimensions. Let the needle spacing be ξ, and denote by $P_\xi(r)$ the probability that a walker released at the height of the needle tips penetrates at least a distance r into the deposit before being absorbed. For model A, we can invoke the well-known electrostatic analogy [48], which replaces the needles with grounded conductors and relates the density of random walkers to the electrostatic potential, to conclude that the penetration probability (and therefore the growth rate of a screened needle) decays exponentially,

$$P_\xi(r) \sim e^{-\pi r/\xi} \text{ (model A).} \tag{2.51}$$

For model R absorption can occur only when the walker returns to the plane $r=0$ (the height of the needle tips). We can analyze the vertical motion using standard results for (discrete) one-dimensional random walks in the presence of a single weak absorber at the origin. The tail of $P_\xi(r)$ is dominated by walkers that return to the origin many times. Asymptotically for long walks the lateral positions of the walker at subsequent returns are uncorrelated, hence the absorption probability per return is $p_a \approx 1/\xi$ ($p_a \sim 1/\xi^d$ in d lateral dimensions). The probability for a walk of length t to return exactly n times is [49] $2^{n-t}(t-n)!/[(t/2)!(t/2-n)!]$, and consequently the

survival probability in the presence of an absorber of strength p_a can be estimated as

$$\psi(t) = \sum_{n=0}^{t/2} (1-p_a)^n 2^{n-t} \frac{(t-n)!}{(t/2)!(t/2-n)!} \approx$$

$$\sqrt{2/\pi} t^{-1/2} \int_0^\infty dn (1-p_a)^n e^{-n^2/2t} \approx \sqrt{2/\pi} t^{-1/2} p_a^{-1}. \tag{2.52}$$

Since the maximal vertical displacement of a walk of length t is $r \sim t^{1/2}$, we can rewrite this as

$$P_\xi(r) \sim \xi/r \quad \text{(model R)} \tag{2.53}$$

in $d=1$, and $P_\xi(r) \sim \xi^d/r$ in general.

We see that the screening capacity of a periodic array of needles is dramatically different in the two models. In particular, only model A features exponentially small growth probabilities in deep fjords, which presumably is an important property of DLA. This is why we expect the needle model A to be more closely related to the full DLA problem; we will return to this point in Section 2.4.4.

Using (2.51) together with the predicted density profile (2.50), we can also give a rough estimate of the growth probabilities in the screened bulk of the model A needle forest. Let us assume, in the spirit of the two-absorber approach, that we can identify a set of 'active' needles of reasonably uniform height $h_a(t)$ and spacing $\xi(h_a) = 1/n(h_a) \approx c h_a / \ln h_a$, with some constant c. Suppose now that we want to probe the growth probability at some height $h = \alpha h_a$, $0 < \alpha < 1$. Under the (admittedly questionable) hypothesis that the screening is dominated by active needles at any height h, we can estimate the growth probability $P_G(h)$ from (2.51), with $r = h_a - h$. The result is of the form

$$P_G(h) \sim h_a^{-\pi(1-\alpha)/c}. \tag{2.54}$$

The growth probability decays as a power law with the 'deposit thickness' h_a, but with a *height-dependent exponent*. In DLA, the dependence of the smallest growth probability on the cluster size has been a hotly debated issue for some time, and functional relations ranging from stretched exponentials to power laws have been proposed [50, 51]. Here, we have a simple but nontrivial prediction, which should be accessible to numerical verification.

For a comparison with the shadowing model we may identify $P_\xi(r)$ with the growth rate $V(\theta)$, and ξ/r (or, in d dimensions, ξ^d/r) with the exposure angle θ. Our considerations then show that model A corresponds to a shadowing model with $V(\theta) \sim e^{-1/\theta}$ for $\theta \to 0$ ($\eta = \infty$ in the notation of Section 2.3.2), while model R corresponds to the standard case $V(\theta) \sim \theta$, $\theta \to 0$ ($\eta = 1$). We have seen in Section 2.3.2 that the two-absorber approximation - equivalently, in the shadowing model,

the sharp distinction between active and shaded needles - becomes more accurate for large values of η (see e.g. eq.(2.37)). Thus, it is no surprise that the assumption of a frozen background of shaded needles is more closely realized for model A, as displayed in Figure 9, than for model R.

2.4.2 Conformal mappings

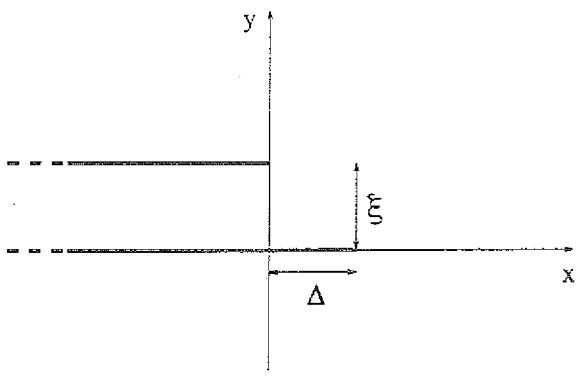

Figure 10: Sketch of the complex z-plane. The bold lines indicate the image of the real axis of the ζ-plane under the mapping (2.55).

The analytic transformation [52]

$$z(\zeta) = -\frac{\xi}{\pi k}\left(\frac{\zeta^2}{2} + (1-k)\zeta - k\mathrm{Log}\zeta - k + \frac{1}{2}\right), \tag{2.55}$$

$z, \zeta \in \mathbb{C}$, maps the real axis of the ζ-plane onto a pair of semiinfinite needles that lie parallel to the real axis of the z-plane (Figure 10). To see this, we evaluate (2.55) for real ζ, noting that $\mathrm{Log}\zeta = \ln\zeta$ for $\zeta > 0$ and $\mathrm{Log}\zeta = \ln|\zeta| + i\pi$ for $\zeta < 0$. With $z = x + iy$ it follows that $y = \mathrm{Im}\zeta = 0$ for $\zeta > 0$ and $y = \xi$ for $\zeta < 0$. Thus, the positive real axis maps onto a needle that lies on the real axis of the z-plane, and the negative real axis maps onto a needle that runs parallel to the real axis, at a distance $y = \xi$. The real part $x(\zeta)$ has two maxima, at $\zeta = -1$ and $\zeta = k$, where $x(-1) = 0$ and

$$\Delta \equiv x(k) = \frac{\xi}{\pi}\left(\frac{k}{2} + \ln k - \frac{1}{2k}\right), \tag{2.56}$$

respectively. The maxima correspond to the needle tips, and the parameter k determines the height difference Δ or, rather, the ratio Δ/ξ. In the relevant limit $\Delta/\xi \ll 1$, (2.56) can be inverted as

$$k \approx 1 + (\pi/2)\Delta/\xi. \tag{2.57}$$

To compute the electrostatic potential close to the tips, we expand (2.55) to second order around $\zeta = -1$ and $\zeta = k$, obtaining

$$z(\zeta) \approx i\xi - \frac{\xi}{2\pi k}(1+k)(\zeta+1)^2, \ \zeta \to -1$$

$$z(\zeta) \approx \Delta - \frac{\xi}{2\pi k^2}(1+k)(\zeta-k)^2, \ \zeta \to k. \tag{2.58}$$

In the ζ-plane, the electrostatic potential is simply $\phi = \mathrm{Im}\zeta$. Setting $\zeta = \zeta_0 + i\phi$ in (2.58), with $\zeta_0 = -1$ and k, respectively, and solving for ϕ we find

$$\phi(x, y=\xi) \approx \sqrt{\left(\frac{2\pi k}{1+k}\right)\frac{x}{\xi}}, \ x \to 0$$

$$\phi(x, y=0) \approx \sqrt{\left(\frac{2\pi k^2}{1+k}\right)\frac{x-\Delta}{\xi}}, \ x \to \Delta. \tag{2.59}$$

The behavior of the potential near the tips gives rise to the familiar square root divergence of the electric field. Here we are interested in the *ratio* of the fields at the two tips, which equals the ratio of the fluxes of random walkers onto the two needles. From (2.59) we have the simple result

$$E_1/E_2 = \sqrt{k} \tag{2.60}$$

with E_1 (E_2) denoting the field at the taller (shorter) needle, and hence the fundamental quantity $\mathcal{P}(\Delta, \xi)$ of the two-absorber approximation is given by

$$\mathcal{P}(\Delta, \xi) = \frac{E_1}{E_1 + E_2} = \frac{\sqrt{k}}{1+\sqrt{k}} \approx \frac{1}{2}\left(1 + \frac{\pi\Delta}{8\xi}\right), \tag{2.61}$$

which confirms the expansion (2.48) and proves that $\nu = 1$, at least for this particular configuration of absorbers.

It is also of interest to consider variants of model A in which all walkers that are absorbed on the sides of the needles contribute to the growth [18]. In that case the electrostatic quantity that determines $\mathcal{P}(\Delta, \xi)$ is the normal electric field - that is, the flux of random walkers - *integrated* over the sides of the needles. For the two-needle configuration considered here, it only makes sense to integrate over the inner sides of the needles, since the outer sides are not subject to screening. It is immediately clear from the definition of the mapping that the ratio of the integrated fluxes is simply k, so

$$\mathcal{P}(\Delta, \xi) = \frac{k}{1+k} \approx \frac{1}{2}\left(1 + \frac{\pi\Delta}{4\xi}\right) \tag{2.62}$$

and $\nu = 1$ as before.

While the mapping (2.55) has the virtue of being simple to analyze, the collective screening effects of the full needle forest are more faithfully represented by a *periodic* needle array, with spacing ξ and alternating heights h_1 and $h_2 = h_1 - \Delta$ (see Figure 5). A conformal mapping that allows one to compute the electrostatic potential around such an array was presented and analyzed in Ref.[12]. The results are equivalent to those derived here: $\mathcal{P}(\Delta,\xi)$ behaves as in (2.48), with $\nu = 1$, and $C = \pi/4$ when only the flux onto the needle tips is considered, and $C = 1$ in the case of the integrated flux.

2.4.3 High dimensionality behavior and mean field theory

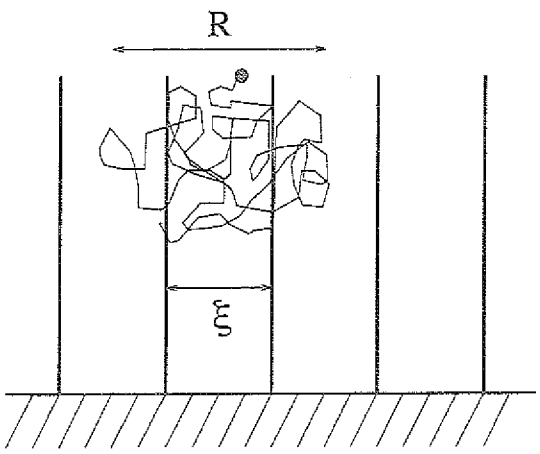

Figure 11: A 'ghost' walker released into a periodic needle array.

We now generalize the discussion of a single random walker penetrating into a periodic needle array to d-dimensional substrates. Our objective is to estimate the distance, R_a, that the walker is able to venture into the forest before being absorbed, in terms of the needle spacing ξ. We have already seen that $R_a \sim \xi$ for both models in $d = 1$ (eqs.(2.51) and (2.53)). Moreover, the estimate of the penetration probability $P_\xi(r) \sim \xi^d/r$ for the d-dimensional model R, derived after eq.(2.53), allows us to determine R_a from (say) $P_\xi(R_a) = 1/2$, hence

$$R_a \sim \xi^d \text{ (model R).} \tag{2.63}$$

For model A we employ an opacity argument [12]. In the $d+1$-dimensional space, the sites visited by a random walk of length t form a cloud of radius $R \sim t^{1/2}$ and density $\rho_w \sim t/R^{d+1} \sim R^{1-d}$ (Figure 11). When this cloud is placed inside the needle forest, the number of absorbing sites N_a within the cloud is $N_a \sim R(R/\xi)^d$. In order to have at least one absorption event we require $\rho_w N_a \approx 1$, or $R \sim R_a$ with

$$R_a \sim \xi^{d/2} \text{ (model A, } d > 1). \tag{2.64}$$

These estimates immediately provide us with bounds on the height distribution exponent γ. Note first that a density profile $n(h) \sim h^{-(\gamma-1)}$ implies that the spacing between needles increases with h as $\xi \sim h^p$ with

$$p = (\gamma - 1)/d \tag{2.65}$$

(this is the d-dimensional version of (2.32)). The absorption length for a needle forest of height h therefore scales as $R_a \sim h^{\gamma-1}$ for model R, and as $R_a \sim h^{(\gamma-1)/2}$ for model A. Consistency clearly requires that $R_a \leq h$: Otherwise, the walkers would be able to reach the substrate and fill up the deposit until the inequality is restored. We conclude

$$\begin{aligned} &\gamma \leq 2 \ \text{(model R)} \\ &\gamma \leq 3 \ \text{(model A)}. \end{aligned} \tag{2.66}$$

Next, we observe that the estimates (2.63) and (2.64) imply a qualitative change in the screening behavior at an *upper critical dimensionality* $d_c = 2$ for model R, and $d_c = 3$ for model A, in the sense that $R_a \gg \xi$ for $d \geq d_c$. In this high dimensionality regime the random walker effectively averages over many needles before being absorbed, and the two-absorber approximation is clearly inappropriate. Instead, one may attempt a continuum description, in which the lateral structure is ignored and the needle forest is represented by a continuous density function $n(h,t)$. Likewise, the density of walkers is given by a function $u(h,t)$, and the two are coupled through the equations of motion

$$\frac{\partial n}{\partial t} = \sigma_R \rho_{tip} u = -\sigma_R \frac{\partial n}{\partial h} u \tag{2.67}$$

$$\frac{\partial u}{\partial t} = \frac{\partial^2 u}{\partial h^2} - \left[\sigma_A n - \sigma_R \frac{\partial n}{\partial h} \right] u. \tag{2.68}$$

Equation (2.67) describes the growth by accretion of walkers at the needle tips, and we have used the fact that the tip density is $\rho_{tip} = -\partial n / \partial h$ [44]; σ_R is an absorption coefficient. Equation (2.68) is a balance equation for the walker density. The absorption term has two parts, one describing the absorption at the sides of needles, which occurs only in model A (model R has $\sigma_A = 0$), and the other accounting for the loss of walkers due to needle growth (this part is the negative of the right hand side of (2.67)). These 'mean field' equations, with $\sigma_A = 0$, were first written down by Cates [46], and further analyzed by Kassner [47].

To extract the essence of these equations, we make a scaling ansatz for the needle density as

$$n(h,t) = h^{-(\gamma-1)} f(h/t^{\kappa}). \tag{2.69}$$

Inserting this into (2.67) we find that the walker density must be of the form

$$u(h,t) = t^{-(1-\kappa)}\, g(h/t^{\kappa}). \tag{2.70}$$

The exponent γ can now be determined by inserting (2.69) and (2.70) into (2.68) and balancing the diffusion and the absorption terms on the right hand side. With $\sigma_A = 0$, this results in [46, 47]

$$\gamma_{MF} = 2 \text{ (model R)}. \tag{2.71}$$

Clearly if $\sigma_A > 0$, the absorption on the sides of the needles dominates that at the tips, and the $\partial n/\partial h$-term on the right hand side of (2.68) can be neglected. Therefore

$$\gamma_{MF} = 3 \text{ (model A)}. \tag{2.72}$$

The mean field exponents saturate the bounds (2.66), as was already noted by Cates [46] for model R.

To fix the dynamic exponent κ we need to invoke the left hand side of (2.68). Not surprisingly, one obtains $\kappa = 1/2$, corresponding to the *diffusive* advancement of the deposit thickness, $h_a(t) \sim t^{1/2}$. Of course, these values for γ and κ only provide *necessary* conditions for scaling solutions of the form (2.69) and (2.70); to actually establish their existence, it must be shown that the resulting equations for the scaling functions f and g admit solutions with physically reasonable behavior. Kassner's detailed analysis [47] shows that all scaling solutions have the property that the walker density u vanishes for $h \to \infty$. Indeed, Cates [46] had noted that the scaling forms (2.69,2.70) do not admit constant flux boundary conditions, $\partial u/\partial h = const.$ for $h \to \infty$; such a boundary condition requires that the scaling variable h/t^{κ} be replaced by $h/e^{\lambda t}$, i.e. the deposit thickness grows exponentially with time, as is obvious from mass balance considerations.

In summary, we have arrived at the following picture for Laplacian needle growth from d-dimensional substrates. In *low dimensionalities*, $d < d_c$, screening is dominated by individual needles and a two-absorber approximation in the spirit of Rossi [41, 44] should be applicable. For model A in $d = 1$, the two-absorber approach was put on a firm basis using the conformal mapping technique; thus we showed that $\nu = 1$ in (2.48), and hence the density profile behaves as (2.50). There is considerable numerical, and some analytic evidence [12] that these results extend to model R in $d = 1$. In *high dimensionalities*, $d \geq d_c$, we expect the mean field equations (2.67,2.68) to provide a reasonable description. This is confirmed by simulations of Rossi [41], who found that $\gamma = \gamma_{MF} = 2$ for model R, both in $d = 2$ and $d = 3$. For model A, $d_c = 3$, so the case $d = 2$ (growth from a plane) should still be in the low dimensionality regime covered by the two-absorber approach. It has been conjectured

[12] that $\nu = 2$ in this case, which would imply, according to (2.46), a coarsening exponent $p = 3/4$ and hence, from (2.65), $\gamma = 5/2$. This prediction, as well as the prediction $\gamma = \gamma_{MF} = 3$ for model A in $d \geq 3$, still has to be verified by numerical simulations. Here, we merely remark an interesting consequence if indeed $\gamma > 2$ in $d \geq 1$: The fact that the average needle height remains bounded (the density profile (2.2) being integrable) even if an infinite amount of mass is added to the deposit; almost all the mass is absorbed on the sides of the needles where it does not contribute to the growth. This scenario is not possible for model R, where all absorbed walkers eventually contribute to the mass of the deposit, as is reflected in the bound (2.66) as well as in the mean field exponent (2.71) which corresponds to a (marginally) nonintegrable density profile.

2.4.4 The relation to DLA

Graff and Sander [18] recently put forward an interesting suggestion on how to relate the behavior of needle models to the full DLA problem, more precisely, to the problem of diffusion-limited deposition onto a d-dimensional substrate. They consider the following modification of the Laplacian model A: In addition to its height h_i, a mass m_i is associated with each needle. While the mass increases in proportion to the *total* flux of random walkers absorbed on the sides as well as on the tip of the needle, the height grows as

$$\frac{dh_i}{dt} = h_i^{-(D_b-1)} \frac{dm_i}{dt}. \tag{2.73}$$

This relation is motivated by viewing each needle as a DLA-branch of fractal dimension $D_b > 1$, such that its mass scales with its height as $m_i \sim h_i^{D_b}$.

From simulations of this model Graff and Sander estimate that the height distribution exponent $\gamma \approx 1.7$ in $d = 1$ (choosing the DLA-value $D_b = 1.7$ [3]), however they remark that, if the needle model were to correctly represent the branch distribution of diffusion limited deposition, one should have

$$\gamma = 1 + d \tag{2.74}$$

asymptotically for d-dimensional substrates. Indeed, under the assumption of the diffusion-limited deposit being an isotropic fractal, it follows that the typical distance $\xi(h)$ of branches increases proportional to h, hence their number density decays as $n(h) \sim h^{-d}$.

A bound on γ can be obtained from mass balance considerations. Assuming a power law needle density profile (2.2) which is cut off at some maximal needle height h_a, we can estimate the average mass of a needle as

$$\langle m \rangle = \int_0^{h_a} dh h^{D_b} N(h) \sim h_a^{D_b - \gamma + 1}. \tag{2.75}$$

Since $\langle m \rangle$ grows in proportion to the number of walkers added to the structure, h_a has to be an increasing function of $\langle m \rangle$. This gives the bound

$$\gamma \leq D_b + 1. \tag{2.76}$$

When combined with the relation (2.74) appropriate for an isotropic fractal, (2.76) reduces to the celebrated 'causality bound' $D_b > d$ for the fractal dimension of DLA [53] (recall that d is the *substrate* dimension, so the space dimension is $d+1$).

We will now argue that the conjectured relation (2.74) cannot hold beyond the upper critical dimensionality $d_c = 3$ of model A. Indeed, in our estimates of d_c we used only the capability of a periodic needle array to *absorb* random walkers; the growth mechanism did not enter. Since the absorption properties of the Graff-Sander model are indistinguishable from those of model A, we conclude that $d_c = 3$ also for the former. Similarly, the bound (2.66) for model A must hold for the Graff-Sander model as well, which rules out (2.74) for $d \geq 3$. This is not hard to understand: In high dimensions, the opacity of the needle forest is insufficient to mimick the properties of a full DLA deposit.

The close similarity between the Graff-Sander model and model A is highlighted by considering the case $d = 1$, where we can invoke the two-absorber approach. Let $F_{1,2} = dm_{1,2}/dt$ denote the total fluxes onto the two needles, which have heights $h_{1,2}$, $h_2 = h_1 - \Delta$, and lateral spacing ξ (Figure 5). From the conformal mapping calculations we know that $(F_1 - F_2)/(F_1 + F_2) \sim \Delta/\xi$ for $\Delta/\xi \ll 1$. Keeping the total flux $F_1 + F_2$ fixed, we have

$$d\Delta/dt \approx F_1 h_1^{-(D_b-1)} - F_2 h_2^{-(D_b-1)}, \tag{2.77}$$

which becomes, in the relevant limit $\Delta \ll \xi \ll h_1$,

$$d\Delta/dt \approx h_1^{-(D_b-1)}(\Delta/\xi). \tag{2.78}$$

At constant flux (2.73) implies that $dh/dt \sim h^{-(D_b-1)}$, so that (2.78) can be rewritten as

$$d\Delta/dh \approx \Delta/\xi \tag{2.79}$$

which is the precise equivalent of (2.24), with $\nu = 1$. Adding noise, as in (2.39), then leads to the same density profile (2.50) as before.

To discuss the high dimensionality regime we adapt the mean field equations for model A to the Graff-Sander growth rule through a simple modification of the growth term in (2.67). The increase in density at height h is due to the growth of needles of height h, whose number is proportional to the tip density $-\partial n/\partial h$; the flux onto these needles is proportional to the random walker density u, integrated

up to height h. Thus

$$\frac{\partial n}{\partial t} = -\sigma_{GS} h^{-(D_b-1)} \frac{\partial n}{\partial h} \int_0^h dy\, u(y,t) \tag{2.80}$$

replaces (2.67). Assuming a scaling form (2.69) for $n(h,t)$, it follows that the walker density satisfies

$$u(h,t) = t^{\kappa(D_b-1)-1} g(h/t^{\kappa}) \tag{2.81}$$

instead of (2.70). However since the height distribution exponent γ is determined only by the balance between the absorption and diffusion terms on the right hand side of (2.68), which are the same as in model A, the mean field value of γ is still given by (2.72), $\gamma = 3$. This *violates*, for $D_b < 2$, the mass balance bound (2.76), indicating that the present formulation of the mean field theory is, in some way, deficient.

Graff and Sander [18] have argued that, in order to at least include density correlations *along* an individual needle, the σ_A-absorption term in (2.68) should be replaced by a term of the form

$$-u n_{\text{eff}} = u \int_h^{\infty} dy\, (\partial n/\partial y) \sigma(h,y) \tag{2.82}$$

where σ represents the absorption strength that a needle of height $y > h$ contributes at height h. Due to self-screening along a needle, tall needles contribute less to the total absorption. More precisely, a simple conformal mapping calculation shows that the flux of random walkers that hits a needle of height y at the vertical position $h < y$ is

$$F \approx h/\sqrt{y^2 - h^2}. \tag{2.83}$$

For $h \ll y$ this behaves as $F \approx h/y$. Since obviously $\sigma = \sigma_{GS} = const.$ at $y = h$, it is plausible to set $\sigma = \sigma_{GS}(h/y)$. Inserting the scaling from (2.69) for the density, we find that $n_{\text{eff}} \sim n \sim h^{-(\gamma-1)}$, and hence the effective absorption strength is of the same order as in the conventional mean field ansatz (2.68) for model A, indicating that the modification (2.82) does not alter the result $\gamma_{MF} = 3$. Here we differ from Graff and Sander, who claim that $\gamma_{MF} = 2$ for their model; at any rate, these considerations are somewhat academic, since they only apply in $d = 1$ (remember that (2.83) is the result of a conformal mapping calculation!) where the mean field approach is inappropriate anyway.

While several aspects of the Graff-Sander model require further clarification, it appears safe to conclude that a straightforward, quantitative relationship between the Laplacian needle models and DLA, as envisioned by Graff and Sander [18], is unlikely to exist. The two problems are fundamentally different in that the needle models possess, due to the effective transparency of needle forests in high dimensionalities, an upper critical dimension, while DLA does not [48]. On the other

hand, the two-absorber approach with its emphasis on the binary competition between branches of comparable height (or mass) provides an appealing picture of the elementary screening process, which should be applicable to DLA as well. We may note in this context that Halsey and Leibig [54] and Halsey [55] have recently presented a quantitative, predictive theory of DLA built precisely on an analysis of the elementary process of binary branch competition.

3. Fundamentals of kinetic roughening

Kinetic roughening phenomena are encountered whenever an interface is set into motion in the presence of fluctuations, be it of thermal, kinetic, or chaotic origin, or due to quenched disorder. The earliest theoretical investigations of surface roughness in growth processes [56, 57, 58] were concerned with the Eden model [59], originally proposed to describe the shape of cell colonies, and [60] with the ballistic deposition model introduced in the previous chapter. Following the progress in understanding the *universal* aspects of these processes which was achieved through the seminal work of Kardar, Parisi and Zhang [14] (KPZ) in 1986, a wide variety of more or less exotic instances of kinetic roughening have been suggested and experimentally investigated. Vicsek, Cserzö and Horváth [61], realizing the original intent of Eden's work, studied the roughening edge of a growing bacterial colony; several groups investigated the roughening of a stable two-fluid interface in a porous medium [62, 63]; and Zhang, Zhang, Alstrom and Levinsen [64] considered the roughening edge of a sheet of paper as it is consumed by fire. Curiously, while all of these experiments were motivated by the KPZ theory, none of them was able to quantitatively confirm its predictions. The discrepancy between theory and experiment has spurred considerable theoretical activity involving modifications of the KPZ theory through the introduction of e.g. correlated [65], non-Gaussian [66, 67] and quenched noise [68, 69]; a review of these developments has been given by Halpin-Healy and Zhang [10].

Here, we shall adopt a somewhat conservative point of view, and introduce the basic concepts of kinetic roughening within the 'classic' context of a moving interface separating two isotropic thermodynamic phases. The reader with some background in statistical mechanics may visualize, for concreteness, an Ising model below its critical temperature, with an interface separating domains of positive and negative magnetization, and subject to an external magnetic field that favors one of the phases, thereby setting the interface into motion (strictly speaking, the permanence of a well-defined interface in such a situation requires a careful tuning of temperature and magnetic field to avoid bulk nucleation of the favored phase [70]). We are going to derive effective, nonlinear equations of motion for the interface, appropriate for different types of interfacial relaxation mechanisms, and then proceed to analyze the roughening process within the *linear* approximation. While not always quantitatively correct, the linear theory already contains the essential ingredients of kinetic roughening phenomena, and provides us with a firm foundation for explorations into the realm of nonlinear theories. As a first step towards a nonlinear theory, the effect of nonlinearities on large scales is estimated using power counting arguments. Retaining only nonlinear terms which are *relevant* in this sense, one arrives, for a particular but broad class of conditions to be specified below, at the

KPZ equation, some aspects of which will be treated Chapter 4.

3.1 Interface equations of motion

Consider an interface oriented on average parallel to a d-dimensional 'substrate' hyperplane in $d+1$-dimensional space. On a somewhat coarse-grained level we may describe the interface position by a height function $x_{d+1} = h(\mathbf{x},t)$, where $\mathbf{x} = (x_1,...,x_d)$ is the substrate coordinate. In the presence of an external field $\mu_0 > 0$ which favors the phase occupying the half space $x_{d+1} < h$ over the phase in $x_{d+1} > h$ (Figure 12), the free energy of the system can be written as

$$\mathcal{F}[h(\mathbf{x},t)] = \sigma \int d^d\mathbf{x}\, \sqrt{1+(\nabla h)^2} - \mu_0 \int d^d\mathbf{x}\, h \tag{3.1}$$

where the interfacial tension σ is assumed, for simplicity, to be independent of orientation. The interfacial free energy in (3.1) corresponds to the 'drumhead' model [71] which neglects the intrinsic interface width (expected to be of the order of the bulk correlation length).

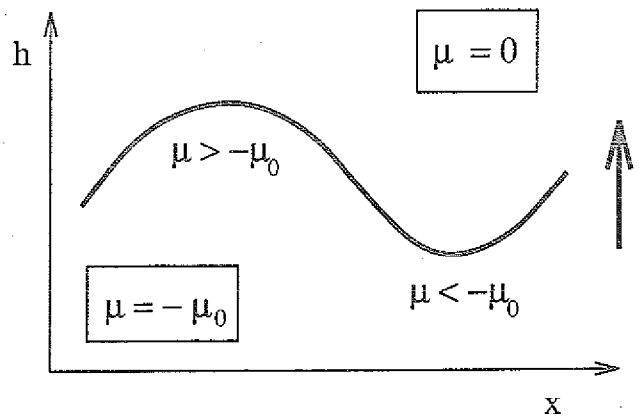

Figure 12: Interface between a favored ($\mu = -\mu_0 < 0$) and an unstable ($\mu = 0$) phase. The chemical potential is increased (reduced) at local maxima (minima). The arrow indicates the direction of interface motion.

The driving force for morphological changes is the interface chemical potential

$$\mu = \delta\mathcal{F}/\delta h. \tag{3.2}$$

A conventional relaxation ansatz for the dynamics then yields the normal interface velocity as

$$v_n = -\Gamma \frac{\delta\mathcal{F}}{\delta h} = -\Gamma\mu \tag{3.3}$$

where $\Gamma > 0$ is the interface mobility [72]; to arrive at an equation of motion for $h(\mathbf{x},t)$ we merely note that, from an obvious geometric construction,

$$\partial h/\partial t = v_n \sqrt{1+(\nabla h)^2}. \tag{3.4}$$

In the interest of keeping the notation transparent, we give explicit expressions only for the case $d=1$, where $h(x,t)$ is a curve. Performing the functional derivative of (3.1) we arrive at

$$\mu = -\frac{\sigma\nabla^2 h}{[1+(\nabla h)^2]^{3/2}} - \mu_0; \tag{3.5}$$

the term multiplying the interfacial tension σ is the local *curvature* (see Figure 12). Thus the full equation of motion reads

$$\frac{\partial h}{\partial t} = \Gamma\sqrt{1+(\nabla h)^2}\left[\mu_0 + \frac{\sigma\nabla^2 h}{[1+(\nabla h)^2]^{3/2}}\right]. \tag{3.6}$$

It is interesting to note that, besides the trivial flat solution $h=\Gamma\mu_0 t$, (3.6) admits (semi-) circular 'droplet' solutions of the form

$$h(x,t) = \sqrt{R^2(t)-x^2},\ x^2 \le R^2, \tag{3.7}$$

where the radius $R(t)$ satisfies

$$dR/dt = \Gamma(\mu_0 - \sigma/R). \tag{3.8}$$

From this we infer the existence of a critical droplet radius $R_c = \sigma/\mu_0$ such that droplets with $R > R_c$ grow while those with $R < R_c$ shrink under surface tension; $R = R_c$ is an unstable equilibrium. Eq.(3.8) (as, indeed, eq.(3.6)) is an expression of the familiar Gibbs-Thomson relation which states that a larger thermodynamic driving force is required to move a curved interface.

Let us now specifically apply these considerations to a solid growing from a vapor phase. The Gibbs-Thomson effect is then microscopically realized through an increased (decreased) evaporation rate at negatively (positively) curved portions of the surface. It turns out, however, that many technologically relevant vapor deposition processes are operated under conditions of negligible evaporation [15, 73]. In such cases the 'evaporation-condensation'-dynamical ansatz (3.3) is inappropriate and has to be replaced by an equation describing relaxation through mass transport *along* the surface [13]. To arrive at such a description, first note that the quantity defined in (3.2) may be interpreted, in the present situation, as the *chemical potential of adatoms*; indeed, $\delta\mathcal{F}/\delta h$ is precisely the change in surface free energy associated with removing or adding a small amount of mass to the surface. When desorption is kinetically suppressed, chemical potential differences that arise due to modulations of the surface profile (as in Figure 12) relax through surface diffusion currents, viz., the migration of adatoms in the direction of chemical potential gradients. Thus, the normal velocity of the surface is given by

$$v_n = -\partial J/\partial s \tag{3.9}$$

where J is (in the one-dimensional situation considered here) the mass current along the arc length

$$s = \int dx \sqrt{1 + (\nabla h)^2}. \tag{3.10}$$

The current being driven by chemical potential gradients, we have

$$J = -\Gamma_a \frac{\partial \mu}{\partial s} = -\frac{\Gamma_a}{\sqrt{1 + (\nabla h)^2}} \frac{\partial \mu}{\partial x} \tag{3.11}$$

with an *adatom mobility* $\Gamma_a > 0$. Putting everything together, we arrive at the equation

$$\frac{\partial h}{\partial t} = -\frac{\partial}{\partial x} \frac{\Gamma_a}{\sqrt{1 + (\nabla h)^2}} \frac{\partial}{\partial x} \frac{\sigma \nabla^2 h}{[1 + (\nabla h)^2]^{3/2}}. \tag{3.12}$$

The explicit form of the two-dimensional generalization of this equation has been derived in several recent papers [74, 75, 76].

The reader will have noticed at this point that the external field μ_0, introduced in (3.1) to set the surface into motion, has effectively disappeared from the description; in fact the surface governed by (3.12) does not move. We can of course cure this deficiency by adding a constant deposition flux F to the right hand side of (3.12), however this implies only a trivial change that can be undone by going to a frame moving at speed F. The physical reason behind this surprising result is clear: Within the framework of the classical theory, as expressed in eqs.(3.9) and (3.11), the surface diffusion processes, being sensitive only to spatial gradients in the chemical potential μ, are not affected by an overall constant shift μ_0. It is also clear that this is unlikely to be the whole truth. A more careful consideration of the microscopic kinetics reveals that the mass transport on the surface can be rather drastically altered by the presence of a deposition flux F. On the level of effective interface equations of motion this implies the appearance of additional *dynamic* nonequilibrium terms in (3.12), the coefficients of which are proportional to F. We postpone to Chapter 5 the detailed discussion of the microscopic origins of these terms, and present here only the main results.

As was first suggested by Villain [15], two types of terms are expected to be present generically. The first set of terms arises because under nonequilibrium conditions the local chemical potential (or, rather, its appropriate nonequilibrium generalization, see Section 5.3) acquires a dependence on the local surface *orientation*; in equilibrium it is clear from the definition (3.2) of μ as a functional derivative, and from the fact that the free energy $\mathcal{F}$ should be invariant under vertical translations $h \to h + const.$, that the leading dependence of μ is on the local *curvature*. From symmetry considerations one expects the nonequilibrium contribution to be an even function of ∇h, and thus to admit an expansion

$$\mu_{NE} = \lambda_2 (\nabla h)^2 + \lambda_4 (\nabla h)^4 + \ldots \tag{3.13}$$

The second type of nonequilibrium effects leads to a contribution to the current J in (3.9) which, rather than being proportional to the gradient of some (equilibrium or nonequilibrium) chemical potential, is itself a function of the local surface orientation [77]. General symmetry arguments and detailed calculations, to be presented in Section 5.2, show that the nonequilibrium current is an odd function of ∇h, such that, in a gradient expansion,

$$J_{NE} = -(\nu_1 + \nu_3(\nabla h)^2 + ...)\,\nabla h. \tag{3.14}$$

Here the leading term $\nu_1 \nabla h$ is of special importance in that it changes the character of the equation of motion already on the level of the linearization around the flat state, which will be the focus of the next section. In particular, if $\nu_1 < 0$ ('uphill' current) the surface can be *destabilized* by (nonequilibrium) surface diffusion (see Section 5.2.4).

Including the nonequilibrium contributions (3.13) and (3.14), through (3.9) and (3.11), in the interface equation of motion leads to a problem of rather formidable complexity. Schematically, the final result reads

$$\frac{\partial h}{\partial t} = \frac{\partial}{\partial x} \frac{\Gamma_a}{\sqrt{1+(\nabla h)^2}} \frac{\partial}{\partial x}(\mu + \mu_{NE}) - \frac{\partial}{\partial x} J_{NE} + F, \tag{3.15}$$

and it should be remembered that $\mu_{NE}, J_{NE} = \mathcal{O}(F)$. Equation (3.15) provides the most general macroscopic description of growth under conditions of volume-conserving surface relaxation. Correspondingly, (3.6) is the general equation of motion for *nonconserved* interface dynamics.

3.2 Linearized fluctuation theory

The theory of kinetic roughening is concerned with the question of how microscopic fluctuations, which are present in virtually any interface displacement process, are transformed, through effective interface equations of the kind derived in the previous section, into large-scale behavior with universal properties. This transformation becomes transparent and easily tractable when the equations of motion are linearized about the flat solution $h(\mathbf{x},t) = v_0 t$. One may hope that the linearization is appropriate when the interface is flat on average, or when one considers length scales on which macroscopic modulations of the interface orientation are negligible. We shall see later that this hope is not quite warranted, due to the possibility of *relevant* nonlinearities which dominate the large scale properties of an interface even in the absence of macroscopic modulations; however in order to appreciate the role of nonlinearities we first need to acquire a thorough understanding of the linear fluctuation theory.

3.2.1 Langevin equations

Fluctuations are commonly modeled by adding a stochastic noise term $\eta(\mathbf{x},t)$ to the right hand side of the interface equation of motion. The noise is assumed to be Gaussian and uncorrelated, with zero mean and covariance

$$\langle \eta(\mathbf{x},t)\eta(\mathbf{x}',t')\rangle = D\delta^d(\mathbf{x}-\mathbf{x}')\delta(t-t'); \tag{3.16}$$

here and in the following the angular brackets imply an average over noise histories. Since we aim at a theory that is as general as possible, we will not, at this point, specify the physical origin of the noise. In processes that operate at or close to equilibrium, the fluctuations are mainly of thermal nature; far from equilibrium additional sources of noise appear, such as shot noise in deposition processes or the frozen disorder in interface displacements in porous media (in the latter case the fluctuations can be modeled by a time-dependent noise term only if the displacement is sufficiently rapid [78]).

However, one remark is in order, regarding the different roles of the noise in the two classes of processes described by eqs.(3.6) and (3.15), respectively. In the case of nonconserved dynamics, eq.(3.6), as exemplified by a moving Ising interface, the noise term $\eta(\mathbf{x},t)$ is present even in equilibrium, when $\mu_0 = 0$; the coefficient D in (3.16) is then proportional to temperature T. In contrast, with mass conserving surface diffusion dynamics as in eq.(3.15), the deposition flux is the sole source of noise that can change the total amount of mass on the surface; the *thermal* fluctuations which arise due to the particulate nature of the surface transport, and which survive in equilibrium, when $F = 0$, conserve the volume of the solid. Mathematically, this is expressed through a *conserved* noise term η_c which can be written as the divergence of a stochastic current, $\eta_c(\mathbf{x},t) = -\nabla\cdot\mathbf{j}_s(\mathbf{x},t)$, and hence has a covariance of the form

$$\langle \eta_c(\mathbf{x},t)\eta_c(\mathbf{x}',t')\rangle = -D_c\nabla^2\delta^d(\mathbf{x}-\mathbf{x}')\delta(t-t') \tag{3.17}$$

with $D_c \sim T$, whereas the coefficient of the nonconserved noise term, D, is proportional to the flux F. In growth processes where surface relaxation occurs mainly through surface diffusion, the noise itself is a nonequilibrium effect; we shall see that this implies very pronounced fluctuations in these systems. The 'mismatch' between nonconserved noise and conserved relaxation dynamics provides a general mechanism for power laws and generic scale invariance also in systems that do not possess the translational symmetry of interfaces [79, 80]. It is intuitively plausible that a nonconserved noise term, when present, dominates the conserved noise η_c on large length and time scales, and that the latter can therefore be neglected; a more precise argument will be given below.

We now linearize the equations of motion (3.6) and (3.15) around a flat, uniformly moving front $h_0(t) = v_0 t$, with $v_0 = \Gamma\mu_0$ for (3.6) and $v_0 = F$ for (3.15). Adding the noise term one has, in the moving frame,

$$\frac{\partial h}{\partial t} = -(-\nu\nabla^2)^m h + \eta. \tag{3.18}$$

The case $m = 1$ includes the linearization of eq.(3.6), where $\nu = \Gamma\sigma$, as well as that of (3.15) in the presence of a stabilizing nonequilibrium current (3.14), such that $\nu = \nu_1 > 0$ (the linearization is clearly useless in the unstable case $\nu_1 < 0$, which will be treated in Section 5.2.4); the fourth order derivative $\nabla^4 h$ that arises from the linearization of the equilibrium equation (3.12) can then be neglected. This leads to an important general conclusion: A nonequilibrium current, provided it is directed downhill so that $\nu_1 > 0$, may effectively mimic evaporation-condensation dynamics (in the sense that $m = 1$ in (3.18)) even if evaporation is kinetically suppressed. If, on the other hand, J_{NE} is absent or negligible, the linearization of (3.15) results in (3.18) with $m = 2$ and $\nu = \Gamma_a\sigma$. Note that while the explicit forms of the full nonlinear equations were given in (3.6) and (3.15) only for $d = 1$, the linearization (3.18) holds in arbitrary dimensionality.

Equation (3.18) with $m = 1$ has been employed to describe the equilibrium dynamics of interfaces e.g. in the contexts of thermal roughening and wetting [81, 82]. In the kinetic roughening literature it is commonly referred to as the Edwards-Wilkinson equation. Edwards and Wilkinson [83] were the first to derive this equation for a nonequilibrium situation, specifically, as a description of the sedimentation of granular particles. In that case the relaxation term $\nu\nabla^2 h$ arises from the expansion (3.14) of a nonequilibrium mass current driven downhill by gravity, and the coefficient ν_1 is proportional to the particle flux. While gravity obviously plays no role on the atomic level, microscopic mechanisms associated e.g. with the transient kinetic energy of the deposited atoms exist [84] which can give rise to downhill currents in vapor deposition processes.

Equation (3.18) with $m = 2$ was first written down and discussed by Golubović and Bruinsma [85] and by Wolf and Villain [86]; since its deterministic form ($\eta = 0$) originates in the work of Mullins [13], we refer to it as the (noisy) *Mullins equation*.

3.2.2 General solution

To solve (3.18) we introduce the Fourier decomposition

$$h(\mathbf{x},t) = \sum_{\mathbf{q}} h_{\mathbf{q}}(t) e^{i\mathbf{q}\cdot\mathbf{x}}$$

$$\eta(\mathbf{x},t) = \sum_{\mathbf{q}} \eta_{\mathbf{q}}(t) e^{i\mathbf{q}\cdot\mathbf{x}} \tag{3.19}$$

where the sums run over the allowed reciprocal vectors of a lattice of linear size L, periodic boundary conditions and a lattice constant a. From (3.16) we find the covariance of the Gaussian noise components

$$\langle \eta_{\mathbf{q}}(t)\eta_{\mathbf{q}'}(t')\rangle = L^{-d} D \delta_{\mathbf{q}+\mathbf{q}'}\delta(t-t'), \tag{3.20}$$

while for the conserved noise defined by (3.17) one has

$$\langle \eta_{c\mathbf{q}}(t)\eta_{c\mathbf{q}'}(t')\rangle = L^{-d} D_c \mathbf{q}^2 \delta_{\mathbf{q}+\mathbf{q}'}\delta(t-t'). \tag{3.21}$$

This shows why η_c can be neglected on large scales (small q), if a nonconserved noise source is present. The Fourier components of h evolve independently according to

$$\frac{\partial}{\partial t} h_{\mathbf{q}} = -\nu |\mathbf{q}|^z h_{\mathbf{q}} + \eta_{\mathbf{q}} \tag{3.22}$$

where we have set $z = 2m$. Odd values of z can appear when the relaxation dynamics is *nonlocal*, e.g. $z = 1$ applies to diffusion-limited erosion [87] and $z = 3$ describes a surface relaxing to equilibrium through volume diffusion [13]. Since there is no difficulty in solving (3.22) for general z, we can treat all these cases on the same footing.

According to (3.22), each mode behaves as a randomly perturbed harmonic oscillator with restoring force $\nu|\mathbf{q}|^z$. The general solution is

$$h_{\mathbf{q}}(t) = e^{-\nu|\mathbf{q}|^z t} h_{\mathbf{q}}(0) + \int_0^t d\tau\, e^{-\nu|\mathbf{q}|^z(t-\tau)}\, \eta_{\mathbf{q}}(\tau). \tag{3.23}$$

Here we will mostly be concerned with the *transient* roughening of an initially flat interface, so we set $h_{\mathbf{q}}(0) = 0$ for all $\mathbf{q}$. Multiplying (3.23) with $h_{\mathbf{q}'}(t)$ and averaging over the noise according to (3.20) we obtain

$$\langle h_{\mathbf{q}}(t) h_{\mathbf{q}'}(t)\rangle = S(q,t)\delta_{\mathbf{q}+\mathbf{q}'} \tag{3.24}$$

with $q = |\mathbf{q}|$ and

$$S(q,t) = L^{-d}\frac{D}{2\nu q^z}(1 - e^{-2\nu q^z t}). \tag{3.25}$$

Since $h_{\mathbf{q}}(t)$ derives from the Gaussian random variable $\eta_{\mathbf{q}}(t)$ through a linear transformation, the height modes themselved are Gaussian and higher order correlation functions are simply related to the covariance (3.24); thus (3.25) completely specifies the statistics of interfacial fluctuations. Two features of (3.25) are noteworthy. First, the relaxation time of a mode with wavenumber q is proportional to q^z, i.e. long wavelength modes relax slowly. Second, the prefactor in (3.25) diverges for $q \to 0$, thus giving large statistical weight to long wavelength modes. Together these two observations bring out the central mechanism of kinetic roughening; note also that both effects are more pronounced the larger the value of z.

To proceed, we translate (3.25) into more conventional measures of interface roughness. Of particular interest are the interface width W, defined through

$$W^2 = \langle (h - \overline{h}(t))^2 \rangle = \sum_{\mathbf{q} \neq \mathbf{0}} S(q,t) \tag{3.26}$$

and the (second order) height difference correlation function

$$G_2 = \langle (h(\mathbf{x}+\mathbf{r},t) - h(\mathbf{x},t))^2 \rangle = \sum_{\mathbf{q}} S(q,t)(1 - \cos \mathbf{q}\cdot\mathbf{r}). \tag{3.27}$$

In (3.26) the instantaneous spatial average $\overline{h}(t) = h_{\mathbf{q}=\mathbf{0}}(t)$ has been subtracted; since the noise operates also at $\mathbf{q}=\mathbf{0}$, $\overline{h}(t)$ performs a random walk with diffusion constant D/L^d.

For a first estimate of the width we approximate the sum in (3.26) by an integral and obtain, up to factors of order unity,

$$W^2 \sim \frac{D}{\nu} \int_{2\pi/L}^{\pi/a} dq\, q^{d-1-z}(1 - e^{-2\nu q^z t}). \tag{3.28}$$

The integral is governed by the interplay of *three length scales*: The lattice constant a, the substrate size L, and the *dynamical correlation length*

$$\xi(t) \equiv (2\nu t)^{1/z}. \tag{3.29}$$

The lattice constant is irrelevant, in the sense that the integral converges for $a \to 0$, below the upper characteristic dimensionality

$$d_c^{(1)} = z. \tag{3.30}$$

For $d > d_c^{(1)}$ we may let $L, t \to \infty$ to obtain a finite limiting interface width $W^2 \approx (D/\nu)a^{z-d}$. This implies that the noise is able to *roughen* the interface, in the sense of a proliferation of long wavelength fluctuations leading to a divergent width for $L, t \to \infty$, only in sufficiently low dimensionalities.

In the rough regime $d < d_c^{(1)}$ the power law prefactor of the integrand in (3.28) implies a divergence at small q which is limited by the smaller of the lengths L and ξ. We may let $a \to 0$ and summarize the dependence on the remaining two length scales in the scaling form [58, 60]

$$W^2(L,t) \sim L^{2\zeta} f(\xi(t)/L) \tag{3.31}$$

with the *roughness exponent*

$$\zeta = (z-d)/2 > 0 \tag{3.32}$$

and the scaling function

$$f(x) = \frac{D}{\nu} \int_{2\pi}^{\infty} dy\, y^{d-1-z}(1 - e^{-(xy)^z}). \tag{3.33}$$

The scaling form (3.31) brings out the significance of the correlation length ξ: The width saturates, that is, it becomes time-independent, when $\xi \sim L$, at a time of the order

$$t_c \approx L^z/\nu. \tag{3.34}$$

This time scale marks the transition from the transient to the *stationary* regime where the memory of the flat initial condition is lost. At early times when $\xi \ll L$, expanding (3.33) shows that the width increases as

$$W^2 \sim (D/\nu)\xi^{2\zeta} \sim t^{2\zeta/z}. \tag{3.35}$$

In the borderline dimensionality $d = d_c^{(1)}$ all three length scales have to be taken into account, and one finds

$$W^2 \sim \begin{cases} (D/\nu)\ln(\nu t/a) & : \quad \xi \ll L \\ (D/\nu)\ln(L/a) & : \quad \xi \gg L. \end{cases} \tag{3.36}$$

For future reference we record some exact expressions for one-dimensional interfaces, $d = 1$, in the rough regime, i.e. for $z > 1$. Consider first the stationary limit, $t \to \infty$. With $a \to 0$ the sum (3.26) can be written as

$$\lim_{t\to\infty} W^2(L,t) = (2\pi)^{-z}\zeta_R(z)(D/\nu)L^{2\zeta}, \tag{3.37}$$

where

$$\zeta_R(z) \equiv \sum_{k=1}^{\infty} \frac{1}{k^z} \tag{3.38}$$

denotes the Riemann zeta function; for even integer values of z, $\zeta_R(z) = 2^{z-1}\pi^z B_{z/2}/z!$ with the Bernoulli numbers B_m, and (3.37) simplifies to

$$\lim_{t\to\infty} W^2(L,t) = \frac{B_{z/2}}{z!}\frac{D}{2\nu}L^{2\zeta}; \tag{3.39}$$

of primary interest are the cases $z = 2$, where $B_1/2! = 1/12$, and $z = 4$ with $B_2/4! = 1/720$.

To evaluate the width in the transient case, $\xi \ll L$, we let $L \to \infty$ as well as $a \to 0$ at fixed t. The sum (3.26) then converges to an integral, which yields, after some simple manipulations,

$$\lim_{L\to\infty} W^2(L,t) = \frac{1}{2\pi}\frac{D}{\nu}\frac{\Gamma(1/z)}{z-1}(2\nu t)^{2\zeta/z}, \tag{3.40}$$

with Γ denoting the gamma function. From (3.37) and (3.40) we can derive a more precise estimate of the crossover time t_c introduced in eq.(3.34). Matching the

two expressions we conclude that the crossover from the transient to the stationary regime occurs when the ratio of the correlation length (3.29) to the system size is

$$\frac{\xi}{L} = \frac{1}{2\pi}\left[\frac{(z-1)\zeta_R(z)}{\Gamma(1/z)}\right]^{1/(z-1)}. \tag{3.41}$$

The numerical value of the right hand side is $\sqrt{\pi}/12 \approx 0.148$ for $z=2$, and ≈ 0.153 for $z=4$.

3.2.3 Anomalous scaling

In the height difference correlation function (3.27) the distance r between the two substrate points introduces a further length scale. In approximation,

$$G_2 \sim \frac{D}{\nu}\int_{2\pi/L}^{\pi/a} dq\, q^{d-1-z}(1-e^{-2\nu q^z t})(1-\cos qr). \tag{3.42}$$

Again, the limit $a \to 0$ exists for $d < d_c^{(1)}$. However we see that the r-dependent factor in the integrand leads to the appearance of a second characteristic dimensionality [85]

$$d_c^{(2)} = z-2 \tag{3.43}$$

such that for $d > d_c^{(2)}$ the limit $L,t \to \infty$ of G_2 at fixed r exists, while for $d \le d_c^{(2)}$ the divergence of the integrand at $q=0$ is too strong to be cured by the factor $1-\cos qr \approx q^2r^2/2$. This implies, for $a \to 0$, two different types of scaling forms for G_2: Above $d_c^{(2)}$ one has 'conventional' scaling,

$$G_2 \sim \begin{cases} r^{2\zeta} g^{(T)}(r/\xi) & : \quad \xi \ll L \\ r^{2\zeta} g^{(S)}(r/L) & : \quad \xi \gg L, \end{cases} \tag{3.44}$$

while for $d < d_c^{(2)}$ the scaling is 'anomalous' [88, 89, 90],

$$G_2 \approx \begin{cases} \xi^{2\alpha} r^{2\tilde{\zeta}} \tilde{g}^{(T)}(r/\xi) & : \quad \xi \ll L \\ L^{2\alpha} r^{2\tilde{\zeta}} \tilde{g}^{(S)}(r/L) & : \quad \xi \gg L. \end{cases} \tag{3.45}$$

The superscripts on the scaling functions refer to the transient (T) and stationary (S) regimes, respectively. All scaling functions tend to constants of order D/ν for small arguments (small r), and the transient scaling functions behave as $g^{(T)}(x) \sim x^{-2\zeta}$, $\tilde{g}^{(T)}(x) \sim x^{-2\tilde{\zeta}}$ for large arguments, consistent with the fact that G_2 becomes independent of r for $r \gg \xi$: At any finite time t, the roughness has only developed up to scale $\xi(t)$. In the stationary case the fact that $G_2(r) = G_2(L-r)$ implies the relation

$$g^{(S)}(x)/g^{(S)}(1-x) = (1/x-1)^{2\zeta} \tag{3.46}$$

and analogously for $\tilde{g}^{(S)}$. The anomalous scaling exponents in (3.45) take the values

$$\alpha = \zeta - 1, \;\; \tilde{\zeta} = 1. \tag{3.47}$$

In general, we observe that since

$$\lim_{r\to\infty} \lim_{L\to\infty} G_2 = 2W^2, \tag{3.48}$$

consistency between (3.45) and (3.35) requires

$$\alpha + \tilde{\zeta} = \zeta \tag{3.49}$$

which is of course satisfied here.

Comparing (3.32) and (3.43) we recognize that the dimensionality $d_c^{(2)}$ is characterized by

$$\zeta(d_c^{(2)}) = 1. \tag{3.50}$$

The value $\zeta = 1$ of the roughness exponent is special because it signals, in a certain sense, that the assumption of a well-defined average orientation of the interface (parallel to the substrate plane) becomes inconsistent: The orientational fluctuations at scale r, estimated e.g. as G_2/r^2, decrease with r only if $\zeta < 1$ [85]. The conclusions that can be drawn if it is found that $\zeta = 1$ for a particular dimensionality depend on the physical context. For equilibrium interfaces $\zeta = 1$ is commonly associated with the breakdown of two-phase coexistence at the lower critical dimensionality of the *bulk* system [91]; e.g. for the pure Ising model $\zeta = (2-d)/2 = 1$ in bulk dimension $d+1 = 1$, while for the Ising model with random fields [92] the Imry-Ma expression $\zeta = (4-d)/3$ shows that the disorder shifts the (bulk) lower critical dimensionality to $d+1 = 2$. Fluid membranes governed by bending elasiticity rather than surface tension have $\zeta = (4-d)/2$, and hence $\zeta = 1$ in the physical dimension $d = 2$; this reflects the tendency of membranes to *crumple* on scales larger than the (possibly astronomical) persistence length [93].

In the present context the anomalous scaling regime described by (3.45) appears only in the case of surface diffusion dynamics without nonequilibrium currents, where $z = 4$ so $\zeta \geq 1$ in dimensionalities $d \leq 2$. Physically, the anomalous behavior is a consequence of the 'mismatch' between mass conserving relaxation dynamics and nonconserving shot noise previously alluded to. Relaxation through surface diffusion is insufficient to counteract the disordering influence of the shot noise even locally; thus *local* roughness measures such as the slope fluctuation $\langle(\nabla h)^2\rangle$ become enslaved by the long wavelength modes and diverge with increasing correlation length (or system size) as $\langle(\nabla h)^2\rangle \sim \xi^{2\alpha}$ with $\alpha > 0$ (cf. (3.45)). While nonlinearities are expected to significantly alter this picture, there is numerical evidence [89, 90, 94] that the

anomalous scaling form (3.45) (possibly with nonuniversal values of the exponents α and $\tilde{\zeta}$) is generic for deposition processes with conserved surface relaxation in low dimensionalities. We will return to the possible origins of this behavior in Section 5.4.1.

3.3 Relevant nonlinearities

To what extent can the linearized fluctuation theory be trusted when it comes to describing real interfaces? The short answer is that the *qualitative* behavior derived above is expected to remain valid. That is, *any* kinetic roughening process entails a dynamic correlation length

$$\xi \sim t^{1/z} \tag{3.51}$$

which enters the scaling forms (3.31), (3.44) and, possibly, (3.45) for the width and the height-difference correlation function, but the values of the *dynamic exponent* z and the roughness exponent ζ, as well as the detailed shapes of the scaling functions may differ from the expressions of the linear theory; in particular, the height fluctuations may become non-Gaussian, involving, in extreme cases [94], separate roughness exponents for different moments of h.

The 'stability' of the large scale behavior of the linear theory against the inclusion of nonlinear terms can be probed by a simple technique referred to as *power counting*, which we illustrate here for the leading growth-induced kinematic nonlinearity of the nonconserved interface equation (3.6). Expanding the square root in front of the square bracket and adding the noise we have, in a frame moving at velocity $v_0 = \Gamma\mu_0$,

$$\frac{\partial h}{\partial t} = \nu\nabla^2 h + \frac{\lambda}{2}(\nabla h)^2 + \eta \tag{3.52}$$

where we have set $\lambda = \Gamma\mu_0 = v_0$. We now perform a rescaling transformation

$$\tilde{h}(\mathbf{x},t) = b^{-\zeta} h(b\mathbf{x}, b^z t) \tag{3.53}$$

with a scaling factor $b > 1$. The transformation of the noise is dictated by the invariance of the covariance (3.16); this yields

$$\tilde{\eta}(\mathbf{x},t) = b^{(d+z)/2}\eta(b\mathbf{x}, b^z t). \tag{3.54}$$

Inserting (3.53) and (3.54) into (3.52) we find that $\tilde{h}$ satisfies (3.52) with the rescaled coefficients

$$\tilde{\nu} = b^{z-2}\nu, \;\; \tilde{D} = b^{z-d-2\zeta} D, \;\; \tilde{\lambda} = b^{z+\zeta-2}\lambda. \tag{3.55}$$

It is easily checked that (3.53) constitutes, for $b > 1$, a *coarse graining* operation. Thus (3.55) provides, for $b \to \infty$, a measure of the relative importance of the various

terms in (3.52) on large scales. In order to evaluate the large scale effects of the nonlinear term we now set ζ and z in (3.55) equal to the values $\zeta = (2-d)/2$, $z = 2$ characteristic of the linear theory. Not surprisingly, the coefficients ν and D that appear already in the linear equation then remain invariant, however the coefficient λ of the nonlinearity *increases*, for $d < 2$, as b^{ζ}. We conclude that this term is *relevant* and presumably alters the scaling behavior of the linear theory. The same kind of analysis applied to higher order terms appearing in the gradient expansion of (3.6), such as $[(\nabla h)^2]^2$ and $(\nabla h)^2 \nabla^2 h$, shows that these are *irrelevant*, that is, their coefficients *decrease* under rescaling. Thus the nonlinear equation (3.52), which was first derived by Kardar, Parisi and Zhang [14] in 1986, gives a complete description of the large scale properties of interfaces moving locally in the direction of the driving force, as in (3.3). Some properties of this equation will be discussed in Chapter 4.

In the case of conserved surface relaxation, as described by (3.15), the situation is much more complicated. First, since the linear theory (without nonequilibrium currents) shows anomalous scaling with $\zeta \geq 1$ for $d \leq 2$, *all* nonlinearities that arise from expanding the geometric factors in (3.12) are relevant [74, 75] in dimensions $d \leq 2$. Similarly the terms $\lambda_{2m}(\nabla h)^{2m}$ in the expansion (3.13) of the nonequilibrium chemical potential are relevant for $d < 4m/(2m-1)$; in $d = 2$ *all* these terms are relevant. Existing renormalization-group treatments of the nonlinearities [75, 95, 96] (see also Section 5.3.3) have taken into account only the lowest order terms, however it is not clear that such a procedure can be justified for infinite sequences of relevant terms.

On the other hand, matters simplify drastically in the presence of a stabilizing (downhill) nonequilibrium current, eq.(3.14) with $\nu_1 > 0$. As already mentioned, the linear theory is then given by the Edwards-Wilkinson equation, (3.18) with $m = 1$, and power counting shows that all conceivable nonlinearities (which are consistent with the conserved nature of the dynamics) are irrelevant [95, 96]. Thus in this instance the linear theory provides the *exact* description of the large scale properties. Below in Section 3.4 we explore some further examples of microscopic models for which the linear theory becomes exact.

Golubović and Bruinsma [85] have investigated the effect of adding the KPZ nonlinearity $(\lambda/2)(\nabla h)^2$ to the fourth order surface diffusion equation, (3.18) with $m = 2$. In that case power counting shows that the nonlinearity is relevant below 8 interface dimensions. It should however be clear from the derivation in Section 3.1 that the Golubović-Bruinsma equation

$$\partial h/\partial t = -\nu \nabla^4 h + (\lambda/2)(\nabla h)^2 + \eta \tag{3.56}$$

does not constitute a consistent description of interface dynamics: Since the KPZ-term does not conserve volume, it should always be accompanied by an evaporation-

condensation term proportional to $\nabla^2 h$. Indeed, the renormalization group analysis of Golubović and Bruinsma does demonstrate the generation of such a term on large length scales, but its sign turns out to be *negative* (i.e., destabilizing) to leading order in $\epsilon = 8 - d$. In view of recent work on the related, deterministic Kuramoto-Sivashinsky equation, to be described in Section 4.4.1, it seems unlikely that this result has any consequences in physical dimensionalities.

The reader should not be left with the impression that power counting always gives fully reliable answers. There are, at least, two kinds of situations where it may fail. The first case is the appearance of a *strong coupling* regime in which a nonlinear term with a *small* (in some dimensionless sense) coefficient is irrelevant, as predicted by power counting, but the same term becomes relevant when the coefficient exceeds some critical value. So far this scenario has been found to apply only to the KPZ-equation and some of its variants (see Chapter 4), but our understanding of the phenomenon is insufficient at present to be able to decide how commonly it occurs in the context of general, nonlinear interface models.

A second case in which linear analysis, including power counting, gives misleading results is growth with conserved relaxation on a one-dimensional vicinal surface stabilized by step edge barriers (see Section 5.2.1). These barriers give rise to a nonequilibrium current $J_{NE}(\nabla h)$ which, when expanded around the average orientation of the vicinal surface, is of the form (3.14) with $\nu_1 > 0$. Thus, following the above line of reasoning, such a surface should be exactly described by the linear (Edwards-Wilkinson) theory. Simulations of a microscopic model (to be briefly described in Section 5.2.1) reveal, however, that the state in which the linear theory applies is *metastable*: At long times fluctuations nucleate large local deviations from the average orientation which bring the surface into a regime where $\nu_1 < 0$, eventually leading to a global instability not anticipated by the linear analysis.

3.4 Microscopic realizations of the linear theory

The large scale behavior of a given microscopic model conforms exactly to the linear theory if (i) all nonlinearities permitted by the physics of the problem turn out to be irrelevant, or (ii) if the model possesses additional (possibly artificial) symmetries that suppress relevant nonlinearities.

An example of the first kind is provided by the process of diffusion-limited erosion (DLE), which was studied numerically by Meakin and Deutch [97] and analytically by Krug and Meakin [87]. DLE is the time-reversed process of DLA: As in DLA, individual diffusing particles are launched far away to wander towards the interface, however instead of accreting to the growing deposit, upon contact they annihilate with a deposit particle, thus eroding the surface. The model applies

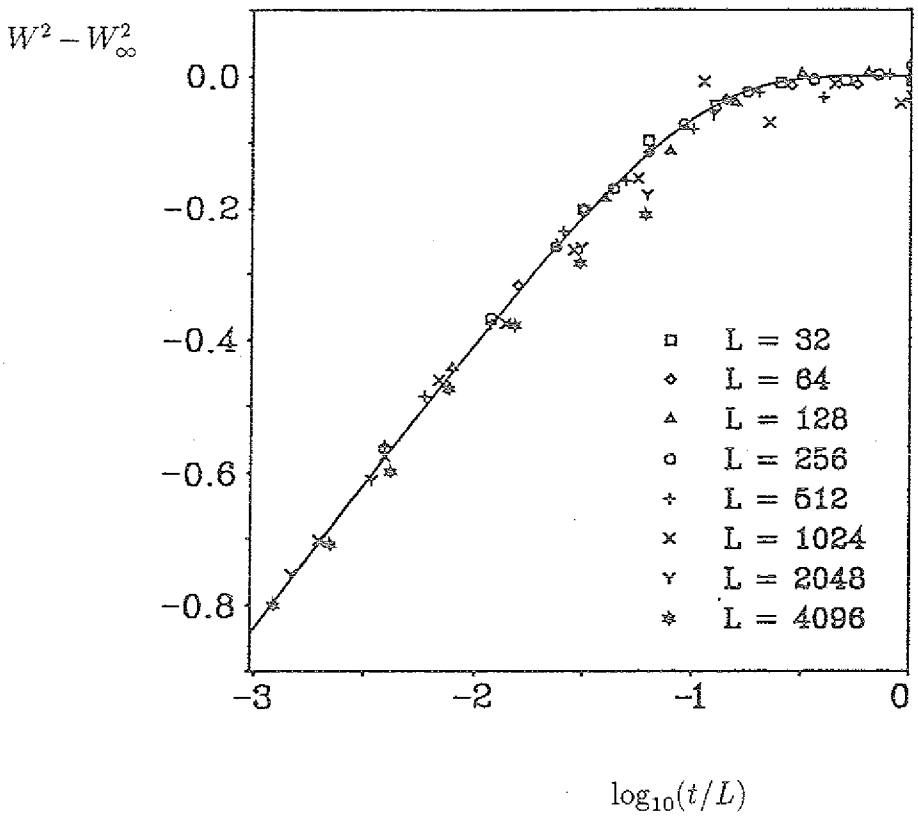

Figure 13: Simulation results (symbols) compared to the theoretical scaling function (3.57) (solid curve) for the surface width in diffusion-limited erosion on the square lattice. The numerical data were averaged over a number of independent runs ranging from 4000 for $L = 32$ to 20 for $L = 4096$. [87]

to diverse processes such as electrolytic polishing and stable fluid invasion in the regime of high capillary numbers [87]. The reversal of the interface motion with respect to the gradient of the diffusion field implies that the destabilizing effect of the latter, as expressed in the conventional stability analysis for solidification fronts [98], is turned into a rather efficient *stabilizing* force, since local protrusions are preferentially eroded.

Krug and Meakin [87] showed that the appropriate linear fluctuation theory for this problem is given by (3.22) with $z = 1$, and the coefficient ν equal to the average interface velocity v; this makes is plain that the relaxation term is of purely nonequilibrium origin. Moreover, all nonlinearities are found to be irrelevant by power counting. The agreement with the linear theory is illustrated in Figure 13, where simulation data for $d = 1$ (the marginal dimensionality $d_c^{(1)}$ for this model) are compared to the analytic expression for the interface width. For $z = 1$, $d = 1$ the

series (3.26) defining W^2 can in fact be summed exactly, with the result

$$W^2 = \frac{D}{2\pi\nu}[\ln(L/a) + \ln(1 - e^{-4\pi\nu t/L})]. \tag{3.57}$$

In the figure, the non-universal short range cutoff a has been removed by subtracting the stationary limit of the width; also, the interface velocity $\nu = 1$ by definition of the time scale, so that the noise strength $D \approx 1.2$ remains as the only fit parameter.

A class of microscopic models tailored to represent the linear continuum theory was recently introduced by Kim and Das Sarma [99], building on earlier work of Family [100]. These models are solid-on-solid (SOS) models [101] in which the position of the surface is specified by an integer-valued height variable $h_{\mathbf{x}}$ defined on the d-dimensional substrate lattice. Deposition occurs by randomly chosing a lattice site $\mathbf{x_0}$, however rather than simply increasing the height at $\mathbf{x_0}$ (which would lead to a trivial model) the depositing particle is allowed to relax in a local neighborhood typically including $\mathbf{x_0}$ and its nearest neighbors. The relaxation is governed by a function $K_{\mathbf{x}}$ of the heights and their discrete derivatives, which is assigned to each lattice site and can be viewed as a representation of the local surface chemical potential. The final deposition site is the site in the neighborhood that has the smallest value of K prior to deposition; if the minimum is not unique, a random choice is made.

In the model of Family [100], the 'chemical potential' K is simply the height itself, $K_{\mathbf{x}} = h_{\mathbf{x}}$. The model may therefore be regarded as a lattice version of the sedimentation process envisioned by Edwards and Wilkinson [83], in which granular particles settle in local surface minima under the influence of gravity. As was pointed out by Krug [102], in the context of sedimentation the assumption of a regular lattice is too strong a simplification: The fact that real sediments are disordered provides a mechanism for the generation of the quadratic KPZ nonlinearity, which invalidates the predictions of the linear theory on large scales (see Chapter 5). On the other hand, a regular lattice appears naturally if one intends to describe epitaxial growth with conserved surface relaxation. In that case the postdeposition relaxation in Family's model could arise from the transient kinetic energy of the depositing particles, which allows them to 'funnel' downhill before being incorporated into the lattice [84]. In the continuum language this causes a downhill current with a stabilizing linear coefficient $\nu_1 > 0$ in (3.14) which, as we have repeatedly argued, supersedes all allowed nonlinearities (the metastability scenario sketched at the end of the previous section cannot alter this conclusion, since the current in Family's model is a monotonic function of inclination, so that $\nu_1 > 0$ for all surface orientations). Thus, this model (including variants with longer ranged, gravity driven relaxation [103]) is an exact realization of the Edwards-Wilkinson equation, as was confirmed by numerical work in one [100] and two [104] dimensions.

For the *curvature model* defined by $K_{\mathbf{x}} = -(\nabla^2 h)_{\mathbf{x}}$ (the right hand side denoting the lattice Laplacian) the corresponding argument [94] requires somewhat greater care. Here, the crucial observation is that, since the dynamics can be formulated solely in terms of the local curvatures, the model is invariant under arbitrary tilts, $h_{\mathbf{x}} \to h_{\mathbf{x}} + \mathbf{u} \cdot \mathbf{x}$. Consequently, any nonlinear contributions to the coarse-grained surface chemical potential have to be powers of second and higher derivatives of h, which are all irrelevant by power counting. Related symmetries are discussed in Section 5.2.2.

Of course, the extra symmetry of the curvature model is due to the somewhat artificial relaxation rule - if the local curvature is replaced e.g. by the coordination number of the deposited atom, as a more realistic representation of the actual atomic kinetics [86, 105, 106] the tilt-invariance is lost and the scaling properties of the model become considerably more complex [89, 90, 94]. Such models are described in Section 5.1.1.

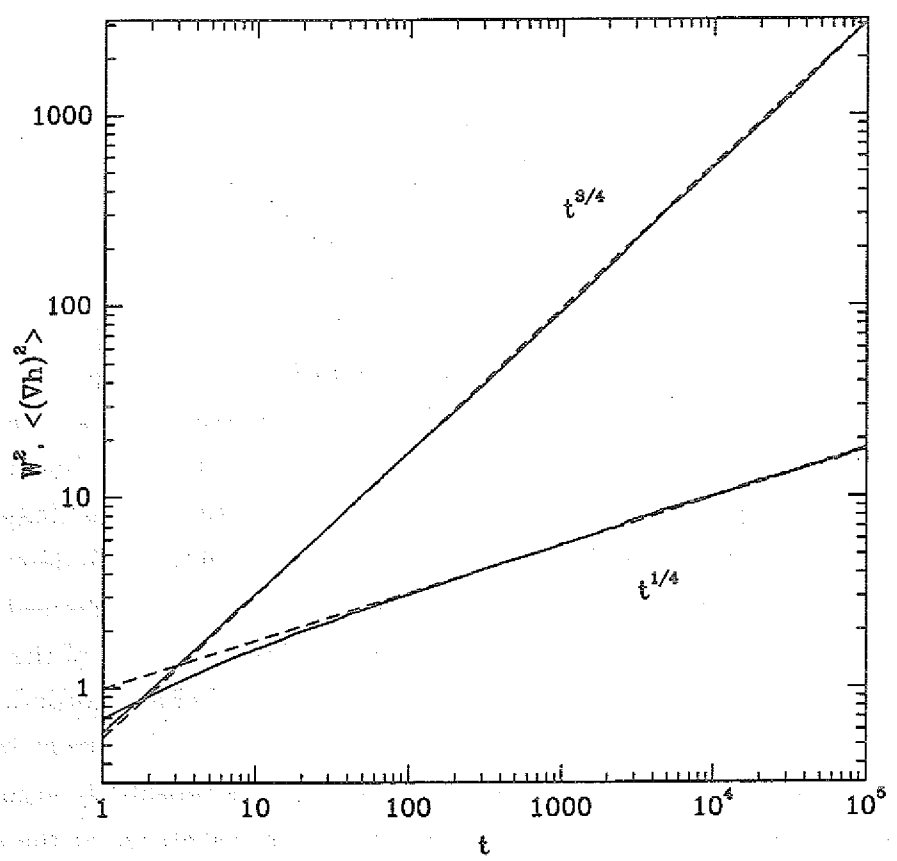

Figure 14: Simulation results for the surface width W^2 and the local height gradient $\langle(\nabla h)^2\rangle$ of the curvature model [94]. The dashed lines are power law fits with the predicted exponents.

Since we expect the large scale behavior of the curvature model to be governed by the linear, noisy Mullins equation (eq.(3.18) with $m=2$), we may utilize the exact expressions derived in Section 3.2.2 both to ascertain our expectation, and to determine the coefficient ν in the continuum equation. The noise strength D is fixed from the outset: In the whole class of models introduced by Kim and Das Sarma [99], particles are deposited *at random* and relax only locally, within a region of a few lattice spacings; therefore the coarse grained noise has Poisson (shot noise) statistics and $D=1$ in units where time is counted in deposited monolayers. In Figure 14 we show simulation data for the width and the mean squared step height $\langle(\nabla h)^2\rangle \equiv \langle(h_{x+1}-h_x)^2\rangle$ for a large ($L=10^5$) one-dimensional system (the precise relaxation rule implemented here is described in Ref.[94]). The predictions of the linear continuum theory for the infinite system can be written as

$$\lim_{t\to\infty} W^2/t^{3/4} = (D/\nu)(2\nu)^{3/4}\Gamma(1/4)/6\pi$$

$$\lim_{t\to\infty} \langle(\nabla h)^2\rangle/t^{1/4} = (D/\nu)(2\nu)^{1/4}\Gamma(3/4)/2\pi. \tag{3.58}$$

From the fits indicated in the figure we estimate $\nu \approx 0.140$ and $D/\nu \approx 7.0$, in accordance with the argument that $D=1$ for this general class of models. The example illustrates how numerical measurements of correlation functions, such as the interface width, can be used to extract the model-dependent parameters that enter the large scale continuum theory. This procedure will recur in the nonlinear context in Sections 4.2 and 5.3.3.

4. Aspects of KPZ theory

The Kardar-Parisi-Zhang equation [14]

$$\frac{\partial h}{\partial t} = \nu \nabla^2 h + \frac{\lambda}{2}(\nabla h)^2 + \eta \tag{4.1}$$

is the most thoroughly studied continuum theory of kinetic roughening. While the derivation in Chapter 3 was based on the macroscopic equation (3.6) for an interface that moves locally normal to itself, it should be recognized that (4.1) is a valid description of large scale interface fluctuations under much more general conditions: The KPZ equation applies whenever the macroscopic interface equation of motion has the form

$$\frac{\partial h}{\partial t} = v(\nabla h) + \text{curvature corrections} \tag{4.2}$$

with an *inclination-dependent growth rate* $v(\nabla h)$ that is a nonlinear function of the local orientation; in the isotropic case of eq.(3.6), $v(\nabla h) = \Gamma \mu_0 \sqrt{1+(\nabla h)^2}$. The characteristic quadratic nonlinearity of (4.1) then results from a gradient expansion of v, [8, 102, 107]

$$v(\nabla h) \approx v(\mathbf{0}) + \sum_{i=1}^{d} \partial_i v(\mathbf{0}) \frac{\partial h}{\partial x_i} + \frac{1}{2} \sum_{i=1}^{d} \lambda_i \left(\frac{\partial h}{\partial x_i} \right)^2 + \ldots \tag{4.3}$$

where the substrate plane coordinates have been chosen such that the matrix of second derivatives $\partial_{ij}^2 v(\mathbf{0})$ is diagonal with eigenvalues λ_i. To arrive at the usual form $(\lambda/2)(\nabla h)^2$ of the nonlinearity one further has to transform to a tilted, comoving frame in which the constant and linear terms in (4.3) vanish, and to assume in-plane isotropy so that $\lambda_i \equiv \lambda$ for all i. This is achieved trivially by a spatial rescaling if all λ_i have the same sign; otherwise novel physics can arise, as will be discussed shortly. The curvature corrections in (4.2) involve second and higher derivatives of h, such as the Gibbs-Thomson term in (3.6). In the presence of a nontrivial inclination-dependent growth rate these terms do not affect the evolution of macroscopic shapes, since they become arbitrarily small under a coarse-graining operation that rescales h- and x-coordinates in the same manner (this should not be confused with the coarse-graining of fluctuations in Section 3.3; there, h and x are treated differently when $\zeta \neq 1$).

Equation (4.2) is useful in clarifying what kind of physical growth processes would be expected *not* to fall into the KPZ universality class. First, the dynamics of h is assumed to be local. This rules out all situations in which the interface motion couples to some nontrivial bulk dynamics, such as the diffusion limited erosion process described in Section 3.4, the competitive growth models of Chapter 2 and the classical continuum theories of solidification [98]. Second, growth with volume

conserving surface relaxation is not covered by the KPZ theory, since in that case the growth rate is controlled entirely by the external deposition flux, $v = F$, and is therefore independent of inclination [102]. We may remark in this context that the orientation-independence of the growth rate is a well-established experimental feature in the molecular beam epitaxy (MBE) of silicon [73], lending support to the application of the conserved growth equation (3.15) to this system; a detailed discussion is found in Chapter 5. Finally, the KPZ theory assumes that the fluctuations in the growth process can be reasonably modeled by a noise term that is a random function of $\mathbf{x}$ and t. This assumption fails for interface motion in a random medium close to the depinning threshold, where the *quenched* nature of the fluctuations, i.e. their dependence on the interface position h, becomes essential [68, 69, 78].

For practical purposes, the mechanisms neglected in the KPZ equation typically define some crossover length scales which limit the applicability of the theory. For example, while desorption may well be negligible in most MBE processes, it is never entirely absent and should in principle lead to a reappearance of KPZ behavior on sufficiently large length scales; defect formation would have the same effect, see Chapter 5. Similarly, an interface moving through a random medium should be describable by the KPZ theory on scales that much exceed the correlation length associated with the depinning transition. Thus, the fact that in many cases the physics on relevant length scales is governed by effects not included in the KPZ equation should not obscure the status of this equation as the *generic* description of the *asymptotic* fluctuation behavior of a broad class of interface displacement processes - though is must be said that non-KPZ physics seems to dominate all experimental situations considered so far, to the extent that no clean experimental confirmation of KPZ behavior has yet emerged!

Strong coupling. From a theoretical perspective, the most intriguing feature of the KPZ equation is the occurrence of a nonequilibrium phase transition for dimensionalities $d > 2$, from a weak coupling phase for small λ where the nonlinearity is irrelevant (as expected on the basis of power counting, see Section 3.3), to a strong coupling phase characterized by nontrivial scaling exponents not accessible to perturbative methods. The physical case $d = 2$ is at the lower critical dimensionality of the transition, which has important implications for the length and time scales required to observe the asymptotic behavior [108]. Most of the work published in the five years following the seminal paper [14] of Kardar, Parisi and Zhang attempted to elucidate the nature of the transition, and to obtain accurate numerical estimates of the strong coupling scaling exponents. These efforts have been reviewed elsewhere [8]; for a representative sample of current numerical work see Ref.[109].

Recent analytic approaches have yielded promising but not quite conclusive

results. Two-loop renormalization group (RG) calculations were presented by Sun and Plischke [110] and by Frey and Täuber [111]. Whereas Sun and Plischke claim to identify the strong coupling fixed point in $d=2$ and derive estimates for the scaling exponents, the analysis of Frey and Täuber indicates a scenario that is similar to the earlier one-loop results [14, 65] - only the critical fixed point governing the phase transition is accessible in an expansion around $d=2$ dimensions, but the strong coupling regime remains elusive.

The non-perturbative nature of this regime suggests that self-consistent mode-coupling approaches [112] may be more appropriate than perturbative RG schemes. Mode-coupling equations were written down earlier in related contexts [113, 114, 115, 116], but only recently have approximate solutions been attempted [117, 118] in order to extract the dimensionality dependence of the strong coupling exponents. Moore, Blum, Doherty, Bouchaud and Claudin [119] have found an *analytic* solution of the mode-coupling equations for $d>4$, which indicates that $d=4$ may play the role of an upper critical dimensionality, in the sense that the dynamic scaling exponent in the strong coupling phase takes on its weak coupling value $z=2$ for $d\geq 4$. Such a scenario was suggested earlier by Halpin-Healy on the basis of a functional RG calculation [120, 121], but so far the numerical evidence [109] does not seem to support it.

A third analytic approach that holds considerable promise with regard to an improved understanding of the strong coupling regime is the study of anisotropic generalizations of the KPZ equation. Building upon the observation of Villain [15] that growth on vicinal crystal surfaces (in the presence of desorption) may display a regime in which the two coefficients λ_1, λ_2 in (4.3) have different signs, Wolf [122] showed that in such a situation the nonlinearities are in fact (marginally) *irrelevant*, i.e. the strong coupling regime disappears and the surface is described by the linear theory (up to logarithmic corrections). Subsequently, Fisher and Grinstein [123] and Hwa [124] considered, in the contexts of electrical transport in insulators and driven flux line liquids, respectively, higher dimensional anisotropic variants of the KPZ equation. Depending on the number of nonzero coefficients λ_i in (4.3) and on their relative signs, strong coupling behavior may or may not be present. Therefore the anisotropic equation can be used to systematically interpolate [124] between the (isotropic) KPZ equation and the problem of driven diffusive systems, DDS [114], which corresponds, roughly speaking, to a situation where only one of the λ_i is nonzero. The DDS problem does not possess a strong coupling regime and is therefore amenable to standard perturbative analysis [125].

Outline of chapter. In the remainder of the chapter we shall be concerned almost exclusively with the *one-dimensional* KPZ equation. The one-dimensional prob-

lem is special due to the validity of a fluctuation-dissipation theorem which fixes the values of the scaling exponents (Section 4.1). This allows one to pose more refined questions regarding scaling functions, universal amplitudes and the probability distribution of height fluctuations [126] (Sections 4.2 and 4.3). Section 4.4 briefly reviews recent work on interface displacement processes in which the fluctuations are of *chaotic* origin [127], while Section 4.5 introduces the well-known 'directed polymer' representation of the KPZ equation. Finally, Section 4.6 addresses the problem of KPZ-type growth in the presence of defects [128] or open boundaries [129], which break the translational symmetry in the substrate (x-) direction. In such situations the nontrivial *dynamic* scaling properties of the KPZ equation reappear in the *spatial* domain in the form of power law height profiles and correlations, which in some cases can be computed exactly [130, 131]. Moreover, morphological phase transitions can be induced by the defects, which have a particularly appealing interpretation in the directed polymer representation [132].

4.1 Exact invariants

The one-dimensional KPZ equation has two important invariance properties, the first of which applies in arbitrary dimensionalities d. To derive it, consider the *tilt transformation*

$$h'(\mathbf{x},t) = h(\mathbf{x}-\mathbf{u_0}t,t) - \frac{1}{\lambda}\mathbf{u_0}\cdot\mathbf{x} + \frac{1}{2\lambda}\mathbf{u_0}^2 t \tag{4.4}$$

parametrized by some d-dimensional vector $\mathbf{u_0}$. It is easily checked that h' satisfies the same KPZ equation (4.1) as h, with a shifted noise term

$$\eta'(\mathbf{x},t) = \eta(\mathbf{x}-\mathbf{u_0}t,t). \tag{4.5}$$

Provided the temporal correlations of η are sufficiently short ranged, the shift does not affect the statistical properties of the noise [65], and we may conclude that the statistics of the height fluctuations are invariant under the transformation (4.4). In the literature this property is often referred to as *Galilean invariance*, since it was first discussed by Forster, Nelson and Stephen [133] in the context of randomly stirred fluids governed by the noisy Burgers equation

$$\frac{\partial \mathbf{u}}{\partial t} + \mathbf{u}\cdot\nabla\mathbf{u} = \nu\nabla^2\mathbf{u} - \lambda\nabla\eta \tag{4.6}$$

which follows from (4.1) with the identification $\mathbf{u} = -\lambda\nabla h$; the tilt transformation (4.4) is precisely a Galilean transformation for the fluid velocity $\mathbf{u}$. In the context of interface motion the tilt invariance appears as a residue of the full rotational symmetry of the isotropic equation (3.6).

The significance of the tilt invariance lies in the fact that the transformation (4.4) contains explicitly the coefficient λ. Thus, if the invariance is to be preserved under coarse graining, it is clear that the rescaling operation (3.53) should not change the value of λ. From the last of eqs.(3.55) we read off that this enforces the exponent identity [19, 65, 115]

$$\zeta + z = 2 \tag{4.7}$$

between the roughness exponent and the dynamic exponent.

In order to determine the values of ζ and z individually, we would require a second identity derived from some invariant combination of the coefficients ν, D and λ. No such invariant is known for $d > 1$; in the one-dimensional case the appropriate combination is the ratio D/ν. In fact a much stronger statement holds [8, 133, 134]: The Gaussian stationary probability distribution of the ($z = 2$) linear theory

$$\mathcal{P}[h] \sim \exp\left[-\frac{\nu}{D}\int dx\,(\nabla h)^2\right] \tag{4.8}$$

is the stationary solution also of the full Fokker-Planck equation that corresponds to the nonlinear KPZ equation. This can be seen by computing the contribution introduced by the KPZ nonlinearity on the right hand side of the Fokker-Planck equation,

$$\frac{\delta}{\delta h}\int dx\,\frac{\lambda}{2}(\nabla h)^2\,\mathcal{P}[h] = \left[\int dx\,\lambda(\nabla h)^2\frac{\nu}{D}\nabla^2 h\right]\mathcal{P}[h] \tag{4.9}$$

which vanishes by partial integration (assuming periodic boundary conditions in x). Similar results can be proved for certain microscopic realizations of the KPZ equation [8].

The remarkable conclusion is that *all* stationary correlations of the nonlinear KPZ equation in one dimension are given *exactly* by the linear theory. Specifically, for the transient roughening of an intially flat interface considered in Section 3.2, we know that the two-point function $S(q,t)$ defined by (3.24) satisfies

$$\lim_{t\to\infty} S(q,t) = L^{-1}\frac{D}{2\nu q^2}; \tag{4.10}$$

corresponding relations for higher order correlations follow immediately from the Gaussian nature of the probability density (4.8). A particular consequence is that the roughness exponent $\zeta = 1/2$ as in the linear case, and the dynamic exponent $z = 3/2$ from the scaling relation (4.7). It is much harder to demonstrate directly that $z = 3/2$; for a particular microscopic model this has been achieved by Gwa and Spohn [135].

We now exploit the invariance of λ and D/ν to determine the full scaling form of $S(q,t)$. First, we derive an expression for the dynamic correlation length $\xi(t)$

using only dimensional arguments. From the KPZ equation (4.1), the dimensions of λ and D/ν are given by

$$[\lambda] = [x]^2/[h][t], \; [D/\nu] = [h]^2/[x]. \tag{4.11}$$

The task is to construct a lateral length scale (of dimension $[x]$) from the invariant quantities λ, D/ν, and the time t. The only solution is

$$\xi(t) = [(D/2\nu)^{1/2}\lambda t]^{2/3} \tag{4.12}$$

where a factor of 2 has been inserted for later convenience. Together with the asymptotic constraint (4.10) it follows that S can be written as

$$S(q,t) = L^{-1}\frac{D}{2\nu q^2} g(q\xi(t)) \tag{4.13}$$

where, in analogy with the expressions (3.25) and (3.29) derived in the linear case, g is now expected to be a *universal* function with the limiting behaviors

$$g(0) = 0, \; \lim_{s\to\infty} g(s) = 1. \tag{4.14}$$

In the linear theory (4.13) holds with $g(s) = 1 - e^{-s^2}$. The scaling function for the KPZ-equation is not known explicitly. Approximate analytic results for a closely related function describing the temporal correlations in the stationary state have been presented by several groups [114, 116, 125]. In the next section we show how the scaling function can be characterized through dimensionless amplitudes of statistical observables such as the interface width.

4.2 Universal amplitudes

Using the scaling form (4.13) we can proceed to compute real space correlation functions from the general formulae (3.26) and (3.27). Since all stationary ($t \to \infty$) correlations are identical to those of the linear theory, the focus is on *transient* quantities, i.e. we take the limit $L \to \infty$ at fixed t. For the width this yields the expression

$$W^2 = c_2[(D/2\nu)^2|\lambda|t]^{2/3} \tag{4.15}$$

with a dimensionless prefactor c_2 that is expressed in terms of the universal scaling function g as

$$c_2 = \frac{1}{\pi}\int_0^\infty \frac{ds}{s^2} g(s). \tag{4.16}$$

Similar expressions can be written for higher order correlation functions and higher moments of the height fluctuation distribution. Of particular interest are quantities that reveal the deviation of the distribution from a Gaussian, such as the skewness

$$\mathcal{S} = \frac{\langle (h - \langle h\rangle)^3\rangle}{\langle (h - \langle h\rangle)^2\rangle^{3/2}} \tag{4.17}$$

and the normalized fourth cumulant

$$\mathcal{Q} = \frac{\langle (h - \langle h \rangle)^4 \rangle}{\langle (h - \langle h \rangle)^2 \rangle^2} - 3. \tag{4.18}$$

The skewness is a measure of the asymmetry of the fluctuation distribution, to be expected because the growth direction breaks the $h \to -h$ symmetry, while $\mathcal{Q}$ gauges the weight contained in the tails of the distribution relative to a Gaussian; for a Gaussian $\mathcal{S} = \mathcal{Q} = 0$. Simulations of a variety of microscopic models belonging to the KPZ universality class indicate [126, 136] that the skewness in the transient regime converges to a universal value $|\mathcal{S}| = 0.28 \pm 0.04$ and the sign of $\mathcal{S}$ is equal to the sign of λ in (4.1); the value of $\mathcal{Q}$ is in the range $\mathcal{Q} \approx 0.12 - 0.16$. The theoretical significance of these results was recently discussed by Friedberg and Yu [137].

A few remarks are in order regarding the numerical procedure [126, 138] employed to extract universal amplitudes like c_2, $\mathcal{S}$ and $\mathcal{Q}$ from simulations of microscopic models. Two steps are involved. First, the transient behavior of the quantity of interest (e.g., the width) is measured, executing care that the asymptotic ($W^2 \sim t^{2/3}$) regime is well established in the time range used to determine the prefactor. Then, in order to arrive at *dimensionless* coefficients such as c_2, the dimensionful invariants D/ν and λ have to be computed for the particular model at hand. In a few cases this can be done analytically [126], however in general one has to resort to simulations. The ratio D/ν figures prominently in the correlation functions of the linear theory, and can therefore be obtained from numerically determined *stationary* quantities, using exact relations like (3.39). The coefficient λ is most easily estimated from a direct measurement of the tilt dependence of the growth rate [107], as defined in (4.3); for this purpose a macroscopic tilt $u = \langle \nabla h \rangle$ is imposed through *helical* boundary conditions, $h(x + L) = h(x) + uL$ (for an example see Figure 17).

The knowledge of the universal amplitude c_2 can be exploited to estimate the crossover time t_c at which the interface width saturates in a finite system, i.e. the nonlinear analogue of (3.41). To this end we match the transient expression (4.15) to the stationary result (3.39) (with $z = 2$), and obtain

$$\xi(t_c)/L = (12 c_2)^{-1} \approx 0.21, \tag{4.19}$$

with the numerical estimate [126] $c_2 \approx 0.40$. Similar considerations apply to the crossover from an intermediate, Edwards-Wilkinson scaling regime in cases where the value of the nonlinearity in (4.1) is small (in a dimensionless sense) compared to the linear term $\nu \nabla^2 h$. Matching the KPZ asymptotics (4.15) to the exact expression (3.40) for the transient regime of the $z = 2$ linear (EW) equation, the crossover is found to occur at a time

$$t_c^{EW \to KPZ} = 32 \pi^{-3} c_2^{-6} \nu^5 D^{-2} |\lambda|^{-4} \approx 252 \; \nu^5 D^{-2} |\lambda|^{-4}. \tag{4.20}$$

This relation has been particularly useful in identifying the asymptotic behavior in models of *chaotic* interfaces, to be described in Section 4.4.

4.3 Finite size effects

An interesting feature of the nonlinear term in the KPZ equation is the coupling that it induces between the spatially averaged, center of mass motion of the interface

$$\overline{h}(t) = h_{q=0}(t) = L^{-1} \int_0^L dx\, h(x,t) \tag{4.21}$$

and the internal fluctuation modes. This is illustrated by writing the instantaneous global interface velocity as

$$v(t) \equiv \frac{d\overline{h}}{dt} = \frac{\lambda}{2} \sum_{q \neq 0} q^2 \, |h_q(t)|^2 + \eta_{q=0}(t). \tag{4.22}$$

Several important conclusions can be drawn from this expression. First, averaging over both sides and taking $t \to \infty$ we find, using (4.10), that the right hand side is a sum over $N-1$ identical terms $L^{-1}(D/2\nu)$, where $N = L/a$ is the total number of modes (the $q=0$ mode does not contribute). It follows that the stationary average growth rate has a universal finite size correction [139]

$$\Delta v = \langle v(L) \rangle - \langle v(\infty) \rangle = -\frac{D\lambda}{4\nu L}; \tag{4.23}$$

the average growth rate itself, $\langle v(\infty) \rangle = D\lambda/4\nu a$, depends on the lattice cutoff a and is therefore nonuniversal. Similarly in the transient regime one finds a correction proportional to $t^{-2/3}$. The non-dimensional coefficient in (4.23) is altered when the periodic boundary conditions are replaced by open ones [132].

Second, the coupling to the internal modes induces [140] *long ranged temporal correlations* in the growth rate, on time scales smaller than the correlation time $t_c \sim L^{3/2}$. This effect is displayed in the center of mass dispersion

$$W_c^2 = \langle (\overline{h} - \langle \overline{h} \rangle)^2 \rangle \tag{4.24}$$

obtained by twice integrating the velocity correlation function $\langle v(t)v(s) \rangle$. In one dimension, this quantity behaves as

$$W_c^2 \sim \begin{cases} L^{-1}\, t^{4/3} & : \quad t \ll L^{3/2} \\ L^{-1/2}\, t & : \quad t \gg L^{3/2}, \end{cases} \tag{4.25}$$

i.e. the dispersion is *superdiffusive* in the transient regime, leading to a $1/f$-type divergence in the velocity power spectrum [114, 123, 140, 141]. In the stationary

regime ordinary diffusion is recovered, however with a prefactor that is enhanced relative to the $1/L$-dependence of the linear theory (see below).

Equation (4.25) highlights the necessity of carefully distinguishing between the ensemble average $\langle h \rangle$ and the spatial average $\overline{h}$ in a finite system. The height fluctuation relative to the *ensemble* average

$$\tilde{W}^2 \equiv \langle (h - \langle h \rangle)^2 \rangle \tag{4.26}$$

is *dominated* by the center of mass dispersion for $t > t_c$, where $W_c^2 \gg W^2$, and $\tilde{W}$ can be equated to the conventional definition (3.26) of the width W only for $t \ll t_c$; of course in simulations $\tilde{W}$ is of little relevance, since the ensemble average $\langle h \rangle$ is generally not known.

These considerations apply also at the level of the linear theory, however there they are comparatively trivial since the center of mass motion only couples to the $q = 0$ mode of the noise, so that $W_c^2 = Dt/L^d$ for all times. Incidentally, this remains true in nonlinear theories with conserved relaxation - indeed, the requirement of volume conservation in all relaxation processes implies precisely that these processes do not couple to the average height. In RG language this leads to the nonrenormalization of the noise strength D and the concomitant exponent identity [80, 86, 95, 96, 140]

$$z = d + 2\zeta, \tag{4.27}$$

as can be read off from the scaling transformation (3.55).

It is instructive to rederive the second part of (4.25) from a scaling argument. Dimensionally, W_c^2 is no different from the width W^2, hence one should be able to write a scaling form analogous to (3.31),

$$W_c^2 = \frac{D}{2\nu} L \, f_c(\xi/L). \tag{4.28}$$

To inform the shape of the scaling function f_c, we note that for times large compared to the correlation time, i.e. for $\xi \gg L$, the interface velocity becomes uncorrelated and one expects that $W_c^2 \sim t$. Since the KPZ correlation length behaves as $\xi \sim t^{2/3}$, this requires that $f_c(s) = c_0 s^{3/2}$ for large arguments, and using the expression (4.12) we obtain

$$W_c^2 = c_0 (D/2\nu)^{3/2} |\lambda| \, L^{-1/2} t \quad (t \gg L^{3/2}) \tag{4.29}$$

which determines also the prefactor in (4.25) up to the universal constant c_0.

Remarkably, the amplitude c_0 is known analytically by virtue of a recent exact solution of a specific model due to Derrida, Evans and Mukamel [142] (DEM). These authors were concerned with the tracer diffusion of particles in a one-dimensional lattice gas with hard core repulsion, the asymmetric simple exclusion process (ASEP).

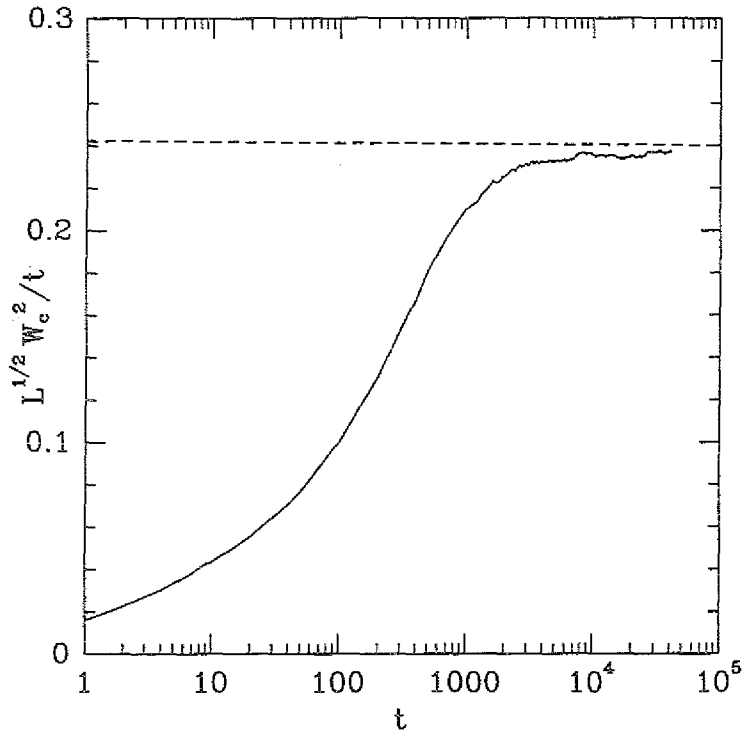

Figure 15: Center of mass fluctuation W_c^2 of the interface in the restricted solid-on-solid growth model of Kim and Kosterlitz [143], scaled by system size ($L = 100$) and time according to the scaling form (4.29). The data represent an average over 10^4 independent runs, extending over 4×10^4 deposition attempts per site. The dashed line is the prediction for the prefactor obtained from (4.29) with the universal amplitude (4.34) and the dimensionful parameters $D/2\nu = 0.81$ and $\lambda = -0.75$ which were determined numerically in Ref.[126].

The equivalence between the ASEP and a simple growth model, the single step model, has been known for some time [8, 19]. Any configuration of lattice gas occupation numbers $\epsilon_i = 0, 1$ can be mapped onto a solid-on-solid interface through the identification $h_{i+1} - h_i = 1 - 2\epsilon_i = \pm 1$, the integer height variables h_i specifying the interface position. In the ASEP particles jump to the right to vacant nearest neighbor sites; each jump increases the local height as $h_i \to h_i + 2$. Thus, h_i measures (twice) the *time-integrated particle current* through bond i. DEM compute the time-integrated displacement Y_t of a tagged particle, and show that, for long times,

$$\langle Y_t^2 \rangle - \langle Y_t \rangle^2 = \Delta\ t \tag{4.30}$$

with a diffusion constant

$$\Delta = \frac{\sqrt{\pi}}{2} \frac{(1-\rho)^{3/2}}{\rho^{1/2}} \frac{1}{L^{1/2}}, \tag{4.31}$$

where $0 < \rho < 1$ denotes the particle density. Equation (4.31) represents the leading

behavior in $1/L$ when the stationary limit $t \to \infty$ is performed first, followed by the limit $L \to \infty$ at fixed density ρ.

To establish the connection with (4.29), note first that since the particle current is equal to the product of density and velocity, the time integrated current is ρY_t and $h = 2\rho Y_t$. Equations (4.30) and (4.31) therefore translate into

$$\tilde{W}^2 = \langle (h - \langle h \rangle)^2 \rangle = 2\sqrt{\pi}[\rho(1-\rho)]^{3/2} t/L^{1/2} \tag{4.32}$$

which is also equal to W_c^2 in the stationary ($t \gg L^{3/2}$) regime considered here. Next we remark that the stationary correlations of the ASEP (with periodic boundary conditions!) are trivial: For $L \to \infty$ every site is occupied independently with probability ρ (for an explicit proof see Refs.[19] and [141]). Consequently it is an easy matter to show that the dimensionful invariants of the equivalent growth model are [126]

$$\lambda = -1, \; D/2\nu = 4\rho(1-\rho). \tag{4.33}$$

Thus (4.32) conforms exactly to the scaling prediction (4.29), and allows us to identify the dimensionless prefactor as

$$c_0 = \sqrt{\pi}/4. \tag{4.34}$$

The universality of this number is illustrated by simulation results for the center of mass dispersion of a different growth model, the restricted solid-on-solid model of Kim and Kosterlitz [143] (Figure 15). For this model the quantities D/ν and λ are known only numerically [126].

4.4 Chaotic interfaces

4.4.1 The Kuramoto-Sivashinsky equation

A number of recent studies have been devoted to purely deterministic models of interface motion where the fluctuations, rather than being induced externally by thermal or kinetic noise, are generated by some local *chaotic* dynamics. The prime representative for this class of systems is the Kuramoto-Sivashinsky equation

$$\partial h/\partial t + \nabla^2 h + \nabla^4 h - (\nabla h)^2 = 0 \tag{4.35}$$

which appears as an asymptotic local approximation to various moving boundary value problems, such as laminar flame propagation [144], solidification at large undercooling [145] and terrace edge evolution during step flow growth [146, 147] (see also Section 5.2.1). Similar equations have been derived also in plasma physics [148] and in the context of chemical turbulence [113, 149].

The units in (4.35) have been chosen such that all coefficients are equal to unity. Usually the one-dimensional equation is considered, with periodic boundary conditions on an interval of length L. The trivial solution $h = const.$ is linearly unstable when $L > 2\pi$. For large L, almost all initial conditions evolve to a state of *spatiotemporal chaos*, which can be viewed as a collection of cell-like structures that split and merge in a random fashion. The cell size is set by the wavelength $\ell_0 = \sqrt{2}(2\pi)$ with the largest growth rate $1/\tau_0 = 1/4$ under the linearized dynamics.

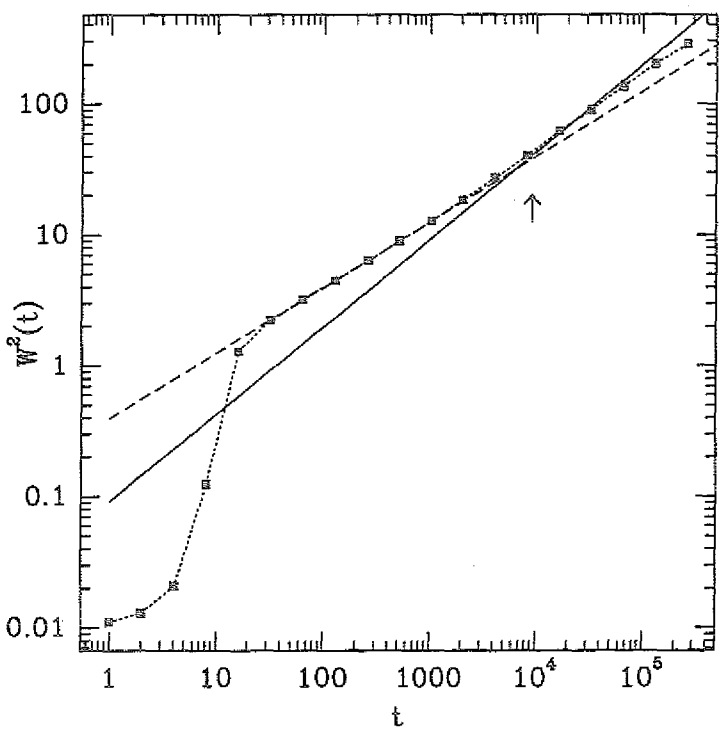

Figure 16: Width of a one-dimensional Kuramoto-Sivashinsky interface of length $L = 65536$. The squares show numerical data obtained by averaging over 70 independent runs. The dashed line is a fit to the early time Edwards-Wilkinson behavior, $W^2 = 0.397\, t^{1/2}$. The full line represents the asymptotic KPZ-behavior, $W^2 = 0.092\, t^{2/3}$, with the prefactor calculated from (4.15) using the numerical estimates of $D/2\nu$ and λ. The arrow indicates the crossover time $t_c^{EW-KPZ} \approx 7000$ predicted from (4.20). The last few data points are already affected by finite size effects - the saturation time determined by (4.19) is about 3×10^5 for this system size. [127]

In the present context, the fundamental question is to what extent the large scale dynamics of this 'turbulent' state, coarse grained beyond the typical cell size ℓ_0, can be described by a *stochastic* theory of kinetic roughening. Yakhot [150] was the first to suggest, on the basis of a renormalization group coarse graining procedure, that the appropriate large scale theory is the KPZ equation (at the time known as

the noisy Burgers equation [133]). Yakhot's conjecture is very plausible intuitively: It only requires that (i) the stabilizing effect of the nonlinearity in (4.35) can be described in terms of a positive, effective interfacial tension $\nu > 0$ on large scales, and (ii) the random cell interaction events are sufficiently uncorrelated to give rise to a white noise forcing.

A careful numerical test of the conjecture was performed by Zaleski [151], who found it exceedingly difficult to assess the asymptotic KPZ regime. A subsequent quantitative crossover analysis [127], utilizing the amplitude relations derived in Section 4.2, estimated that the asymptotic behavior sets in only on length scales $L > 2500$ and time scales $t > 7000$ (Figure 16). Somewhat paradoxically, the crossover time (4.20) is large because of the large value of the effective interface tension ν, which starts out being *negative* on the 'microscopic' (= sub cell size) level. Assuming that ν is generated by the cell dynamics, a rough estimate involving the characteristic cell scales is $\nu = \ell_0^2/\tau_0 = 19.7$. Numerically, one finds $\nu = 10.5 \pm 0.6$ [127].

The intuitive picture suggests that a KPZ-type large scale description should apply also in higher dimensions. Recent numerical work in two dimensions [152, 153] has not succeeded in unambiguously confirming this hypothesis, and the issue remains controversial. It is unclear at present whether the problem is only one of computational resources, or whether the two-dimensional equation is different from the one-dimensional case in some more fundamental way.

We briefly comment on the relationship between the Kuramoto-Sivashinsky equation (4.35), and the Golubović-Bruinsma equation (3.56), which may be viewed as the $\nu_0 \to 0$ limit of the generalized KPZ-equation

$$\partial h/\partial t = \nu_0 \nabla^2 h - \nabla^4 h + (\nabla h)^2 + \eta. \tag{4.36}$$

The work summarized in this section has shown that an interface governed by (4.35) with zero external noise strength, $D = 0$, and a *negative* bare interface tension $\nu_0 < 0$ can be described on large scales by an equation with a nonzero intrinsic noise strength $D_{\rm intr} > 0$ and a *positive* effective tension $\nu > 0$. It appears plausible that the properties of the chaotic state of (4.35) should not be qualitatively altered by the addition of an external noise source. Moreover, if the nonlinearity in (4.36) is capable of generating a positive interface tension out of a negative bare value $\nu_0 < 0$, this should remain true in the limit $\nu_0 \to 0^-$. Thus, one is lead to conclude that a positive interface tension would be generated also in the case of eq.(3.56), in contradiction to the $\epsilon = 8 - d$ expansion of Golubović and Bruinsma [85].

The argument is somewhat less firm than it seems, because it presupposes that the limit $\nu_0 \to 0$ in (4.36) (which takes (4.36) to (3.56)) commutes with the limit $D \to 0$ (which takes (4.36) to (4.35)). To gain some insight into this issue, consider

(4.36) with $D=0$ and $\nu_0<0$. This reduces to the parameter-free equation (4.35) through the transformation

$$\tilde{h}(x,t)=|\nu_0|^{-1}h(|\nu_0|^{-1/2}x,|\nu_0|^{-2}t). \tag{4.37}$$

Using this transformation together with the results obtained for (4.35) in Ref.[127], it is an easy matter to show that the effective large scale interface tension of the deterministic version of (4.36) vanishes as $\nu\sim-\nu_0$, and the intrinsic noise strength vanishes as $D_{\rm intr}\sim|\nu_0|^{7/2}$ when $\nu_0\to 0$. If the limit $\nu_0\to 0$ is performed at fixed external noise strength $D>0$, one therefore enters a regime where the external noise dominates over that generated by the chaotic fluctuations, and which may behave differently from the deterministic equation (4.35). The transition between the two regimes was studied numerically by Karma and Misbah [147], who find a smooth crossover with no singular features.

4.4.2 Coupled circle maps

It should be emphasized that, since (4.35) contains no control parameters apart from the system size L, the large crossover scale in one (and possibly also two) dimensions is an *intrinsic* property of the equation. This lack of versatility was one of the motivations that lead Bohr and coworkers [154, 155] to introduce lattices of *coupled circle maps* as a new class of chaotic interface models. These models are defined in terms of real, unbounded height variables $h_t(i)$ that live in discrete time and on a discrete space (the integer lattice, for the present discussion). In the absence of coupling each variable is updated according to a rule that is a combination of a constant shift (to break the $h\to -h$ symmetry) and a nonlinear map on the unit interval acting on the fractional part of h,

$$h\to F(h)=h+f(h-[h]). \tag{4.38}$$

A typical choice is the logistic map, $f(x)=Rx(1-x)$. Two kinds of coupling schemes have been considered [154, 155]: A *diffusive* coupling defined by

$$h_{t+1}(i)=F(h_t(i))+\epsilon(h_t(i+1)+h_t(i-1)-2h_t(i)) \tag{4.39}$$

and a *totalistic* coupling

$$h_{t+1}(i)=F(\{h_t(i+1)+h_t(i)+h_t(i-1)\}/3). \tag{4.40}$$

It turns out [155] that the magnitude of the KPZ nonlinearity in the large scale dynamics, and therefore the observability of KPZ scaling, depends crucially on the choice of coupling. This is illustrated in Figure 17, which shows the variation

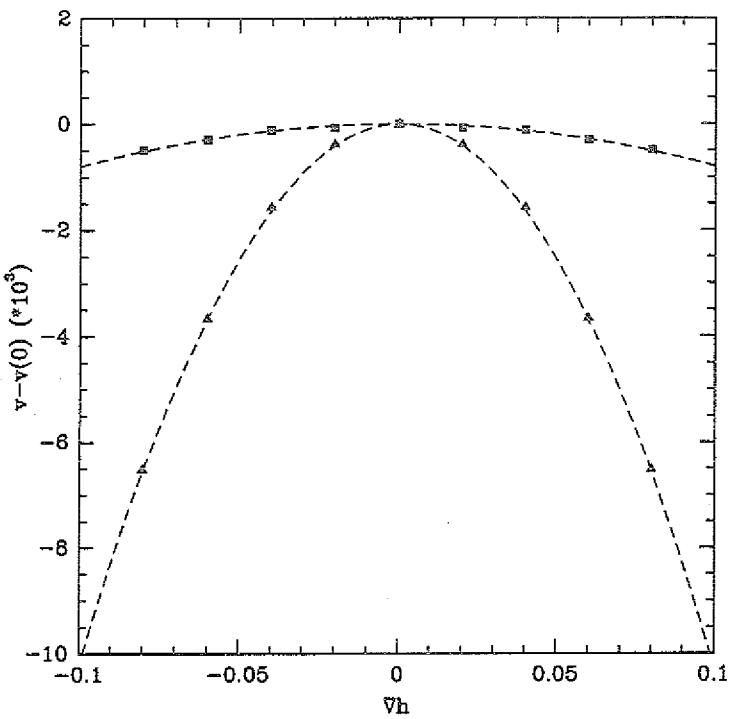

Figure 17: Inclination dependence of the interface velocity v for coupled circle maps with diffusive (squares) and totalistic (triangles) coupling. The local updating rule (4.38) was the logistic map with $R=4$ in both cases. The data were obtained from simulations of systems of size $L=1000$, with a duration of 10^6 time steps per data point. The dashed lines indicate parabolic fits.

of the average interface velocity $v=\langle h_{t+1}(i)-h_t(i)\rangle$ with inclination $\nabla h=\langle h_t(i+1)-h_t(i)\rangle$, for the two coupling schemes (4.39) (with $\epsilon=0.2$) and (4.40). From the indicated parabolic fits one estimates that $\lambda\approx -0.16$ for the diffusive coupling, and $\lambda\approx -2.0$ in the totalistic model. According to (4.20), this implies that the crossover times to asymptotic KPZ behavior differ by a factor of 2.4×10^4! Indeed, while clean KPZ scaling was observed in simulations of the totalistic rule, with the diffusive coupling only the preasymptotic EW regime could be accessed [155].

Clearly, the coupled map models differ from the Kuramoto-Sivashinsky equation (4.35) in several, possibly important, respects. Here, the chaotic fluctuations arise (for appropriate choices of f) simply from the local updating rule (4.38); there is no analogue of the unstable spatial coupling in (4.35), nor of the resulting cellular structure. Also, the coupled map models have only discrete translational symmetry in i and h; moreover, in two dimensions the continuous *rotational* symmetry of (4.35) is lost. Nevertheless, the great variability that can be achieved by different choices of local maps and different coupling schemes makes them promising objects

for explorative studies of spatiotemporal chaos.

4.5 Directed polymers in random media

The directed polymer representation [14, 65] of the KPZ equation provides a link between the *nonequilibrium* dynamics of interfaces and the *equilibrium* statistical mechanics of flexible lines in a quenched random environment. The conceptual basis of the mapping between the two problems is quite simple. The d-dimensional substrate space of the interface is enlarged into a $d+1$-dimensional space by treating the time direction as an additional coordinate. Thereby each noise history $\eta(\mathbf{x},t)$ can be viewed as a realization of a quenched random potential in $d+1$ dimensions. The time evolution of the interface is then encoded by an ensemble of 'infection paths', to be specified shortly, which are directed along the t-axis. The statistical weight of each path can be written as a Boltzmann factor with an energy that comprises an elastic term and a random contribution due to the disorder potential. Thus, the paths can be identified with conformations of physical objects such as flux lines, directed polymers or (in $d=1$) *equilibrium* interfaces.

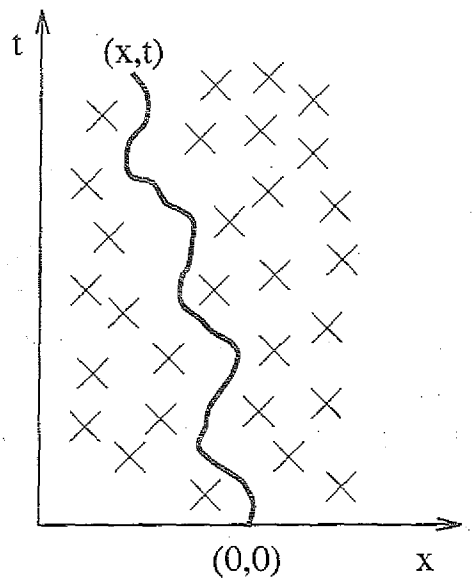

Figure 18: Directed line in a random potential, indicated by the crosses.

Mathematically, the mapping is achieved through the Cole-Hopf transformation, which was discovered some forty years ago as a means to exactly linearize the (deterministic, one-dimensional) Burgers equation [156]. Here, we shall proceed in the converse direction - we first state the directed polymer problem, and then show how it leads to the KPZ equation. Throughout this section we will be working with a general number of transverse dimensions d, and return to specific applications to $d=1$ in Section 4.6.

Consider then a directed line that runs through the random potential η, connecting the origin $(\mathbf{0},0)$ to some endpoint $(\mathbf{x},t)$ (Figure 18). The total energy of the line can be written as

$$\mathcal{H}[\mathbf{y}(s)] = \int_0^t ds \left[\frac{\gamma}{2} \left(\frac{d\mathbf{y}}{ds} \right)^2 + \eta(\mathbf{y}(s), s) \right] \tag{4.41}$$

with a line tension $\gamma > 0$. The restricted partition function of all conformations that run from $(\mathbf{0},0)$ to $(\mathbf{x},t)$ takes the form of a path integral,

$$\mathcal{Z}(\mathbf{x},t) = \int_{(\mathbf{0},0)}^{(\mathbf{x},t)} \mathbf{D}\mathbf{y}[\cdot] e^{-\mathcal{H}[\mathbf{y}]/k_B T}. \tag{4.42}$$

By standard techniques [157] this is brought into the differential form of a diffusion equation,

$$\frac{\partial \mathcal{Z}}{\partial t} = \frac{k_B T}{2\gamma} \nabla^2 \mathcal{Z} - \frac{1}{k_B T} \eta \mathcal{Z}. \tag{4.43}$$

In the last step we introduce the restricted free energy

$$\mathcal{F}(\mathbf{x},t) = -k_B T \ln \mathcal{Z}(\mathbf{x},t) \tag{4.44}$$

which satisfies, according to (4.43), the KPZ equation

$$\frac{\partial \mathcal{F}}{\partial t} = \frac{k_B T}{2\gamma} \nabla^2 \mathcal{F} - \frac{1}{2\gamma} (\nabla \mathcal{F})^2 + \eta \tag{4.45}$$

with coefficients $\nu = k_B T / 2\gamma$ and $\lambda = -1/\gamma$. The equivalence between (4.42) and (4.45) was first observed by Huse, Henley and Fisher [134].

Several remarks are in order. First, since (4.45) is written for $\mathcal{F}$ rather than for $\mathcal{Z}$, the *thermal* average is already implicitly performed when describing the directed polymer by the KPZ equation, whereas the conventional noise average in the interface dynamics corresponds to a subsequent *disorder* average. The succession of the two averages implies that we are dealing with a case of *quenched* disorder. Second, it should be noted that the natural initial condition for $\mathcal{F}$ is different from the flat initial state commonly considered in the interface context: From the definition of the path integral (4.42) we have $\mathcal{Z}(\mathbf{x},0) = \delta^d(\mathbf{x})$, corresponding to a deep narrow groove in the 'interface' $\mathcal{F}(\mathbf{x},t)$. Third, it is clear from the derivation that the mapping always leads to the *isotropic* KPZ equation; different signs of the λ_i in (4.3) cannot be accomodated [122]. This hints at some fundamental differences between the isotropic and anisotropic equations, which still wait to be elucidated.

Readers who feel uneasy about the formal manipulations of the continuum path integral (4.42) will be reassured to learn that the mapping can be formulated and explicitly carried out also on the level of microscopic, stochastic lattice growth models [8, 132, 158]. In these cases the resulting directed polymer problem typically

resides as *zero temperature*, so that the thermal average is replaced by the selection of a single, optimal ground state path. This is nonessential as long as the finite (low) temperature behavior and the behavior at $T=0$ fall into the same universality class, which is true for the standard directed polymer (see below) but fails e.g. in the presence of columnar disorder [159] (see Section 4.6.3).

We summarize the main correspondences induced by the mapping (details can be found in the cited literature). The rough interface configuration $h(\mathrm{x},t)$ translates into the rugged free energy landscape felt by a polymer of length t. The interface velocity equals the free energy per unit length $f=\partial\mathcal{F}/\partial t$. This immediately provides us with an appealing interpretation of the finite size correction to the stationary interface velocity derived in Section 4.3: Identifying the coefficients from (4.45) we see that (4.23) expresses the increase in the free energy per unit length

$$\Delta f=\frac{D}{2k_BTL} \tag{4.46}$$

due to the *confinement* of the polymer to a cylinder of circumference L. The effect is analogous to the increase in free energy incurred by a thermally excited line (in the absence of disorder) confined to a region of lateral extent L, due to the loss of configurational *entropy* [160]. The corresponding expression

$$\Delta f_{\mathrm{thermal}}\sim\frac{(k_BT)^2}{\gamma L^2} \tag{4.47}$$

is easily derived [132] from (4.45) with $\eta=0$ and appropriate boundary conditions. Besides the different L-dependences of (4.46) and (4.47), which show that the disorder always dominates the behavior on scales large than $L_c=(k_BT)^3/\gamma D$, it is interesting to note the opposite roles played by temperature in the two cases, as well as the fact that (4.46), in contrast to (4.47), is independent of the line tension γ.

Somewhat less obviously, the dynamic correlation length $\xi(t)\sim t^{1/z}$ turns out to be proportional to the *transverse displacement* of the polymer

$$\delta x(t)=\langle[\mathrm{x}(t)]^2\rangle^{1/2}\sim\xi(t)\sim t^{1/z}, \tag{4.48}$$

where square (angular) brackets indicate thermal (disorder) averages. The displacement is superdiffusive when $z<2$, due to the random potential which encourages large transverse fluctuations; diffusive behavior, $z=2$, is characteristic of the entropic wandering of a thermally excited line.

The directed polymer representation has been instrumental in developing an intuitive understanding of the weak coupling/strong coupling phase transition of the KPZ equation in dimensions $d>2$. In the directed polymer context the transition

appears as a thermal phase transition between a disorder-dominated, glassy low temperature phase (strong coupling) and a high temperature phase in which the polymer is essentially unobstructed by the disorder (weak coupling). Rigorous proofs for the existence of the transition, and bounds on the transition temperature have been obtained [8, 161].

Another issue that deserves more than summary treatment is the interpretation of the tilt (or Galilean) invariance of the KPZ equation in the directed polymer language. We have argued in Section 4.1 that, as a consequence of the invariance of the equation under the tilt transformation (4.4), the coefficient λ of the nonlinearity is not renormalized. From (4.45) we see that this implies the nonrenormalization of the polymer line tension γ. Indeed, by applying the tilt invariance argument on the level of the partition function (4.42) it can be shown [162] that the *average* elastic response of the polymer is completely unaffected by the disorder, in the sense that the average free energy profile for a polymer of length t, fixed at the origin, is

$$\langle \mathcal{F}(\mathbf{x},t) - \mathcal{F}(\mathbf{0},t) \rangle = \frac{\gamma \mathbf{x}^2}{2t}. \tag{4.49}$$

Since the transverse displacement of the endpoint from $\mathbf{0}$ to $\mathbf{x}$ stretches the polymer, to leading order, by the amount $\mathbf{x}^2/2t$, (4.49) is simply a manifestation of Hookes law with the line tension γ of the *pure* system. This is a highly nontrivial result, which has its roots in the statistical translational invariance of the disorder potential, i.e. the fact that η' and η in (4.5) have the same correlation functions; statistical translational invariance, when regarded as a symmetry property, has powerful consequences for a large class of disordered systems [163]. The simplicity of the *average* free energy (4.49) notwithstanding, the *actual* response of a polymer in a single realization of randomness is dominated by rare, large fluctuations drawn from a nontrivial power law distribution [164].

While the line tension remains unrenormalized, the temperature T does not - from (4.45) we see that $T \sim \nu$, and hence, according to the scaling transformation (3.55), temperature is driven to zero under renormalization, provided $z < 2$; the low temperature (strong coupling) phase of the directed polymer is governed by a zero-temperature fixed point [120]. This is the reason for the equivalence of zero and finite temperature scaling properties alluded to previously. The equivalence may break down if the translational invariance of the disorder potential is broken, as is the case in the situations discussed in the following section.

4.6 Inhomogeneous growth

In this section we shall concern ourselves with situations where the translational invariance parallel to the interface (in the substrate plane) is broken due to the

presence of an external, position dependent contribution to the local growth rate. There is no principal difficulty in studying this problem in general dimensionalities, however since almost all studies so far have addressed the one-dimensional case, we will specialize to $d=1$ from the outset. Consider then the following generalization of the KPZ equation,

$$\frac{\partial h}{\partial t} = \nu \nabla^2 h + \frac{\lambda}{2}(\nabla h)^2 + \eta(x,t) + V(x). \tag{4.50}$$

We will discuss two types of growth rate inhomogeneities $V(x)$. In the first case (the *single defect* case), $V(x)$ is localized in a small spatial region and can be modeled, in the continuum limit, by a δ-function,

$$V(x) = V_0 \delta(x - x_0), \tag{4.51}$$

where x_0 may be located either in the bulk, or at the boundary of the system; the latter possibility is realized in the dynamics of an interface of finite lateral extent L in which growth rate inhomogeneities arise at $x=0$ and $x=L$ due to some set of 'free' boundary conditions [129, 132]. Here the main interest is in *morphological phase transitions* that may occur, by a mechanism to be explained shortly, as the strength V_0 of the inhomogeneity is varied. In the second case (*many defects*), $V(x)$ is a random function with short ranged correlations. Not surprisingly, as will be shown in Section 4.6.3, this turns out to severely modify the roughness of the interface.

4.6.1 Morphological transitions

The basic mechanism whereby a growth rate inhomogeneity of the type (4.51) can change the large scale morphology of the interface is easily accounted for [128] (Figure 19). Consider an interface with a growth rate that is a symmetric function of inclination, $v(\nabla h) = v(0) + (\lambda/2)(\nabla h)^2$, and suppose for concreteness that $\lambda > 0$. This implies that the interface can *increase* its growth rate by assuming a nonzero tilt. Consequently, a macroscopic hill can form in response to a sufficiently large, positive growth rate inhomogeneity $V_0 > 0$: Since the sides of the hill are tilted by some amount $\pm u$ relative to the reference line, the hill grows faster than the planar interface and thus allows the system to accomodate the external bias. This is not possible if the growth rate is *reduced* at x_0, i.e. if $V_0 < 0$, since the planar interface already propagates as slowly as possible and cannot slow down by tilting; a defect with $V_0 < 0$ does not affect the large scale morphology. Clearly the roles of positive ($V_0 > 0$) and negative ($V_0 < 0$) inhomogeneities are reversed if $\lambda < 0$.

It is natural to regard the magnitude of the induced tilt, u, as an order parameter of the transition, and to write

$$u \sim |V_0 - V_0^c|^\beta, \quad V_0 \to V_0^c \tag{4.52}$$

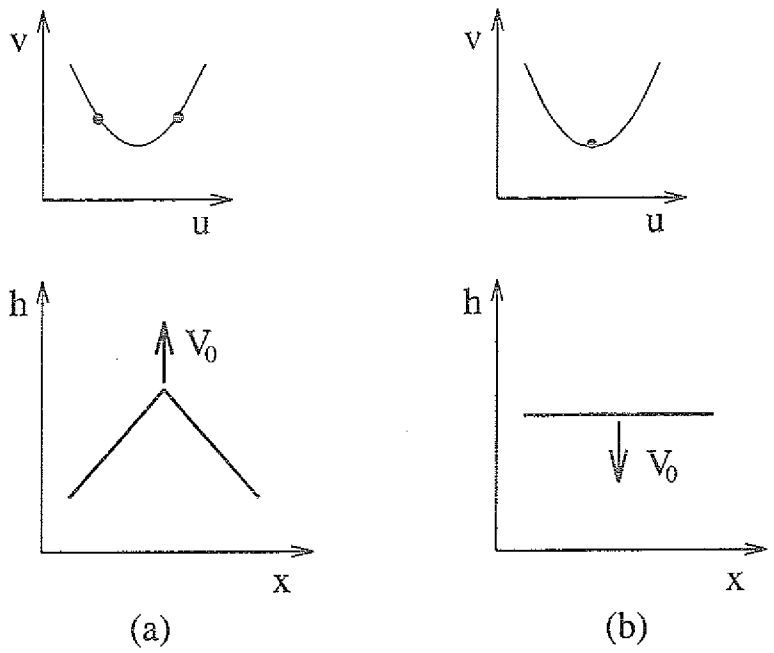

Figure 19: Illustration of the mechanism for tilting transitions induced by a localized growth rate inhomogeneity. The growth rate v is assumed to be an increasing function of inclination u. (a) If $V_0 > 0$, the interface can increase its growth rate by forming a macroscopic hill; the slopes of the hillsides are indicated by dots in the $v(u)$-graph. (b) If $V_0 < 0$, no transition occurs because the flat interface is already moving as slowly as possible.

to define an order parameter exponent β (note that possibly $V_0^c = 0$). The transition is associated with a diverging correlation length, which can be identified as follows. In the tilted state, we consider the interface fluctuations about the average profile $h_0(x,t) = ux + v(u)t$, i.e. setting $h(x,t) = h_0(x,t) + \hat{h}(x,t)$ one has

$$\frac{\partial \hat{h}}{\partial t} = \nu \nabla^2 \hat{h} + \lambda u \nabla \hat{h} + \frac{\lambda}{2}(\nabla \hat{h})^2 + \eta(x,t) + V(x). \tag{4.53}$$

The essential feature is the linear term $\lambda u \nabla \hat{h}$ induced by the tilt. This term describes a drift of fluctuations with velocity $c = -\lambda u$. In contrast to the translational invariant situation discussed subsequent to eq.(4.3), here the drift term cannot be eliminated by going to a suitably chosen moving frame, since such a transformation would not be compatible with the inhomogeneity $V(x)$. Instead, the drift is expected to play an essential role in the dynamics [129] (for a related situation see [165]). In view of the dimensional arguments employed in Section 4.1, the primary effect of the additional term is that it provides us with a third dimensionful coefficient, the drift velocity c, that can be used together with the invariants λ and D/ν to construct a *time-independent* length scale

$$\ell(u) = \lambda^2 (D/\nu)|c|^{-2} = (D/\nu)|u|^{-2} \tag{4.54}$$

which diverges upon approaching the transition. Introducing the correlation length exponent ψ through

$$\ell \sim |V_0 - V_0^c|^{-\psi} \tag{4.55}$$

it follows that $\psi = 2\beta$.

It is informative to contrast the quadratic divergence of (4.54) with the corresponding behavior in a 'mean field' approximation [128, 129] to (4.50), in which the noise term $\eta(x,t)$ is neglected. In the absence of noise the invariant quantities of the equation are λ, the drift velocity c and the coefficent ν of the Laplacian term. Since the dimension of ν is $[\nu] = [x]^2/[t]$, a length scale can be constructed from ν and c,

$$\ell_{MF}(u) = \nu/|c| = (\nu/|\lambda|)|u|^{-1} \tag{4.56}$$

which diverges *linearly* in $1/|u|$. This indicates that the presence of noise changes the universal features of the transition. To clarify these issues we now turn to the interpretation of inhomogeneous growth in the directed polymer representation.

4.6.2 Delocalization and unbinding

To arrive, via the mapping described in Section 4.5, at the generalized KPZ equation (4.50), we have to start from the energy expression

$$\mathcal{H}[\mathbf{y}(s)] = \int_0^t ds \left[\frac{\gamma}{2} \left(\frac{d\mathbf{y}}{ds} \right)^2 + \eta(\mathbf{y}(s), s) + V(y(s)) \right] \tag{4.57}$$

which contains an additional potential term V acting on the polymer. Since V is independent of the 'time' coordinate t, a localized inhomogeneity (4.51) corresponds to a defect line that traverses the random energy landscape parallel to the t-axis (Figure 18). Noting that $\lambda < 0$ in the KPZ equation (4.45) for the polymer free energy, it becomes evident why a phase transition can be expected to occur for $V_0 < 0$: The defect potential being *attractive*, it competes with the roughening tendency of the bulk disorder η and may, if sufficiently strong, *bind* the transverse position of the polymer close to x_0; in the bound phase the restricted free energy $\mathcal{F}(x,t)$ increases linearly with the distance from the defect, corresponding to a macroscopically tilted interface. Thus the morphological transitions induced by the growth rate inhomogeneity reemerge in the guise of unbinding or delocalization transitions of a kind that has been much studied in the context of thermal and disorder-induced fluctuations of equilibrium interfaces [160].

At this point it becomes important to distinguish between the two possible locations of the defect position x_0 in the bulk or at the boundary of the system, respectively. When the defect resides in the bulk, the defect potential $V(x)$ is symmetric in $x - x_0$. This property is inherited by the positional probability distribution

of the polymer. Consequently the average position will be equal to x_0 irrespective of whether the polymer is bound to the defect or not; in order to observe the transition, the width (second moment) of the probability distribution has to be monitored. Following Forgacs, Lipowsky and Nieuwenhuizen [160] this case will be referred to as a *delocalization* transition. In contrast, if the defect is located at the boundary of the system ($x_0 = 0$, say), the polymer is subject to an additional 'hard wall' potential which arises from the constraint that $y(s) \geq 0$ for all paths (this corresponds [132] to a free boundary condition for the interface). Therefore the *total* defect potential has a repulsive hard core and an attractive short range part of strength V_0. In this case the liberation of the polymer from the defect will result in a divergence of the *average* distance from the boundary, a phenomenon known as [160] *unbinding*. In both cases the 'liberation' of the polymer from the defect is expressed in the divergence of the correlation length ℓ, which measures the typical distance of the polymer from the defect; for this reason the exponent ψ in (4.55) is occasionally referred to as the liberation exponent.

To appreciate why the two situations may lead to qualitatively different behaviors, it is useful to first consider the 'mean field' version of the problem in which $\eta = 0$ in (4.50) and (4.57). Note that this simplification has a very natural interpretation in the directed polymer language: In the absence of disorder (4.57) reduces to the energy of a *thermally* excited line (or one-dimensional interface) subject to an external potential, a class of problems much studied in diverse contexts ranging from wetting phenomena [160] to the adhesion and unbinding of fluid membranes [93].

In the thermal case the study of the delocalization or unbinding of a line reduces to an exercise in elementary quantum mechanics. Taking the limit $t \to \infty$, the diffusion equation (4.43) for the restricted partition function $\mathcal{Z}(x,t)$ (derived from the Hamiltonian (4.57)) becomes a stationary Schrödinger equation

$$\left[-\frac{(k_B T)^2}{2\gamma} \nabla^2 + V \right] \mathcal{Z} = f_0 \mathcal{Z}, \tag{4.58}$$

where f_0 denotes the free energy per unit length. The transition is associated with the disappearance of the last bound state of the Schrödinger problem and the concomitant vanishing of the eigenvalue f_0. Outside the range of V such a bound state decays exponentially on a scale $\ell = k_B T / \sqrt{-2\gamma f_0}$, hence the order parameter $u = \partial \mathcal{F} / \partial x$ is $u = k_B T / \ell$ in accordance with (4.56) (note that from (4.45) we have $\nu / |\lambda| = k_B T / 2$). From the well-known fact that a symmetric, attractive potential always possesses at least one bound state in one dimension we conclude that the delocalization transition occurs at zero potential strength, $V_0^c = 0$, while the threshold for unbinding is expected to be nonzero. Specifically, if the potential is modeled by

a square well of width a and depth $-V_0$, one obtains

$$\ell = \frac{k_B T}{u} = \frac{(k_B T)^2}{\gamma a}(V_0^c - V_0)^{-1} \tag{4.59}$$

with $V_0^c = 0$ for delocalization and $V_0^c = -(k_B T)^2(\pi/2a)^2/2\gamma < 0$ for unbinding. Comparing with (4.52) we see that the order parameter exponent $\beta = 1$ in the thermal case, both for delocalization and unbinding.

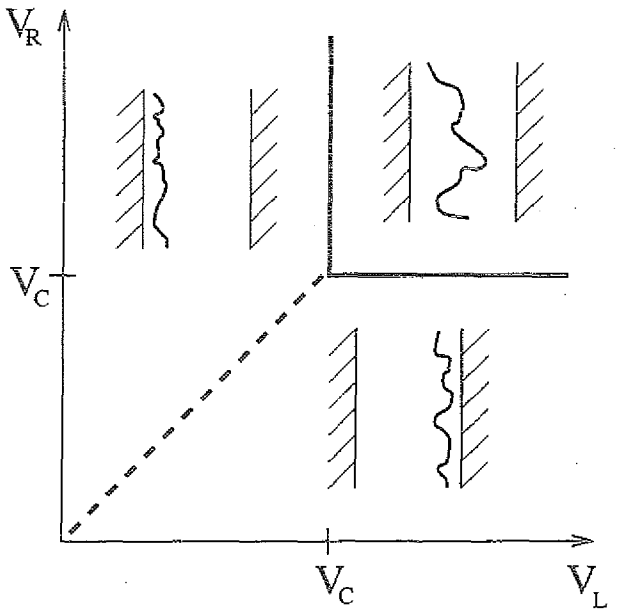

Figure 20: Phase diagram for a directed polymer confined by two attractive walls, as obtained from the exact solution of the ASEP with open boundary conditions [132]. V_L and V_R denote the (negative) contact potentials at the left and right walls. The bold lines indicate continuous unbinding transitions, while the dashed line represents a first order transition between two bound phases.

Delocalization and unbinding transitions in the presence of quenched bulk disorder constitute a highly nontrivial class of problems that has been intensely studied in the years following the pioneering work of Kardar [166]. It was pointed out only very recently [132] that the particular problem of zero-temperature disorder-induced unbinding affords an *exact* solution in one transverse dimension, $d = 1$. The solution is obtained in a somewhat indirect fashion, through a sequence of mappings that take a zero temperature, discrete directed polymer problem to a growth model (the single step model briefly discussed at the end of Section 4.3) and further to a version of the asymmetric simple exclusion model (ASEP, see Section 4.3) with open boundaries originally introduced by Krug [129]. The ASEP, in turn, was solved exactly by Derrida, Evans, Hakim and Pasquier [130] and independently by Schütz and Domany [131].

The main features of the unbinding transition that emerge from the exact solution are as follows (see also Figure 20). The transition occurs at a finite value of the binding potential, and the order parameter exponent in (4.52) is $\beta = 1$ as in the thermal case (in fact the entire phase diagram of the model is reproduced *exactly* by the mean-field/thermal approximation, for reasons that are not completely understood). The relation (4.54) would then suggest that the liberation exponent ψ defined by (4.55) should take the value $\psi = 2$, different from the thermal result $\psi = 1$ (see (4.59)). This was already predicted by Kardar [166], and is explicitly confirmed by the exact solution [132].

While early numerical studies [166, 167] suggested that disorder-induced delocalization may be rather similar to unbinding, recent analytic and numerical work [168, 169, 170] seems to converge on the view that the two problems are in fact fundamentally different. First, as in the thermal case, delocalization occurs at zero potential strength, $V_0^c = 0$. Second, and more importantly, the values of the exponents β and ψ are formally infinite, in the sense that the power law divergence (4.55) is replaced by an essential singularity

$$\ell \sim \exp(-C/V_0), \tag{4.60}$$

with $C > 0$, for $V_0 < 0$; the relation (4.54) is nevertheless satisfied [170]. Needless to say, the direct numerical verification of (4.60) is exceedingly difficult [168, 169].

4.6.3 Many defects

Much of the recent work on the disorder-induced delocalization of directed polymers has been motivated by the application to flux lines in dirty high-temperature superconductors [169]. There, the localizing potential is provided by a *columnar defect* which may either be present in the material in the form of a screw dislocation, or may be deliberately created by ion irradiation, with the intent of increasing the critical current through enhanced pinning. Localization at the defect is counteracted by thermal fluctuations (i.e., entropy) as well as by bulk disorder that appears in the form of *point defects* such as oxygen vacancies.

In this context it is very natural to consider the behavior of a flux line in an array of *many* columnar defects with randomly distributed pinning strengths. Within the continuum theory defined by (4.57), this can be modeled by chosing the potential V as a Gaussian random variable with zero mean and short ranged correlations,

$$\langle V(x)V(x')\rangle = V_0^2 \delta(x - x'). \tag{4.61}$$

In terms of interfaces described by the inhomogeneous KPZ equation (4.50), this corresponds to a growth rate with a time-independent, spatially random component

(not to be confused with the quenched, h-dependent noise that appears in the study of interface displacement in random media [68, 69]). Since a physical realization of such an interface growth process seems somewhat hard to imagine, in the following discussion we will mostly use the directed polymer language.

As it stands, the KPZ equation (4.50) with random inhomogeneities poses a rather formidable problem, the directed polymer being subject to the conflicting influences of point disorder, columnar defects and thermal fluctuations. The problem without point disorder ($\eta = 0$) has a rich history [159, 171], with applications ranging from the conformation of (undirected!) Gaussian polymers in random media to the evolution of biological species. Here, we shall focus on two special cases, (i) the purely columnar problem ($\eta = 0$) at *finite* temperature, and (ii) the zero temperature problem in the presence of both columnar and point disorder. We will argue that the thermal fluctuations and the point disorder play very similar roles in counteracting the localizing tendency of the columnar defects in the two cases, and can in fact be treated on the same footing [172]. In passing, we note that the *zero* temperature, purely columnar problem shows nonuniversal behavior [159] that is different from that at finite temperature, while the finite temperature problem in the presence of *both* columnar and point defects has not been studied so far.

To avoid some subtleties associated with the continuum formulation of the problem, we envision, for the purposes of the present discussion, a suitable discretization. For example, in the case of directed paths on the square lattice with the transverse displacement restricted to at most one lattice spacing per time step, the discrete version of the diffusion equation (4.43) for the restricted partition function reads [159, 172]

$$Z(x,t+1) = e^{-(\eta(x,t)+V(x))/k_BT}[Z(x,t) + Z(x-1,t) + Z(x+1,t)]. \qquad (4.62)$$

In the zero temperature limit this reduces to a recursion for the ground state energies $E(x,t) = -\lim_{T\to 0} k_BT \ln Z(x,t)$.

The competition between the localizing defect and the delocalizing influence of thermal or point disorder fluctuations has already been emphasized as the driving force behind delocalization and unbinding transitions. In the presence of a random array of columnar defects, this competition extends to all scales, thereby dramatically enhancing the transverse wandering of the polymer. To see this, we first need to identify the 'optimal' disorder regions to which the polymer is attracted. In the presence of either point disorder or thermal fluctuations, the (free) energy cost per unit length required to localize the polymer in a region of transverse extent ℓ is of order $\ell^{-\tau}$, where (for $d = 1$ transverse dimension) $\tau = 1$ for point disorder, and $\tau = 2$ in the thermal case (see eqs.(4.46) and (4.47)). Due to the confinement energy, the polymer is primarily attracted to *wide* regions in which all columnar defect energies

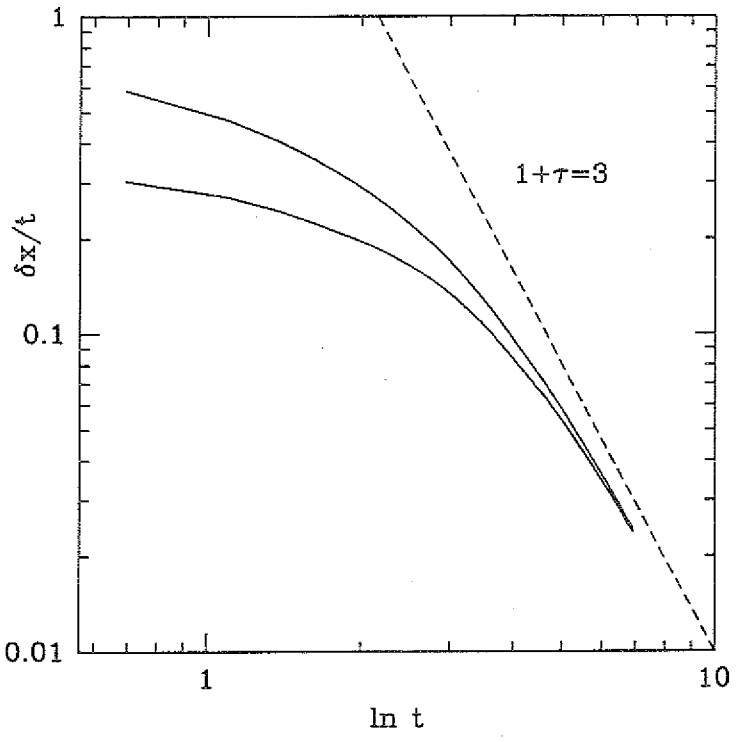

Figure 21: Measures of the transverse wandering of a finite temperature directed polymer in 1+1 dimensions, subject to binary columnar disorder, but no point disorder ($\eta = 0$ in (4.62)). The upper and the lower curves show $\langle [x(t)^2] \rangle^{1/2}$ and $\langle [x(t)]^2 \rangle^{1/2}$, respectively, divided by the path length t. The dashed line indicates the prediction (4.64) for the logarithmic prefactor, with $\tau = 2$ in the entropic case. The data were obtained by averaging over 10^4 realizations of disorder. [159]

are lower than average; naturally, such regions are rare, and to reach them large transverse fluctuations are necessary.

For a quantitative estimate, consider e.g. a binary distribution of columnar defect energies, $V = -V_0$ with probability p and $V = 0$ with probability $1-p$. The probability for finding ℓ subsequent attractive defects (which have $V = -V_0$) is then p^ℓ, and the (free) energy per unit length for a polymer residing in such a region can be estimated as $-V_0 + \epsilon$, with $\epsilon \sim 1/\ell^\tau$. This translates into a 'density of states'

$$\rho(\epsilon) \sim p^\ell \sim \exp\left[-\frac{|\ln p|}{\epsilon^{1/\tau}}\right]; \tag{4.63}$$

a similar form is obtained for continuous, bounded disorder distributions. A standard variable range hopping argument [159, 172] applied to (4.63) then shows that the transverse displacement increases as

$$\delta x(t) \sim \frac{t}{(\ln t)^{1+\tau}}, \tag{4.64}$$

in reasonable agreement with simulations [159, 172] (see Figure 21). In d transverse dimensions the exponent of the logarithmic factor in (4.64) is $1+\tau/d$. The result $\delta x \sim t/(\ln t)^3$ for the thermal case in one dimension has been rigorously confirmed by Sznitman [173].

In case (ii), point and columnar defects at zero temperature, the result (4.64) has the surprising, and somewhat counterintuitive, feature that the displacement due to the combined effect of both types of defects is larger than that produced by any of the two types alone: The pure point problem has the standard KPZ behavior $\delta x \sim t^{1/z} = t^{2/3}$, while purely columnar defects at zero temperature, with a uniform distribution of defect energies, lead to a wandering as $\delta x \sim t^{1/2}$ [159].

Returning to the kinetic roughening of interfaces described by the KPZ equation (4.50) with random inhomogeneities, the main interest is in the temporal behavior of the interface width W, rather than the correlation length $\xi \sim \delta x$ described by (4.64). Arguments of the type sketched above indicate that the width increases as

$$W \sim \frac{t}{(\ln t)^\tau} \tag{4.65}$$

in one transverse dimension, where $\tau = 1$ ($\tau = 2$) in the presence (absence) of a time-dependent noise term η. The $t/\ln t$ behavior has in fact been observed in numerical simulations of a growth model that combines time-dependent noise and spatially random, quenched growth rates [174].

Up to higher order corrections (which may however decay very slowly, as powers of $(\ln(\ln t))^{-1}$ [159]), these arguments apply whenever the distribution of columnar defect strengths $V(x)$ in (4.62) has finite support. For *rapidly* decaying, unbounded distributions (e.g. Gaussian or exponential) the wandering is still subballistic, $\delta x \sim t/(\ln t)^\mu$, but the value of μ differs from that in (4.64) [159]. The effect of *slowly* decaying (power law) distributions of columnar disorder has so far been studied only in the absence of both thermal fluctuations and point disorder, where it typically leads to ballistic wandering, $\delta x \sim t$, and nonextensive behavior of the ground state energy [159].

5. The rôle of surface diffusion

Despite the challenging unresolved problems posed by the KPZ theory, over the last few years the attention of the kinetic roughening community has turned increasingly towards a class of surface growth processes that are *not* described by the KPZ equation. The shift of focus is motivated mainly by a critical reassessment [15] of the physical relevance of the KPZ nonlinearity in *deposition* processes, which would appear to provide the most natural realization of kinetic roughening phenomena.

We have emphasized in Chapter 4 that the origin of the (kinematic) KPZ nonlinearity lies in a nontrivial inclination-dependence of the growth rate v, measured in the vertical (h-) direction (see eq.(4.3)). However, as was first pointed out by Krug [102], in the most simplistic model of crystal growth from the vapor (the Wilson-Frenkel model; see [101] and [73]), in which every atom impinging on the surface is immediately incorporated into a perfect crystal lattice, the growth rate is manifestly *independent* of inclination. In suitable units it can be written as

$$v = F/\rho \tag{5.1}$$

where F denotes the deposition flux and ρ is the deposit density (equivalently, $1/\rho$ is the atomic volume); in the situation just described, both are independent of surface orientation. In the framework of the derivation of the isotropic continuum equation (3.6) in Section 3.1, this result may be regarded as a consequence of crystalline anisotropy, which enforces an orientation dependence of the normal surface velocity v_n that precisely cancels the geometric factor $\sqrt{1+(\nabla h)^2}$ in (3.4).

Equation (5.1) is useful in identifying the mechanisms by which the simplistic Wilson-Frenkel picture fails in real deposition processes. At *low temperatures*, the mobility on the surface is insufficient for every deposited atom to reach a lattice site before the arrival of other atoms, and a finite concentration of vacancies and other defects results. This implies a shift in the deposit density which, as is well known for the extreme case of ballistic deposition [23] (see also Section 2.1), is a function of the surface inclination relative to the deposition beam. On an inclined surface one has a higher concentration of steps, at which overhangs and, eventually, overgrown vacancies can form; consequently the density ρ decreases, and, according to (5.1), the growth rate increases with the tilt [102].

At *high temperatures* there is a nonnegligible probability for a deposited atom to redesorb from the surface; the sticking coefficient is less than unity. As the desorption probability depends on the local bonding environment, the desorption flux varies e.g. with the step density, and hence with surface inclination. To account for desorption, the total deposition flux in (5.1) should be replaced by a net flux $F - F_{\text{desorp}}(\nabla h)$,

which, again, induces an inclination dependence in v. This mechanism is also evident in the celebrated Burton-Cabrera-Frank (BCF) expression for the growth rate of a vicinal surface [73, 175] (see also Section 5.2.1)

$$v_{\mathrm{BCF}} = 2F(\sqrt{D_s\tau}/\ell)\tanh(\ell/2\sqrt{D_s\tau}), \tag{5.2}$$

where $\ell = |\nabla h|^{-1}$ is the step distance, D_s is the surface diffusion coefficient, and τ is the inverse desorption rate. In the limit $\tau \to \infty$ (no desorption) (5.2) reduces to (5.1), $v_{\mathrm{BCF}} \to F$.

In the context of simple stochastic growth models, the 'desorption' mechanism may be viewed as being responsible for the inclination-dependence of the growth rate for the class of restricted solid-on-solid (RSOS) models introduced by Meakin et al. [19], Kim and Kosterlitz [143] and others [109, 176]. In these models deposition attempts are accepted only if certain conditions on the local height configuration are met; obviously this can be interpreted in terms of a zero sticking coefficient, or immediate redesorption, for some local environments.

The conclusion is that vapor deposition processes *do* fall into the KPZ universality class, however the two underlying mechanisms apply mainly at either high or low temperatures. It turns out that technologically relevant deposition methods - in particular molecular beam epitaxy (MBE) - are often operated in the temperature window where *both* mechanisms, desorption as well as defect formation, can be neglected. This is perhaps not entirely surprising, since the practitioner would attempt to optimize the process towards growing perfect crystals (no defects) at maximal yield (no desorption). Empirically, the absence of the two mechanisms is demonstrated directly by the observed independence of the growth rate on miscut angle (that is, inclination), e.g. in the MBE of silicon [73].

Given the widespread interest in MBE applications, and availability of MBE growth chambers as well as sophisticated experimental techniques for the characterization of the growing surface, it is obviously desirable to bring the concepts of kinetic roughening to bear upon the MBE process. This has prompted a large amount of theoretical work devoted to the limiting case, termed *ideal MBE* by Lai and Das Sarma [95], of deposition in the complete absence of both desorption and defect formation. The fundamental interest in this class of processes arises from the hope of finding new, nontrivial universality classes - distinct from the KPZ-class which is excluded by construction. As we shall see in this chapter, the removal of the dominant KPZ-term opens up a Pandoras box of possible behaviors. Moreover, the assignment of a universality class (represented by a specific large scale equation of motion) to a given microscopic model turns out to be a rather subtle problem, with seemingly minor details playing a decisive role in a way unprecedented by the experience with KPZ-type models.

Ideal MBE. In the absence of desorption all relaxation processes on the surface conserve the mass of the growing film. The assumption of perfect crystalline structure transforms mass conservation into volume (or height) conservation. Thus, apart from the deposition flux, which is by definition uncorrelated with the surface configuration, ideal MBE is a *conservative* growth process that can be described by a driven continuity equation

$$\frac{\partial h}{\partial t} + \nabla \cdot \mathbf{J} = F, \tag{5.3}$$

where F includes the average deposition flux as well as shot noise fluctuations. Clearly, the question of universality classes reduces to a classification of the possible forms for the surface diffusion current $\mathbf{J}$.

We remarked already in Section 3.1 that, in addition to the classical equilibrium surface diffusion current, two types of nonequilibrium contributions generically occur. Here, we reemphasize that these contributions are fundamentally different from the KPZ nonlinearity, in the following sense. The KPZ-term is obtained from a purely kinematic relation, eq.(3.4), and arises physically simply because the interface is moving on average. In contrast, for the MBE equation (5.3) the mean motion is irrelevant, because it *does not couple to the surface fluctuations* (compare to Section 4.3). Instead, the nonequilibrium contributions to the current $\mathbf{J}$ are of *dynamical* origin, reflecting the perturbation of the surface diffusion processes imposed by the external deposition flux. Consequently, the microscopic interpretation of these contributions requires considerable insight into the behavior of adatoms on the surface.

The purpose of this chapter is to review the current theoretical understanding of nonequilibrium effects in ideal MBE. The two types of nonequilibrium contributions - inclination-dependent currents and inclination-dependent chemical potentials - are discussed separately in Sections 5.2 and 5.3. A central theme is provided by the idea that the main effect of the deposition flux is to *remove the constraints* imposed on equilibrium surface diffusion by the requirement of detailed balance in microscopic processes. This view is supported by the fact that closely analogous nonequilibrium effects arise if a surface is driven out of equilibrium by some mechanism other than growth, provided detailed balance is broken [77, 177, 178]. In Section 5.4. the emerging picture is summarized, and the experimental situation is evaluated. To set the stage, we begin in Section 5.1 with a survey of microscopic models.

5.1 A survey of MBE models

5.1.1 Limited mobility models

The first example of a growth model that conforms to the 'ideal MBE' restrictions of no desorption and no defect formation was proposed by Family in 1986 [100]; we have described the model in Section 3.4. Although the title of Family's paper features the term 'surface diffusion', the basic assumption of the model - that the motion of adatoms is biased in the direction of decreasing absolute height - is hardly realistic in the context of MBE (unless one posits that the adatom dynamics is completely dominated by transient mobility and downward funneling effects, which may well be true on metal surfaces at low temperatures [84, 179, 180]). Recognizing this weakness, Wolf and Villain [86] and Das Sarma and Tamborenea [105] independently proposed variants of Family's model in which the preferred incorporation sites for the adatom are determined by the local bonding environment; roughly speaking, the function K_x introduced in Section 3.4, which the mobile adatom seeks to minimize, is identified with the negative coordination number.

In fact the two models introduced by Wolf and Villain [86] and by Das Sarma and Tamborenea [105] differ slightly in their microscopic rules. For later reference, we make the effort to precisely define *three* versions of these models, the first two of which (DT1 and DT2) are probably close to the model actually simulated by Das Sarma and Tamborenea, while the third (WV) is the model proposed by Wolf and Villain. Bizarre as it may seem at this point, we will argue in Section 5.2.3 that all three models belong to different universality classes asymptotically - a striking example of the sensitive dependence on microscopic details alluded to above.

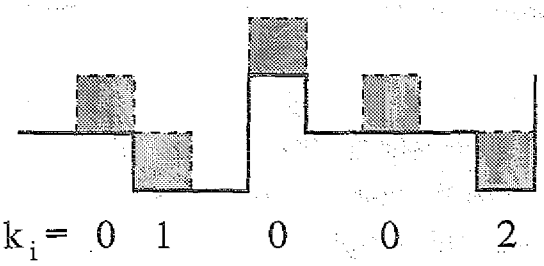

Figure 22: Illustration of the lateral coordination number defined in (5.4). The shaded squares are virtual atoms about to be deposited onto the (bold) surface.

To keep matters simple, we restrict the discussion to one-dimensional surfaces, and allow the freshly deposited atom to search for an incorporation site only among the nearest neighbors of the deposition site. As in Section 3.4, the surface configuration is described by a set of integer height variables h_i defined on the one-dimensional substrate lattice $i = 1, ..., L$ (with periodic boundary conditions, say). The bonding

environment at each site i is characterized by the lateral coordination number k_i (that is, the number of lateral nearest neighbor bonds) that *an additional atom would have if it were deposited at* i,

$$k_i = \begin{cases} 0 & : \quad h_i \geq h_{i+1} \text{ and } h_i \geq h_{i-1} \\ 1 & : \quad h_{i-1} \leq h_i < h_{i+1} \text{ or } h_{i-1} > h_i \geq h_{i+1} \\ 2 & : \quad h_i < h_{i-1} \text{ and } h_i < h_{i+1} \end{cases} \tag{5.4}$$

(see Figure 22). In one deposition step, a site i is chosen at random and the coordination numbers (k_{i-1}, k_i, k_{i+1}) are examined.

In the *DT models*, sites with $k_i = 1$ or 2 are permanent traps; the freshly deposited atom is moved to one of the neighboring sites $i \pm 1$ only if $k_i = 0$ *and* $k_{i-1} > 0$ or $k_{i+1} > 0$. The atom is moved to the right if $(k_{i-1}, k_{i+1}) = (0,1)$ or $(0,2)$, and to the left if $(k_{i-1}, k_{i+1}) = (1,0)$ or $(2,0)$. In a symmetric environment, $(k_{i-1}, k_{i+1}) = (1,1)$ or $(2,2)$, a random choice is made to move the atom left or right with equal probability. The two versions DT1 and DT2 differ in their treatment of the cases $(k_{i-1}, k_{i+1}) = (1,2)$ and $(2,1)$. Rule DT1 treats them as symmetric configurations, i.e. one of the two neighboring sites is chosen at random, while DT2 always moves the atom to the site with the largest value of k_i, i.e. to the right for $(k_{i-1}, k_{i+1}) = (1,2)$ and to the left for $(k_{i-1}, k_{i+1}) = (2,1)$.

The *WV rule* coincides with DT2 when $k_i = 0$, however in addition atoms deposited on sites where $k_i = 1$ are allowed to move, if they can increase the coordination number. The atom is moved to the right if $(k_i, k_{i+1}) = (1,2)$ and to the left if $(k_{i-1}, k_i) = (2,1)$; the symmetric case $(k_{i-1}, k_i, k_{i+1}) = (2,1,2)$ cannot occur.

It is worthwhile to point out that in all three models (DT1, DT2 and WV) the height of the incorporation site is always less or equal to that of the deposition site, i.e. there are no 'uphill' jumps (this is no longer true if next nearest neighbor jumps are included). Naively, one might expect this asymmetry to give rise to a 'downhill' nonequilibrium current, as discussed in Chapter 3, and consequently place all models in the Edwards-Wilkinson universality class (see Section 3.2). We will show in Section 5.2.2 why this simple minded reasoning fails.

The work of Wolf and Villain [86] and Das Sarma and Tamborenea [105] was of great importance because it numerically demonstrated, for the first time, the possibility of scaling behavior in vapor deposition processes that is distinct from the familiar Edwards-Wilkinson and KPZ universality classes. A confusing variety of related models have been subsequently proposed, with rules that are not always easy to decipher from the published description [95, 106, 181, 182, 183, 184].

A particularly interesting variant, which will play a certain role in the final classification attempted in Section 5.4.1, was introduced very recently by Kim, Park and Kim [185]. This model is a *restricted* solid-on-solid (RSOS) model in which a

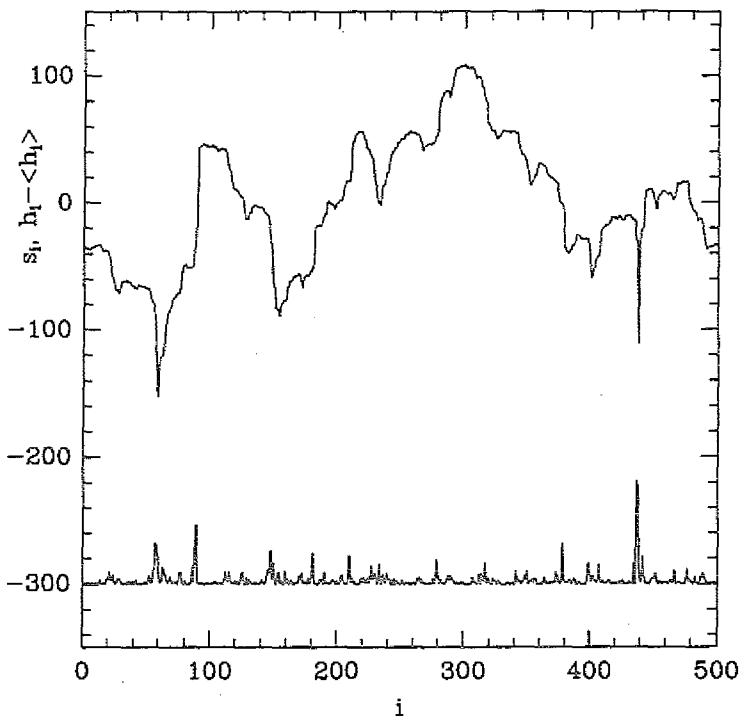

Figure 23: Surface configuration $h_i - \langle h \rangle$ (upper curve) and local step size $s_i = |h_{i+1} - h_i|$ (lower curve shows $s_i - 300$) generated by the DT1 rule. A total of 10^5 monolayers were deposited on a substrate of $L = 500$ lattice sites. [94]

strict constraint on the absolute magnitude of nearest neighbor height differences is enforced at all times. Since it is required, under the rules of ideal MBE, that every deposited atom be incorporated somewhere on the surface, such a constraint can be maintained only if the region around the deposition site in which the atom searches for an eligible incorporation site is unlimited. In the implementation of Kim et al.[185] the search is conducted in shells of ever increasing radius around the deposition site.

The common feature of all these models (and the rationale for subsuming them under the 'limited mobility' heading) is that only freshly deposited atoms are regarded as mobile; once the preferred incorporation site has been chosen, according to some rule, in the neighborhood of the deposition site, the deposited atom is placed there permanently. If, as is commonly done, the potential incorporation region is restricted to the nearest neighbors of the deposition site, the adatom mobility is very limited indeed, and the model strongly overemphasizes the disordering influence of the shot noise in the atomic beam. Consequently, the surface morphology is extremely rough (Figure 23). In a certain sense the limited mobility models do not allow for any true surface relaxation, since there is *no dynamics when the beam is*

turned off. The crucial improvement afforded by the collective diffusion models, to be described next, addresses precisely this problem.

These remarks make it clear that the limited mobility models have the status of toy models, rather than providing a (semi-) realistic description of MBE. We should mention, however, that a realistic interpretation of these models does exist, in terms of a coarse-grained algorithm for island nucleation and growth, when the growth rule is supplemented by a noise-reduction algorithm [186].

5.1.2 Collective diffusion models

An important number for characterizing epitaxial growth is the ratio of the surface diffusion constant D_s to the deposition flux F. To arrive at a properly nondimensional quantity, we express the flux in terms of the monolayer completion time τ_{ML} and the diffusion constant through the atomic hopping rate R, as

$$F = (a^d \tau_{\mathrm{ML}})^{-1}, \;\; D_s = a^2 R \tag{5.5}$$

where a is the lattice constant, and d the substrate dimension. The relevant number is then $R\tau_{\mathrm{ML}}$. Note that D_s refers to the *tracer* diffusion of a single adatom on a perfect, flat surface without steps or islands; the *collective* diffusion constant, which determines the adatom mobility in the macroscopic theory, eq.(3.11), can be significantly reduced relative to D_s [187].

For an order of magnitude estimate, consider MBE of silicon at 600° C and a growth rate of one monolayer per second [73]. The conventional Arrhenius ansatz for the hopping rate reads

$$R = \omega_0 \exp(-E_s/k_B T) \tag{5.6}$$

with a vibrational attempt frequency $\omega_0 \approx 2k_B T/h = 3.64 \times 10^{13} s^{-1}$ (here h denotes Plancks constant). With the experimental estimate $E_s \approx 1.3\, eV$ for the surface diffusion activation barrier, this yields $R\tau_{\mathrm{ML}} \approx 1.1 \times 10^6$. At higher temperatures, lower flux rates or for metal surfaces where the activation energies are lower, values of $R\tau_{\mathrm{ML}} \approx 10^{10}$ and more are possible. Thus, growth under MBE conditions must be viewed as a competition between two opposing processes - disordering through deposition and smoothening through diffusion - that occur on *widely separated time scales*. The models described in this section are designed to deal with this situation, at least in principle (in practice computational resources limit the values of $R\tau_{\mathrm{ML}}$ that can actually be achieved). Accordingly, their dynamics consists of two sets of rules - a deposition rule and a diffusion rule - that can be applied at widely different rates.

Arrhenius dynamics. The most popular model in this class is the Arrhenius model introduced and investigated by Vvedensky and coworkers several years prior to the advent of ideal MBE in the kinetic roughening community [188, 189, 190] (see also [191] and references therein). These early studies were concerned mainly with reproducing experimentally observed features of the early stages of growth, such as the characteristic oscillations in the RHEED (reflection high-energy electron diffraction) signal.

The surface is modeled in the conventional solid-on-solid (SOS) fashion [101], its position being specified by a set of integer height variables $h_{\mathbf{x}}$ above the substrate ($\mathbf{x}$-) lattice. Deposition occurs, at a rate F, by selecting a site $\mathbf{x}$ at random and letting $h_{\mathbf{x}} \rightarrow h_{\mathbf{x}} + 1$; more involved deposition schemes, in which the kinetic energy of the depositing atom allows it to search, in the spirit of the limited mobility models, for a highly coordinated site in the neighborhood of the deposition site, have also been implemented [192].

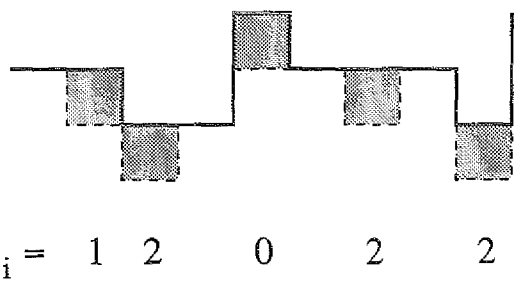

Figure 24: Definition of the coordination numbers (5.8). The surface configuration is identical to that in Figure 22, but here the relevant environments are those of (shaded) surface atoms that attempt to hop.

The modeling of the diffusion step adheres to the Arrhenius form (5.6) for the hopping rate, however with an activation barrier that depends on the local bonding environment. The barrier is assumed to be of the form

$$E = E_s + nE_N \tag{5.7}$$

where E_s is the barrier on a flat surface used in (5.6), and E_N is a bonding contribution multiplying the number n of in-plane (lateral) nearest neighbor bonds of the adatom that attempts to jump. It is important to point out that the lateral coordination number n is different from the coordination numbers k_i introduced in Section 5.1.1, since it refers to an atom that is actually present on the surface, rather than to a 'virtual' atom about to be deposited. For clarity we give here the definition of

n for a one-dimensional surface, in analogy with (5.4),

$$n_i = \begin{cases} 0 & : \quad h_i > h_{i+1} \text{ and } h_i > h_{i-1} \\ 1 & : \quad h_{i-1} < h_i \leq h_{i+1} \text{ or } h_{i-1} \geq h_i > h_{i+1} \\ 2 & : \quad h_i \leq h_{i-1} \text{ and } h_i \leq h_{i+1}, \end{cases} \tag{5.8}$$

see Figure 24. Since jumps of isolated adatoms ($n=0$) constitute the fastest process in the problem, they define the time scale and are accepted with unit probability (note that this implies a considerable speedup, by a factor of $\exp(E_s/k_BT)$, compared to a molecular dynamics simulation that operates at the attempt frequency ω_0 in (5.6)). Jumps of more highly coordinated atoms ($n>0$) are executed with probability $\exp(-nE_N/k_BT)$. It should be emphasized that, within the SOS model, the topmost atom above *each* substrate site is a potentially mobile adatom; even fully coordinated surface atoms, which have $n=2d$ on a d-dimensional surface, can move, albeit at a very small rate.

When a jump occurs, the atom is removed ($h_{\mathbf{x}} \to h_{\mathbf{x}} - 1$) and placed at a *randomly* chosen nearest neighbor site $\mathbf{y}$ ($h_{\mathbf{y}} \to h_{\mathbf{y}} + 1$). At least in this basic, most commonly used version of the model, the jump rate is independent of the bonding environment at the final site; variants which abandon this simplifying (and, as we shall see, crucial) assumption have been considered recently [192, 193, 194]. A noteworthy feature of the *equilibrium* ($F=0$) dynamics of the basic Arrhenius model is a simple relation between the collective and the tracer surface diffusion coefficients, viz. their ratio is $\exp(-dE_N/k_BT)$ for a d-dimensional surface [195].

Detailed balance. It was first suggested by Siegert and Plischke [74, 196](see also [197]) that, as a minimal criterion in the choice of surface diffusion rules in MBE models, one should require the surface to relax into a reasonable thermodynamic equilibrium state when the beam is turned off. This would ensure that the observed nonequilibrium effects are really associated with the external particle flux, rather than being artifacts of the surface diffusion dynamics. A sufficient condition is that the jump rates satisfy detailed balance with respect to some short-ranged energy function $\mathcal{H}$. Explicitly, denoting by $R_{\mathbf{xy}}$ the jump rate from site $\mathbf{x}$ to a nearest neighbor site $\mathbf{y}$, the condition reads

$$R_{\mathbf{xy}}(H)/R_{\mathbf{yx}}(H^{\mathbf{xy}}) = \exp[-(\mathcal{H}(H^{\mathbf{xy}}) - \mathcal{H}(H))/k_BT], \tag{5.9}$$

where H is a shorthand notation for a height configuration $\{h_{\mathbf{x}}\}$ and $H^{\mathbf{xy}}$ is the configuration obtained from H by moving an atom from $\mathbf{x}$ to $\mathbf{y}$; for clarity, the dependence of the jump rates on the configuration has been indicated also.

Simple energy expressions for a solid-on-solid surface are the Hamiltonians

$$\mathcal{H}_q = K_q \sum_{(\mathbf{xy})} |h_{\mathbf{x}} - h_{\mathbf{y}}|^q, \tag{5.10}$$

the sum running over nearest neighbor pairs. The case $q=1$ is known as the standard SOS model, and $q=2$ is the discrete Gaussian model [198]. It is easily checked that the basic Arrhenius rules for surface diffusion satisfy detailed balance with respect to the standard SOS model ($q=1$), provided the bonding contribution to the activation barrier is set to $E_N = 2K_1$.

Of course, the requirement of detailed balance is fulfilled by a large variety of jump rates. Siegert and Plischke [74, 196] chose the 'Metropolis' function

$$R_{\mathbf{xy}} = [1+\exp((\mathcal{H}(H^{\mathbf{xy}}) - \mathcal{H}(H))/k_B T)]^{-1} \tag{5.11}$$

and studied the effect of varying the power q in (5.10), with rather remarkable results (see Section 5.2.2). One motivation for considering different values of q comes from the observation [199] that the Hamiltonian (5.10) mimics, for $q>1$, the effect of *step edge barriers* (also referred to as *Schwoebel barriers* [200, 201]) which are known to exist on certain metal surfaces. Field-ion microscopy studies [202, 203, 204] show that atoms diffusing on a terrace can be reflected when attempting to jump down from the terrace edge. This is interpreted in terms of an increased energy barrier for inter-layer diffusion, due to the reduced bonding experienced by the atom at an edge position (the energy landscape is illustrated in Figure 28).

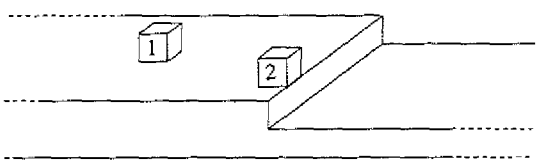

Figure 25: The excess step edge energy (5.12) is the energy difference between atom 2 and atom 1.

To see that the Hamiltonian (5.10) incorporates this effect, consider adding an isolated adatom ($n=0$) to a perfectly flat terrace (Figure 25). From (5.10) the excess energy associated with the atom is $2dK_q$ in d dimensions. Now imagine moving the atom to the cliff edge of a straight, monoatomic step. At such an edge site the energy of the atom is $(2d-1)K_q + (2^q-1)K_q$, since one of the neighboring sites is now *two* lattice units lower, rather than one. Thus, the energy at a step edge is increased by an amount

$$\Delta\mathcal{H} = (2^q-2)K_q > 0 \tag{5.12}$$

for $q>1$. If the jump rates are sensitive to the energy at the final site (this is true e.g. for the rates (5.11)), then a diffusing atom approaching a step from above is likely to be reflected, rather than being incorporated at the step. This effect is one of the main microscopic mechanisms that give rise to a nonequilibrium surface diffusion current [15] and will be discussed in detail in Section 5.2.1.

In our opinion, the requirement of detailed balance for surface diffusion processes is a useful guiding principle that should be abandoned only if compelling reasons exist to do so; as we shall see below, matters are sufficiently complicated even without artifacts arising from ill-chosen diffusion dynamics. Nevertheless, a number of investigations of collective diffusion models of MBE have been carried out in which surface diffusion is governed by energetic considerations, but detailed balance is *not* (or only approximately) fulfilled. For example, in some studies of the Arrhenius model the slowest processes, involving the motion of atoms with $n=2$ in $d=1$, are completely suppressed for numerical convenience [105, 106]; this clearly violates detailed balance, though the effects may be small at low temperatures. Phillips and Chrzan [199] proposed a model of crystal growth (in the presence of desorption) in which surface diffusion is governed by the Gaussian Hamiltonian, $q=2$, but the system is updated *in parallel*, in violation of detailed balance [197]. Finally, in some recent papers [184, 214] Arrhenius-type dynamics is supplemented with an additional rule that prevents atoms from jumping up, a further source for possibly artificial, non-detailed balance behavior.

5.1.3 Beyond the SOS approximation

All models described so far are of the SOS-type, wherein the crystal is viewed as an array of columns of heights $h_{\mathbf{x}}$ above the substrate lattice. The SOS restriction is quite natural in the context of ideal MBE, since it prevents, by construction, the formation of bulk defects. Nevertheless it has been been criticized as becoming unphysical in the presence of high surface steps [205, 206]. Indeed, since atoms move laterally, from the top of one column to another, irrespective of the height difference involved, the *vertical* motion is effectively instantaneous, as the time required for diffusion does not depend on the distance *along* the surface. This is hardly a problem for collective diffusion on two-dimensional surfaces, especially for realistically large values of $R\tau_{\mathrm{ML}}$, since high steps are exceedingly rare in that case; but the criticism is clearly relevant in one dimension, where fluctuation effects can create large local height gradients, especially in the limited mobility models. Furthermore, it is of some interest to understand the crossover from ideal MBE to (presumably) KPZ scaling once overhangs are allowed to form through 'vertical' diffusion.

Deposition models which include both surface diffusion and defect formation have long been considered in the optical thin film community [207] as well as in the detailed microscopic modeling of semiconductor MBE [208, 209], however in these works the emphasis was not on obtaining information about the statistical properties of the surface. Because of the significant computational demands associated with a realistic modeling of isotropic surface diffusion, only a few, exploratory studies

of this problem have been performed to date in the context of kinetic roughening. Yan [205] introduced two models on the square lattice ($d=1$) which are essentially isotropic variants of the limited mobility models of Section 5.1.1. Deposition occurs either in the manner of ballistic deposition (sticking at the first empty site with an occupied nearest neighbor, see Section 2.1), or as in the SOS models (deposition onto the topmost atom in a lattice column). The freshly deposited atom then performs a number of random walk steps along the arclength of the surface, vertically or horizontally. The atom is trapped permanently at sites with two or more nearest neighbors, or else it stops walking when the number of steps has reached a prescribed threshold L_{RW}. For both kinds of deposition rules a rather gradual crossover from an early time regime possibly described by the noisy Mullins equation (see Section 3.2), to KPZ-type scaling was observed, and it was confirmed that the deposit acquires a finite density of defects $1-\rho$ which approaches zero upon increasing L_{RW}.

The model of Kessler, Levine and Sander [206] is closer in spirit to the collective diffusion models of Section 5.1.2, in the sense that any atom that is not fully coordinated may move, even if it was not recently deposited. A move occurs if a more highly coordinated site can be found within a box of length and height $2L_D+1$, where the 'diffusion length' L_D is to be roughly identified with $L_{\mathrm{RW}}^{1/2}$ in Yan's model. The model was studied on the square lattice, with a 'ballistic' deposition rule (see above). In this case the crossover from an early time regime, apparently characterized by Edwards-Wilkinson scaling (see Section 3.2), to the KPZ-regime is observed to be rather violent, with a rapid intermediate increase of the width attributed to the sudden proliferation of bulk defects.

A similar scenario was found by Das Sarma, Lanczycki, Ghaisas and Kim [210] in simulations on both two- and three-dimensional lattices ($d=1$ and 2) with the 'ballistic' deposition rule. These authors employed an Arrhenius-type collective diffusion model in which the activation barrier is proportional to the *total* number of (horizontal and vertical) nearest neighbors of the atom. If the hopping attempt is accepted, the atom is moved to a randomly chosen nearest or next nearest neighbor site, provided the landing site is at the surface, i.e. it possesses at least one occupied nearest neighbor. It should be noted that this rule includes the possibility of the deposit becoming disconnected - e.g. if part of the deposit is connected to the rest only through a single, doubly coordinated atom which hops away; this problem is not specifically addressed by Das Sarma et al. The simulations show an early time 'epitaxial' regime consistent with Edwards-Wilkinson scaling ($W\sim t^{1/4}$ in $d=1$ and $W\sim\mathcal{O}(\log t)$ in $d=2$), followed by a rapid increase of the width and a final power-law regime, which is clearly resolved (and consistent with KPZ behavior) only at low temperatures, in $d=1$. The crossover time (or thickness) at which epitaxial growth

breaks down shows the expected, strong temperature dependence. By monitoring the deposit density, Das Sarma et al. verified that the crossover is associated with the onset of bulk defect formation. The defect density is rather small in the square lattice simulations, about 1 % at 700 K, but the three-dimensional cubic lattice deposits turn out to be extremely porous, with a saturation defect density of about 2/3 which, moreover, appears to be temperature independent.

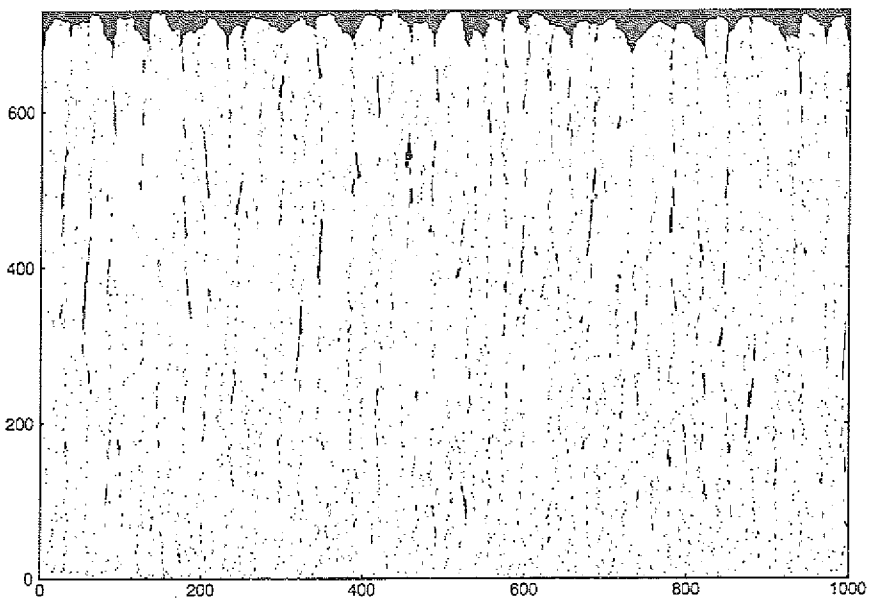

Figure 26: Two-dimensional deposit grown with a rule that allows for the formation of defects through isotropic surface diffusion. Courtesy of Martin Schimschak.

Schimschak [211] recently carried out a detailed study of the defect-induced cross-over to KPZ scaling in which both the pre-asymptotic 'epitaxial' regime, and the KPZ regime were clearly resolved, and the available information about the universal KPZ amplitudes was exploited. The model was defined on the square lattice, and the rules were chosen as a compromise between realism and tractability. First, to avoid defect formation already in the deposition stage, an SOS deposition rule was used in which particles slide down lattice columns until they reach the topmost occupied site (cf. [205]); physically this can be viewed as a consequence of transient mobility [84]. Second, a collective diffusion rule in the spirit of Das Sarma et al. [210] was employed, however diffusion was limited to singly coordinated atoms, in order to ensure the connectivity of the deposit; in this sense the model is the low temperature limit of that of Das Sarma et al. [210]. Diffusion proceeds along the arclength of the surface, and hops to nearest and next nearest neighbor sites (from the point of view of the square lattice) occur at equal probability; the inclusion of

step edge barriers which suppress 'around the corner' jumps to next nearest neighbor sites is straightforward.

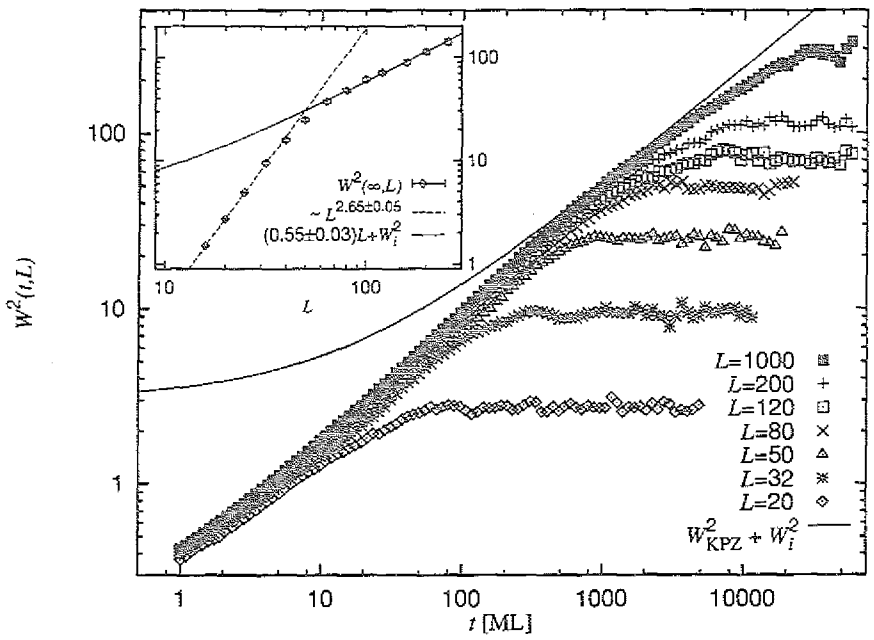

Figure 27: Surface width W as a function of the number of monolayers, t, for system sizes $L = 20 - 1000$. The ratio of hopping rate to deposition rate is $R\tau_{\mathrm{ML}} = 200$. The full line is the KPZ prediction (4.15), evaluated with the numerically determined KPZ parameters $D/2\nu = 6.6 \pm 0.4$ and $\lambda = 0.0314 \pm 0.0006$, and corrected for the intrinsic width W_i. The inset shows the stationary ($t \to \infty$) width as a function of system size. The dashed line corresponds to a roughness exponent $\zeta \approx 1.3$; the slope of the full line has been used to determine $D/2\nu$ according to (3.39). Courtesy of Martin Schimschak.

The control parameter in the model is the ratio $R\tau_{\mathrm{ML}}$ of the hopping rate to the deposition rate. A typical deposit grown at $R\tau_{\mathrm{ML}} = 200$ is shown in Figure 26. The most striking feature is the appearance of vertical void chains that seem to originate from deep narrow grooves in the surface; at least in this regime of rather high-quality epitaxial growth (the deposit density is about 0.98), the bulk defects are seen to be *induced by surface fluctuations*. The surface grooves themselves are reminiscent of structures found in the one-dimensional limited mobility models (compare to Figure 23). Indeed, the analysis of spatial and temporal correlation functions reveals that the surface fluctuations on short length and time scales (up to about 50 lattice spacings and 1000 monolayers) are virtually identical to those found in the limited mobility models of Wolf and Villain [86] and Das Sarma and Tamborenea [105], *including* the anomalous scaling of the height difference correlation function [89, 90, 94] (see also Sections 3.2 and 5.4.1).

The crossover to KPZ scaling that occurs on larger scales is illustrated in Figure

27. While the scaling range available for determining the asymptotic exponents is quite limited, KPZ universality can be unambiguously identified by including the prefactors into the analysis. As was described in Section 4.2, the relevant numbers are D/ν, which can be extracted, via eq.(3.39), from the stationary surface width shown in the inset of Figure 27, and λ, which is obtained from a measurement of the tilt dependence of the deposit density (compare to (4.3) and (5.1)). The prediction for the KPZ asymptotics resulting from (4.15) is plotted in Figure 27; it is interesting to note that, in contrast to the crossover from Edwards-Wilkinson scaling (Figure 16), here the asymptote is approached from below.

5.2 Nonequilibrium surface currents

As was noted in the preliminary discussion of nonequilibrium effects in Section 3.1, the central importance of the nonequilibrium surface current (3.14) lies in the fact that it changes the surface dynamics already on the level of the *linearized* equation of motion, and hence ultimately decides the stability of the surface. Possible mechanisms for generating an 'Edwards-Wilkinson' (EW) term $\nu\nabla^2 h$ under MBE conditions were discussed by Wolf and Villain [86] in their pioneering paper; numerical evidence for the presence of such a term was reported by Kessler et al. [206] and by Kessler and Orr [212], but its origin remained unclear. The thoughtful study of Villain [15] focused the attention on the role of step edge barriers (termed 'diffusion bias' by Villain) in producing an EW term with a coefficient that could be either stabilizing ($\nu > 0$) or destabilizing ($\nu < 0$); unknowingly Villain rediscovered the results of Schwoebel [200, 201], who had investigated the effects of step edge barriers in the framework of a step dynamical model (see Section 5.2.1).

Subsequently, Krug, Plischke and Siegert [77] offered a somewhat different point of view by proposing that inclination-dependent surface currents with an expansion (3.14) should be regarded as a *generic* consequence of the nonequilibrium conditions of MBE growth. The core of the argument can be phrased as follows: On a vicinal surface the in-plane direction of the miscut induces an asymmetry in the statistics of local bonding environments; for example, the density of up steps differs from that of down steps. Generically, an adatom moving on the surface will be influenced by the asymmetry, and consequently acquire a systematic drift along the direction of the miscut, *unless* some constraint is present which prevents the asymmetric bonding environments to be reflected in the hopping rates. In equilibrium, such a constraint is always present in the form of detailed balance. However, once detailed balance is broken by the presence of a deposition flux, or some other external influence, the drift of the particles adds up to a systematic mass current directed either 'uphill' or 'downhill'. The step edge barrier arguments of Schwoebel and Villain focus on one

particular set of bonding environments, however it is clear that many other configurations potentially play a role in determining the overall current. This implies, in particular, that nonequilibrium surface currents can appear also on surfaces where the simplest kind of step edge barriers [202, 203] is absent or undetectably weak.

An analogy may be useful in clarifying the spirit of this argument. There has been much recent interest in the Brownian motion of particles in one-dimensional, periodic, 'ratchet'-like potentials ([213] and references therein). According to a famous remark of Feynman, the left-right asymmetry of the potential is unable to induce a drift in the particle motion *provided* the stochastic dynamics satisfies the fluctuation-dissipation relation of thermal equilibrium. On the other hand, fluctuations that are of nonequilibrium origin, modeled e.g. by a 'colored' noise term in the Langevin equation, do generically produce a systematic motion of the particle, even if the fluctuations themselves are symmetric. While the magnitude of the induced current is of the order of the correlation time of the noise, as would be expected, the *sign* of the drift results from an interplay between the shape of the potential and the detailed noise statistics, in a way not easily accessible to intuitive reasoning. It is our contention that the nonequilibrium surface currents in MBE growth can be viewed as a similar, though more complex phenomenon. Indeed, rather than dealing with a single particle in an external potential, we are confronted with the *collective* diffusion of adatoms on a surface whose structure is determined by the moving atoms themselves.

Krug et al.[77] corroborated their hypothesis by numerically measuring the surface current as a function of misorientation, for MBE models of the 'collective diffusion' and the 'limited mobility' varieties, as well as for models of nonequilibrium surface diffusion *without* growth, in which detailed balance is broken by a suitable choice of hopping rates [177]. Here, we focus on the (rather limited) *analytic* understanding of these effects. Three types of analytic results have been obtained so far. First, in Section 5.2.1 the growth-induced surface current is calculated for the classic step dynamical model of crystal growth at vicinal orientations [73, 175]. This model is intermediate between continuum theories (as introduced in Section 3.1) and atomistic models, in the sense that certain microscopic structures - steps - are retained, but deposition and surface diffusion are described in terms of a continuous adatom density. While the neglect of fluctuation and nucleation effects leads to some artificial features, the results are useful for the order-of-magnitude comparison with experiments that will be attempted in Section 5.2.4. Second, for some of the models described in Section 5.1 hidden symmetries can be identified that force the nonequilibrium current to be zero, despite the absence of detailed balance in the conventional sense; these 'negative' results are summarized in Section

5.2.2. Third, in Section 5.2.3 an approximate, microscopic calculation of the current is presented for the one-dimensional limited mobility models introduced in Section 5.1.1. In these models only a few local configurations contribute to the current, the statistical weights of which can be reasonably estimated.

5.2.1 Burton-Cabrera-Frank theory with step edge barriers

The classic BCF theory [175] (here we follow the presentation of Ghez and Iyer [73]) considers a vicinal surface consisting of perfectly straight steps at a fixed spacing ℓ. The (effectively one-dimensional) geometry, and the basic processes are indicated in Figure 28. Particles impinge on the surface at a flux F, diffuse on the terraces with a diffusion constant D_s, and incorporate into the crystal at the steps; the presence of step edge barriers is modeled through the rates $r_\pm$ at which atoms coming from the lower (r_+) and the upper (r_-) terrace are incorporated; the conventional behavior corresponds to $r_+ > r_-$ [200, 201]. As usual in ideal MBE, desorption is neglected.

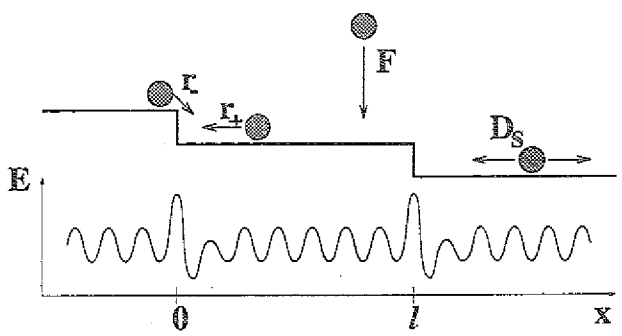

Figure 28: Schematic of a vicinal surface according to Burton, Cabrera and Frank [175]. The underlying adatom energy landscape is also indicated.

We adopt the quasistatic approximation, assuming that the adatom population on the terrace equilibrates on a time scale that is fast compared to the step motion; the consistency of this approximation will be addressed shortly. The adatom density $n(x)$ on the terrace (more precisely, the deviation of the density from its equilibrium value) then satisfies, in steady state, the stationary diffusion equation ($n'(x) = dn/dx$, $n''(x) = d^2n/dx^2$)

$$D_s n'' + F = 0 \tag{5.13}$$

with the incorporation boundary conditions [73]

$$D_s n'(0) = r_+ n(0), \quad D_s n'(\ell) = -r_- n(\ell). \tag{5.14}$$

The resulting parabolic density profile is easily written down. For later reference we note that the density scale is

$$n_0 = F\ell^2/D_s, \tag{5.15}$$

as could be guessed from dimensional considerations.

Here we are mainly interested in the surface current, which is obtained by averaging the local diffusion current $j = -D_s n'$ over the terrace. This yields

$$J = (D_s/\ell)[n(0) - n(\ell)] = J_\infty \left(\frac{\ell_- - \ell_+}{\ell + \ell_- + \ell_+} \right) \tag{5.16}$$

where the length scales

$$\ell_\pm = D_s / r_\pm \tag{5.17}$$

have been introduced, and

$$J_\infty = -\frac{1}{2} F \ell \tag{5.18}$$

refers to the maximal current that results when mass transport between layers is completely inhibited, $r_- = 0$; eq.(5.18) was previously derived by Villain [15]. Under normal conditions ($r_+ > r_-$) the current is negative because particles preferentially attach at the left, in the *uphill* direction (Figure 28).

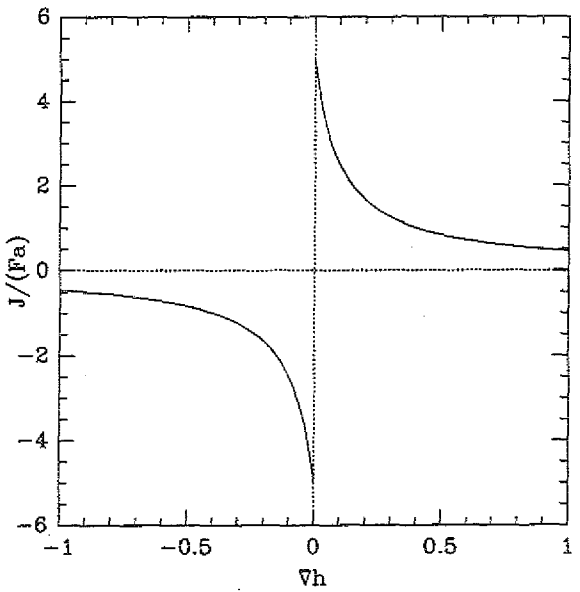

Figure 29: Growth-induced current (5.22) computed from the BCF theory without nucleation. The incorporation length is $\ell_-/a = 10$.

For an estimate of the length scales $\ell_\pm$ we write, in analogy to (5.6),

$$r_\pm = \omega_0 a \exp(-E_\pm / k_B T) \tag{5.19}$$

with $E_\pm$ denoting the energy barriers that have to be overcome to attach to the step (compare to Figure 28). Together with the expression (5.5,5.6) for D_s this implies

$$\ell_\pm = a \exp(\Delta E_\pm / k_B T) \tag{5.20}$$

where $\Delta E_\pm = E_\pm - E_s$. Since attachment from below the step is expected to be facilitated, $\Delta E_+ < 0$; consequently ℓ_+ is at most of the order of the lattice constant, and can be neglected relative to ℓ and ℓ_- in (5.16). In contrast, ℓ_- can be significantly larger than a, e.g. using the experimental estimate $\Delta E_- \approx 0.2eV$ for tungsten [203], one obtains $\ell_-/a \approx 2300$ at room temperature. The meaning of the incorporation length ℓ_- is clarified by considering the probability p_+ (p_-) that a deposited atom will be incorporated at the upward (downward) step. Since the total flux impinging onto the terrace is $F\ell$, we have (neglecting ℓ_+)

$$p_+ = \frac{D_s n'(0)}{F\ell} \approx \frac{1/2 + \ell_-/\ell}{1 + \ell_-/\ell}, \quad p_- = 1 - p_+. \tag{5.21}$$

Hence incorporation becomes symmetric, $p_+ \approx p_-$, for terraces much wider than ℓ_-. In the same approximation ($\ell_+ \to 0$)

$$J \approx J_\infty [1 + \ell/\ell_-]^{-1}, \tag{5.22}$$

illustrating the reduction of the current relative to J_∞ due to the finite interlayer transport.

Island nucleation. In Figure 29 the current (5.22) is plotted as a function of the surface inclination $\nabla h = -a/\ell$. The current is discontinuous at the high symmetry orientation $\nabla h = 0$, because (5.22) has a finite limit $-F\ell_-/2$ for $\ell \to \infty$. This is of course an artifact of not allowing for the nucleation of islands on the terraces, a process that becomes important when the terrace width ℓ exceeds the *diffusion length* ℓ_D which characterizes the typical island size on the singular ($\nabla h = 0$) surface. Studies of submonolayer epitaxial growth [215] show that ℓ_D is typically given by a relation of the form

$$\ell_D \sim (D_s/F)^\gamma \tag{5.23}$$

where the exponent γ depends on the size of the smallest stable island, the fractal dimensionality of islands, etc. In the simplest case of stable dimers and compact islands, one finds $\gamma = 1/(2d+2)$ for a d-dimensional surface.

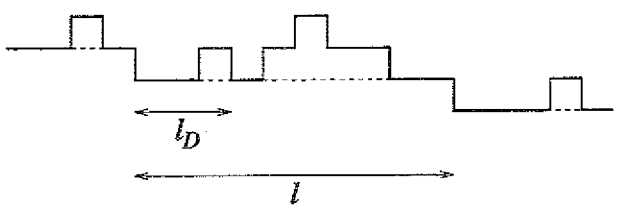

Figure 30: Schematic of a vicinal surface in the nucleation dominated regime, $\ell > \ell_D$. The dashed line indicates the original surface prior to growth.

Heuristically, the effect of island nucleation can be treated as follows [15, 216]. When $\ell \gg \ell_D$, the surface morphology more closely resembles Figure 30 than Figure 28: Rather than a well-ordered step train, one has to consider a disordered array of steps of both signs, with a small fraction ℓ_D/ℓ of excess (down) steps representing the overall vicinality of the surface. Only the excess steps contribute to the current, and the contribution of each is given by (5.22) evaluated at $\ell = \ell_D$. Thus the current vanishes for $\ell \to \infty$, as required by symmetry. Specifically, $J \approx \nu_1(a/\ell) = -\nu_1 \nabla h$ as in (3.14), with a coefficient

$$\nu_1 \approx \begin{cases} -F\ell_D^2/a & : \quad \ell_- \gg \ell_D \\ -F(\ell_D \ell_-)/a & : \quad \ell_- \ll \ell_D. \end{cases} \tag{5.24}$$

Myers-Beaghton and Vvedensky [217, 218] have proposed to include island nucleation in the BCF theory through a quadratic pair-formation term in the balance equation (5.13). In the following we show that this extended BCF theory, supplemented with the boundary conditions (5.14), reproduces the behavior of the current expected on heuristic grounds. At high adatom densities, where nucleation becomes significant, one may also expect the steps to move sufficiently fast to invalidate the quasistatic approximation [73]. Thus, the stationarity condition replacing (5.13) reads, in a frame moving with the step velocity c [217]

$$D_s n'' + cn' + F = ma^2 Fn + r_2 D_s n^2. \tag{5.25}$$

The first loss terms on the right hand side accounts for events in which an atom is deposited next to an adatom (m is the number of nearest neighbor sites of the adatom and ma^2 the corresponding capture area), while the second term describes loss of adatoms due to dimer formation, which occurs with probability r_2. In the absence of desorption the step velocity is $c = \ell/\tau_{ML} = a^2 F\ell$ by mass balance (compare to eq.(5.5)).

The significance of the various terms in (5.25) can be assessed by going over to scaled quantities, $n(x) = n_0 \rho(x/\ell)$, with the BCF density scale (5.15). This results in

$$\rho'' + (\ell/\ell_0)^2 \rho' + 1 = m(\ell/\ell_0)^2 \rho + (\ell/\ell_D)^4 \rho^2 \tag{5.26}$$

where the length scales

$$\ell_0 = (D_s/Fa^2)^{1/2} = (D_s \tau_{ML})^{1/2}, \quad \ell_D = (D_s/Fr_2)^{1/4} \tag{5.27}$$

have been introduced. The length ℓ_0 is the distance covered by a freely diffusing adatom during the monolayer completion time, while ℓ_D can be identified with the diffusion length introduced above. The value $\gamma = 1/4$ for the exponent in (5.23) results because the dominant nucleation effect has been assumed to be the formation

of dimers; in fact it is much more likely that an adatom is captured by a preexisting island, which would give $\gamma = 1/6$ [220]. This effect could be included by writing a separate equation for the island density [217, 218, 219].

For the purpose of the present discussion, the main point is that $\ell_D \ll \ell_0$ for $R\tau_{\rm ML} \gg 1$. Thus, the leading correction to the quasistatic, linear equation (5.13) is due to the pairwise nucleation term, and both the convection term cn' and the deposition term ma^2Fn in (5.25) can be neglected. Keeping the relevant terms, we rewrite (5.25) as

$$n'' = -F/D_s + r_2 n^2 = -V'(n) \tag{5.28}$$

to emphasize the analogy with a Newtonian particle of unit mass, moving in a cubic potential $V(n) = (F/D_s)n - (r_2/3)n^3$. This analogy is very useful in extracting the behavior of the density profile in the limit $\ell \to \infty$. Since ℓ is the total travel time of the particle, for $\ell \to \infty$ it has to spend most of its time close to the unstable equilibrium position $n_1 > 0$ where $V'(n_1) = 0$. Thus, the adatom density on the terrace approaches, for $\ell \to \infty$, the value

$$n_1 = \sqrt{F/D_s r_2} = F\ell_D^2/D_s \tag{5.29}$$

which is, not surprisingly, of the same form as (5.15). The boundary values $n(0)$ and $n(\ell)$ that determine the current (5.16) can now be obtained from the law of energy conservation for the particle problem (5.28), which states that the quantity

$$E(x) = (n'(x))^2/2 + V(n(x)) \tag{5.30}$$

is independent of x. Indeed, since the particle is almost at rest (the density profile is almost constant) close to n_1, for $\ell \to \infty$ the energy converges to $E = V(n_1)$. Using the bondary conditions (5.14), the boundary densities are then given by two uncoupled cubic equations,

$$(n(0)/\ell_+)^2/2 + V(n(0)) = (n(\ell)/\ell_-)^2/2 + V(n(\ell)) = V(n_1). \tag{5.31}$$

We now specialize to the case where attachment to the step from below is rapid, so that $\ell_+ = 0$ and $n(0) = 0$ is ensured. The current (5.16) is then simply $J = -(D_s/\ell)n(\ell)$. Writing $n(\ell) = \mu n_1$, the dimensionless coefficient μ satisfies

$$(\ell_D/\ell_-)^2\mu^2/2 + \mu - \mu^3/3 - 2/3 = 0, \tag{5.32}$$

which implies that $\mu \approx 1$ for $\ell_D \ll \ell_-$, and $\mu \approx (2/\sqrt{3})\ell_-/\ell_D$ for $\ell_D \gg \ell_-$. As expected, the current vanishes linearly in $\nabla h = -a/\ell$, and the coefficient is given by

$$\nu_1 = \begin{cases} -F\ell_D^2/a & : \quad \ell_- \gg \ell_D \\ -(2/\sqrt{3})F(\ell_D\ell_-)/a & : \quad \ell_- \ll \ell_D \end{cases} \tag{5.33}$$

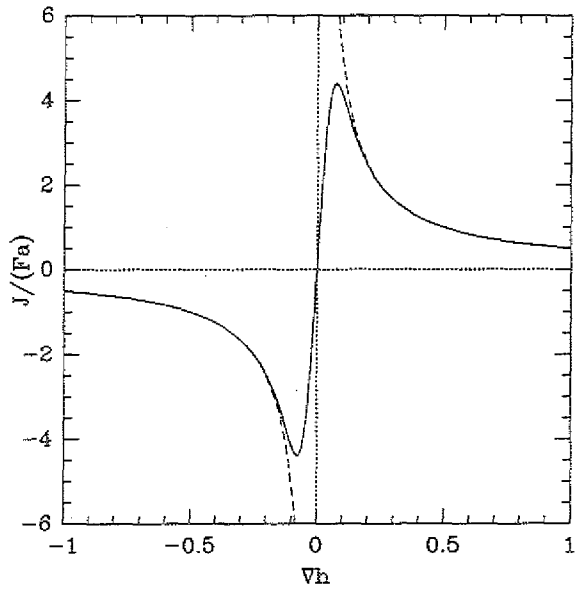

Figure 31: Growth-induced current in the presence of island nucleation, for $\ell_- = \infty$ and $\ell_D/a = 10$. The full line shows the lower bound (5.34), and the dashed line shows the current (5.18) obtained in the absence of nucleation.

in accordance with (5.24).

To obtain the full inclination dependence of the current one would require the solution of the mechanical problem (5.28) for arbitrary ℓ, which is not available in closed form. For the case of perfect step edge barriers ($r_- = 0$, $r_+ = \infty$), the lower bound

$$J \geq J_b = 2J_\infty (\ell_D/\ell)^4 [\sqrt{1 + (\ell/\ell_D)^4} - 1] \tag{5.34}$$

can be derived, which reproduces the exact asymptotics for $\ell \ll \ell_D$ and $\ell \gg \ell_D$. The expression (5.34) is shown in Figure 31, together with the current (5.18) obtained in the absence of nucleation. A similar, heuristic interpolation formula was proposed by Johnson et al. [194].

Stability. Irrespective of its derivation, the bound (5.34) is representative of the generic form of the inclination-dependent surface current induced by step edge barriers, and can be used to discuss the stability of the growing surface. We consider the physical dimensionality $d = 2$, and assume in-plane isotropy. The nonequilibrium contribution to the surface current $\mathbf{J}$ in (5.3) can then be written as [77]

$$\mathbf{J}_{NE} = \phi(|\nabla h|^2)\, \nabla h \tag{5.35}$$

where the function ϕ corresponding to (5.34) is

$$\phi(u^2) = F(\ell_D^2/a)[\sqrt{(u\ell_D/a)^4 + 1} - (u\ell_D/a)^2]. \tag{5.36}$$

The important (and generic) features of (5.36) are that $\phi \approx -\nu_1$ for $u \ll a/\ell_D$ and $\phi \approx Fa/2u^2$ for $u \gg a/\ell_D$.

We now insert (5.35) into (5.3) and expand the equation of motion about a growing surface uniformly tilted in the x-direction,

$$h(x,y,t) = ux + Ft + \epsilon(x,y,t). \tag{5.37}$$

We disregard for the moment the fourth order derivatives due to the equilibrium part of the current, since they do not affect the stability with respect to long wavelength fluctuations (see Section 5.2.4). This results in

$$\frac{\partial \epsilon}{\partial t} = \nu_{\|} \frac{\partial^2 \epsilon}{\partial x^2} + \nu_{\perp} \frac{\partial^2 \epsilon}{\partial y^2} \tag{5.38}$$

with

$$\nu_{\|} = -(\phi(u^2) + 2u^2 \phi'(u^2))$$

$$\nu_{\perp} = -\phi(u^2). \tag{5.39}$$

The stability coefficient in the tilt direction can be written in terms of the BCF current function $J(\ell)$ as

$$\nu_{\|} = -(\ell^2/a) dJ/d\ell \tag{5.40}$$

which changes sign at $\ell \approx \ell_D$. Thus, as was first pointed out by Schwoebel and Shipsey [200], the step edge barriers *stabilize* the surface in the step flow regime, $\ell < \ell_D$, but the same effect acts to *destabilize* it once island nucleation becomes appreciable for $\ell > \ell_D$ [15]. However even in the step flow regime the surface is not completely stable, because the transverse coefficient $\nu_{\perp} < 0$ for all u.

The transverse instability is related to the meandering instability of terrace edges discussed by Bales and Zangwill [221] (see also [146, 147]). In the context of the present continuum theory, a terrace edge is simply a height contour line in the (x,y)-plane. In the regime of step flow growth treated by Bales and Zangwill, the surface is stable in the tilt direction, $\nu_{\|} > 0$. It is then reasonable to consider perturbations that vary only in the transverse direction, $\epsilon = \epsilon(y,t)$ in (5.37). Defining the position of the $h = Ft$ contour line by the relation $x = \chi(y,t)$, we see from (5.37) that $\chi = -\epsilon/u$ and χ evolves according to

$$\frac{\partial \chi}{\partial t} = \nu_{\perp} \frac{\partial^2 \chi}{\partial y^2}. \tag{5.41}$$

For a quantitative comparison with Ref.[221], consider the case of absolute step edge barriers ($r_- = 0$, $r_+ = \infty$), where $\nu_{\perp} = (\ell/a) J_{\infty}$. The growth rate for a transverse modulation of wavenumber q is then equal to $(1/2)(F\ell^2/a)q^2$, which coincides with

the appropriate limit (no desorption, $q\ell \ll 1$) of the expression derived by Bales and Zangwill [221].

The converse scenario of transverse stability ($\nu_\perp > 0$) and longitudinal instability ($\nu_\parallel < 0$) is possible if adatoms preferentially approach the step from *above* ('reverse' Schwoebel effect). Due to the strongly anisotropic surface diffusion rates on the dimer-reconstructed terraces, this case is approximately realized on vicinal Si(001) [222].

We conclude that truly stable growth requires that (i) the current is a decreasing function of inclination, so that $\nu_\parallel > 0$, and (ii) the current is in the downhill direction, $\phi \leq 0$, to ensure that $\nu_\perp > 0$ also. Within the BCF theory the latter condition can be met only by assuming 'reversed' step edge barriers with $r_+ < r_-$ (this may be possible in the presence of surfactants [223]), while the former requires the surface to be in the nucleation-dominated regime, $\ell > \ell_D$. On the other hand, the BCF theory is expected to apply only to orientations vicinal to a high symmetry direction, and it is quite conceivable that a more refined treatment will reveal additional features of the current, such as zeroes related to other crystallographic symmetries [77] or 'hot atom' effects [193, 216], which favor stable growth.

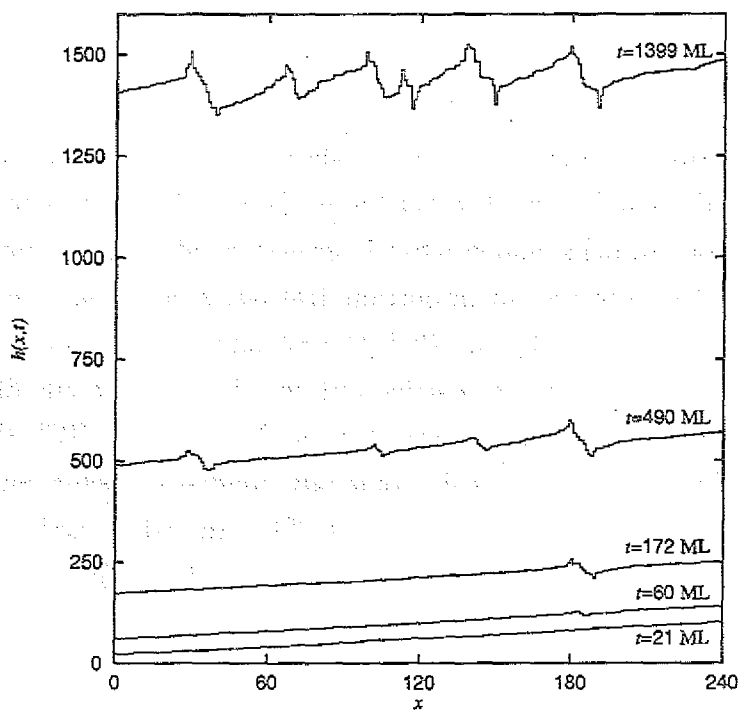

Figure 32: Evolution of a one-dimensional vicinal surface ($\ell/a = 3$) in the presence of absolute step edge barriers. The ratio of hopping to deposition rate is $R\tau_{ML} = 5 \times 10^5$. Note the nucleation of an unstable region after 60 monolayers, and the development of an approximately periodic pattern at late times. Courtesy of Martin Schimschak.

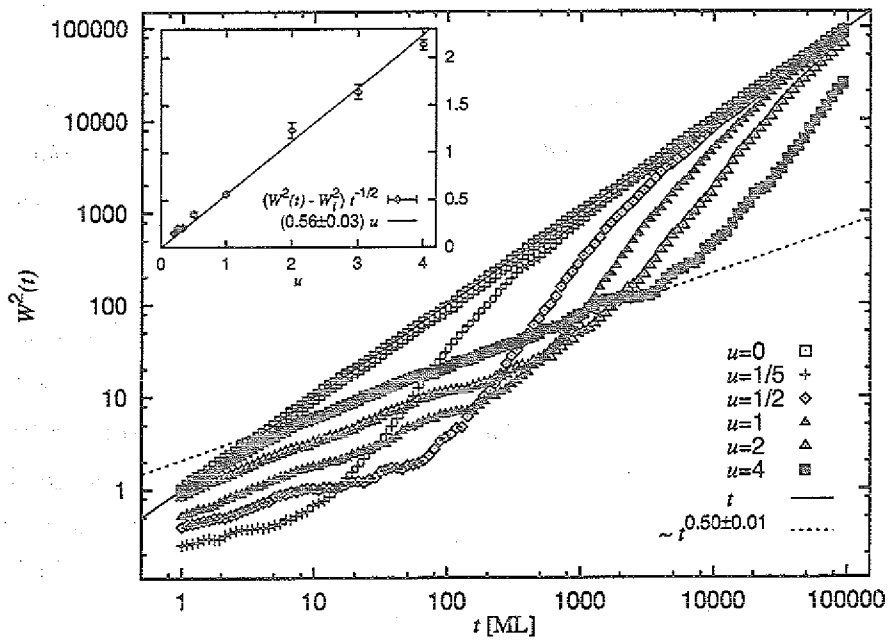

Figure 33: Time evolution of the surface width for various values of $u = -a/\ell$, at $R\tau_{ML} = 5 \times 10^5$. Initially $W^2 \sim t^{1/2}$ with a prefactor that is correctly predicted by the EW equation (inset). After the nucleation of unstable regions (Figure 32) W^2 increases faster than linearly in order to catch up with the Poisson behavior (5.42). Courtesy of Martin Schimschak.

Since the transverse destabilization is absent for one-dimensional surfaces, one may hope that the stable step-flow regime envisioned by Schwoebel may be realizable at least in one-dimensional stochastic growth models. This conclusion appears to be invalidated by the second important feature, apart from the transverse step fluctuations, that is left out by the BCF theory, namely the shot noise in the deposition flux. Schimschak [211] has carried out simulations of a one-dimensional SOS model that incorporates the basic processes of the extended BCF theory described above - deposition at rate F, diffusion of singly bonded adatoms, and the formation of immobile islands when two adatoms meet. The step edge barriers are assumed to be absolute ($r_- = 0$) so that mass transport between layers is completely inhibited. For the singular orientation, $\nabla h = 0$, this is well known to give rise to a Poisson distribution of layer coverages, and a width that increases diffusively,

$$W^2 = Ft \tag{5.42}$$

with no saturation even on a finite substrate [224]. On vicinal surfaces, for large values of $R\tau_{ML}$ (typically $R\tau_{ML} = 5 \times 10^5$), step flow behavior is observed that conforms to the predictions of BCF theory for the current (equation (5.18)), as well as for the fluctuations, described by the Edwards-Wilkinson equation with $\nu = \nu_{\|} > 0$

(see Section 3.2). However, the step flow regime is *metastable* and terminates at a transition time t_c (measured in units of τ_{ML}) that empirically scales as

$$t_c \sim u^{2.3} (R\tau_{ML})^{0.7} \tag{5.43}$$

with the surface inclination u and the diffusion rate. The transition proceeds through the nucleation of a large fluctuation in the local orientation that brings the surface into the regime where $\nu_{\|} < 0$ (Figure 32). For times $t \gg t_c$ the surface configurations resemble the strongly disordered morphology obtained on a flat substrate ($u = 0$), and the width asymptotically approaches the maximal 'Poisson' randomness given by (5.42). It is interesting to note that W^2 increases *faster* than linearly with t in the transition region (Figure 33).

5.2.2 Symmetry arguments

In this section we return to the microscopic level, and begin by formulating a precise microscopic definition of the nonequilibrium surface current for SOS models. To unburden the notation we focus on a one-dimensional surface described by discrete height variables h_i, $i = 1, ..., L$. The average heights then evolve according to

$$\frac{d}{dt}\langle h_i \rangle + \langle J_i - J_{i-1} \rangle = F, \tag{5.44}$$

the discrete analogue of (5.3), where the current is given in terms of the jump rates R_{ij} between neighboring sites, $j = i \pm 1$, as

$$J_i = R_{ii+1} - R_{i+1i}. \tag{5.45}$$

The inclination-dependent current of the macroscopic description is obtained by averaging (5.45) with respect to the stationary probability distribution of height configurations of *fixed average tilt* $u = \langle h_{i+1} - h_i \rangle$, imposed e.g. through helical boundary conditions

$$h_{i+L} = h_i + uL. \tag{5.46}$$

Thus we would like to evaluate the expectation

$$J(u) = \langle R_{ii+1} - R_{i+1i} \rangle_u. \tag{5.47}$$

Numerically, this is done simply by keeping track of the cumulative number of jumps executed to the right and to the left [77]. Note that the vertical displacements of the atoms - whether their *actual* height is increased or decreased by a jump - plays no role in determining the current. Therefore, in the following we shall use the terms 'uphill' and 'downhill' motion to imply moves in the direction of increasing or

decreasing *average* height, respectively. If $u > 0$ in (5.46), uphill jumps are directed to the right, downhill jumps to the left.

The analytic computation of (5.47) is difficult because the stationary distribution of the growth process is not known. However, in some cases either the jump rates or the stationary state itself possess a symmetry that forces J to vanish identically. This is obviously true if the rates satisfy detailed balance. It is also true for the Arrhenius growth model introduced in Section 5.1.2. There, the key point is that the jump rates depend only on the bonding environment at the initial site, $R_{ii+1} = \exp(-n_i E_N/k_B T)$, where n_i denotes the number of lateral neighbors at site i. Thus

$$J = \langle e^{-n_i E_N/k_B T} \rangle_u - \langle e^{-n_{i+1} E_N/k_B T} \rangle_u = 0 \tag{5.48}$$

by translational invariance. Physically, the current vanishes because the jump rates do not couple to the asymmetry of the local environment.

A somewhat different argument applies to the discrete Gaussian model, defined by (5.10) with $q = 2$, equipped with random deposition and the Metropolis-type jump rates (5.11). These rates depend on the initial *and* final position of the atom, and therefore the motion does couple to the asymmetry of local environments. Instead, in this case the stationary state at fixed tilt u turns out to be *independent* of u; since the current vanishes by symmetry at $u = 0$, it then has to vanish identically for all u. The tilt-invariance follows from writing the energy difference involved in a jump as [225] (the notation is explained in Section 5.1.2)

$$\begin{aligned} K_2^{-1}[\mathcal{H}(H^{ii+1}) - \mathcal{H}(H)] &= 6 - 2(h_{i+2} + h_i - 2h_{i+1}) + 2(h_{i+1} + h_{i-1} - 2h_i) \\ &= 6 - 2[(\nabla^2 h)_{i+1} - (\nabla^2 h)_i]. \end{aligned} \tag{5.49}$$

The dynamics depends only on differences in the discrete local curvature, and is therefore invariant[1] under global tilts, $h_i \to h_i + ui$. In this sense, the discrete Gaussian 'collective diffusion' model is similar to the 'limited mobility' curvature model introduced in Section 3.4, and the conclusion drawn for this model applies here also: As a consequence of the tilt-invariance there are *no relevant nonlinearities*, and the large scale properties of the surface should be given exactly by the linear noisy Mullins equation. While the original simulations of Siegert and Plischke [74] seemed to indicate a different behavior, more recent numerical results are in accord with this prediction [225].

Two comments are in order. First, we recall having argued, in Section 5.1.2, that the discrete Gaussian model has a sizable step edge barrier [199] (see eq.(5.12)),

[1] Strictly speaking the argument only implies invariance for *integer* values of the tilt. Indeed, careful simulations of the discrete Gaussian model [226] reveal a nonzero current that is a *periodic* function of the tilt, with unit period; however its amplitude ($\approx 2 \times 10^{-7}$) is so small as to make it negligible for all practical purposes.

nevertheless we have shown here that the nonequilibrium surface current vanishes identically. Thus, the presence of step edge barriers is not sufficient to produce a nonzero net current, because their effect can be cancelled by other, less conspicuous local configurations. Second, the fact that the step edge barrier energy (5.12) is an increasing function of q, vanishing at $q=1$, leads to a plausible conjecture regarding the q-dependence of the current: Since $J=0$ at $q=2$, we expect a net current in the uphill (downhill) direction for $q>2$ ($q<2$). This conclusion is corroborated by a detailed analysis of how the jump rates in various local environments change as q is moved away from $q=2$ [227]. It is further confirmed by the direct measurement of the current for $q=1$ and $q=4$ [77], as well as by the resulting behavior of the surface, which shows clean Edwards-Wilkinson scaling for $q=1$ [196], and unstable growth for $q=4$ [74, 225].

The symmetry arguments for the Arrhenius and the Gaussian models apply in arbitrary surface dimensionalities. In contrast, our last example, the version DT1 of the limited mobility rules described in Section 5.1.1, can be simply analyzed only in $d=1$. For the present discussion, the important property of the rule is that it does not distinguish between incorporation sites with one ($k_i=1$) and two ($k_i=2$) lateral nearest neighbors (the coordination numbers k_i are defined in (5.4)). The behavior of adatoms on the surface can therefore be predicted on the basis of a *two-state* variable $\tilde{k}_i=\min[k_i,1]=0,1$ assigned to each site i. The local environments that contribute to the current are $(\tilde{k}_{i-1},\tilde{k}_i,\tilde{k}_{i+1})=$ $(0,0,1)$ and $(1,0,0)$, where the atom is thought to be deposited at i and incorporates at $i+1$ or $i-1$, respectively.

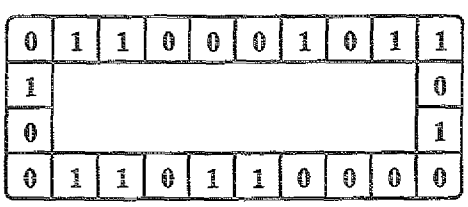

Figure 34: In a random sequence of 0's and 1's on a ring, the number of triples (001) is equal to the number of triples (100).

For a fixed height configuration $H=\{h_i\}$ subject to helical boundary conditions (5.46), we now consider the spatially and temporally averaged surface current $\bar{J}$ defined by depositing many 'test' atoms onto each site i, and recording where they would incorporate. Clearly,

$$\bar{J}(H)=L^{-1}(N_{001}(H)-N_{100}(H)) \tag{5.50}$$

where N_{lmn} is the number of local environments $(\tilde{k}_{i-1},\tilde{k}_i,\tilde{k}_{i+1})=(l,m,n)$ in the configuration H. The crucial observation is that $N_{001}=N_{100}$ for *any* string of 0's and

1's with periodic boundary conditions, both numbers being equal to the number of clusters of at least two consecutive 0's (Figure 34). Thus, $\bar{J}(H)=0$ for any configuration, and the ensemble average over H vanishes also. The proof is easily extended to versions of the rule where the atoms are allowed to search in a larger neighborhood for a favorable incorporation site, as long as the property of having only two possible values for the effective coordination number $\tilde{k}_i$ is preserved. The remaining two rules defined in Section 5.1.1, DT2 and WV, do not have this property and hence give rise to a nonzero current, which is approximately computed in the next section.

5.2.3 Approximate microscopic theory

Having established that the surface current vanishes identically for rule DT1, we may conclude that the current for the more elaborate rules DT2 and WV must be due solely to configurations in which these rules differ from DT1. For DT2, these are the asymmetric configurations $(k_{i-1},k_i,k_{i+1})=(1,0,2)$ and $(2,0,1)$, which bias the deposited particles to the right and to the left, respectively. We may therefore write

$$J_{\mathrm{DT2}}=\mathrm{Prob}(1,0,2)-\mathrm{Prob}(2,0,1). \tag{5.51}$$

For the Wolf-Villain rule WV, an additional contribution comes from the motion of particles deposited onto a site with $k_i=1$ that has a neighbor for which $k_j=2$. Thus

$$J_{\mathrm{WV}}=J_{\mathrm{DT2}}+\mathrm{Prob}(1,2)-\mathrm{Prob}(2,1). \tag{5.52}$$

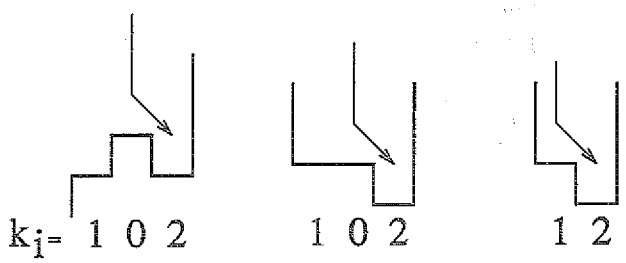

Figure 35: Height configurations contributing to the current in the limited mobility rules DT2 and WV.

In order to evaluate the probabilities occurring in (5.51) and (5.52), we now make two rather drastic approximations. First, we assume that the local height differences (also referred to as *step heights*) $\sigma_i=h_{i+1}-h_i$ at different sites are *statistically independent*. The probabilities in (5.51) and (5.52) can then be expressed as products of the three numbers p_+, p_- and p_0 defined by

$$p_+=\mathrm{Prob}\{\sigma_i>0\},\ p_-=\mathrm{Prob}\{\sigma_i<0\},\ p_0=\mathrm{Prob}\{\sigma_i=0\}. \tag{5.53}$$

The height configurations contributing to Prob(1,0,2) and Prob(1,2) are illustrated in Figure 35. We conclude that

$$\text{Prob}(1,0,2) = (p_0 + p_+)p_+^2 p_- + p_0 p_-^2 p_+, \ \text{Prob}(1,2) = p_-^2 p_+ \tag{5.54}$$

and therefore

$$J_{\text{DT2}} = p_+ p_- (p_+^2 - p_-^2)$$

$$J_{\text{WV}} = J_{\text{DT2}} + p_+ p_- (p_- - p_+) = -p_+ p_- p_0 (p_+ - p_-). \tag{5.55}$$

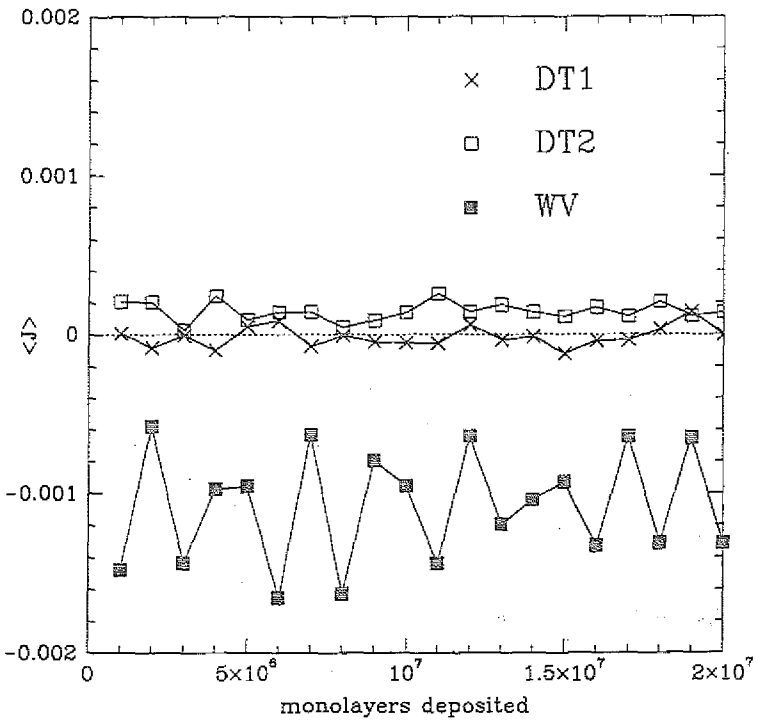

Figure 36: Simulation results for the growth-induced current, at surface inclination $\nabla h = 1$, obtained using the three limited mobility rules described in Section 5.1.1. Each data point represents an average over 10^6 monolayers deposited onto a substrate of size $L = 100$.

If the surface is flat on average, $p_+ = p_-$ by symmetry and the currents vanish. A positive average surface inclination increases p_+ relative to p_-. Thus, a first conclusion from the expressions (5.55) is that the current is directed *uphill* for the DT2 model, $J_{\text{DT2}}(u > 0) > 0$, while $J_{\text{WV}}(u > 0) < 0$. The two rules belong to different universality classes, in the sense of different signs for the coefficient ν_1 in the expansion (3.14). This is confirmed by the direct numerical measurement of the currents (Figure 36). Note, however, that J_{DT2} is extremely small and barely distinguishable from the noise. The fact that $\nu_1 < 0$ for this model therefore does not lead to any observable consequences on accessible time and length scales.

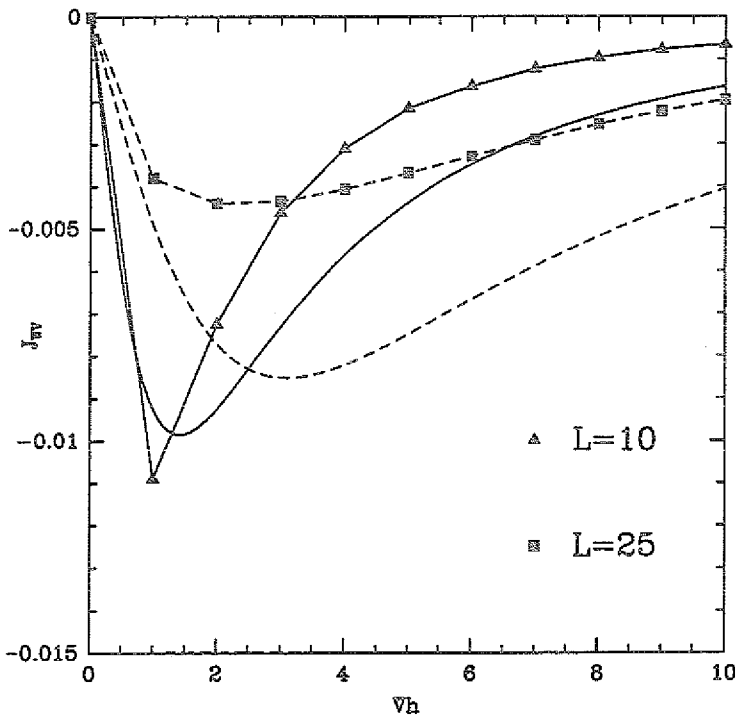

Figure 37: The inclination-dependent current in the one-dimensional Wolf-Villain model. The symbols show simulation results for two different system sizes, obtained by averaging over 10^8 monolayers per data point. The full and dashed lines without symbols show the corresponding analytic approximation.

The inclination dependence of the currents can be obtained by making a second assumption regarding the probability distribution of the step heights σ_i. For convenience, we choose an exponential distribution

$$P(\sigma) = \frac{1}{Z} \exp(-K|\sigma| + m\sigma), \tag{5.56}$$

where the 'slope chemical potential' m controls the average inclination through the relation

$$u = \langle \sigma \rangle = \frac{\sinh m}{\cosh K - \cosh m}; \tag{5.57}$$

the coupling K controls the spread of the distribution, which can be characterized, for $u = m = 0$, by the variance

$$\langle \sigma^2 \rangle = (\cosh K - 1)^{-1}; \tag{5.58}$$

and $Z(K,m)$ is a normalization constant. Eq.(5.56) would be exact if the surface were in equilibrium, governed by the Hamiltonian (5.10) with $q = 1$. The actual height difference distribution for the one-dimensional limited mobility models is

much broader, and better described by a stretched exponential (Krug, 1994a). In view of the uncontrolled approximations inherent in the present approach, however, the form (5.56) is quite sufficient for our purposes. The generalization to other choices for $P(\sigma)$ is straightforward.

Using (5.56), the probabilities $p_\pm$, p_0 and thus the currents are easily evaluated. In the following we discuss only the Wolf-Villain rule. In Figure 37 the calculated current is compared to the results of direct simulations. Since the current tends to strongly decrease with increasing system size (see below), we have chosen small systems for the simulations - $L=10$ and $L=25$ - , and averaged over 10^8 monolayers for each value of the inclination. For comparison with the simulations, the parameter K in the exponential distribution (5.56) was chosen such that the variance (5.58) matches that of the numerically determined step height distribution; for $L=10$ this gives $K=0.797$ (in this case $\langle\sigma^2\rangle \approx 2.986$), and for $L=25$ we chose $K=0.361$ (corresponding to $\langle\sigma^2\rangle \approx 15.21$). It can be seen that the approximate theory reproduces the overall inclination dependence rather well, but the magnitude of the current is significantly overestimated, especially at larger tilts.

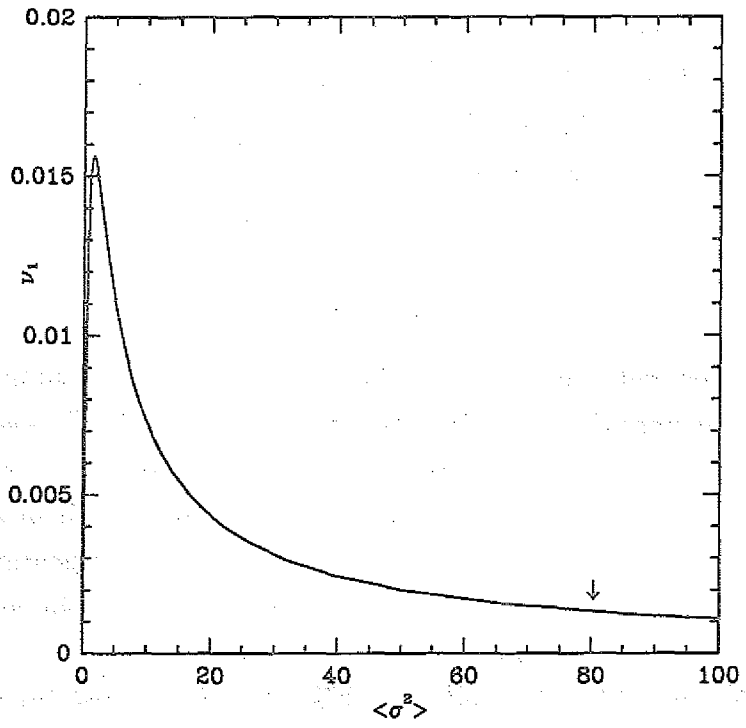

Figure 38: The expression (5.59) for the (negative) derivative of J_{WV} at zero tilt, as a function of the variance of the step height distribution. The arrow indicates the value at which $\langle\sigma^2\rangle$ saturates for large systems sizes and long times.

It is of particular interest to understand how the shape of the current-inclination

curve changes as the step height distribution $P(\sigma)$ broadens, e.g. by decreasing K in (5.56). Qualitatively, Figure 37 shows that the minimum in $J(u)$ shifts to larger slopes, such that the absolute magnitude of the current decreases with decreasing K for slopes smaller than the minimum, but increases for large slopes. On a more quantitative level, one obtains the following simple expressions for the derivative at zero slope,

$$\nu_1 = -J'_{WV}(0) = \frac{e^{-2K}(1-e^{-K})^2}{(1+e^{-K})^4} \tag{5.59}$$

and for the asymptotics for $u \to \infty$ at fixed K,

$$J_{WV}(u) \approx -\frac{e^{-K}}{2\sinh K}\frac{1}{u^2}, \quad u \to \infty. \tag{5.60}$$

Thus, ν_1 vanishes as $\nu_1 \sim K^2/16$ for $K \to 0$, while the prefactor in (5.60) diverges for small K. In Figure 38 (5.59) is plotted as a function of the variance (5.58). Somewhat surprisingly, the asymptotic $1/u^2$ behavior predicted by (5.60) seems to be confirmed by simulations of the WV model (Figure 39). Note that this asymptotics is distinct from that obtained using simple step-edge barrier arguments, which always lead to a decay of the current as $1/u$ (see Section 5.2.1).

These considerations can be used to discuss the strong size dependence of the current in the Wolf-Villain model observed by Krug et al.[77]. Recent numerical work [89, 90, 94] has revealed that the one-dimensional limited mobility models are generally characterized by a stationary step size distribution $P(\sigma)$ that broadens with increasing system size L; more precisely, the moments appear to satisfy scaling laws of the form [94]

$$\langle \sigma^q \rangle^{1/q} \sim L^{\alpha_q} \tag{5.61}$$

with nontrivial, q-dependent exponents α_q. We have encountered a simple form of this 'anomalous' scaling behavior in our investigation of the noisy Mullins equation in Section 3.2; in that case $P(\sigma)$ is a Gaussian of width $\sim L^{1/2}$ in one dimension. From our approximate theory we conclude that such broadening will result in a decrease of the current with increasing system size. This is not hard to understand: If the step height distribution is very broad, the excess steps introduced by an external tilt will have little effect, and thus the current will be small.

For the Wolf-Villain model, Schroeder et al.[89] found that the broadening of $P(\sigma)$ ceases when the system size exceeds $L \approx 250$, at which point the variance has reached a value of $\langle \sigma^2 \rangle \approx 80$. From (5.58) we see that this corresponds to a value of $K \approx 0.158$ and, using (5.59), $\nu_1 \approx 0.00132$ (see Figure 38). In comparison, in the direct numerical measurements reported by Krug et al.[77] the current was found to become size independent at $L \approx 320$, where $J(u=1) \approx -0.0008$. Thus, the approximate theory appears to provide a reasonable description of the relation

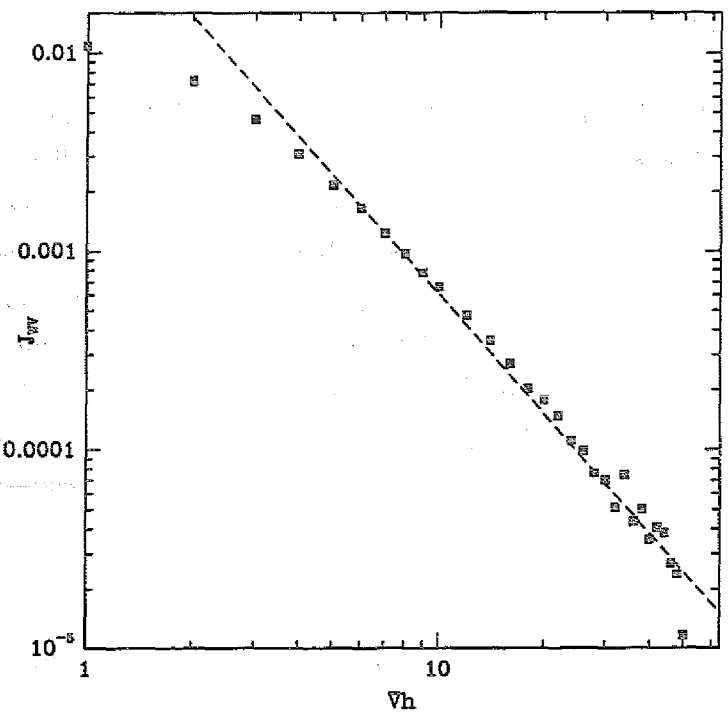

Figure 39: Inclination-dependent current in the one-dimensional Wolf-Villain model, for a small system ($L = 10$) and large slopes. Each data point corresponds to an average over 10^8 monolayers. The dashed line indicates the $|\nabla h|^{-2}$ decay predicted by the approximate theory.

between the statistics of step heights and the resulting nonequilibrium current. It does not, however, explain why the step height distribution broadens according to (5.61) in the first place (see also Section 5.4.1). We may note in this context that the broadening appears to continue indefinitely for the DT1 rule [94], which allows no current by symmetry (Section 5.2.2), indicating that the saturation of $P(\sigma)$ observed for the WV rule is indeed due to the fact that J_{WV} is nonzero.

5.2.4 Unstable growth: Theory vs. experiment

Perhaps the most remarkable corollary of the ubiquity of growth-induced surface currents is the conclusion that ideal MBE growth is *generically unstable*, in the sense that destabilizing 'uphill' currents occur as frequently as stabilizing 'downhill' currents. Among the models discussed in the preceding sections we have encountered examples of both kinds - the Metropolis model (5.11) with Hamiltonian (5.10) is stable when $q = 1$ but unstable when $q = 4$, and similarly the limited mobility model WV is stable, while DT2 is (asymptotically) unstable. Indeed, if we adopt the common view that nonequilibrium currents arise on real surfaces mainly due to

repulsive step edge barriers, unstable growth on singular surfaces should be the rule rather than the exception.

Experiments. It is therefore gratifying that several recent MBE experiments have obtained surface morphologies that are indicative of a growth instability of the kind anticipated by theory. Albrecht, Fritzsche and Gradmann [228] observed the formation of a periodic array of one-dimensional ridges during the early stages of low temperature (200 K) homoepitaxy of Fe on Fe(110). The ridges appeared after the deposition of the first few monolayers (ML), and the wavelength perpendicular to the ridges remained constant, at about 60 atomic distances, throughout the experiment, which comprised the deposition of a total of 10 ML. The amplitude of the ridges was found to increase roughly as the square root of the film thickness, and correspondingly the sides of the ridges steepened, the average terrace width decreasing from 6.1 atomic distances at 2.8 ML to 3.6 atomic distances at 9 ML.

Qualitatively similar behavior was observed by Ernst, Fabre, Folkerts and Lapujoulade [229] in a study of low temperature MBE on the Cu(100) surface. Growing up to about 100 ML at temperatures of 160 K and 200 K, they concluded from helium scattering measurements that pyramidal structures form on the surface. As in the case of Fe(110), the sides of the pyramids were found to steepen as a function of time, and their height (monitored through the surface width) increased as the square root of the film thickness $\bar{h}$ at $T = 200\text{K}$, and as $\bar{h}^{0.26}$ at $T = 160\text{K}$. For long times (beyond 50 ML) the sides of the pyramids appeared to approach a fixed crystallographic orientation, which was identified as (115) at 200 K, and (113) at 160 K. The lateral size of the pyramids, as estimated from the correlation length of the height-height correlation function, was about 22 Å at 160 K, and 106 Å at 200 K, after deposition of 60 ML. No information about the evolution of the lateral scale with film thickness was given.

A second set of experiments was carried out for the GaAs(001) surface [230]. Compared to the metal surfaces, the scales of the developing morphology are much larger in this case. Using the atomic force microscope (AFM) to scan areas of $2.5 \times 2.5\mu m$, Smith, Pidduck, Whitehouse, Glasper and Spowart [231] observed the formation of ridges running parallel to the $[\bar{1}10]$ direction. The transverse spacing (in the [110] direction) was about $0.1\mu m$ at a film thickness $\bar{h} = 0.2\mu m$, and subsequently coarsened to a value of $0.3\mu m$ at $\bar{h} = 2\mu m$. The ridges were found to be remarkably shallow, with slopes between 1.5° and 3.5° that appeared to remain constant during growth. These gentle slopes and the large lateral scale may explain why the ridge structure was overlooked in earlier studies - on scales smaller than the ridge spacing, which can be scanned using e.g. the scanning tunneling microscope (STM), the surface would appear perfectly flat, though somewhat miscut [232].

The key features of the instability on GaAs(001) were confirmed by the detailed study of Orme, Johnson, Sudijono, Leung and Orr [233] (see also [194]). In the following we will refer to this work in a preliminary attempt to *quantitatively* interpret the experimental observations in the light of the theory presented in this section. It is vital that such a quantitative comparison be attempted, and eventually refined, since it provides the only way to ascertain that the mechanism underlying the observed phenomenon is in fact that described by the theory.

Orme et al.[233] grew GaAs(001) films by MBE at $555°C$ and a growth rate of $0.18\mu m/h$. At various stages the growth was quenched and the surface was scanned using an AFM. The ridge structure first appeared after the deposition of 270 bilayers, with a transverse ridge spacing of $0.25\mu m$. From an STM study of the same surface grown under identical conditions, the diffusion length was estimated to be $\ell_D \approx 165$ Å [232]. Thus, the initial ridge spacing exceeds the diffusion length by a factor of 15. The first task of the theory must be to explain the appearance of such a large length scale.

Initial wavelength. Some insight can be gained from the linearized interface equation of motion. To linear order the general MBE equation (3.15) reduces to

$$\partial h/\partial t = \nu_1 \nabla^2 h - \kappa \nabla^4 h + F \tag{5.62}$$

where, as usual, ν_1 is the leading coefficient in the expansion of the nonequilibrium current (3.14), and $\kappa = \Gamma_a \sigma$ is the product of adatom mobility and surface tension. In the unstable case, $\nu_1 < 0$, the fastest growing wavelength under (5.62) is

$$\lambda^* = 2\pi\sqrt{-2\kappa/\nu_1}. \tag{5.63}$$

This mode growth exponentially $\sim \exp(t/\tau^*)$, with a time constant

$$\tau^* = (\lambda^*)^2/(2\pi^2\nu_1). \tag{5.64}$$

We use the generalized BCF estimate $\nu_1 \approx -F\tilde{\ell}_D^2/a$ derived in Section 5.2.1, where

$$\tilde{\ell}_D = \min[\ell_D, \sqrt{\ell_D \ell_-}] \tag{5.65}$$

is an effective diffusion length. Multiplying both sides of (5.64) by the deposition flux F, we obtain a relation between the film thickness $h^* = F\tau^*$ at which the modulation first becomes visible, the initial wavelength λ^*, and $\tilde{\ell}_D$, which we write as

$$\lambda^* = \pi\sqrt{2h^*/a}\ \tilde{\ell}_D. \tag{5.66}$$

Thus, the initial wavelength exceeds the effective diffusion length by a factor which is proportional to the square root of the number of deposited layers.

We can now ask whether the step edge barriers on GaAs(001) are 'strong', in the sense that the incorporation length $\ell_- > \ell_D$ and $\tilde{\ell}_D = \ell_D$ (see Section 5.2.1), or 'weak', $\ell_- < \ell_D$. Setting $\tilde{\ell}_D = \ell_D = 165$ Å, (5.66) predicts an initial wavelength of $1.2\mu m$, a factor 5 larger than what is observed. Thus we may assume that $\ell_- < \ell_D$, and use the experimental value $\lambda^* = 0.25\mu m$ to estimate that $\ell_- \approx 7$ Å . This can be converted into an estimate of the step edge barrier energy ΔE_- by invoking the relation (5.20). With $a \approx 2.8$ Å, the bilayer thickness, and $T = 555°C$ we obtain $\Delta E_- \approx 0.06eV$, a very small number compared to the energy barrier $E_s \approx 1.3eV$ for surface diffusion on GaAs(001) [234]. Direct experimental information on the magnitude of ΔE_- is not available. Šmilauer and Vvedensky [235] obtained $\Delta E_- \approx 0.175eV$ by fitting the results of an Arrhenius-type computer simulation (see Section 5.1.2) to reflection high energy electron diffraction (RHEED) data monitoring the thermal smoothening of MBE grown vicinal surfaces. The two estimates agree at least to the extent that both predict a *weak* barrier, in the sense that $\Delta E_- \ll E_s$.

While the arguments given here clearly are of a rather tentative character, they do indicate that the observed phenomenology for the growth-induced instability of the GaAs(001) surface is consistent with a mechanism involving weak, repulsive step edge barriers.

Slope selection and coarsening. The experiments described above suggest two possible scenarios for the nonlinear evolution of the surface morphology, beyond the validity of the linearized dynamics (5.62). In the case of Fe(110) (and possibly also for Cu(100)) the *wavelength* of the pattern was found to be independent of film thickness $\bar{h}$, while the *slopes* of the ridges increased as a power law with $\bar{h}$. In contrast, in the GaAs experiments a considerable *coarsening*, that is, an increase of the lateral wavelength of the pattern was observed, but the slopes of the ridges remained constant.

To disentangle these behaviors it is useful to first consider unstable growth in one dimension. We start from the interface equation (3.15), including a general nonequilibrium current $J_{NE}(\nabla h)$ but neglecting both the nonequilibrium chemical potential μ_{NE} and the nonlinearities induced by the geometric factors in (3.15) and (3.5). The equation for the local slope $u(x,t) = \nabla h(x,t)$ can then be written in the form

$$\frac{\partial u}{\partial t} = \frac{\partial^2}{\partial x^2} \frac{\delta \mathcal{V}}{\delta u}$$

$$\mathcal{V}[u(x,t)] = \int dx \left[\frac{\kappa}{2} (\frac{\partial u}{\partial x})^2 + V(u(x,t)) \right], \tag{5.67}$$

which is the Cahn-Hilliard equation for a conserved order parameter u [236]. Here

$\kappa = \Gamma_a \sigma$, and the 'free energy density' V is the integral of the nonequilibrium current,

$$V(u) = -\int_0^u dv J_{NE}(v). \tag{5.68}$$

In the situation of unstable growth, $V(u)$ has an unstable stationary point (a maximum) at $u = 0$, and therefore an initially flat surface (a homogeneous system prepared at $u = 0$) will phase separate through the process of spinodal decomposition [236]; the analogy between growth instabilities and spinodal decomposition was first pointed out by Golubović and Karunasiri [237].

Spinodal decomposition proceeds in two stages. The initial evolution is governed by the linearized dynamics (5.62), which selectively amplifies fluctuations at the most unstable wavelength (5.63). During this stage, which may correspond to the regime observed in the experiments on metal surfaces, the wavelength of the pattern does not change, but the amplitude (and therefore the slopes of the surface morphology) increases. Once the surface modulations have reached an amplitude where the nonlinear terms in (5.67) can no longer be neglected, a *domain structure* of typical wavelength λ^* is established. This domain structure further evolves through coarsening, a process in which larger domains grow at the expense of smaller ones. In the coarsening stage the wavelength ξ of the pattern typically increases according to a power law,

$$\xi(t) \sim t^{1/z} \tag{5.69}$$

characterized by a dynamic exponent z (see also Section 2.3.1).

The nature of the coarsening process depends crucially on the shape of the slope potential $V(u)$. A domain structure with fixed, time independent slopes of the kind observed in the GaAs experiments is possible only if $V(u)$ has stable minima at some slopes $\pm u_0$, corresponding to zeroes in the current $J_{NE}(u)$ [77]. For example, for a cubic current function (compare to (3.14))

$$J_{NE}(u) = -\nu_1 u - \nu_3 u^3 \tag{5.70}$$

the potential (5.68) becomes the familiar φ^4 Landau-Ginzburg-Wilson model which describes (for $\nu_1 < 0$ and $\nu_3 > 0$) the coexistence between two phases located at $u = \pm\sqrt{-\nu_1/\nu_3}$. Coarsening in the one-dimensional φ^4 model is well understood. In the absence of fluctuations the domain size grows logarithmically with time [40], while in the presence of fluctuations (as would be furnished e.g. by the shot noise in the MBE process) one obtains power law coarsening with $z = 3$ [238], at least up to the point where $\xi(t)$ reaches the (finite) correlation length of the one-dimensional system.

However, as we have seen in the preceding sections, simple models for the growth induced currents (such as the generalized BCF theory) typically do not produce any

zeroes in $J_{NE}(u)$, apart from the symmetry condition that $J_{NE}(0)=0$. In such cases a stable domain structure cannot be established, but rather the domains continue to steepen even during the coarsening stage. It seems plausible that the shape of an individual domain (a ridge or pyramid on the surface) would approach, for large ξ, the stationary solution of the Cahn-Hilliard equation (5.67) with wavelength ξ. The stationarity condition $\delta\mathcal{V}/\delta u=0$ takes the form of Newton's equation for a particle moving in the potential $-V(u)$, $\kappa u''=V'(u(x))$ [236]. In the case of interest here $-V$ is a potential well with a single minimum at $u=0$. The stationary solutions of wavelength ξ correspond to 'trapped' periodic trajectories with period ξ. Using energy conservation, the relationship between the wavelength and the maximal slope $u_{\max}$ (that is, the turning point of the particle trajectory) can be written as

$$\xi=4\int_0^{u_{\max}} du\,\sqrt{2(V(u_{\max})-V(u))}^{-1}. \tag{5.71}$$

For example, if the current decays to zero as

$$J_{NE}(u)\sim u^{-\gamma},\ u\to\infty, \tag{5.72}$$

evaluation of (5.71) yields

$$u_{\max}\sim\xi^{2/(1+\gamma)}. \tag{5.73}$$

Together with (5.69) this predicts how the morphology steepens as a function of time.

A detailed study of the BCF-case $\gamma=1$ has been performed by Hunt, Orme, Williams, Orr and Sander [239]. On the basis of an analysis of the lifetime of stationary solutions of fixed wavelength [40], as well as from a numerical solution of the Cahn-Hilliard equation, they estimate a coarsening exponent $z\approx 4$ in the absence of noise. Another case of interest is $\gamma=0$, corresponding to a finite limiting current for $u\to\infty$. This behavior was found numerically for the $q=4$ Metropolis model [77]. With $\gamma=0$, (5.73) predicts that $u_{\max}\sim\xi^2$, which is reasonably close to the result $u_{\max}\sim\xi^{2.6}$ obtained in simulations of the model [74, 225]. However the agreement may well be fortuitous, since the anisotropies in the surface tension and the adatom mobility probably have significant effects at the large slopes involved [195].

The simultaneous coarsening and steepening of the surface pattern can lead to a rather rapid temporal increase of the modulation *amplitude*. Combining (5.69) and (5.73), the amplitude $\delta h\sim u_{\max}\xi$ is seen to grow as

$$\delta h\sim t^{(3+\gamma)/z(1+\gamma)}. \tag{5.74}$$

Depending on the values of z and γ, the exponent in (5.74) may well exceed $1/2$, the value describing the most rapid *stochastic* roughening of a surface through purely

random deposition, with no relaxation whatsoever. For example, Siegert and Plischke [225]) found $\delta h \sim t^{0.61}$ in simulations of the one-dimensional $q=4$ Metropolis model (see Section 5.1.2), where $z \approx 6$ and $u_{\max} \sim \xi^{2.6}$, see above. This observation could be relevant to recent experiments on the epitaxial growth of silicon, where a *linear* increase of surface roughness with film thickness was found both on the Si(100) and the Si(111) surface [240, 241]. A rapid development of surface roughness was earlier conjectured by Eaglesham, Gossmann and Cerrullo [242] to be at the heart of the crystalline/amorphous transition that determines the limiting film thickness for low temperature MBE of silicon, and Eaglesham and Gilmer [240] tentatively attributed the observed behavior to the presence of step edge barrires. However, the available information about the surface morphology does not allow one to decide at this time whether an unstable growth scenario in fact applies here.

Returning to the GaAs experiments, it appears that the observed phenomenology - lateral coarsening at fixed slope - is consistent only with a current that vanishes at the selected inclinations; at least the experiments are *not* consistent with a BCF-type current, $\gamma = 1$, which would predict that the ridges steepen at the same rate as they coarsen. Krug et al.[77] pointed out that additional zeroes in J_{NE} should be expected simply due to crystalline symmetry, however the small values of the ridge slopes observed on GaAs(001) make it unlikely that these orientations would be selected by symmetry. Another possibility is that the current is driven to zero by additional effects such as knockout processes [193], which compete with the step edge barriers [216]. It seems fair to say, however, that our understanding of the microscopic origins of the growth-induced surface currents on real surfaces is insufficient to allow for any firm conclusions at this point.

Of course, in order to be relevant to real surfaces these considerations should be extended to two dimensions (though the strong anisotropy of the patterns on GaAs(001) may provide some justification for using a one-dimensional model). In two dimensions the order parameter $\mathbf{u} = \nabla h$ is a vector field satisfying the potential condition $\nabla \times \mathbf{u} = 0$. Theories of phase ordering [243] predict a coarsening exponent $z = 4$ for a vector order parameter with continuous symmetry (corresponding to in-plane isotropy of the current J_{NE}), and $z = 3$ if the symmetry is discrete (in-plane anisotropy). Siegert and Plischke [216] have numerically solved the deterministic continuum growth equation with a surface current that has symmetry-related zeroes, finding $z \approx 4$ both with and without in-plane anisotropy. An analytic understanding of this result would be of interest also for the problem of *thermal* faceting of a thermodynamically unstable crystal surface, which is governed (for the case of evaporation-condensation relaxation) by the same equation of motion as the MBE problem [216, 244].

5.3 The nonequilibrium chemical potential

The conserved KPZ equation

$$\frac{\partial h}{\partial t} = -\nabla^2[\nu\nabla^2 h + \frac{\lambda}{2}(\nabla h)^2] + \eta \tag{5.75}$$

was proposed in 1989 by Sun, Guo and Grant [245] in a first exploration of non-KPZ universality classes. These authors were concerned with the nonequilibrium dynamics of interfaces under conditions of local volume conservation, and therefore chose the noise term η to be of the conserving type, characterized by the covariance (3.17). The equation reemerged, equipped with nonconserving 'shot noise', in the first papers on ideal MBE [86, 105]. In both contexts the quadratic nonlinearity in (5.75) was written down by appealing to symmetry considerations, and to the analogy with the KPZ equation (see Chapter 4).

A physical interpretation was suggested by Villain [15], who pointed out that the nonlinearity in (5.75) could be thought to arise from an inclination dependence of the *adatom density* under growth conditions; such a dependence is easily demonstrated e.g. in the framework of the BCF-type theories discussed in Section 5.2.1. Villain's picture is very close to the point of view adopted in Section 3.1, where nonlinear terms of the form $\nabla^2(\nabla h)^{2n}$ were argued to represent the inclination dependence of a nonequilibrium contribution to the *adatom chemical potential* μ_{NE}, see eq.(3.13). In the notation of Section 3.1, the coefficients in (5.75) are $\nu = \Gamma_a\sigma$ and $\lambda = -2\Gamma_a\lambda_2$.

The goal of this section is to give a precise microscopic meaning to the notion of an inclination dependent, nonequilibrium chemical potential. We will be working mostly in the context of the Arrhenius MBE model described in Section 5.1.2. Besides having the advantage of a simple equilibrium dynamics [195], this model suits our purposes because, as shown in Section 5.2.2, it does not allow any nonequilibrium surface current. According to the power counting arguments of Section 3.3, this implies that the nonlinearity in (5.75) is a relevant term which governs the large scale behavior of the surface. We noted in Section 3.3 that the role of higher order corrections of the form $\nabla^2(\nabla h)^{2n}$ with $n \geq 2$, i.e. the consistency of keeping only the leading term in the gradient expansion (3.13), is not well understood, especially in low dimensionalities; here we will follow the common practice and disregard this complication.

Once the physics behind the nonequilibrium chemical potential has been elucidated for the case of growth, it is straightforward to devise other microscopic mechanisms that give rise to the same kind of effects under conditions of volume conservation, and thus to construct models that are described by the (fully) conserved KPZ equation originally envisioned by Sun et al.[245]. This will be addressed briefly in Section 5.3.2. In Section 5.3.3 we summarize what is known analytically

about the properties of (5.75), with conserved or nonconserved noise.

5.3.1 Microscopic origin in the Arrhenius model

As a starting point, consider the change in the ensemble-averaged local height $\langle h_{\mathbf{x}} \rangle$ induced by deposition and diffusion processes. For the purpose of the present discussion, we envision an ensemble of microscopic surface configurations that correspond to the same, slowly varying macroscopic surface shape. Due to deposition, $\langle h_{\mathbf{x}} \rangle$ increases at constant rate F; diffusion processes remove particles from site $\mathbf{x}$ and add particles coming from the neighboring sites. The resulting dynamics can be written as

$$\frac{d}{dt}\langle h_{\mathbf{x}} \rangle = \frac{1}{2d} \sum_{n.n.} \langle R_{\mathbf{yx}} - R_{\mathbf{xy}} \rangle + F, \tag{5.76}$$

with the sum over the averaged rates including the nearest neighbor sites $\mathbf{y}$ of $\mathbf{x}$. For the standard Arrhenius model described in Section 5.1.2, $R_{\mathbf{xy}} = \exp(-2K_1 n_{\mathbf{x}}/k_B T)$ which is independent of the final site $\mathbf{y}$ (recall that K_1 is the coupling constant of the SOS Hamiltonian $\mathcal{H}_1$ in (5.10)). Consequently the sum on the right hand side of (5.76) takes the form of the lattice Laplacian of the quantity

$$M_{\mathbf{x}} \equiv \langle \exp(-2K_1 n_{\mathbf{x}}/k_B T) \rangle \tag{5.77}$$

and the coarse grained equation of motion reads

$$\frac{\partial h}{\partial t} = \frac{1}{2d} \nabla^2 M + F. \tag{5.78}$$

It is clear from a comparison with the conserved interface equation (3.15) that M should be associated with the chemical potential μ (the geometric prefactor $\sqrt{1+(\nabla h)^2}$ in (3.15) does not appear in the large scale description of SOS models, see [178, 195]). In particular, a term $\nabla^2(\nabla h)^2$ appears in the equation of motion if and only if the local value of M depends on the local surface slope.

In fact a more precise connection can be established [195]. In (global) thermal equilibrium ($F = 0$) it can be shown that $M = \exp(-2dK_1/k_B T)$ independent of inclination. Moreover, if the surface is constrained by an inhomogeneous chemical potential $\mu_{\mathbf{x}}$ to adopt a modulated, *local* equilibrum shape, one finds

$$M_{\mathbf{x}} = \exp[-(2dK_1 - \mu_{\mathbf{x}})/k_B T]. \tag{5.79}$$

We give here a simple proof due to H.T. Dobbs. Let the total energy of a surface configuration $H = \{h_{\mathbf{x}}\}$ be given by (compare to (5.10))

$$\mathcal{H} = K_1 \sum_{\langle \mathbf{xy} \rangle} |h_{\mathbf{x}} - h_{\mathbf{y}}| - \sum_{\mathbf{x}} \mu_{\mathbf{x}} h_{\mathbf{x}}, \tag{5.80}$$

and let $H' = \{h'_{\mathrm{y}}\}$ denote the configuration obtained from $\{h_{\mathrm{y}}\}$ by removing a particle at site x,

$$h_{\mathrm{y}} = \begin{cases} h_{\mathrm{y}} - 1 & : \quad \mathrm{y} = \mathrm{x} \\ h_{\mathrm{y}} & : \quad \mathrm{y} \neq \mathrm{x}. \end{cases} \tag{5.81}$$

The energy difference between the two configurations is readily shown to be

$$\mathcal{H}(H') - \mathcal{H}(H) = 2K_1(n_{\mathrm{x}} - d) + \mu_{\mathrm{x}}. \tag{5.82}$$

Consequently,

$$\left\langle e^{-(2K_1(n_{\mathrm{x}}-d)+\mu_{\mathrm{x}})/k_BT} \right\rangle = \frac{1}{Z} \sum_H e^{-(\mathcal{H}(H)+2K_1(n_{\mathrm{x}}-d)+\mu_{\mathrm{x}})/k_BT} =$$

$$\left(\sum_H e^{-\mathcal{H}(H)/k_BT} \right)^{-1} \sum_{H'} e^{-\mathcal{H}(H')/k_BT} = 1 \tag{5.83}$$

and (5.79) follows.

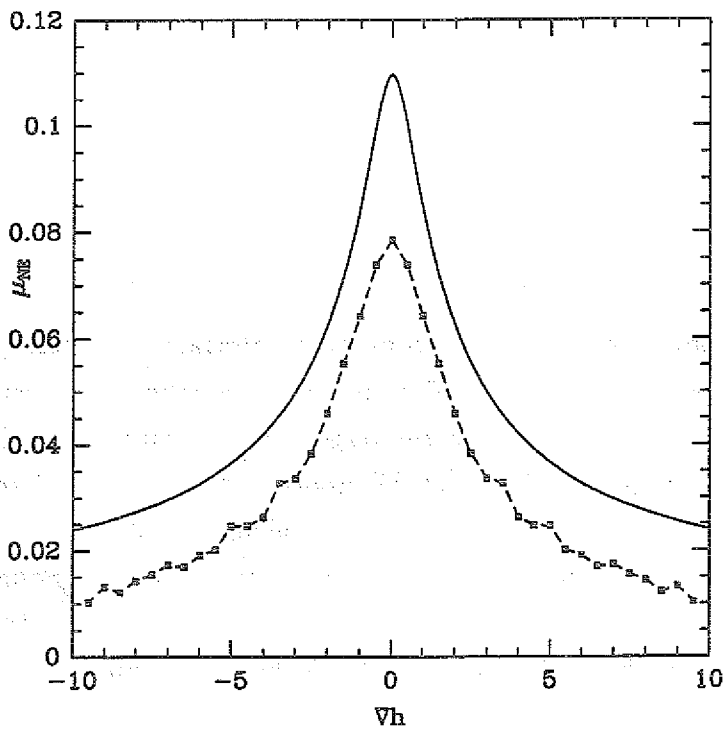

Figure 40: Inclination-dependent nonequilibrium chemical potential for the one-dimensional Arrhenius model, at reduced inverse temperature $K_1/k_BT = 1.15$ and deposition rate $F = 0.01$. The symbols represent numerical results from simulations of a system of size $L = 40$, averaged over 10^7 Monte Carlo steps per site (10^5 monolayers) for each data point. The full line is the result of the approximate analytic theory.

Turning the relation (5.79) around, we see that the quantity

$$\mu(\mathrm{x}) \equiv k_B T \ln\langle \exp(-2K_1 n_{\mathrm{x}}/k_B T)\rangle + 2dK_1 \tag{5.84}$$

provides a direct measure of the local chemical potential which can be used also in a nonequilibrium situation. In Figure 40 we show a measurement of the chemical potential as a function of inclination, for the one-dimensional Arrhenius MBE model with parameters $K_1/k_BT = 1.15$ and $F = 0.01$. The chemical potential is seen to be increased relative to its equilibrium value $\mu = 0$, with a distinct peak at zero slope. In a slope expansion as in (3.13) this implies a *negative* value of λ_2, which is estimated from the data to be $\lambda_2 \approx -0.015$. It should be no surprise that this is a small number: Since μ_{NE} is induced by the growth, its scale is set by the deposition rate F. This will be made more precise shortly.

To gain some insight into the behavior of the chemical potential, we note that (5.77) can be expressed as [246]

$$M = \sum_{n=0}^{2d} c_n \exp(-2K_1 n/k_B T) \tag{5.85}$$

where c_n is the probability that a surface atom has n lateral nearest neighbors. The c_n depend on the surface inclination even in thermal equilibrium. For example, in $d = 1$ all sites have $n = 1$ for strongly tilted surfaces, so that $c_1 \to 1$ and $c_{0,2} \to 0$ for $\nabla h \to \pm\infty$. It is only the specific linear combination (5.85) that is slope-independent in equilibrium, due to the subtle constraint of detailed balance. Conversely, it is evident that virtually *any* nonequilibrium influence disrupting detailed balance will also make M a slope-dependent quantity.

In the case of growth, one expects that the deposition beam will create isolated adatoms and thereby increase c_0 relative to the c_n with $n > 0$. Since c_0 enters the sum (5.85) with the largest coefficient, this results in an overall increase of M, and also of the chemical potential $\mu = k_B T \ln M + 2dK_1$. On the other hand, for large slopes it is easy to see that sites with $n = d$ will dominate, thereby resetting M and μ to their equilibrium values $M = \exp(-2dK_1/k_BT)$, $\mu = 0$. Consequently, the behavior of the nonequilibrium chemical potential depicted in Figure 40 - $\mu_{NE} > 0$, with a peak at zero inclination and $\mu_{NE} \to 0$ for large slopes - should be generally valid.

For the one-dimensional case a simple scheme can be devised to approximately calculate the nonequilibrium chemical potential. Let g_{mn} denote the probability that deposition onto a site occupied by an atom with m lateral nearest neighbors will create an atom with n lateral nearest neighbors. Nonzero off-diagonal elements of g are g_{10} (creation of an isolated adatom on a step edge), g_{20} (creation of an adatom on a flat portion of the surface) and g_{21} (deposition below a step edge), see Figure

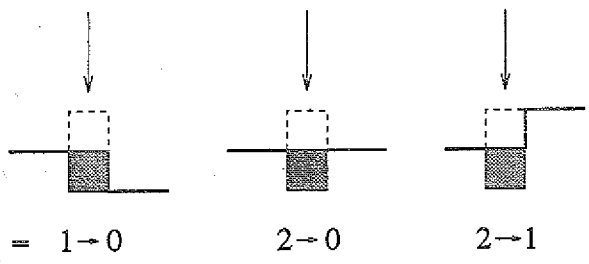

Figure 41: Changes in the local coordination numbers n_i due to the deposition of atoms.

41. For a one-dimensional equilibrium surface governed by the Hamiltonian $\mathcal{H}_1$ in (5.10), the g_{mn} are easily calculated as a function of surface inclination. To leading order in the deposition flux, the changes δc_n in the coordination number densities can then be expressed as

$$\delta c_n = F \sum_m (g_{mn} - g_{nm}) \tag{5.86}$$

which, inserted into (5.85), yields the changes in M and in μ. The result of this calculation is shown as the full line in Figure 40. The overall behavior of the chemical potential is well reproduced, though the magnitude is considerably overestimated. The situation appears to be similar, in this respect, to the calculation of the slope-dependent current in Section 5.2.3.

5.3.2 Conserved nonequilibrium dynamics

In their original work on eq.(5.75) with conserving noise, Sun et al.[245] proposed a microscopic realization based on the restricted solid-on-solid (RSOS) model of Kim and Kosterlitz [143]. It was subsequently pointed out by Rácz et al.[177] that this model in fact possesses detailed balance, and therefore cannot display the nonlinear term in (5.75). Rácz et al.[177] showed how to break detailed balance in the RSOS rule, however in the process a nonequilibrium surface current was also generated [77]. As a consequence, the large scale dynamics of their model contains a Laplacian term $\nu_1 \nabla^2 h$ which supersedes the effect of the nonlinearity (see Section 3.3), except at a special parameter value where ν_1 is (close to) zero.

From the dicussion in the preceding section it is clear how to construct a model of conserved surface dynamics that is described by the conserved KPZ equation (5.75) for *arbitrary* parameter values. We have seen that the essential effect of the deposition current in the Arrhenius MBE model is to upset the delicate balance between the terms in the sum (5.85) defining the local chemical potential, such that the conserved KPZ nonlinearity is generated in the large scale equation of motion. Thus, the task is to break detailed balance *without* violating the symmetry of the Arrhenius model that disallows a net nonequilibrium surface current (see Section

5.2.2).

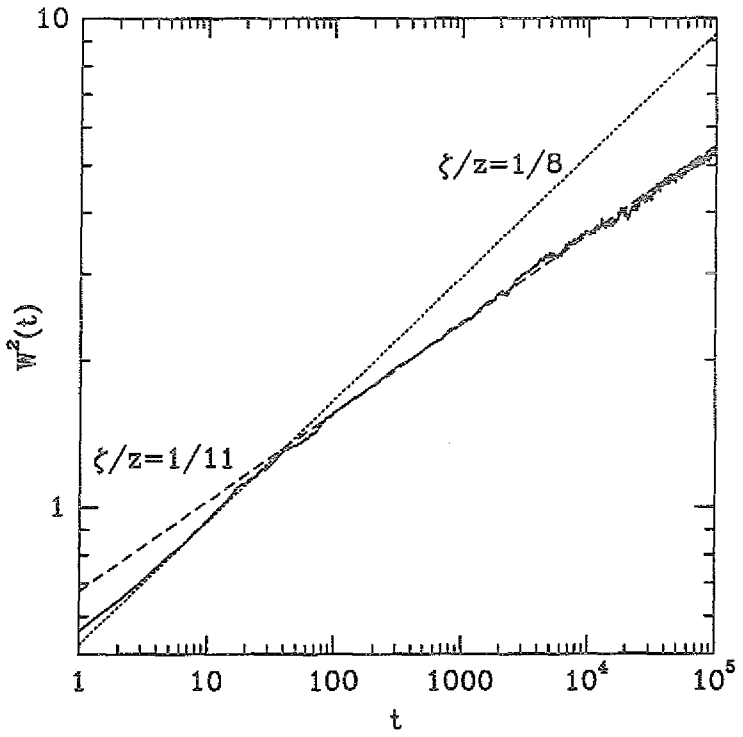

Figure 42: Simulation results for the simple symmetric nonequilibrium surface diffusion model described in the text. The full line shows the surface width (squared) as a function of time, for a one-dimensional surface of length $L = 2 \times 10^5$. The dotted line indicates an initial Mullins-regime, with $\zeta/z = 1/8$, while the dashed line $W^2 \approx 0.68\, t^{2/11}$ shows the asymptotic behavior predicted by the conserved KPZ equation, see (5.93).

It is easy to imagine nonequilibrium processes that have this effect, and that do not change the amount of mass on the surface. For example, consider a surface exposed to a beam of energetic ions. The kinetic energy provided by the beam allows particles on the surface to move to neighboring sites without thermal activation [247]. Within an Arrhenius-type model, we may suppose that an adatom is 'kicked' by the beam with probability p, and performs a thermal jump with probability $1-p$. The total jump rate is then

$$R_{\mathrm{xy}} = p + (1-p)\exp(-2K_1 n_{\mathrm{x}}), \tag{5.87}$$

which is still independent of the final site y, but no longer satisfies detailed balance; the deviation from equilibrium is governed by the parameter p, the analogue of the deposition flux in the MBE case. A straightforward simulation verifies that an inclination-dependent nonequilibrium chemical potential is indeed generated. Since the total volume of the solid is conserved, one therefore expects this model to be

described asymptotically by the conserved KPZ equation, eq.(5.75), with conserving noise.

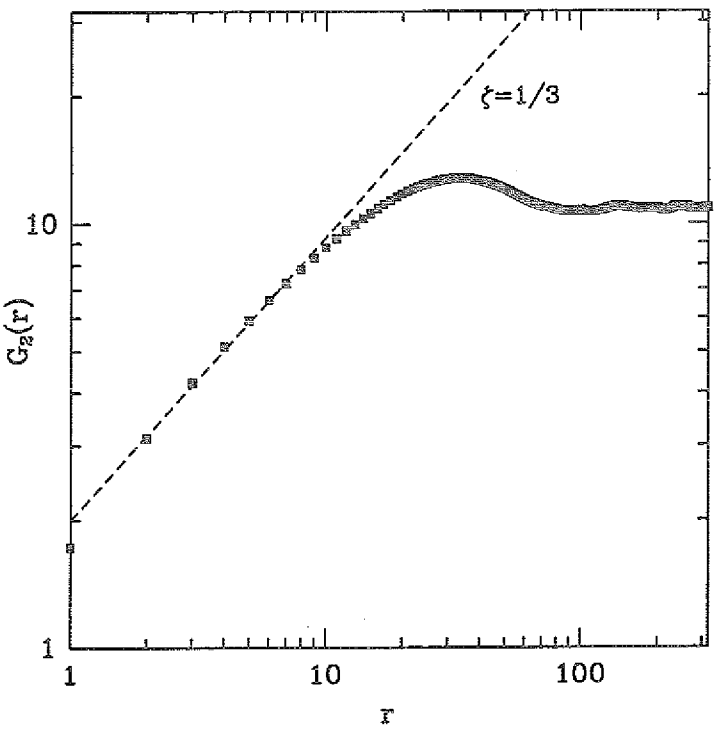

Figure 43: Height-difference correlation function at time $t = 10^5$, from the simulation shown in Figure 42. The dashed line indicates the predicted roughness exponent $\zeta = 1/3$ (see (5.92)), $G_2 \approx 2.0\, r^{2/3}$.

A simpler (and computationally more efficient) rule with the same properties is obtained as follows. A site $\mathbf{x}$ is chosen at random. It is checked whether the height at any one of the neighboring sites *exceeds* $h_{\mathbf{x}}$, by at least one lattice spacing. If so, the particle at $\mathbf{x}$ is regarded as immobile and a new site is chosen; if not, the particle at $\mathbf{x}$ is moved to a randomly chosen neighbor site. Note that, under this rule, particles incorporated into a perfect, flat singular surface are mobile. Simulation results for this rule are shown in Figures 42 and 43. The exponents are in good agreement with the theoretical predictions for eq.(5.75), which we describe next.

5.3.3 Properties of the conserved KPZ equation

One-loop renormalization group analyses of eq.(5.75) were reported by Sun et al.[245] for the case of conserved noise, and by Lai and Das Sarma [95] for the case of nonconserved noise; the latter work was extended by Tang and Nattermann [96] by including the effect of a lattice pinning potential, which turns out to be irrelevant

on large length scales. In the conserved case the lattice potential gives rise to a Kosterlitz-Thouless-type roughening transition in $d=2$ [248].

These calculations suggest a remarkably simple picture. We noted above in Section 4.3 that the lack of coupling between the average motion of the surface, and the internal fluctuations, which is a common feature of all ideal MBE processes described by equations of the type (5.3), enforces the *exact* exponent identity $z = d+2\zeta$ (eq.(4.27)). Replacing the deposition noise η by the conserving noise η_c defined by (3.17) merely shifts the dimensionality $d \to d+2$ and implies the relation

$$z = d+2+2\zeta. \tag{5.88}$$

While the scale-independence of the noise strength D is an exact property of these equations, the one-loop calculations indicate that the coefficient λ of the nonlinearity in (5.75) is also invariant under rescaling, implying the second identity

$$\zeta + z = 4, \tag{5.89}$$

the analogue of the Galilean invariance relation (4.7) for the KPZ equation. The relation (5.89) was implicitly used by Villain [15] in a Flory-type estimate of the scaling exponents.

The invariance of λ is commonly believed to hold to all orders, though this has not been rigorously established; it is not clear what symmetry plays the role of Galilean invariance in the conventional KPZ context (see [96, 177, 245] for discussions of this point). Here we follow the common view and *assume* that λ is scale-independent. This leaves us in the fortunate situation encountered previously in the treatment of the *one-dimensional* KPZ equation in Section 4.1: Having two invariant quantities, D and λ, at our disposal, both exponents and scaling forms can be determined exactly, up to universal scaling functions and amplitudes [138]. Using (4.27) and (5.89) we obtain the exponents [15, 95]

$$\zeta = (4-d)/3,\ z = (8+d)/3,\ d \le d_c = 4 \tag{5.90}$$

for (5.75) with nonconserved noise, and [245]

$$\zeta = (2-d)/3,\ z = (10+d)/3,\ d \le d_c = 2 \tag{5.91}$$

for the conserved noise case.

Specializing to the case of conserved noise in $d=1$ dimensions, we can further introduce universal amplitudes through the relations

$$G_2(r,t) \approx a_2 (D/\lambda)^{2/3} r^{2/3},\ r \ll \xi(t) \tag{5.92}$$

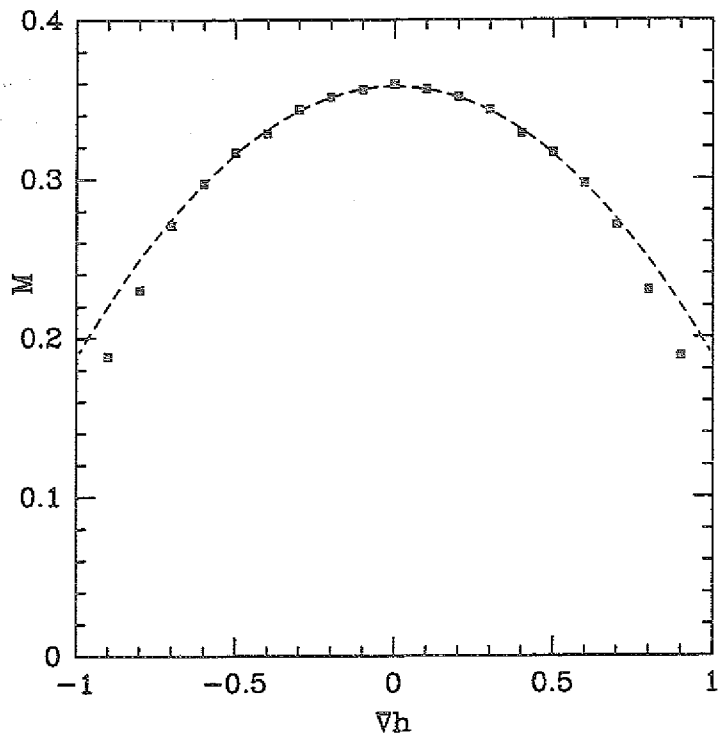

Figure 44: Average jump rate M as a function of inclination for the nonequilibrium surface diffusion model described in Section 5.3.2. The data were obtained from simulations of a system of size $L = 200$; each point constitutes an average over 10^7 attempted moves per site. The dashed line is a parabolic fit $M = 0.358 - 0.17(\nabla h)^2$. The large scale equation of motion for this model is, in analogy to (5.78), $\partial h/\partial t = (1/2)\nabla^2 M$, hence comparison with (5.75) shows that $\lambda \approx 0.17$.

for the stationary height difference correlation function (see Section 3.2), and

$$W^2(L,t) \approx c_2 (D^4/\lambda^3)^{2/11} t^{2/11}, \quad \xi(t) \ll L. \tag{5.93}$$

For the simple model described in Section 5.3.2, a measurement of the average jump rate as a function of surface inclination (which is the equivalent of the quantity M defined in (5.77) for the Arrhenius growth model) yields the value $\lambda \approx 0.17$ (see Figure 44). Together with the prefactors of G_2 and W^2 obtained from the data in Figures 42 and 43, this allows us to estimate the universal amplitude ratio

$$\mathcal{R} \equiv c_2^{11/12}/a_2 \approx 0.47. \tag{5.94}$$

In view of the somewhat uncertain status of the scaling relation (5.89), it is clearly desirable to confirm the predictions (5.90) and (5.91) for the scaling exponents through a direct numerical integration of the equation (5.75). Chakrabarti [249] carried out such a study for the equation with conserved noise, and found

agreement with (5.91). For the case of nonconserved noise the numerical integration has been attempted by Tu [250] and Moser [251]. Both authors encountered severe difficulties in integrating the equation for $d=1$, which they attributed to the large value $\zeta=1$ of the roughness exponent (see eq.(5.90)). Tu found the temporal behavior of the width to be consistent with the prediction, $W\sim t^{1/3}$, up to a finite transition time at which the interface developed singularities and the algorithm broke down. He conjectured that the development of finite time singularities might be an intrinsic feature of the *deterministic* conserved KPZ equation, (5.75) with $\eta=0$.

This seems unlikely in view of recent analytic work by Putkaradze, Bohr and Krug [252], who show that (i) cusp-like singularities can develop in finite time, but only if the stabilizing linear term in (5.75) is absent, i.e. if $\nu=0$, and (ii) the solutions remain bounded even when singularities do develop. Nevertheless, it is worth pointing out that the behavior of the deterministic, conserved KPZ equation is much less understood (and potentially more interesting) than its nonconserved counterpart, which can be exactly linearized using the Cole-Hopf transformation [156] (see also Section 4.5).

In $d=2$ dimensions the equation is numerically better behaved. Tu [250] estimates that $\zeta/z=0.21\pm0.03$ and $\zeta\approx0.71$, in reasonable agreement with the predictions 1/5 and 2/3, respectively. The extensive simulations of Moser [251] yield the estimate $\zeta/z=0.183\pm0.010$, somewhat smaller than predicted, however the deviation is attributed to a finite-time effect. Thus, at present there appears to be no compelling reason to doubt the values (5.90) of the scaling exponents.

5.4 Conclusion: The universality classes of MBE

In this chapter we have attempted to provide microscopic derivations of the nonequilibrium contributions to the conserved growth equation (3.15), which allow, at least in principle, to estimate their magnitude under conditions of real MBE growth. The relevance of these terms for the large scale surface fluctuations was discussed already in Section 3.3. The emerging picture is that of a 'nested' sequence of universality classes:

(I) Under generic circumstances, the behavior is dominated by the linear part of the nonequilibrium surface current $J_{NE}(\nabla h)$. Depending on the sign of the leading coefficient ν_1 in the gradient expansion (3.14), one obtains either Edwards-Wilkinson (EW) scaling, with logarithmic roughness in $d=2$ surface dimensions (see Section 3.2), or unstable growth of the kind discussed in Section 5.2.4.

(II) If, for reasons of symmetry (or, more realistically, because asymmetric con-

figurations such as step edges are dynamically unimportant), $J_{NE} \equiv 0$, the most relevant terms are those generated by the nonequilibrium chemical potential, eq.(3.13), and one expects the surface to be described by the conserved KPZ equation with the exponents (5.90) (at the conserved KPZ fixed point the geometric nonlinearities in (3.15) are believed to be irrelevant [95]).

(III) Finally, if the symmetry of the system not only prohibits nonequilibrium surface currents, but also imposes an invariance of the dynamics under arbitrary tilts, all conceivable nonlinearities are irrelevant and one is left with a surface described exactly by the noisy Mullins equation, with $\zeta = 1$ and $z = 4$ in $d = 2$ (see Section 3.4).

Strictly speaking, this list does not exhaust all possibilities. For example, one should also consider the case were both $J_{NE} \equiv 0$ and $\mu_{NE} \equiv 0$ in (3.15), and ask what scaling behavior results from the interplay of the geometric nonlinearities with the nonconserved shot noise [75, 76]. As was mentioned in Section 3.3, this problem is difficult to control, because all geometric nonlinearities are relevant below $d = 2$. However, it is hard to imagine a situation where $\mu_{NE} \equiv 0$, except for the case of tilt-invariance, which suppresses the geometric nonlinearities at the same time. Thus, for the present discussion we restrict our attention to the three cases I - III.

The purpose of this section is to examine to what extent the available numerical and experimental results on ideal MBE growth is consistent with the picture sketched above. The case of unstable growth was already dealt with in Section 5.2.4, and will not be discussed here. We begin with a survey of computer simulations, following the classification of Section 5.1.

5.4.1 Computer simulations

Limited mobility models. A surprising result of the numerical measurement of nonequilibrium surface currents in Ref.[77] was the prediction of a crossover to Edwards-Wilkinson scaling for the Wolf-Villain (WV) model both in one and two substrate dimensions; the crossover time was estimated to be $t_c \approx 10^6$ monolayers in $d = 1$, and $t_c \approx 2 \times 10^4$ ML in $d = 2$. Direct numerical evidence for such a crossover has been presented in two recent studies [253, 254]. Moreover, the measurement of surface currents for a variety of limited mobility rules introduced by Das Sarma and Ghaisas [183] indicates that J_{NE} is nonzero generically for these models [255]. This is to be expected, since their dynamics, which is governed by a comparison of local coordination numbers (see Section 5.1.1), does not possess any symmetries that would enforce $J_{NE} \equiv 0$; the only exception is the one-dimensional rule DT1 (Section 5.2.2). Both uphill and downhill currents have been observed [255]. The

most spectacular manifestation of uphill currents and unstable growth was displayed by Šmilauer and Kotrla [256] in a study of the WV model in $d=3$ and $d=4$ substrate dimensions.

However, clean and unambiguous EW scaling is observed in these models only when the dynamics favors downhill moves in some obvious way, through funneling [179, 180] or an explicit suppression of down jumps [183, 257]. In all other cases the downhill currents are very weak, and the scaling on numerically relevant length and time scales is governed by some *effective continuum theory* that is often difficult to identify. In one dimension this effective theory would also be expected to govern the *asymptotic* behavior of the DT1 model, which has no EW term.

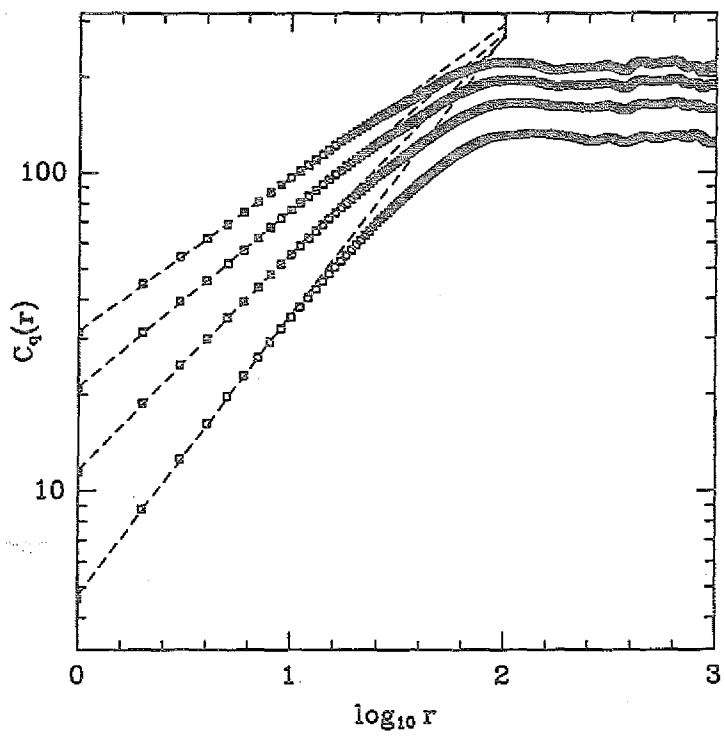

Figure 45: Generalized height difference correlation functions $C_q(r)$, defined in (5.95), from a simulation of the DT1 limited mobility model. From top to bottom, the data sets correspond to $q=4$, 3, 2 and 1. [94]

Early results obtained for the surface width $W(L,t)$ in *one dimension* suggested that the effective behavior might be described simply by the linear noisy Mullins equation [86, 105], but recent studies of the full height-difference correlation function point at a much more complex scenario [89, 90, 94]. It appears that limited mobility models in one dimension generically show anomalous scaling of correlation functions, as in (3.45), with exponents α and $\tilde{\zeta}$ that cannot easily be associated with continuum theories. Microscopically, the anomalous behavior manifests itself in an extremely

broad (stretched exponential) distribution of local height differences, with moments scaling according to (5.61). This can lead to *multiscaling* of the generalized height-difference correlation functions C_q,

$$C_q(r) = \langle |h(x+r) - h(x)|^q \rangle^{1/q} \sim r^{\tilde{\zeta}_q} \tag{5.95}$$

with q-dependent exponents, through the dominance of rare, large slope fluctuations for large q [94], see Figure 45.

While the origin of these anomalous fluctuations is yet unknown, there are two indications that their explanation lies outside the realm of continuum theories. First, Schroeder [258] has investigated the effect of increasing the incorporation range in the WV model (see Section 5.1.1). He finds that this dramatically decreases the value of α in (3.45), while leaving the roughness exponent $\tilde{\zeta}$ essentially unchanged. Thus, the long wavelength fluctuations described by $\tilde{\zeta}$, which are the only feature that can be modeled by a continuum theory, do not appear to be influenced by the divergence of the short range slope fluctuations expressed by the scaling $G_2(1,t) \sim \xi^{2\alpha}$. This suggests a picture of a conventionally rough surface 'decorated' by anomalous local fluctuations, which can be eliminated by local smoothening, e.g. by increasing the diffusion range.

The actual value of the roughness exponent, $\tilde{\zeta} = 0.78 \pm 0.05$, is close to that associated with the continuum equation

$$\frac{\partial h}{\partial t} = \nu_3 \nabla (\nabla h)^3 - \kappa \nabla^4 h + \eta \tag{5.96}$$

which is obtained if the next-to-leading, cubic term in the gradient expansion (3.14) of J_{NE} dominates over the leading linear term. Balancing the nonlinear term in (5.96) against the time derivative one obtains the relation $2\zeta + z = 4$, which together with the general exponent identity (4.27) yields [95, 183]

$$\zeta = \tilde{\zeta} = (4-d)/4, \quad z = (4+d)/2, \tag{5.97}$$

hence $\zeta = 0.75$ in $d = 1$. However the validity of this result, and in particular its relevance for the description of microscopic growth models, must be questioned. It is easy to see [259] that the cubic nonlinearity in conjunction with the noise in (5.96) gives rise to an effective surface diffusion current which is in fact *linear* in the imposed surface inclination, with a coefficient $\tilde{\nu}_1 \approx \nu_3 \kappa / D$. Thus, as it stands equation (5.96) gives rise to either Edwards-Wilkinson scaling (if $\nu_3 > 0$), or to unstable growth (if $\nu_3 < 0$). Different behavior (possibly described by (5.97)) can be expected only if a 'bare' Laplacian term $\nu_1 \nabla^2 h$ is added to the right hand side of (5.96), and the coefficient ν_1 is tuned such that $\nu_1 + \tilde{\nu}_1 = 0$. It seems unlikely that such fine tuning would take place in any 'generic' microscopic model.

A second indication for the decoupling of the anomalous slope fluctuations from the long wavelength behavior in the one-dimensional limited mobility models derives from the work of Kim, Park and Kim [185] on a restricted SOS model briefly described in Section 5.1.1. In this model large local slopes are suppressed by definition. The resulting scaling behavior is in excellent agreement with the predictions (5.90) of the conserved KPZ equation. Thus, once the anomalous local fluctuations are eliminated, the simple scenario sketched at the beginning of this section is reinstated. The inclination-dependent surface current was not measured in the work of Kim et al.[185], therefore it is not known when (or if at all) a crossover to EW behavior should be expected.

In *two dimensions*, anomalous scaling, while still detectable [255], is much weaker; Šmilauer and Kotrla [253] estimate that $\alpha/z \approx 0.05$ for the $d=2$ WV model, as compared to $\alpha/z \approx 0.19$ in one dimension with nearest neighbor incorporation. Consequently, the identification of the effective behavior prior to the crossover to EW scaling is less problematic. For the WV model Kotrla et al.[257] and Šmilauer and Kotrla [253] obtain results consistent with the exponents (5.90) of the conserved KPZ equation. For some of the variants considered by Das Sarma and Ghaisas [183], the measured exponents are closer to the values (5.97) associated with the cubic equation (5.96) [260]. As mentioned already, the reason for the applicability of this equation needs to be clarified.

Collective diffusion models. We have shown in this chapter that (i) the Arrhenius model of MBE has no net surface current, and (ii) a nonequilibrium chemical potential $\mu_{NE} > 0$, quantified by the expression (5.84), is generated under growth conditions. Thus, the large scale behavior of this model should be governed *asymptotically* by the conserved KPZ equation (5.75) with nonconserved noise. This conclusion is supported by simulations of Wilby, Vvedensky and Zangwill [261] in dimensionalities $d=1$, 2 and 3, though the scaling range in these simulations, especially in $d=1$ and 3, was quite small. In the one-dimensional case, part of the difficulty probably arises from the appearance of anomalous scaling of the kind discussed above, particularly at low temperatures [184, 225]. A detailed crossover analysis for this model as a function of temperature and deposition rate would be quite useful.

The behavior of the Metropolis model, defined by the Hamiltonian (5.10) and the jump rates (5.11), can be understood completely from the consideration of the surface current [77, 225]. For $q=1$ one observes a considerable downhill current, and clean EW scaling [196]. For $q=4$ the current is uphill and the surface is unstable [74, 225]. Finally, for $q=2$ the symmetry argument given in Section 5.2.2 implies that the surface should be governed by the linear Mullins equation, in agreement with recent simulations [225].

Among the collective diffusion simulations with detailed balance violating diffusion algorithms mentioned in Section 5.1.2, we discuss here only the careful work of Pal and Landau [214]. In their model, the suppression of upward jumps would be expected to induce a downhill current. Indeed, the logarithmic roughening characteristic of the two-dimensional EW equation is observed, though the dynamic exponent is estimated to be $z = 1.61 \pm 0.02$, rather than the EW value $z = 2$; it appears, however, that the data are not inconsistent with $z = 2$.

5.4.2 Kinetic roughening experiments

Over the last few years, an increasing number of deposition experiments have been performed with the aim of verifying the dynamic scaling scenario, and estimating the universal scaling exponents widely advertised by theoreticians. In carrying out such experiments and interpreting their results in the light of theory, one is faced with two somewhat unrelated difficulties.

First, real surfaces are immensely more complex than the theorist's mental images. They typically display a wide variety of characteristic length scales, associated with e.g. grain boundaries, defects and impurities, and it is often hard to ensure that the phenomena occurring at the scale accessible to a particular experimental technique are indeed governed by the simple processes described by theoretical models; also, the substrate on which growth occurs is usually not perfectly flat, but possesses a roughness that can be quite comparable to that developed kinetically during growth. Second, all experimental techniques that can access the micro- and mesoscopic scales of interest are, to a larger or lesser degree, *indirect* in the sense that the interpretation of data requires additional assumptions and theoretical input.

These inherent difficulties place high demands on the versatility and inventiveness of the experimental investigation. To unambiguously determine that kinetic roughening is taking place, it is crucial that the *dynamic* development of the roughness be monitored (e.g. through the increase of the surface width W or the correlation length ξ) in addition to its spatial characterization through the roughness exponent ζ. This requires either the use of some *in situ* technique by which the surface morphology can be observed during growth, or the preparation of a sequence of samples with different film thicknesses (that is, deposition times) that are then investigated *ex situ*. An interesting third possibility is the growth of multilayer films, where the surface configurations at various stages of the deposition process are preserved in the bulk of the film in the form of solid-solid interfaces [240, 262, 263]. Similarly, in order to overcome the limitations of any particular experimental probe of surface roughness, it is essential that the same system be investigated using different, complementary techniques [264].

In the following, a few recent key experiments are described that have gone a long way in meeting the requirements formulated above, and that were moreover conducted under conditions reasonably close to the 'ideal MBE' process envisioned in this chapter.

Iron. The first set of experiments concerns the epitaxial growth of iron. Chevrier, Le Thanh, Buys and Derrien [265] deposited iron films of up to 2500 Å thickness onto the Si(111) surface at $50°C$. Analyzing the broadening of the peaks in the RHEED (reflection high energy electron diffraction) pattern as a function of deposition time, they found that the surface width W increased with film thickness $\bar{h}$ as a power law,

$$W \sim \bar{h}^{\beta}, \tag{5.98}$$

where β was in the range 0.22-0.3. Since the measured value of β is close to the prediction of KPZ simulations, $\beta = \zeta/z \approx 0.24$ [109], the experiment was initially interpreted as being indicative of a KPZ-type roughening mechanism.

This conclusion had to be revised when He, Yang, Lu and Wang [266] reported results on a closely related system (Fe on Fe(001)) obtained with a technique (high resolution low energy electron diffraction, HRLEED) that allows for the simultaneous measurement of dynamic and static scaling properties. While the value of β estimated by HRLEED, $\beta = 0.22 \pm 0.02$, is fully compatible with that of Chevrier et al.[265], the large value $\zeta = 0.79 \pm 0.05$ of the roughness exponent clearly rules out KPZ behavior. The observed exponents are roughly halfway between those predicted by the linear Mullins theory ($\beta = \zeta/z = 1/4$, $\zeta = 1$ in $d = 2$) and by the conserved KPZ equation ($\beta = 1/5, \zeta = 2/3$ from (5.90)), perhaps slightly closer to the latter.

More significantly, the scaling relation (4.27), characteristic of all ideal MBE-type processes, is well satisfied by the experimental exponent estimates. In terms of the experimentally accessible exponents, the relation (4.27) reads

$$2\beta(1 + 1/\zeta) = 1, \tag{5.99}$$

while the values given by He et al.[266] imply $2\beta(1 + 1/\zeta) = 1.0 \pm 0.1$. In contrast, the KPZ identity (4.7) would predict $\zeta(1 + 1/\beta) = 2$, whereas experimentally $\zeta(1 + 1/\beta) = 4.4 \pm 0.6$. This provides quite strong evidence that the epitaxial growth of iron films at ambient temperatures falls into the ideal MBE category (note, however, the rather different behavior found in the low temperature epitaxy on Fe(110), as described in Section 5.2.4; we will return to this point at the end of the section).

Silver. A detailed study of room temperature vapor deposition of silver films onto silicon and quartz substrates was recently carried out by Thompson, Palasantzas,

Feng, Sinha and Krim [267] and by Palasantzas and Krim [268]. Thompson et al.[267] used an *in situ* apparatus where thermal deposition could be alternated with X-ray reflectivity measurements. In these measurements, the increase of the surface width is monitored through the decrease in specular reflection, while the height difference correlation function is extracted from the diffuse scattering [269]. Examining a range of film thicknesses $100\text{Å} \leq \bar{h} \leq 1500\text{Å}$, the surface width was found to increase as in (5.98) with $\beta = 0.26 \pm 0.05$. The estimate for the roughness exponent obtained from the diffuse scattering intensity was $\zeta = 0.63 \pm 0.05$. Correcting for the influence of the 'buried' Si/Ag interface lead to larger values, in the range $0.65 < \zeta < 0.75$. A larger value for ζ is also suggested by an STM analysis of the surface, which yields $\zeta = 0.78 \pm 0.014$ from a direct measurement of the height difference correlation function. The final estimate given by the authors is $\zeta = 0.7 \pm 0.1$.

In principle, the diffuse scattering of X-rays provides a measure also of the dynamic correlation length ξ, and thus of the dynamic exponent z defined through $\xi \sim t^{1/z}$ [269]. Thompson et al.[267] conclude that, in their system, the correlation length is too small to be accurately determined in this way, however the data are consistent with a power law dependence on film thickness, $\xi \sim \bar{h}^{1/z}$ with $z = \zeta/\beta \approx 2.7$ obtained from the experimental estimates for ζ and β. This issue was reexamined in the STM study of Palasantzas and Krim [268]. For silver films of thicknesses between 100 and 10000 Å, deposited onto quartz substrates, they estimated that $\beta = 0.29 \pm 0.06$ and $\zeta = 0.82 \pm 0.05$, in good agreement with the X-ray results. In addition, the increase of the dynamic correlation length with film thickness was explicitly verified, and the dynamic exponent was estimated to be $z = 2.53 \pm 0.50$. Within the error bars, these numbers satisfy the ideal MBE scaling relation (5.99) as well as the (theoretically self-evident) relation $\beta = \zeta/z$. Additional direct evidence for the applicability of ideal MBE models to this system derives from the observation [267] that the film density is close to the bulk density of silver (no defects), and the sticking coefficient is close to unity (no desorption).

Discussion. The silver deposition studies of Thompson, Krim and coworkers provide the most detailed confirmation to date of the dynamic scaling scenario for the kinetic roughening of surfaces. They also highlight the typical difficulties mentioned at the beginning of this section.

First, since the substrates used in this work (silicon and quartz) are not wetted by the silver, the initial stage of growth proceeds through the formation of three-dimensional islands, which lead to a polycrystalline film structure and considerable long-wavelength roughness not associated with the stochasticity in the deposition process [267]. The polycrystallinity can be neglected only as long as the size of the crystalline domains much exceeds the dynamic correlation length ξ [270]. In addi-

tion, a considerable amount of substrate roughness was present in the experiments, which had to be subtracted from the measured (squared) surface width prior to analysis [267, 268].

Second, X-ray scattering, while being an extremely powerful technique for the study of correlated surface roughness, is also a typical example of an indirect method, the results of which can be strongly affected by the assumptions put into the data analysis. In order to extract the roughness exponent ζ and the correlation length ξ from the diffuse scattering intensity, a model for the full height difference correlation function has to be provided. The traditional choice (see e.g. [269])

$$G_2(r) = 2W^2(1 - \exp[-(r/\xi)^{2\zeta}]) \tag{5.100}$$

combines the proper asymptotics for $r/\xi \ll 1$ and $r/\xi \gg 1$ in a simple way, but it is motivated by convenience rather than supported by theory or experiment. Palasantzas and Krim [271] have proposed alternative forms for G_2, and shown that the value of ξ extracted from diffuse X-ray data depends sensitively on the precise shape of the scaling function.

These comments do not intend to criticize the admirable and highly encouraging experimental efforts. Rather, it is hoped that they will inspire future theoretical work addressing the pertinent issues, i.e. (i) the effects that a polycrystalline domain structure and a rough substrate have on the kinetic roughening process, and (ii) an improved model for the shape of the height correlation function, to replace the heuristic ansatz (5.100).

One may wonder, finally, why the EW universality class, purportedly the most robust and generic class of ideal MBE processes, does not appear in the experiments described here (rather convincing evidence for EW scaling has been found in the growth of *amorphous* multilayers, however [263]). A tentative explanation was given in Section 5.2.4: If repulsive step edge barriers are primarily responsible for nonequilibrium surface currents on real surfaces, then destabilizing currents ($\nu_1 < 0$) should occur more commonly than stabilizing ones ($\nu_1 > 0$, EW scaling). This view would reconcile the iron film experiments described in this section with those discussed in Section 5.2.4: Under the low temperature conditions considered by Albrecht et al.[228], step edge barriers may be sufficiently effective to instigate unstable growth, while at room temperature effectively $\nu_1 = 0$ and higher order terms in the general interface equation of motion (3.15) become important.

Indirect evidence that points in the same direction is provided by studies of kinetic roughening during the MBE of GaAs(001). Johnson et al.[232] observed that the increase of roughness as a function of film thickness is exceedingly slow, consistent with the logarithmic behavior expected from the EW theory. In view of the subsequently discovered growth-induced instability of the GaAs surface, this

result should be interpreted as describing the kinetic roughening of the sides of the evolving ridge structures (see Section 5.2.4). Whatever the mechanism that selects the slopes of these ridges, it is clear that the slopes have to lie in the stable region of the inclination dependent current, where $\nu_1 = -J' > 0$, and hence their roughening should indeed be of EW type.

Note added: The experimental situation in this area is very much in a state of flux. Recent work by Stroscio *et al.* [272] suggests that the scaling behavior observed in the iron deposition experiments described above [265, 266] may in fact be due to *unstable* growth of the kind discussed in Section 5.2.4, at least for the case of deposition onto atomically flat, single crystal surfaces. On the other hand, the real space images of Palasantzas and Krim [268] seem to rule out an unstable growth scenario for the silver/quartz system. Two recent experimental studies of scaling in *heteroepitaxial* growth [273, 274] emphasize the need to incorporate droplet formation and coalescence in the initial stages of deposition, and the subsequent formation of a polycrystalline domain structure, into the kinetic roughening theories.

Acknowledgements

Much of this work originated from most enjoyable collaborations with Tomas Bohr, Harvey Dobbs, Geoff Grinstein, Tim Halpin-Healy, Mogens Jensen, Klaus Kassner, Mike Plischke, Martin Schimschak, Martin Siegert, Kim Sneppen and Lei-Han Tang. I am particularly indebted to Paul Meakin for his contributions to the study of competitive growth processes. I am grateful to Jim Evans, Terry Hwa, Martin Rost, Herbert Spohn, Dietrich Wolf and Andy Zangwill for sharing their insights; to Richard Ghez for introducing me to the BCF-theory of crystal growth; and to Uwe Klemradt for alerting me to the subtleties of kinetic roughening experiments. Last not least, Reinhard Lipowsky has provided continuous guidance and encouragement while this work was in progress.

Some important ideas were developed during productive visits to Simon Fraser University and NORDITA. I also wish to thank the organizers of the recent summer schools on *Complex Systems* (Humlebæk, August 1993) and *Scale invariance, interfaces and nonequilibrium dynamics* (Cambridge, UK, June 1994) for giving me the opportunity to deliver the lectures around which this article was built.

References

[1] T.A. Witten and L.M. Sander, Diffusion limited aggregation: A kinetic critical phenomenon, *Phys. Rev. Lett.* 47:1400 (1981).

[2] T. Vicsek, "Fractal Growth Phenomena", World Scientific, Singapore (1989).

[3] P. Meakin, The growth of fractal aggregates and their fractal measures, *in:* "Phase Transitions and Critical Phenomena", Vol. 12, C. Domb and J.L. Lebowitz, eds., Academic, New York (1988).

[4] B.B. Mandelbrot, "The Fractal Geometry of Nature", W.H. Freeman and Co., San Francisco (1982).

[5] L.P. Kadanoff, Fractals - where's the physics ?, *Physics Today*, February 1986, p. 6.

[6] P. Bak, C. Tang and K. Wiesenfeld, Self-organized criticality - an explanation of $1/f$ noise, *Phys. Rev. Lett.* 59:381 (1987).

[7] G. Grinstein, Generic scale invariance and self-organized criticality, to appear in "Scale Invariance, Interfaces and Non-Equilibrium Dynamics", M. Droz, A.J. McKane, J. Vannimenus and D.E. Wolf, eds., Plenum Press, New York.

[8] J. Krug and H. Spohn, Kinetic roughening of growing surfaces, *in:* "Solids Far From Equilibrium", C. Godrèche, ed., Cambridge University Press, Cambridge (1991), pp. 479.

[9] P. Meakin, The growth of rough surfaces and interfaces, *Phys. Rep.* 235:189 (1993).

[10] T.J. Halpin-Healy and Y.C. Zhang, Kinetic roughening phenomena, stochastic growth, directed polymers and all that, *Phys. Rep.* (to appear).

[11] J. Krug and P. Meakin, Scaling properties of the shadowing model for sputter deposition, *Phys. Rev. E* 47:R17 (1993).

[12] J. Krug, K. Kassner, P. Meakin and F. Family, Laplacian needle growth, *Europhys. Lett.* 27:527 (1993).

[13] W.W. Mullins, Solid surface morphologies governed by capillarity, *in:* "Metal Surfaces: Structure, Energetics and Kinetics", N.A. Gjostein and W.D. Robertson, eds., American Society of Metals, Metals Park (1963).

[14] M. Kardar, G. Parisi and Y.C. Zhang, Dynamic scaling of growing interfaces, *Phys. Rev. Lett.* 56:889 (1986).

[15] J. Villain, Continuum models of crystal growth from atomic beams with and without desorption, *J. Phys. France I* 1:19 (1991).

[16] H.-A. Bahr, U. Bahr, and A. Petzold, *1-d* deterministic crack pattern formation as a growth process with restrictions, *Europhys. Lett.* 19:485 (1992).

[17] Y. Couder, F. Argoul, A. Arnéodo, J. Maurer and M. Rabaud, Statistical properties of fractal dendrites and anisotropic diffusion-limited aggregates, *Phys. Rev. A* 42:3499 (1990).

[18] D.S. Graff and L.M. Sander, Branch-height distribution in diffusion-limited deposition, *Phys. Rev. E* 47:R2273 (1993).

[19] P. Meakin, P. Ramanlal, L.M. Sander and R.C. Ball, Ballistic deposition on surfaces, *Phys. Rev. A* 34:5091 (1986).

[20] H.J. Leamy, G.H. Gilmer and A.G. Dirks, The microstructure of vapor deposited thin films, *in* "Current Topics in Materials Science", E. Kaldis, ed., North-Holland, New York (1980).

[21] P. Meakin and J. Krug, Columnar microstructure in three-dimensional ballistic deposition, *Europhys. Lett.* 11:7 (1990).

[22] P. Meakin and J. Krug, Three-dimensional ballistic deposition at oblique incidence, *Phys. Rev. A* 46:3390 (1992).

[23] J. Krug and P. Meakin, Columnar growth in oblique incidence ballistic deposition: Faceting, noise reduction and mean-field theory, *Phys. Rev. A* 43:900 (1991).

[24] J. Krug and P. Meakin, Microstructure and surface scaling in ballistic deposition at oblique incidence, *Phys. Rev. A* 40:2064 (1989).

[25] P. Meakin and J. Krug, Scaling structure in simple screening models for columnar growth, *Phys. Rev. A* 46:4654 (1992).

[26] M. Matsushita and P. Meakin, Cluster-size distribution of self-affine fractals, *Phys. Rev. A* 37:3645 (1988).

[27] T. Nagatani, Scaling structure in a simple growth model with screening: forest formation model, *J. Phys. A* 24:L449 (1991).

[28] E.J. Gumbel, "Statistics of Extremes", Columbia University Press, New York (1958).

[29] J. Krug and H. Spohn, Universality classes for deterministic surface growth, *Phys. Rev. A* 38:4271 (1988).

[30] C. Tang, S. Alexander and R. Bruinsma, Scaling theory for the growth of amorphous films, *Phys. Rev. Lett.* 64:772 (1990).

[31] M. Westoby, The self-thinning rule, *Adv. Ecol. Res.* 14:167 (1984).

[32] J. White, The allometric interpretation of the self-thinning rule, *J. theor. Biol.* 89:475 (1981).

[33] T. Hara, A stochastic model and the moment dynamics of the growth and size distribution in plant populations, *J. theor. Biol.* 109:173 (1984).

[34] R.P.U. Karunasiri, R. Bruinsma and J. Rudnick, Thin-film growth and the shadow instability, *Phys. Rev. Lett.* 62:788 (1989).

[35] G.S. Bales, R. Bruinsma, E.A. Eklund, R.P.U. Karunasiri, J. Rudnick and A. Zangwill, Growth and erosion of thin solid films, *Science* 249:264 (1990).

[36] G.S. Bales and A. Zangwill, Macroscopic model for columnar growth of amorphous films by sputter deposition, *J. Vac. Sci. Tech. A* 9:145 (1991).

[37] J.H. Yao, C. Roland and H. Guo, Interfacial dynamics with long-range screening, *Phys. Rev. A* 45:3903 (1992).

[38] J.H. Yao and H. Guo, Shadowing instability in three dimensions, *Phys. Rev. E* 47:1007 (1993)

[39] C. Tang and S. Liang, Patterns and scaling properties in a ballistic deposition model, *Phys. Rev. Lett.* 71:2769 (1994).

[40] J.S. Langer, Theory of spinodal decomposition in alloys, *Ann. Phys.* 65:53 (1971).

[41] G. Rossi, Diffusion-limited aggregation without branching: A detailed analysis, *Phys. Rev. A* 35:2246 (1987).

[42] C. Roland and H. Guo, Interface growth with a shadow instability, *Phys. Rev. Lett.* 66:2106 (1991).

[43] P. Meakin, Diffusion-limited surface deposition in the limit of large anisotropy, *Phys. Rev. A* 33:1984 (1986).

[44] G. Rossi, Diffusion-limited aggregation without branching, *Phys. Rev. A* 34:3543 (1986).

[45] X.R. Wang, Scaling of the shortest-path aggregation, *Phys. Rev. A* 40:6767 (1989).

[46] M.E. Cates, Diffusion-limited aggregation without branching in the continuum approximation, *Phys. Rev. A* 34:5007 (1986).

[47] K. Kassner, Solutions to the mean-field equations of branchless diffusion-limited aggregation, *Phys. Rev. A* 42:3637 (1990).

[48] T.A. Witten and L.M. Sander, Diffusion-limited aggregation, *Phys. Rev. B* 27:5686 (1983).

[49] W. Feller, "An Introduction to Probability Theory and Its Applications", Vol. 1, Wiley, New York (1957).

[50] S. Schwarzer, J. Lee, A. Bunde, S. Havlin, H.E. Roman and H.E. Stanley, Minimum growth probability of diffusion-limited aggregates, *Phys. Rev. Lett.* 65:603 (1990).

[51] R.C. Ball and R. Blumenfeld, Exact results on exponential screening in two-dimensional diffusion limited aggregation, *Phys. Rev. A* 44:R828 (1991).

[52] E. Durand, "Electrostatique", Masson, Paris (1966).

[53] R.C. Ball and T.A. Witten, Causality bound on the density of aggregates, *Phys. Rev. A* 29:2966 (1984).

[54] T.C. Halsey and M. Leibig, Theory of branched growth, *Phys. Rev. A* 46:7793 (1992).

[55] T.C. Halsey, Diffusion-limited aggregation as branched growth, *Phys. Rev. Lett.* 72:1228 (1994).

[56] H.P. Peters, D. Stauffer, H.P. Höltes and K. Loewenich, Radius, perimeter, and density profile for percolation clusters and lattice animals, *Z. Phys. B* 34:399 (1979).

[57] M. Plischke and Z. Rácz, Active zone of growing clusters: Diffusion-limited aggregation and the Eden model, *Phys. Rev. Lett.* 53:415 (1984).

[58] R. Jullien and R. Botet, Scaling properties of the surface of the Eden model in $d=2,3,4$, *J. Phys. A* 18:2279 (1985).

[59] M. Eden, A probabilistic model for morphogenesis, *in:* "Symposium on Information Theory in Biology", Pergamon Press, New York (1958).

[60] F. Family and T. Vicsek, Scaling of the active zone in the Eden process on percolation networks and the ballistic deposition model, *J. Phys. A* 18:L75 (1985).

[61] T. Vicsek, M. Cserzö and V.K. Horváth, Self-affine growth of bacterial colonies, *Physica A* 167:315 (1990).

[62] M.A. Rubio, C.A. Edwards, A. Dougherty and J.P. Gollub, Self-affine fractal interfaces from immiscible displacement in porous media, *Phys. Rev. Lett.* 63:1685 (1989).

[63] S. He, G.L.M.K.S. Kahanda and P.-z. Wong, Roughness of wetting fluid invasion fronts in porous media, *Phys. Rev. Lett.* 69:3731 (1992).

[64] J. Zhang, Y.C. Zhang, P. Alstrom and M.T. Levinsen, Modeling forest fire by a paper-burning experiment, a realization of the interface growth mechanism, *Physica A* 189:383 (1992).

[65] E. Medina, T. Hwa, M. Kardar and Y.C. Zhang, Burgers equation with correlated noise: Renormalization-group analysis and applications to directed polymers and interface growth, *Phys. Rev. A* 39:3053 (1989).

[66] Y.C. Zhang, Non-universal roughening of kinetic self-affine interfaces, *J. Physique* 51:2129 (1990).

[67] J. Krug, Kinetic roughening by exceptional fluctuations, *J. Physique I* 1:9 (1991).

[68] Z. Csahók, K. Honda and T. Vicsek, Dynamics of surface roughening in disordered media, *J. Phys. A* 24:L171 (1993).

[69] L.A.N. Amaral, A.-L. Barabási and H.E. Stanley, Universality classes for interface growth with quenched disorder, *Phys. Rev. Lett.* 73:62 (1994).

[70] P. Devillard, Interface motion in a two-dimensional Ising model with a field, *J. Stat. Phys.* 62:443 (1991).

[71] H.W. Diehl, D.M. Kroll and H. Wagner, The interface in a Ginsburg-Landau-Wilson model: Derivation of the drumhead model in the low-temperature limit, *Z. Phys. B* 36:329 (1980).

[72] H. Spohn, Interface motion in models with stochastic dynamics, *J. Stat. Phys.* 71:1081 (1993).

[73] R. Ghez and S.S. Iyer, The kinetics of fast steps on crystal surfaces and its application to the molecular beam epitaxy of silicon, *IBM J. Res. Dev.* 32:804 (1988).

[74] M. Siegert and M. Plischke, Instability in surface growth with diffusion, *Phys. Rev. Lett.* 68:2035 (1992).

[75] T. Sun and M. Plischke, Renormalization group study of a driven continuum model for molecular beam epitaxy, *Phys. Rev. Lett.* 71:3174 (1993).

[76] F. Family and J.G. Amar, The morphology and evolution of the surface in epitaxial and thin film growth: A continuum model with surface diffusion, *Fractals* 1:753 (1993).

[77] J. Krug, M. Plischke and M. Siegert, Surface diffusion currents and the universality classes of growth, *Phys. Rev. Lett.* 70:3271 (1993).

[78] J. Koplik and H. Levine, Interface moving through a random background, *Phys. Rev. B* 32:280 (1985).

[79] G. Grinstein, D.H. Lee and S. Sachdev, Conservation laws, anisotropy, and 'self-organized criticality' in noisy nonequilibrium systems, *Phys. Rev. Lett.* 64:1927 (1990).

[80] T. Hwa and M. Kardar, Avalanches, hydrodynamics and discharge events in models of sandpiles, *Phys. Rev. A* 45:7002 (1992).

[81] R. Lipowsky, Nonlinear growth of wetting layers, *J. Phys. A* 18:L585 (1985).

[82] M. Grant, Dynamics of roughening and complete wetting, *Phys. Rev. B* 37:5705 (1988).

[83] S.F. Edwards and D.R. Wilkinson, The surface statistics of a granular aggregate, *Proc. Roy. Soc. London* A381:17 (1982).

[84] J.W. Evans, Factors mediating smoothness in epitaxial thin-film growth, *Phys. Rev. B* 43:3897 (1991).

[85] L. Golubović and R. Bruinsma, Surface diffusion and fluctuations of growing interfaces, *Phys. Rev. Lett.* 66:321 (1991); Erratum 67:2747.

[86] D.E. Wolf and J. Villain, Growth with surface diffusion, *Europhys. Lett.* 13:389 (1990).

[87] J. Krug and P. Meakin, Kinetic roughening of Laplacian fronts, *Phys. Rev. Lett.* 66:703 (1991).

[88] J.G. Amar, P.-M. Lam and F. Family, Groove instabilities in surface growth with diffusion, *Phys. Rev. E* 47:3242 (1993).

[89] M. Schroeder, M. Siegert, D.E. Wolf, J.D. Shore and M. Plischke, Scaling of growing surfaces with large local slopes, *Europhys. Lett.* 24:563 (1993).

[90] S. Das Sarma, S.V. Ghaisas and J.M. Kim, Kinetic super-roughening and anomalous dynamic scaling in nonequilibrium growth models, *Phys. Rev. E* 49:122 (1994).

[91] M.E. Fisher, Interface wandering in adsorbed and bulk phases, pure and impure, *J. Chem. Soc. Faraday Trans. 2* 82:1569 (1986).

[92] T. Nattermann and J. Villain, Random-field Ising systems: A survey of current theoretical views, *Phase Transitions* 11:5 (1988).

[93] R. Lipowsky, The conformation of membranes, *Nature* 349:475 (1991).

[94] J. Krug, Turbulent interfaces, *Phys. Rev. Lett.* 72:2907 (1994).

[95] Z.-W. Lai and S. Das Sarma, Kinetic growth with surface relaxation: Continuum versus atomistic models, *Phys. Rev. Lett.* 66:2348 (1991).

[96] L.-H. Tang and T. Nattermann, Kinetic roughening in molecular beam epitaxy, *Phys. Rev. Lett.* 66:2899 (1991).

[97] P. Meakin and J.M. Deutch, The formation of surfaces by diffusion limited annihilation, *J. Chem. Phys.* 85:2320 (1986).

[98] B. Caroli, C. Caroli and B. Roulet, Instabilities of planar solidification fronts, *in:* "Solids Far From Equilibrium", C. Godrèche, ed., Cambridge University Press, Cambridge (1991), pp. 155.

[99] J.M. Kim and S. Das Sarma, Discrete models for conserved growth equations, *Phys. Rev. Lett.* 72:2903 (1994).

[100] F. Family, Scaling of rough surfaces: effects of surface diffusion, *J. Phys. A* 19:L441 (1986).

[101] J.D. Weeks and G.H. Gilmer, Dynamics of crystal growth, *Adv. Chem. Phys.* 40:157 (1979).

[102] J. Krug, Classification of some growth and deposition processes, *J. Phys. A* 22:L769 (1989).

[103] P. Meakin and R. Jullien, Restructuring effects in the rain model for random deposition, *J. Physique* 48:1651 (1987).

[104] D. Liu and M. Plischke, Universality in two- and three-dimensional growth and deposition models, *Phys. Rev. B* 38:4781 (1988).

[105] S. Das Sarma and P. Tamborenea, A new universality class for kinetic growth: One-dimensional molecular beam epitaxy, *Phys. Rev. Lett.* 66:325 (1991).

[106] P.I. Tamborenea and S. Das Sarma, Surface-diffusion-driven kinetic growth on one-dimensional substrates, *Phys. Rev. E* 48:2575 (1993).

[107] J. Krug and H. Spohn, Mechanism for rough-to-rough transitions in surface growth, *Phys. Rev. Lett.* 64:2232 (1990).

[108] L.-H. Tang and T. Nattermann, Kinetic surface roughening. I. The Kardar-Parisi-Zhang equation in the weak coupling regime, *Phys. Rev. A* 45:7156 (1992).

[109] T. Ala-Nissila, T. Hjelt, J.M. Kosterlitz and O. Venäläinen, Scaling exponents for kinetic roughening in higher dimensions, *J. Stat. Phys.* 72:207 (1993).

[110] T. Sun and M. Plischke, Field-theory renormalization approach to the Kardar-Parisi-Zhang equation, *Phys. Rev. E* 49:5046 (1994).

[111] E. Frey and U.C. Täuber, Two-loop renormalization group analysis of the Burgers - Kardar-Parisi-Zhang equation, *Phys. Rev. E* 50:1024 (1994).

[112] J.P. Doherty, M.A. Moore, J.M. Kim and A.J. Bray, Generalizations of the Kardar-Parisi-Zhang equation, *Phys. Rev. Lett.* 72:2041 (1994).

[113] H. Fujisaka and T. Yamada, Theoretical study of a chemical turbulence, *Progr. Theor. Phys.* 57:734 (1977).

[114] H. van Beijeren, R. Kutner and H. Spohn, Excess noise for driven diffusive systems, *Phys. Rev. Lett.* 54:2026 (1985).

[115] J. Krug, Scaling relation for a growing interface, *Phys. Rev. A* 36:5465 (1987).

[116] T. Hwa and E. Frey, Exact scaling function of interface growth dynamics, *Phys. Rev. A* 44:R7873 (1991).

[117] M. Schwartz and S.F. Edwards, Nonlinear deposition: a new approach, *Europhys. Lett.* 20:301 (1992).

[118] J.P. Bouchaud and M. Cates, Self-consistent approach to the Kardar-Parisi-Zhang equation, *Phys. Rev. E* 47:1455; Erratum 48:635 (1993).

[119] M.A. Moore, T. Blum, J.P. Doherty, J.-P. Bouchaud and P. Claudin, Glassy solutions of the Kardar-Parisi-Zhang equation (preprint).

[120] T. Halpin-Healy, Disorder-induced roughening of diverse manifolds, *Phys. Rev. A* 42:711 (1990).

[121] T. Nattermann and H. Leschhorn, Interfaces and directed polymers in disordered systems: a three-parameter renormalization group approach, *Europhys. Lett.* 14:603 (1991).

[122] D.E. Wolf, Kinetic roughening of vicinal surfaces, *Phys. Rev. Lett.* 67:1783 (1991).

[123] M.P.A. Fisher and G. Grinstein, Nonlinear transport and $1/f^{\alpha}$ noise in insulators, *Phys. Rev. Lett.* 69:2322 (1992).

[124] T. Hwa, Nonequilibrium dynamics of driven line liquids, *Phys. Rev. Lett.* 69:1552 (1992).

[125] H.K. Janssen and B. Schmittmann, Field theory of long time behavior in driven diffusive systems, *Z. Phys. B* 63:517 (1986).

[126] J. Krug, P. Meakin and T. Halpin-Healy, Amplitude universality for driven interfaces and directed polymers in random media, *Phys. Rev. A* 45:638 (1992).

[127] K. Sneppen, J. Krug, M.H. Jensen, C. Jayaprakash and T. Bohr, Dynamic scaling and crossover analysis for the Kuramoto-Sivashinsky equation, *Phys. Rev. A* 46:R7351 (1992).

[128] D.E. Wolf and L.-H. Tang, Inhomogeneous growth processes, *Phys. Rev. Lett.* 65:1591 (1990).

[129] J. Krug, Boundary-induced phase transitions in driven diffusive systems, *Phys. Rev. Lett.* 67:1882 (1991).

[130] B. Derrida, M.R. Evans, V. Hakim and V. Pasquier, Exact solution of a 1D asymmetric exclusion model using a matrix formulation, *J. Phys. A* 26:1493 (1993).

[131] G. Schütz and E. Domany, Phase transitions in an exactly soluble one-dimensional exclusion process, *J. Stat. Phys.* 72:277 (1993).

[132] J. Krug and L.-H. Tang, Disorder-induced unbinding in confined geometries, *Phys. Rev. E* 50:104 (1994).

[133] D. Forster, D.R. Nelson and M.J. Stephen, Large-distance and long-time properties of a randomly stirred fluid, *Phys. Rev. A* 16:732 (1977).

[134] D.A. Huse, C.L. Henley and D.S. Fisher, Huse, Henley, and Fisher respond, *Phys. Rev. Lett.* 55:2924 (1985).

[135] L.-H. Gwa and H. Spohn, Bethe solution for the dynamical-scaling exponent of the noisy Burgers equation, *Phys. Rev. A* 46:844 (1992).

[136] J.M. Kim, M.A. Moore and A.J. Bray, Zero-temperature directed polymers in a random potential, *Phys. Rev. A* 44:2345 (1991).

[137] R. Friedberg and Y.-K. Yu, Replica model at low integer N for directed polymers in $(1+1)$ dimensions, *Phys. Rev. E* 49:4157 (1994).

[138] J.G. Amar and F. Family, Universality in surface growth: Scaling functions and amplitude ratios, *Phys. Rev. A* 45:5378 (1992).

[139] J. Krug and P. Meakin, Universal finite-size effects in the rate of growth processes, *J. Phys. A* 23:L987 (1990).

[140] J. Krug, $1/f$ noise for driven interfaces, *Phys. Rev. A* 44:R801 (1991).

[141] L.M. Sander and H. Yan, Temporal characteristics in nonequilibrium surface-growth models, *Phys. Rev. A* 44:4885 (1991).

[142] B. Derrida, M.R. Evans and D. Mukamel, Exact diffusion constant for one-dimensional asymmetric exclusion models, *J. Phys. A* 26:4911 (1993).

[143] J.M. Kim and J.M. Kosterlitz, Growth in a restricted solid-on-solid model, *Phys. Rev. Lett.* 62:2289 (1989).

[144] G.I. Sivashinsky, Instabilities, pattern formation, and turbulence in flames, *Ann. Rev. Fluid Mech.* 15:179 (1983).

[145] C. Misbah, H. Müller-Krumbhaar and D.E. Temkin, Interface structure at large supercooling, *J. Phys. I* 1:585 (1991).

[146] I. Bena, C. Misbah and A. Valance, Nonlinear evolution of a terrace edge during step-flow growth, *Phys. Rev. B* 47:7408 (1993).

[147] A. Karma and C. Misbah, Competition between noise and determinism in step flow growth, *Phys. Rev. Lett.* 71:3810 (1993).

[148] R.E. LaQuey, S.M. Mahajan, P.H. Rutherford and W.M. Tang, Nonlinear saturation of the trapped-ion mode, *Phys. Rev. Lett.* 34:391 (1975).

[149] Y. Kuramoto, "Chemical Oscillations, Waves, and Turbulence", Springer, Berlin (1984).

[150] V. Yakhot, Large-scale properties of unstable systems governed by the Kuramoto-Sivashinksi (*sic*) equation, *Phys. Rev. A* 24:642 (1981).

[151] S. Zaleski, A stochastic model for the large scale dynamics of some fluctuating interfaces, *Physica D* 34:427 (1989).

[152] I. Procaccia, M.H. Jensen, V.S. L'vov, K. Sneppen and R. Zeitak, Surface roughening and the long-wavelength properties of the Kuramoto-Sivashinsky equation, *Phys. Rev. A* 46:3220 (1992).

[153] C. Jayaprakash, F. Hayot and R. Pandit, Universal properties of the two-dimensional Kuramoto-Sivashinsky equation, *Phys. Rev. Lett.* 71:12 (1993).

[154] T. Bohr, G. Grinstein, C. Jayaprakash, M.H. Jensen and D. Mukamel, Chaotic interface dynamics: A model with turbulent behavior, *Phys. Rev. A* 46:4791 (1992).

[155] T. Bohr, G. Grinstein, C. Jayaprakash, M.H. Jensen, J. Krug and D. Mukamel, Turbulence, power laws and Galilean invariance, *Physica D* 59:177 (1992).

[156] J.M. Burgers, 1974, "The Nonlinear Diffusion Equation", Reidel, Dordrecht.

[157] L.S. Schulman, "Techniques and Applications of Path Integration", Wiley, New York (1981).

[158] L.-H. Tang, J. Kertész and D.E. Wolf, Kinetic roughening with power-law waiting time distribution, *J. Phys. A* 25:L1193 (1991).

[159] J. Krug and T. Halpin-Healy, Directed polymers in the presence of columnar disorder, *J. Physique I* 3:2179 (1993).

[160] G. Forgacs, R. Lipowsky and Th.M. Nieuwenhuizen, The behavior of interfaces in ordered and disordered systems, *in* "Phase Transitions and Critical Phenomena", Vol. 14, C. Domb and J.L. Lebowitz, eds., Academic Press, London (1991).

[161] M.R. Evans and B. Derrida, Improved bounds for the transition temperature of directed polymers in a finite-dimensional random medium, *J. Stat. Phys.* 69:427 (1992).

[162] D.S. Fisher and D.A. Huse, Directed paths in a random potential, *Phys. Rev. B* 43:10728 (1991).

[163] U. Schultz, J. Villain, E. Brézin and H. Orland, Thermal fluctuations in some random field models, *J. Stat. Phys.* 51:1 (1988).

[164] T. Hwa and D.S. Fisher, Anomalous fluctuations of directed polymers in random media, *Phys. Rev. B* 49:3136 (1994).

[165] B. Derrida, J.L. Lebowitz, E.R. Speer and H. Spohn, Dynamics of an anchored Toom interface, *J. Phys. A* 24:4805 (1991).

[166] M. Kardar, Depinning by quenched randomness, *Phys. Rev. Lett.* 55:2235 (1985).

[167] J. Wuttke and R. Lipowsky, Universality classes for wetting in two-dimensional random bond systems, *Phys. Rev. B* 44:13042 (1991).

[168] L.-H. Tang and I.F. Lyuksyutov, Directed polymer localization in a disordered medium, *Phys. Rev. Lett.* 71:2745 (1993).

[169] L. Balents and M. Kardar, Disorder-induced unbinding of a flux line from an extended defect, *Phys. Rev. B* 49:13030 (1994).

[170] H. Kinzelbach and M. Lässig, Depinning in a random medium (preprint, cond-mat/9405088).

[171] T. Nattermann and W. Renz, Diffusion in a random catalytic environment, polymers in random media, and stochastically growing interfaces, *Phys. Rev. A* 40:4675 (1989).

[172] I. Arsenin, T. Halpin-Healy and J. Krug, Competing effects of point versus columnar disorder on the roughening of directed polymers in random media, *Phys. Rev. E* 49:R3561 (1994).

[173] A.-S. Sznitman, Brownian confinement and pinning in a Poissonian potential (preprint).

[174] J. Krug, Kinetic roughening in the presence of quenched random phases, *in* "Surface Disordering: Growth, Roughening and Phase Transitions", R. Jullien, J. Kertész, P. Meakin and D.E. Wolf, eds., Nova Science, Commack, NY (1992) p. 177.

[175] W.K. Burton, N. Cabrera and F.C. Frank, The growth of crystals and the equilibrium structure of their surfaces, *Phil. Trans. Roy. Soc. (Lond.) A* 243:299 (1951).

[176] B.M. Forrest and L.-H. Tang, Surface roughening in a hypercube-stacking model, *Phys. Rev. Lett.* 64:1405 (1990).

[177] Z. Rácz, M. Siegert, D. Liu and M. Plischke, Scaling properties of driven interfaces: Symmetries, conservation laws and the role of constraints, *Phys. Rev. A* 43:5275 (1991).

[178] J. Krug and H.T. Dobbs, Current-induced faceting of crystal surfaces, *Phys. Rev. Lett.* 73:1947 (1994).

[179] H.C. Kang and J.W. Evans, Scaling analysis of surface roughness in simple models for molecular-beam epitaxy, *Surf. Sci.* 269/270:784 (1992).

[180] H.C. Kang and J.W. Evans, Scaling analysis of surface roughness and Bragg oscillation decay in models for low-temperature epitaxial growth, *Surf. Sci.* 271:321 (1992).

[181] H. Park, A. Provata and S. Redner, Interface growth with competing surface currents, *J. Phys. A* 24:L1391 (1991).

[182] P.-M. Lam and F. Family, Surface growth in a model of molecular-beam epitaxy with correlated noise, *Phys. Rev. A* 44:4854 (1991).

[183] S. Das Sarma and S.V. Ghaisas, Solid-on-solid rules and models for nonequilibrium growth in 2+1 dimensions, *Phys. Rev. Lett.* 69:3762 (1992).

[184] C.J. Lanczycki and S. Das Sarma, Nonequilibrium influence of upward atomic mobility in one-dimensional molecular-beam epitaxy, *Phys. Rev. E* 50:213 (1994).

[185] Y. Kim, D.K. Park and J.M. Kim, Conserved growth in a restricted solid-on-solid model, *J. Phys. A* 27:L533 (1994).

[186] D.E. Wolf, Computer simulation of molecular beam epitaxy, to appear in "Scale Invariance, Interfaces and Non-Equilibrium Dynamics", M. Droz, A.J. McKane, J. Vannimenus and D.E. Wolf, eds., Plenum Press, New York.

[187] H.P. Bonzel, Surface diffusion of metals - a comparison of intrinsic and mass transfer measurements, *CRC Crit. Rev. Solid State Sci.* 6:171 (1976).

[188] S. Clarke and D.D. Vvedensky, Origin of reflection high-energy electron-diffraction intensity oscillations during molecular-beam epitaxy: A computational modeling approach, *Phys. Rev. Lett.* 58:2235 (1987).

[189] D.D. Vvedensky and S. Clarke, Recovery kinetics during interrupted epitaxial growth, *Surf. Sci.* 225:373 (1990).

[190] S. Clarke, M.R. Wilby and D.D. Vvedensky, Theory of homoepitaxy on Si(001), I. Kinetics during growth, *Surf. Sci.* 255:91 (1990).

[191] S. Das Sarma, Numerical studies of epitaxial kinetics: What can a computer simulation tell us about nonequilibrium crystal growth?, *J. Vac. Sci. Technol. A* 8:2714 (1990).

[192] P. Šmilauer, M.R. Wilby, and D.D. Vvedensky, Reentrant layer-by-layer growth: A numerical study, *Phys. Rev. B* 47:4119 (1993).

[193] D.D. Vvedensky, A. Zangwill, C.N. Luse and M.R. Wilby, Stochastic equations of motion for epitaxial growth, *Phys. Rev. E* 48:852 (1993).

[194] M.D. Johnson, C. Orme, A.W. Hunt, D. Graff, J. Sudijono, L.M. Sander and B.G. Orr, Stable and unstable growth in molecular beam epitaxy, *Phys. Rev. Lett.* 72:116 (1994).

[195] J. Krug, H.T. Dobbs and S. Majaniemi, Adatom mobility for the solid-on-solid model, to appear in *Z. Phys. B* (1995).

[196] M. Siegert and M. Plischke, Scaling behavior of driven solid-on-solid models with diffusion, *J. Phys. I France* 3:1371 (1993).

[197] M. Plischke and M. Siegert, Comment on 'Kinetic phase diagram for crystal growth: A (1+1)-dimensional model', *Phys. Rev. Lett.* 68:2854 (1992).

[198] J.D. Weeks, The roughening transition, *in* "Ordering in strongly fluctuating condensed matter systems", T. Riste, ed., Plenum Press, New York 1980.

[199] R. Phillips and D.C. Chrzan, Kinetic phase diagram for crystal growth: A (1+1)-dimensional model, *Phys. Rev. Lett.* 67:220 (1991).

[200] R.L. Schwoebel and E.J. Shipsey, Step motion on crystal surfaces, *J. Appl. Phys.* 37:3682 (1966).

[201] R.L. Schwoebel, Step motion on crystal surfaces II, *J. Appl. Phys.* 40:614 (1969).

[202] G. Ehrlich and F.G. Hudda, Atomic view of surface self-diffusion: Tungsten on tungsten, *J. Chem. Phys.* 44:1039 (1966).

[203] S.-C. Wang and T.T. Tsong, Measurement of the barrier height of the reflective W(110) plane boundaries in surface diffusion of single atoms, *Surf. Sci.* 121:85 (1982).

[204] S.C. Wang and G. Ehrlich, Adatom motion to lattice steps: A direct view, *Phys. Rev. Lett.* 70:41 (1993).

[205] H. Yan, Kinetic growth with surface diffusion: The scaling aspect, *Phys. Rev. Lett.* 68:3048 (1992).

[206] D. Kessler, H. Levine and L.M. Sander, Molecular-beam epitaxial growth and surface diffusion, *Phys. Rev. Lett.* 69:100 (1992).

[207] R.B. Sargent, Effects of surface diffusion on thin-film morphology: a computer study, *in* "Modeling of Optical Thin Films II", M.R. Jacobson, ed., *Proc. SPIE* 1324:13 (1990).

[208] I.K. Marmorkos and S. Das Sarma, Kinetic simulation of molecular beam epitaxial growth dynamics, *Surf. Sci. Lett.* 237:L411 (1990).

[209] I.K. Marmorkos and S. Das Sarma, Atomistic numerical study of molecular-beam- epitaxial growth kinetics, *Phys. Rev. B* 45:11262 (1992).

[210] S. Das Sarma, C.J. Lanczycki, S.V. Ghaisas and J.M. Kim, Defect formation and crossover behavior in the dynamic scaling properties of molecular-beam epitaxy, *Phys. Rev. B* 49:10963 (1994).

[211] M. Schimschak, Modelle zur Beschreibung von Oberflächenwachstum, diploma thesis, University of Cologne (1994).

[212] D.A. Kessler and B.G. Orr, Diffusion in MBE growth (unpublished manuscript).

[213] C.R. Doering, W. Horsthemke and J. Riordan, Nonequilibrium fluctuation-induced transport, *Phys. Rev. Lett.* 72:2984 (1994).

[214] S. Pal and D.P. Landau, Monte Carlo simulation and dynamic scaling of surfaces in MBE growth, *Phys. Rev. B* 49:10597 (1994).

[215] J. Villain, A. Pimpinelli, L. Tang and D. Wolf, Terrace sizes in molecular beam epitaxy, *J. Phys. I France* 2:2107 (1992).

[216] M. Siegert and M. Plischke, Slope selection and coarsening in molecular beam epitaxy, *Phys. Rev. Lett.* 73:1517 (1994).

[217] A.K. Myers-Beaghton and D.D. Vvedensky, Nonlinear equation for diffusion and adatom interactions during epitaxial growth on vicinal surfaces, *Phys. Rev. B* 42:5544 (1990).

[218] A.K. Myers-Beaghton and D.D. Vvedensky, Generalized Burton-Cabrera-Frank theory for growth and equilibration on stepped surfaces, *Phys. Rev. A* 44:2457 (1991).

[219] V. Fuenzalida, Cluster-size distribution during epitaxial growth from the vapor on strongly misoriented surfaces, *Phys. Rev. B* 44:10835 (1991).

[220] J. Villain, A. Pimpinelli and D. Wolf, Layer by layer growth in molecular beam epitaxy, *Comments Cond. Mat. Phys.* 16:1 (1992).

[221] G.S. Bales and A. Zangwill, Morphological instability of a terrace edge during step-flow growth, *Phys. Rev. B* 41:5500 (1990).

[222] F. Wu, S.G. Jaloviar, D.E. Savage and M.G. Lagally, Roughening of steps during homoepitaxial growth on Si(001), *Phys. Rev. Lett.* 71:4190 (1993).

[223] I. Markov, Kinetics of surfactant-mediated epitaxial growth, *Phys. Rev. B* 50:11271 (1994).

[224] P.I. Cohen, G.S. Petrich, P.R. Pukite, G.J. Whaley and A.S. Arrott, Birth-death models of epitaxy: I. Diffraction oscillations from low index surfaces, *Surf. Sci* 216:222 (1989).

[225] M. Siegert and M. Plischke, Solid-on-solid models of molecular beam epitaxy, *Phys. Rev. E* 50:917 (1994).

[226] M. Plischke (private communication).

[227] J.D. Shore (private communication).

[228] M. Albrecht, H. Fritzsche and U. Gradmann, Kinetic facetting in homoepitaxy of Fe(110) on Fe(110), *Surf. Sci.* 294:1 (1993).

[229] H.-J. Ernst, F. Fabre, R. Folkerts and J. Lapujoulade, Observation of a growth instability during low temperature molecular beam epitaxy, *Phys. Rev. Lett.* 72:112 (1994).

[230] D.D. Vvedensky, New slant on epitaxial growth, *Physics World*, March 1994, p. 30.

[231] G.W. Smith, A.J. Pidduck, C.R. Whitehouse, J.L. Glasper and J. Spowart, Real-time laser-light scattering studies of surface topography development during GaAs MBE growth, *J. Cryst. Growth* 127:966 (1993).

[232] M.D. Johnson, J. Sudijono, A.W. Hunt and B.G. Orr, Growth mode evolution during homoepitaxy of GaAs(001), *Appl. Phys. Lett.* 64:484 (1994).

[233] C. Orme, M.D. Johnson, J.L. Sudijono, K.T. Leung and B.G. Orr, Large scale surface structure formed during GaAS(001) homoepitaxy, *Appl. Phys. Lett.* 64:860 (1994).

[234] J.H. Neave, P.J. Dobson and B.A. Joyce, Reflection high-energy electron diffraction oscillations from vicinal surfaces - a new approach to surface diffusion measurements, *Appl. Phys. Lett.* 47:100 (1985).

[235] P. Šmilauer and D.D. Vvedensky, Step-edge barriers on GaAs(001), *Phys. Rev. B* 48:17603 (1993).

[236] J.S. Langer, An introduction to the kinetics of first-order phase transitions, *in* "Solids far from equilibrium", C. Godrèche, ed., Cambridge University Press (1991).

[237] L. Golubović and R.P.U. Karunasiri, Spinodal decomposition of the interface in nonlinear Edwards-Wilkinson model, *Phys. Rev. Lett.* 66:3156 (1991).

[238] T. Kawakatsu and T. Munakata, Kink dynamics in a one-dimensional conserved TDGL system, *Prog. Theor. Phys.* 74:11 (1985).

[239] A.W. Hunt, C. Orme, D.R.M. Williams, B.G. Orr and L.M. Sander, Instabilities in MBE growth, *Europhys. Lett.* 27:611 (1994).

[240] D.J. Eaglesham and G.H. Gilmer, Roughening during Si deposition at low temperatures, *in* "Surface disordering: Growth, roughening and phase transitions", R. Jullien, J. Kertész, P. Meakin and D.E. Wolf, eds., Nova Science, New York (1992) p. 69.

[241] J. Chevrier, A. Cruz, N. Pinto, I. Berbezier and J. Derrien, Influence of kinetic roughening on the epitaxial growth of silicon, *J. Phys. I France* 4:1309 (1994).

[242] D.J. Eaglesham, H.-J. Gossmann and M. Cerullo, Limiting thickness h_{epi} for epitaxial growth and room-temperature Si growth on Si(100), *Phys. Rev. Lett.* 65:1227 (1990).

[243] A.J. Bray, Exact renormalization-group results for domain-growth scaling in spinodal decomposition, *Phys. Rev. Lett.* 62:2841 (1989).

[244] F. Liu and H. Metiu, Dynamics of phase separation of crystal surfaces, *Phys. Rev. B* 48:5808 (1993).

[245] T. Sun, H. Guo and M. Grant, Dynamics of driven interfaces with a conservation law, *Phys. Rev. A* 40:6763 (1989).

[246] C.N. Luse, A. Zangwill, D.D. Vvedensky and M.R. Wilby, Adatom mobility on vicinal surfaces during epitaxial growth, *Surf. Sci. Lett.* 274:L535 (1992).

[247] J.Y. Cavaillé and M. Drechsler, Surface self-diffusion by ion impact, *Surf. Sci.* 75:342 (1978).

[248] T. Sun, B. Morin, H. Guo and M. Grant, Roughening transition of a driven interface with a conservation law, *in* "Surface disordering: Growth, roughening and phase transitions", R. Jullien, J. Kertész, P. Meakin and D.E. Wolf, eds., Nova Science, New York (1992) p. 45.

[249] A. Chakrabarti, Computer simulation of stochastically growing interfaces with a conservation law, *J. Phys. A* 23:L919 (1990).

[250] Y. Tu, Instability in a continuum kinetic-growth model with surface relaxation, *Phys. Rev. A* 46:R729 (1992).

[251] K. Moser, Stochastische Differentialgleichungen für rauhe Oberflächen, doctoral thesis, University of Cologne (1993).

[252] V. Putkaradze, T. Bohr and J. Krug, Global estimates for the solutions of the noiseless conserved Kardar-Parisi-Zhang equation (preprint).

[253] P. Šmilauer and M. Kotrla, Crossover effects in the Wolf-Villain model of epitaxial growth in 1+1 and 2+1 dimensions, *Phys. Rev. B* 49:5769 (1994).

[254] K. Park, B. Kahng and S.S. Kim, Surface dynamics of the Wolf-Villain model for epitaxial growth in 1+1 dimensions, *Physica A* 210:146 (1994).

[255] M. Plischke, J.D. Shore, M. Schroeder, M. Siegert and D.E. Wolf, Comment on "Solid-on-solid rules and models for nonequilibrium growth in 2+1 dimensions", *Phys. Rev. Lett.* 71:2509 (1993).

[256] P. Šmilauer and M.Kotrla, Kinetic roughening in growth models with diffusion in higher dimensions, *Europhys. Lett.* 27:261 (1994).

[257] M. Kotrla, A.C. Levi and P. Šmilauer, Roughness and nonlinearities in (2+1)- dimensional growth models with diffusion, *Europhys. Lett.* 20:25 (1992).

[258] M. Schroeder, Modelle mit Bezug zum epitaktischen Kristallwachstum, diploma thesis, University of Duisburg (1993).

[259] S. Das Sarma and R. Kotlyar, Dynamical renormalization group analysis of fourth-order conserved growth nonlinearities, *Phys. Rev. E* 50:R4275 (1994).

[260] S. Das Sarma and S.V. Ghaisas, Das Sarma and Ghaisas reply, *Phys. Rev. Lett.* 71:2510 (1993).

[261] M.R. Wilby, D.D. Vvedensky and A. Zangwill, Scaling in a solid-on-solid model of epitaxial growth, *Phys. Rev. B* 46:12896 (1992); Erratum 47:16068 (1993).

[262] D.J. Miller, K.E. Gray, R.T. Kampwirth and J.M. Murduck, Studies of growth instabilities and roughening in sputtered NbN films using a multilayer decoration technique, *Europhys. Lett.* 19:27 (1992).

[263] T. Salditt, T.H. Metzger and J. Peisl, Kinetic roughness of amorphous multilayers studied by diffuse X-ray scattering, *Phys. Rev. Lett.* 73:2228 (1994).

[264] R. Chiarello, V. Panella, J. Krim and C. Thompson, X-ray reflectivity and adsorption isotherm study of fractal scaling in vapor-deposited films, *Phys. Rev. Lett.* 67:3408 (1991).

[265] J. Chevrier, V. Le Thanh, R. Buys and J. Derrien, A RHEED study of epitaxial growth of iron on a silicon surface: Experimental evidence for kinetic roughening, *Europhy. Lett.* 16:737 (1991).

[266] Y.-L. He, H.-N. Yang, T.-M. Lu and G.-C. Wang, Measurement of dynamic scaling from epitaxial growth front: Fe film on Fe(001), *Phys. Rev. Lett.* 69:3770 (1992).

[267] C. Thompson, G. Palasantzas, Y.P. Feng, S.K. Sinha and J. Krim, X-ray reflectivity study of the growth kinetics of vapor-deposited silver films, *Phys. Rev. B* 49:4902 (1994).

[268] G. Palasantzas and J. Krim, Scanning tunneling microscopy study of the thick film limit of kinetic roughening, *Phys. Rev. Lett.* 73:3564 (1994).

[269] W. Weber and B. Lengeler, Diffuse scattering of hard x rays from rough surfaces, *Phys. Rev. B* 46:7953 (1992).

[270] G. Palasantzas, Finite-size effects on self-affine fractal surfaces due to domains, *Phys. Rev. B* 49:10544 (1994).

[271] G. Palasantzas and J. Krim, Effect of the form of the height-height correlation function on diffuse x-ray scattering from a self-affine surface, *Phys. Rev. B* 48:2873 (1993).

[272] J.A. Stroscio, D.T. Pierce, M. Stiles, A. Zangwill and L.M. Sander, Coarsening of unstable surface features during Fe(001) homoepitaxy (preprint).

[273] W.M. Tong, R.S. Williams, A. Yanase, Y. Segawa and M.S. Anderson, Atomic force microscope study of growth kinetics: Scaling in the heteroepitaxy of CuCl on CaF_2(111), *Phys. Rev. Lett.* 72:3374 (1994).

[274] H. Zeng and G. Vidali, Measurement of growth kinetics in a heteroepitaxial system: Pb on Cu(100), *Phys. Rev. Lett.* 74:582 (1995).

FORSCHUNGSZENTRUM JÜLICH GmbH

KFA

Jül-3031
February 1995
ISSN 0944-2952